



# C–H bond functionalization: recent discoveries and future directions

Edited by Indranil Chatterjee

## Imprint

Beilstein Journal of Organic Chemistry  
[www.bjoc.org](http://www.bjoc.org)  
ISSN 1860-5397  
Email: [journals-support@beilstein-institut.de](mailto:journals-support@beilstein-institut.de)

The *Beilstein Journal of Organic Chemistry* is published by the Beilstein-Institut zur Förderung der Chemischen Wissenschaften.

Beilstein-Institut zur Förderung der  
Chemischen Wissenschaften  
Trakehner Straße 7–9  
60487 Frankfurt am Main  
Germany  
[www.beilstein-institut.de](http://www.beilstein-institut.de)

The copyright to this document as a whole, which is published in the *Beilstein Journal of Organic Chemistry*, is held by the Beilstein-Institut zur Förderung der Chemischen Wissenschaften. The copyright to the individual articles in this document is held by the respective authors, subject to a Creative Commons Attribution license.



# C–H bond functionalization: recent discoveries and future directions

Indranil Chatterjee

## Editorial

Open Access

### Address:

Department of Chemistry, Indian Institute of Technology Ropar,  
Nangal Road, Rupnagar, Punjab 140001, India

### Email:

Indranil Chatterjee - indranil.chatterjee@iitrpr.ac.in

### Keywords:

C–H bond functionalization

*Beilstein J. Org. Chem.* **2023**, *19*, 1568–1569.

<https://doi.org/10.3762/bjoc.19.114>

Received: 20 September 2023

Accepted: 08 October 2023

Published: 17 October 2023

This article is part of the thematic issue "C–H bond functionalization: recent discoveries and future directions".

Guest Editor: I. Chatterjee



© 2023 Chatterjee; licensee Beilstein-Institut.  
License and terms: see end of document.

The process of C–H bond functionalization can be defined as the replacement of an activated or nonactivated C–H bond with a functional group. This discipline surfaced within the last few decades and proved to be a powerful synthetic tactic due to some remarkable advantages. It has drawn immense attention from the scientific community, thanks to some significant opportunities, such as the use of readily available feedstocks, the introduction of functionality at specific positions of molecules without requiring any prefunctionalized precursors, and the conversion of light alkanes to higher-value analogues [1,2]. The nonnecessity of prefunctionalization provides a step-economic alternative to classical reactions as well as famous Noble-prize-winning cross-couplings, therefore approaching another step up towards sustainability.

Likewise, a free-radical process is also a classical way to functionalize nonactivated C–H bonds in which site selectivity arises either from the relative strength of the C–H bonds or from the abstraction of intramolecular hydrogen atoms. Radical chemistry is a viable alternative to the two-electron process, in-

volving C–H bond functionalization in the absence of any ligand and using low-cost redox-active metals (Fe, Cu, Mn, etc.) rather than heavy metals (Rh, Ir, etc.). Although radical strategies are age-old processes, they were initially cumbersome due to the stoichiometric use of heavy metal salts, peroxides, and other toxic materials as well as the generation of heavy organic and inorganic wastes. In modern days, new strategies are being developed, dealing with photoredox chemistry and its combination with organometallic chemistry for site-selective C–H bond functionalization [3,4]. Recent years have witnessed many viable strategies for the synthesis of complex targets utilizing photoredox catalysis, electroorganic catalysis, Lewis acid catalysis, and transition-metal-free techniques. Some energy-economic reactors such as ball mill, microwave, ultrasound and, most importantly, flow reactors have also evolved towards a more sustainable future.

To showcase the modern approaches in this domain, this thematic issue in the *Beilstein Journal of Organic Chemistry* gathers recent reports from several research groups, including

photochemical as well as transition-metal-mediated C–H bond functionalization. This mixing of traditional and classical with modern-day research will surely encourage synthetic chemists to sketch new methodologies.

Indranil Chatterjee

Rupnagar, September 2023

## ORCID® iDs

Indranil Chatterjee - <https://orcid.org/0000-0001-8957-5182>

## References

1. Lam, N. Y. S.; Wu, K.; Yu, J.-Q. *Angew. Chem., Int. Ed.* **2021**, *60*, 15767–15790. doi:10.1002/anie.202011901
2. Sinha, S. K.; Guin, S.; Maiti, S.; Biswas, J. P.; Porey, S.; Maiti, D. *Chem. Rev.* **2022**, *122*, 5682–5841. doi:10.1021/acs.chemrev.1c00220
3. Prier, C. K.; Rankic, D. A.; MacMillan, D. W. C. *Chem. Rev.* **2013**, *113*, 5322–5363. doi:10.1021/cr300503r
4. Romero, N. A.; Nicewicz, D. A. *Chem. Rev.* **2016**, *116*, 10075–10166. doi:10.1021/acs.chemrev.6b00057

## License and Terms

This is an open access article licensed under the terms of the Beilstein-Institut Open Access License Agreement (<https://www.beilstein-journals.org/bjoc/terms>), which is identical to the Creative Commons Attribution 4.0 International License (<https://creativecommons.org/licenses/by/4.0>). The reuse of material under this license requires that the author(s), source and license are credited. Third-party material in this article could be subject to other licenses (typically indicated in the credit line), and in this case, users are required to obtain permission from the license holder to reuse the material.

The definitive version of this article is the electronic one which can be found at:  
<https://doi.org/10.3762/bjoc.19.114>





# NaI/PPh<sub>3</sub>-catalyzed visible-light-mediated decarboxylative radical cascade cyclization of *N*-arylacrylamides for the efficient synthesis of quaternary oxindoles

Dan Liu, Yue Zhao and Frederic W. Patureau\*

## Letter

Open Access

Address:  
Institute of Organic Chemistry, RWTH Aachen University,  
Landoltweg 1, 52074 Aachen, Germany

Email:  
Frederic W. Patureau\* - Frederic.patureau@rwth-aachen.de

\* Corresponding author

Keywords:  
decarboxylative cascade cyclization; iodide catalysis; metal-free photocatalysis; oxindole; phosphine catalysis

*Beilstein J. Org. Chem.* **2023**, *19*, 57–65.  
<https://doi.org/10.3762/bjoc.19.5>

Received: 03 October 2022  
Accepted: 08 December 2022  
Published: 16 January 2023

This article is part of the thematic issue "C–H bond functionalization: recent discoveries and future directions".

Guest Editor: I. Chatterjee

© 2023 Liu et al.; licensee Beilstein-Institut.  
License and terms: see end of document.

## Abstract

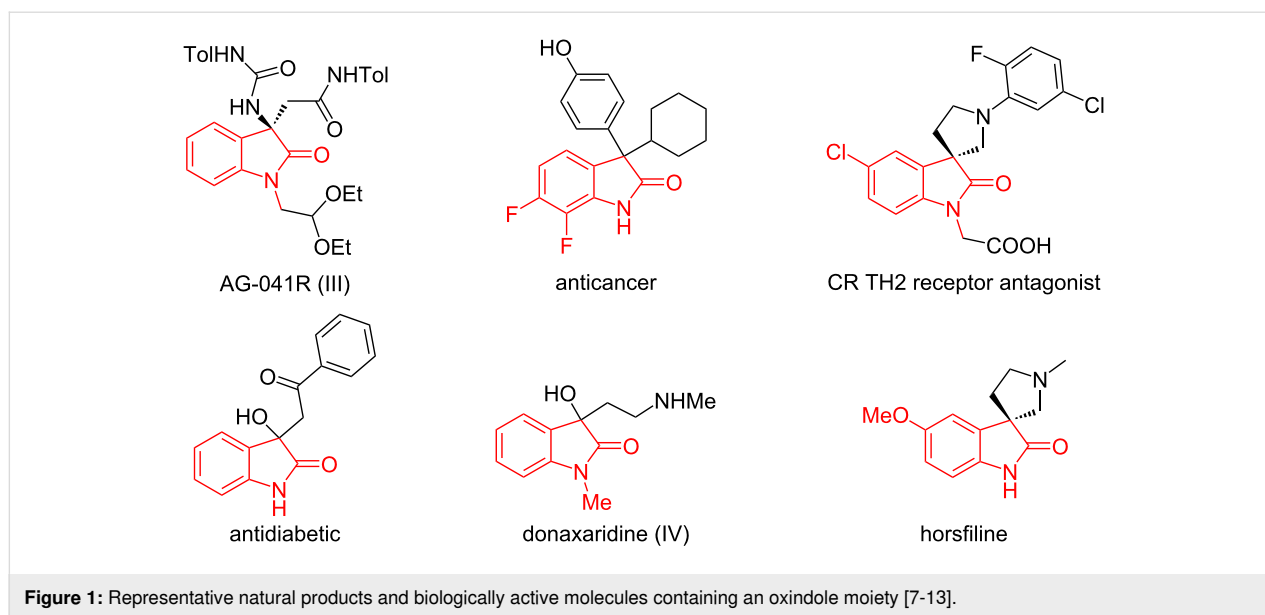
A practical NaI/PPh<sub>3</sub>-catalyzed decarboxylative radical cascade cyclization of *N*-arylacrylamides with redox-active esters is described, which is mediated by visible light irradiation. A wide range of substrates bearing different substituents and derived from ubiquitous carboxylic acids, including  $\alpha$ -amino acids, were synthesized and examined under this very mild, efficient, and cost effective transition-metal-free synthetic method. These afforded various functionalized oxindoles featuring a C3 quaternary stereogenic center. Mechanistic experiments suggest a radical mechanism.

## Introduction

Radical-initiated cascade reactions constitute a powerful synthetic approach to construct multiple C–C or C–X bonds in one pot. As such, these tend to allow facile access to many complex natural molecules and drugs [1–6]. Recently, radical-initiated cascade cyclizations involving acrylamides have attracted considerable attention due to their propensity to build important oxindole scaffolds. These are broadly found in natural products, pharmaceuticals, and bioactive molecules (Figure 1) [7–13]. Although a number of synthetic approaches have already been explored [14–20], these existing methods generally require stoi-

chiometric, often onerous reagents [21–28], and/or high temperatures [29–38].

In the past few years, photocatalytic processes have become one of the most powerful tools in developing radical-initiated addition/cyclization cascades from acrylamides for the synthesis of oxindoles [39–41]. The radicals are typically generated from alkyl halides [42–44], carboxylic acids [45–47], simple alkanes [48], alkylboronic acids [49], isocyanides [50], or other [51–53]. In this context, the group of Fu reported a Ru(bpy)<sub>3</sub>Cl<sub>2</sub>-cata-



lyzed synthesis of *N*-Boc proline oxindole derivatives under visible-light assistance [47]. Therein, *N*-hydroxyphthalimide (NPhth) esters were utilized as alkyl radical precursors, which can be readily prepared from highly available carboxylic acids. In 2015, Cheng and co-workers disclosed a visible light-mediated radical tandem cyclization of *N*-arylacrylamides with *N*-(acyloxy)phthalimides to access 3,3-dialkylated oxindoles in the presence of [Ru(bpy)<sub>3</sub>Cl<sub>2</sub>] $\cdot$ 6H<sub>2</sub>O [46]. However, these seminal methods remain limited by the need of noble-metal-based photocatalysts, excess additives and limited substrate scopes (Scheme 1a).

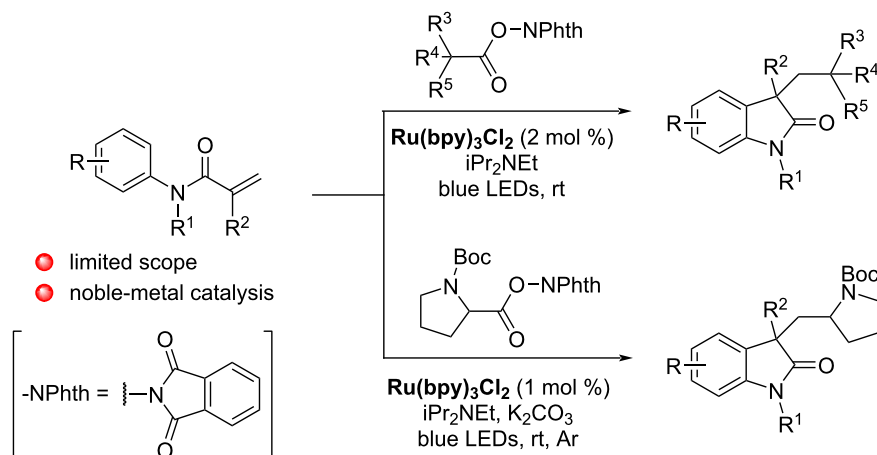
With the rapid development of sustainable chemistry, developing low-cost and transition-metal-free photocatalytic methods has become a strategic priority. In 2019 [54], the groups of Fu and Shang pioneered the photocatalytic decarboxylative alkylation of silyl enol ethers and *N*-heteroarenes by using a novel catalytic system based on sodium iodide (NaI) and triphenylphosphine (PPh<sub>3</sub>), suggested to function as an electron donor–acceptor (EDA) complex [55-60]. Compared to previously reported radical reactions, this novel catalytic system has the key advantage of circumventing the need for external redox additives and/or noble metals, using readily available and cost-effective NaI and PPh<sub>3</sub> under mild reaction conditions. In a broader context, phosphine organocatalysis is probably still underappreciated in organic synthesis, and could lead to important future synthetic developments [61-67]. The NaI/PPh<sub>3</sub> system has been further broadly applied to the functionalization of alkenes [68-70], as well as to decarboxylative C(sp<sup>3</sup>)–X bond formation [71], cyclization of 1,7-enynes [72,73] and other reactions [74-77]. Inspired by these advances, we developed here a visible light-mediated decarboxylative radical cascade

cyclization of *N*-arylacrylamides under NaI/PPh<sub>3</sub> catalysis, for the most efficient and practical synthesis of quaternary oxindoles (Scheme 1b and 1c). It should be noted that during the finalization of this work, a similar, however stoichiometric CsI/PPh<sub>2</sub>Cy-mediated method appeared from the Yang and Li groups (Scheme 1b) [28]. In contrast, the method we present here is 1) catalytic, 2) it employs the far less onerous NaI/PPh<sub>3</sub> system, and 3) it displays a considerably broader substrate scope.

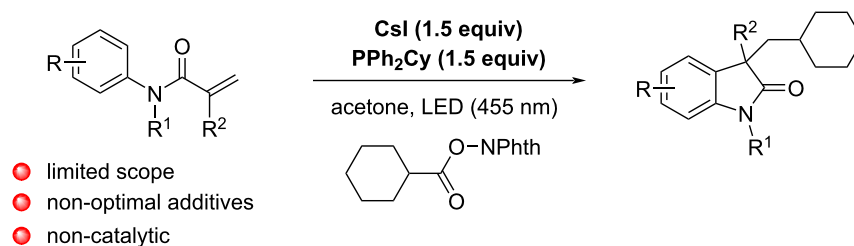
## Results and Discussion

Key elements of reaction optimization are summarized in Table 1. With NaI (20 mol %) and PPh<sub>3</sub> (20 mol %), acrylamide **1a** and redox-active ester **2a** were used as model substrates to react for 36 h in acetonitrile (MeCN) under blue LEDs irradiation and N<sub>2</sub> atmosphere, delivering the desired oxindole derivative **3aa** with 72% isolated yield (Table 1, entry 1). Other iodide sources, such as LiI, KI, RbI, CsI, CaI<sub>2</sub>, and a quaternary ammonium iodide, while also effective, provided slightly lower yields (Table 1, entries 2–7). It should be noted that all tested iodide sources were found soluble under those conditions. Some diverse phosphines were then screened. Aromatic phosphines performed best (Table 1, entries 8 and 9), the cheapest PPh<sub>3</sub> remaining however optimal. In contrast, tricyclohexylphosphine PCy<sub>3</sub> performed poorly (Table 1, entry 10), and bulky tri-*o*-tolylphosphine almost shut down the reaction (Table 1, entry 11). These results indicate that the accessibility of the phosphorus center is important. Next, the solvent was investigated. Replacing acetonitrile with dimethyl sulfoxide (DMSO), or dimethylacetamide (DMA), or acetone, or ethyl acetate (EA), resulted in inferior yields (Table 1, entries 12–15), and no product was detected when using 1,4-dioxane or

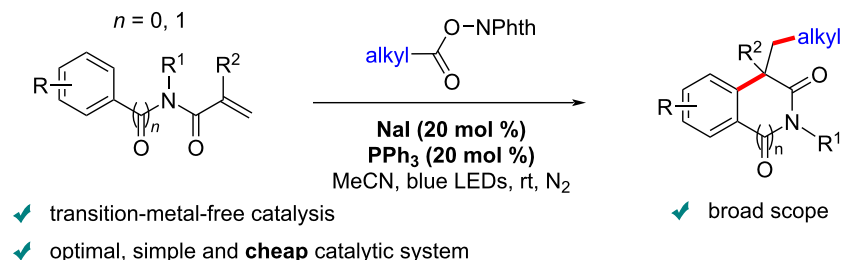
a) previous works: photocatalytic decarboxylative cyclization via transition metal catalysis



b) appeared during the preparation of this work:



c) this work: photocatalytic decarboxylative cyclization via NaI/PPh<sub>3</sub> catalysis



**Scheme 1:** Selected photocatalytic decarboxylative radical cascade reactions of *N*-arylamides.

dichloromethane (DCM) as reaction solvent (Table 1, entries 16 and 17). Although the reaction also proceeded without NaI, only a low yield of **3aa** was then obtained (Table 1, entry 18). PPh<sub>3</sub> and irradiation are however both essential for this decarboxylative cascade cyclization process (Table 1, entries 19 and 20).

With the optimized conditions in hand, we then explored the scope of *N*-arylacrylamides with different substituents. A series of acrylamides showed good compatibility under standard conditions, offering the desired oxindoles in moderate to good yields (Scheme 2). Electron-donating groups at the *para*-posi-

tion of the phenyl ring, such as methyl or methoxy groups, decreased slightly the yield, to 68% and 66%, respectively (**3ba** and **3ca**). When these substituents were replaced by common halogens or electron-withdrawing groups, good yields of the corresponding oxindoles (**3da–ga**) were achieved. A trifluoromethyl-substituted acrylamide afforded the product **3fa** in very high 85% yield. In addition, *ortho*-substitution at the *N*-aryl moiety was also well tolerated, albeit with slightly decreased yields (**3ha–ka**, 50–63%).

Interestingly, a cyclic *N*-arylamide derivative was also well tolerated, furnishing polycyclic structure **3la** in 67% yield. In

Table 1: Optimization table<sup>a</sup>.

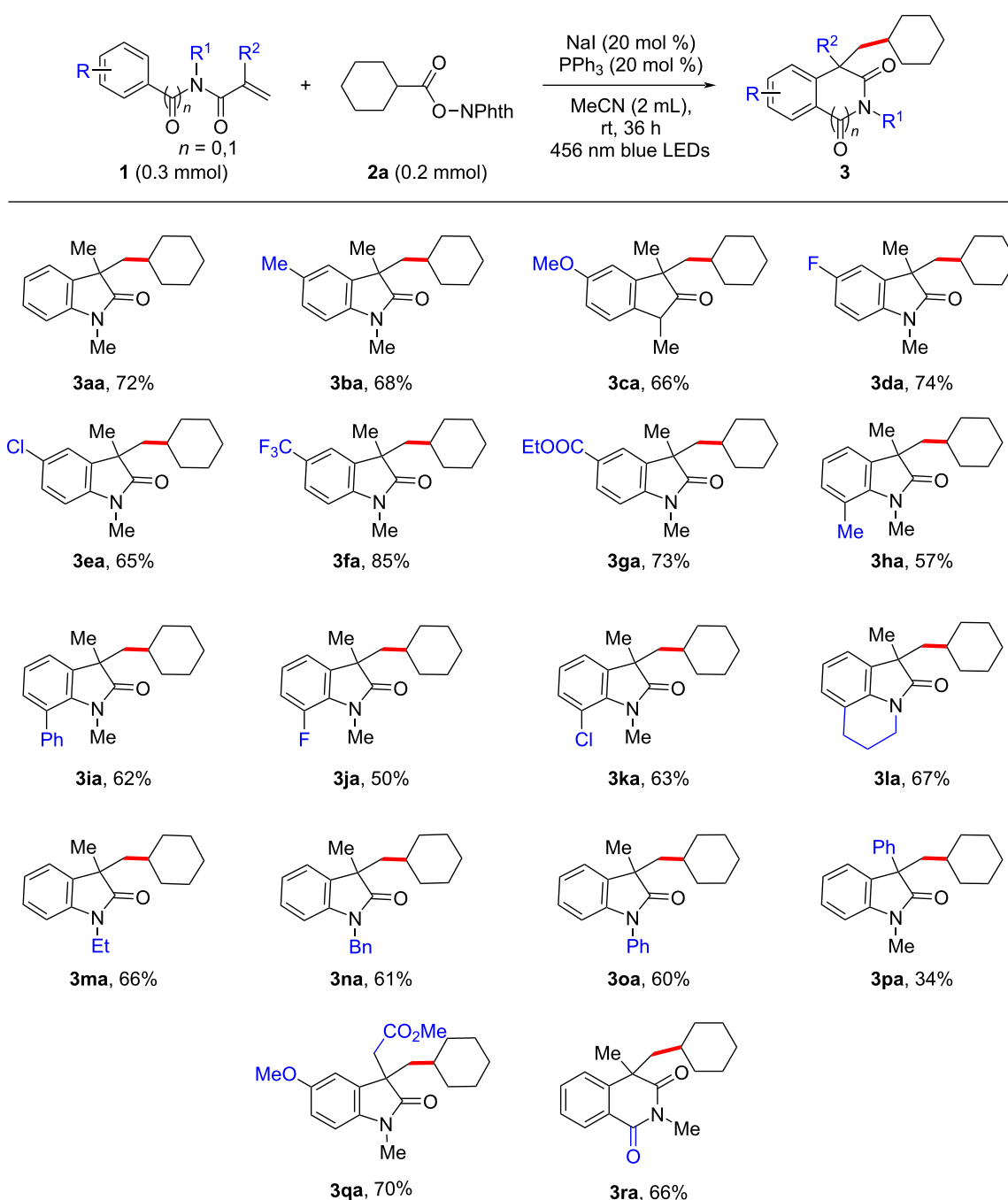
Entry	Variation from standard conditions	<b>3aa</b> , Yield (%) <sup>b</sup>
1	none	76 (72) <sup>c</sup>
2	Lil instead of NaI	70
3	KI instead of NaI	62
4	RbI instead of NaI	64
5	CsI instead of NaI	39
6	CaI <sub>2</sub> instead of NaI	56
7	<i>n</i> -Bu <sub>4</sub> NI instead of NaI	57
8	P(4-F-C <sub>6</sub> H <sub>4</sub> ) <sub>3</sub> instead of PPh <sub>3</sub>	73
9	P(4-OMe-C <sub>6</sub> H <sub>4</sub> ) <sub>3</sub> instead of PPh <sub>3</sub>	60
10	PCy <sub>3</sub> instead of PPh <sub>3</sub>	23
11	P(2-Me-C <sub>6</sub> H <sub>4</sub> ) <sub>3</sub> instead of PPh <sub>3</sub>	trace
12	DMSO instead of MeCN	60
13	DMA instead of MeCN	44
14	acetone instead of MeCN	52
15	EA instead of MeCN	57
16	DCM instead of MeCN	nr
17	1,4-dioxane instead MeCN	nr
18	without NaI	14
19	without PPh <sub>3</sub>	0
20	without blue LED	0

<sup>a</sup>Unless otherwise noted, the standard reaction conditions were as follows: **1a** (0.3 mmol), **2a** (0.2 mmol), solvent (2 mL); <sup>b</sup>the yield was determined by <sup>1</sup>H NMR analysis of the crude reaction mixture using 1,3,5-trimethoxybenzene as an internal standard; <sup>c</sup>isolated yield.

addition, substrates with different *N*-substituents, such as ethyl, benzyl, and phenyl, could be converted into the expected products **3ma–oa** in good yields. It should be noted that replacing the methyl with a phenyl group at the *N*-arylacrylamide core significantly affected the reaction efficiency from 72% to 34% yield (**3pa**). Satisfyingly, substrate **1q** could successfully undergo decarboxylative cascade cyclization to afford **3qa** with 70% yield, which is used as a key intermediate in the synthesis of (±)-physovenine and (±)-physostigmine alkyl analogues exhibiting inhibitory activity against acetylcholinesterase and butyrylcholinesterase [30,78–84]. Subsequently, we expanded the scope of this protocol to include a benzamide derived acrylamide **1r**. The expected six-membered ring structure **3ra** could be successfully isolated with a good yield (66%).

A number of alkyl radical precursors were then synthesized and evaluated in the reaction (Scheme 3). We found that redox-active esters derived from primary, secondary, and tertiary ali-

phatic carboxylic acids were all compatible with the method. Cyclic substrates bearing cyclobutyl, cyclopentyl, and indenyl groups could deliver the corresponding desired products with good yields (**3ab–ad**, 63–74%), while an adamantyl-derived substituent proved more challenging (**3ae**, 40%). The use of other cyclic substituents such as oxygen-containing and nitrogen-containing rings gave good yields of the target oxindoles (**3af–ah**, 65–76%). In addition, a symmetrically  $\alpha$ -substituted redox-active esters furnished the corresponding quaternary oxindole **3ai** with 69% yield. Moreover, an asymmetrically  $\alpha$ -branched starting material could react with similar efficiency, affording oxindole **3aj** as a 1:1.1 mixture of diastereomers. Interestingly, this method also enabled the synthesis of the highly sterically demanding oxindole **3ak** in good yield when using a *tert*-butyl *N*-hydroxyphthalimide ester as the *tert*-butyl radical precursor. Importantly, a redox-active ester derived from methionine could be converted effectively to  $\alpha$ -aminoalkylation product **3al** in overall 70% yield, which thus

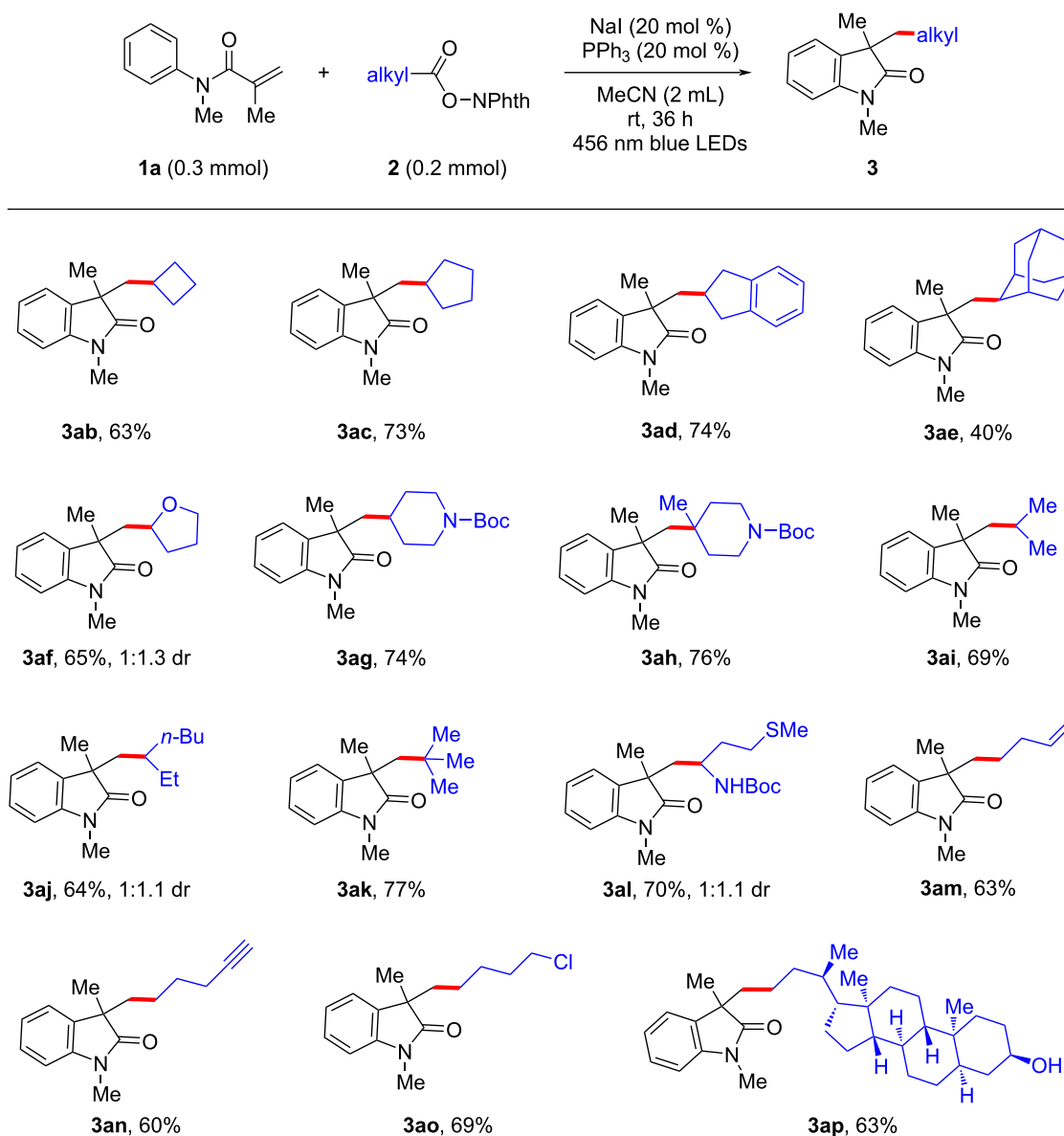


**Scheme 2:** Arylamide substrate scope with isolated yields of products.

provides a mild method for the functionalization and derivation of abundant natural or unnatural amino acids. Some functional groups such as a terminal alkene in **3am**, a terminal alkyne in **3an**, and an alkyl chloride in **3ao** proved compatible, associated with encouraging yields. In order to further demonstrate the utility of our protocol, a complex scaffold derived from litho-

cholic acid was tested, and was found to smoothly undergo the decarboxylative cyclization towards oxindole **3ap** in 63% yield.

In order to gain insight into the reaction mechanism, some control experiments were further performed. When a radical scavenger such as 2,2,6,6-tetramethyl-1-piperidinyloxy



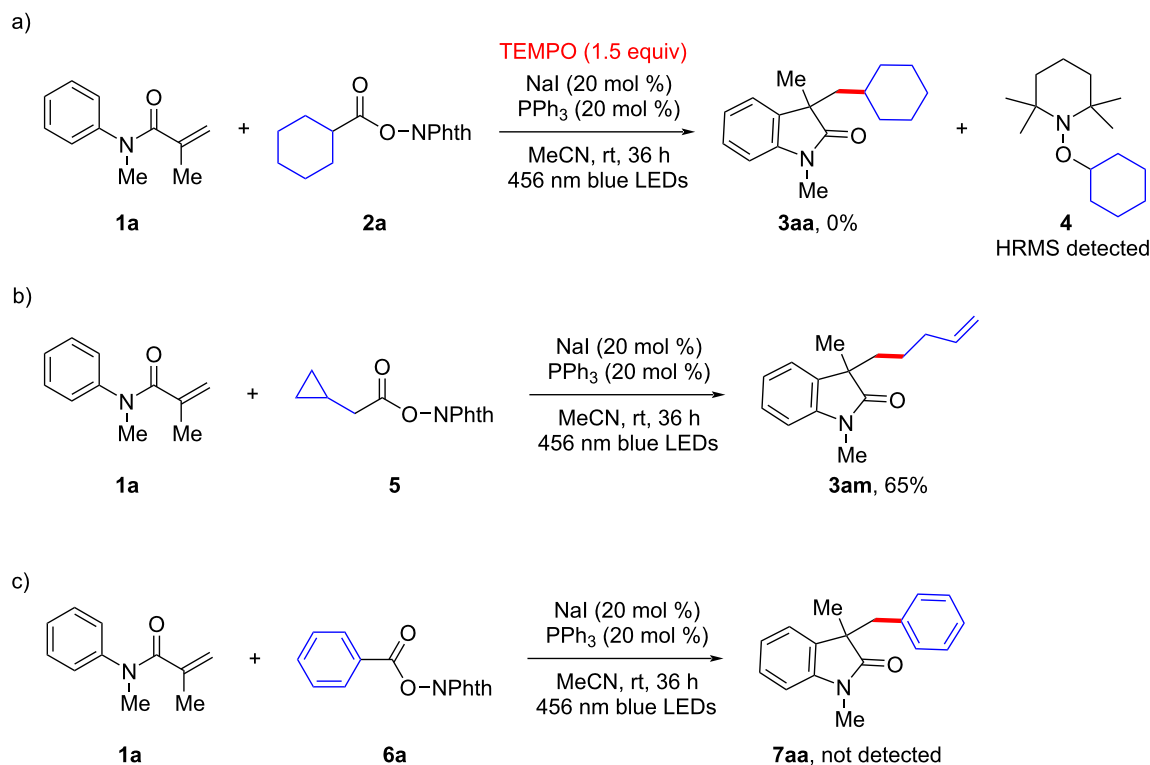
**Scheme 3:** Alkyl radical precursor scope with isolated yields of products.

(TEMPO) was added to the catalytic system under standard conditions, the reaction was fully inhibited, and a TEMPO-trapped adduct (**4**) was detected by HRMS (Scheme 4a). Moreover, the radical-mediated ring-opening product **3am** could be obtained with 66% yield in a radical clock experiment when redox-active ester **5** was engaged to react with acrylamide **1a** under standard conditions (Scheme 4b). Finally, it should be noted that benzoyl ester substrate **6a** did not deliver the corresponding cyclized product **7aa** (Scheme 4c). All of these outcomes indicate that a radical species should be involved in this decarboxylative cascade cyclization towards oxindoles under NaI/PPh<sub>3</sub> catalysis. Thus, the mechanism should run in a

similar fashion to related well-documented previous reports [54,68–77], through a light-induced, phosphine-assisted, intermolecular electron transfer from sodium iodide to the redox-active ester.

## Conclusion

In summary, we developed an effective photocatalytic decarboxylative radical cascade cyclization of *N*-arylacrylamides with various redox-active esters derived from common and/or important carboxylic acids under mild conditions. Complementary to traditional transition metal photocatalysis and organo-photocatalysis [85], the readily available and inexpen-



Scheme 4: Selected mechanistic experiments.

sive NaI/PPh<sub>3</sub> can operate as an efficient photoredox catalyst, providing an economical access to construct important oxindole scaffolds containing a quaternary carbon center. This synthetic method features a broad substrate scope, good functional group tolerance and operational simplicity. Mechanistic investigations revealed that this cyclization reaction proceeds via a cascade radical pathway. We expect these results to encourage the further development of NaI/PPh<sub>3</sub>-catalyzed and related synthetic methods.

## Supporting Information

### Supporting Information File 1

Experimental section and characterization of synthesized compounds.

[<https://www.beilstein-journals.org/bjoc/content/supplementary/1860-5397-19-5-S1.pdf>]

## Funding

ERC project 716136: 2O2ACTIVATION is acknowledged for generous financial support. We are also thankful to the Chinese Scholarship Council (CSC) for financial support to Dan Liu (No. 202106230113), and Yue Zhao (No. 201908320377).

## ORCID® iDs

Dan Liu - <https://orcid.org/0000-0002-8517-1161>

Frederic W. Patureau - <https://orcid.org/0000-0002-4693-7240>

## References

- Molander, G. A.; Harris, C. R. *Chem. Rev.* **1996**, *96*, 307–338. doi:10.1021/cr950019y
- Snider, B. B. *Chem. Rev.* **1996**, *96*, 339–364. doi:10.1021/cr950026m
- Nair, V.; Mathew, J.; Prabhakaran, J. *Chem. Soc. Rev.* **1997**, *26*, 127–132. doi:10.1039/cs9972600127
- McCarroll, A. J.; Walton, J. C. *Angew. Chem., Int. Ed.* **2001**, *40*, 2224–2248. doi:10.1002/1521-3773(20010618)40:12<2224::aid-anie2224>3.0.co;2-f
- Albert, M.; Fensterbank, L.; Lacote, E.; Malacria, M. Tandem Radical Reactions. In *Radicals in Synthesis II*; Gansäuer, A., Ed.; Springer: Berlin, 2006; pp 1–62. doi:10.1007/128\_026
- Wille, U. *Chem. Rev.* **2013**, *113*, 813–853. doi:10.1021/cr100359d
- Ding, K.; Lu, Y.; Nikolovska-Coleska, Z.; Wang, G.; Qiu, S.; Shangary, S.; Gao, W.; Qin, D.; Stuckey, J.; Krajewski, K.; Roller, P. P.; Wang, S. *J. Med. Chem.* **2006**, *49*, 3432–3435. doi:10.1021/jm051122a
- Christensen, M. K.; Erichsen, K. D.; Trojel-Hansen, C.; Tjørnelund, J.; Nielsen, S. J.; Frydenvang, K.; Johansen, T. N.; Nielsen, B.; Sehested, M.; Jensen, P. B.; Ikaunieks, M.; Zaichenko, A.; Loza, E.; Kalvinsh, I.; Björklund, F. *J. Med. Chem.* **2010**, *53*, 7140–7145. doi:10.1021/jm100763j
- Millemaggi, A.; Taylor, R. J. K. *Eur. J. Org. Chem.* **2010**, 4527–4547. doi:10.1002/ejoc.201000643

10. Rudrangi, S. R. S.; Bontha, V. K.; Manda, V. R.; Bethi, S. *Asian J. Res. Chem.* **2011**, *4*, 335.
11. Yu, B.; Yu, D. Q.; Liu, H. M. *Eur. J. Med. Chem.* **2015**, *97*, 763. doi:10.1016/j.ejmech.2014.06.056
12. Kaur, M.; Singh, M.; Chadha, N.; Silakari, O. *Eur. J. Med. Chem.* **2016**, *123*, 858–894. doi:10.1016/j.ejmech.2016.08.011
13. Ye, N.; Chen, H.; Wold, E. A.; Shi, P.-Y.; Zhou, J. *ACS Infect. Dis.* **2016**, *2*, 382–392. doi:10.1021/acsinfecdis.6b00041
14. Klein, J. E. M. N.; Taylor, R. J. K. *Eur. J. Org. Chem.* **2011**, 6821–6841. doi:10.1002/ejoc.201100836
15. Dalpozzo, R.; Bartoli, G.; Bencivenni, G. *Chem. Soc. Rev.* **2012**, *41*, 7247. doi:10.1039/c2cs35100e
16. Mai, W.; Wang, J.; Yang, L.; Yuan, J.; Mao, P.; Xiao, Y.; Qu, L. *Chin. J. Org. Chem.* **2014**, *34*, 1958. doi:10.6023/cjoc201405006
17. Li, C.-C.; Yang, S.-D. *Org. Biomol. Chem.* **2016**, *14*, 4365–4377. doi:10.1039/c6ob00554c
18. Cao, Z.-Y.; Zhou, F.; Zhou, J. *Acc. Chem. Res.* **2018**, *51*, 1443–1454. doi:10.1021/acs.accounts.8b00097
19. Marchese, A. D.; Larin, E. M.; Mirabi, B.; Lautens, M. *Acc. Chem. Res.* **2020**, *53*, 1605–1619. doi:10.1021/acs.accounts.0c00297
20. Boddy, A. J.; Bull, J. A. *Org. Chem. Front.* **2021**, *8*, 1026–1084. doi:10.1039/d0qo01085e
21. Xu, Z.; Yan, C.; Liu, Z.-Q. *Org. Lett.* **2014**, *16*, 5670–5673. doi:10.1021/ol502738a
22. Dai, Q.; Yu, J.; Jiang, Y.; Guo, S.; Yang, H.; Cheng, J. *Chem. Commun.* **2014**, *50*, 3865. doi:10.1039/c4cc01053a
23. Zhou, D.; Li, Z.-H.; Li, J.; Li, S.-H.; Wang, M.-W.; Luo, X.-L.; Ding, G.-L.; Sheng, R.-L.; Fu, M.-J.; Tang, S. *Eur. J. Org. Chem.* **2015**, 1606–1612. doi:10.1002/ejoc.201403499
24. He, Z.-Y.; Guo, J.-Y.; Tian, S.-K. *Adv. Synth. Catal.* **2018**, *360*, 1544–1548. doi:10.1002/adsc.201800012
25. Shi, Y.; Xiao, H.; Xu, X.-H.; Huang, Y. *Org. Biomol. Chem.* **2018**, *16*, 8472–8476. doi:10.1039/c8ob02457j
26. Wang, X.-Y.; Zhong, Y.-F.; Mo, Z.-Y.; Wu, S.-H.; Xu, Y.-L.; Tang, H.-T.; Pan, Y.-M. *Adv. Synth. Catal.* **2021**, *363*, 208–214. doi:10.1002/adsc.202001192
27. Wu, H.; Zhou, M.; Li, W.; Zhang, P. *Catal. Commun.* **2020**, *133*, 105832. doi:10.1016/j.catcom.2019.105832
28. Fan, X.; Liu, H.; Ma, S.; Wang, F.; Yang, J.; Li, D. *Tetrahedron* **2022**, *117–118*, 132849. doi:10.1016/j.tet.2022.132849
29. Fan, J.-H.; Wei, W.-T.; Zhou, M.-B.; Song, R.-J.; Li, J.-H. *Angew. Chem., Int. Ed.* **2014**, *53*, 6650–6654. doi:10.1002/anie.201402893
30. Biswas, P.; Paul, S.; Guin, J. *Angew. Chem., Int. Ed.* **2016**, *55*, 7756–7760. doi:10.1002/anie.201603809
31. Tang, S.; Zhou, D.; Li, Z.-H.; Fu, M.-J.; Jie, L.; Sheng, R.-L.; Li, S.-H. *Synthesis* **2015**, *47*, 1567–1580. doi:10.1055/s-0034-1379902
32. Wang, H.; Guo, L.; Duan, X.-H. *J. Org. Chem.* **2016**, *81*, 860–867. doi:10.1021/acs.joc.5b02433
33. Yang, Z.; Cheng, Y.; Long, J.; Feng, X.; Tang, R.; Wei, J. *New J. Chem.* **2019**, *43*, 18760–18766. doi:10.1039/c9nj04458b
34. Che, F.; Zhong, J.; Yu, L.; Ma, C.; Yu, C.; Wang, M.; Hou, Z.; Zhang, Y. *Adv. Synth. Catal.* **2020**, *362*, 5020–5025. doi:10.1002/adsc.202000600
35. Zhang, L.; Zhou, H.; Bai, S.; Li, S. *Dalton Trans.* **2021**, *50*, 3201–3206. doi:10.1039/d0dt04295a
36. Zhang, L.; Wang, Y.; Yang, Y.; Zhang, P.; Wang, C. *Org. Chem. Front.* **2020**, *7*, 3234–3241. doi:10.1039/d0qo00953a
37. Wang, C.; Liu, L. *Org. Chem. Front.* **2021**, *8*, 1454–1460. doi:10.1039/d0qo01508c
38. Su, L.; Sun, H.; Liu, J.; Wang, C. *Org. Lett.* **2021**, *23*, 4662–4666. doi:10.1021/acs.orglett.1c01400
39. Festa, A. A.; Voskressensky, L. G.; Van der Eycken, E. V. *Chem. Soc. Rev.* **2019**, *48*, 4401–4423. doi:10.1039/c8cs00790j
40. Singh, J.; Sharma, A. *Adv. Synth. Catal.* **2021**, *363*, 4284–4308. doi:10.1002/adsc.202100515
41. Ghosh, S.; Qu, Z.-W.; Pradhan, S.; Ghosh, A.; Grimme, S.; Chatterjee, I. *Angew. Chem., Int. Ed.* **2022**, *61*, 10.1002/anie.202115272. doi:10.1002/anie.202115272
42. An, Y.; Li, Y.; Wu, J. *Org. Chem. Front.* **2016**, *3*, 570. doi:10.1039/c6qo00055j
43. Muralirajan, K.; Kancherla, R.; Gimnkhani, A.; Rueping, M. *Org. Lett.* **2021**, *23*, 6905–6910. doi:10.1021/acs.orglett.1c02467
44. Du, J.; Wang, X.; Wang, H.; Wei, J.; Huang, X.; Song, J.; Zhang, J. *Org. Lett.* **2021**, *23*, 5631–5635. doi:10.1021/acs.orglett.1c01698
45. Xie, J.; Xu, P.; Li, H.; Xue, Q.; Jin, H.; Cheng, Y.; Zhu, C. *Chem. Commun.* **2013**, *49*, 5672. doi:10.1039/c3cc42672f
46. Tang, Q.; Liu, X.; Liu, S.; Xie, H.; Liu, W.; Zeng, J.; Cheng, P. *RSC Adv.* **2015**, *5*, 89009–89014. doi:10.1039/c5ra17292f
47. Jin, Y.; Jiang, M.; Wang, H.; Fu, H. *Sci. Rep.* **2016**, *6*, 20068. doi:10.1038/srep20068
48. Li, Z.; Zhang, Y.; Zhang, L.; Liu, Z.-Q. *Org. Lett.* **2014**, *16*, 382–385. doi:10.1021/ol4032478
49. Li, X.; Han, M.-Y.; Wang, B.; Wang, L.; Wang, M. *Org. Biomol. Chem.* **2019**, *17*, 6612–6619. doi:10.1039/c9ob01023h
50. Zhao, Y.; Li, Z.; Sharma, U. K.; Sharma, N.; Song, G.; Van der Eycken, E. V. *Chem. Commun.* **2016**, *52*, 6395–6398. doi:10.1039/c6cc02024k
51. Xu, P.; Xie, J.; Xue, Q.; Pan, C.; Cheng, Y.; Zhu, C. *Chem. – Eur. J.* **2013**, *19*, 14039–14042. doi:10.1002/chem.201302407
52. Chen, J.-Q.; Wei, Y.-L.; Xu, G.-Q.; Liang, Y.-M.; Xu, P.-F. *Chem. Commun.* **2016**, *52*, 6455–6458. doi:10.1039/c6cc02007k
53. Wang, Y.-Z.; Lin, W.-J.; Zou, J.-Y.; Yu, W.; Liu, X.-Y. *Adv. Synth. Catal.* **2020**, *362*, 3116–3120. doi:10.1002/adsc.202000609
54. Fu, M.-C.; Shang, R.; Zhao, B.; Wang, B.; Fu, Y. *Science* **2019**, *363*, 1429–1434. doi:10.1126/science.aav3200
55. Rosokha, S. V.; Kochi, J. K. *Acc. Chem. Res.* **2008**, *41*, 641–653. doi:10.1021/ar700256a
56. Lima, C. G. S.; de M. Lima, T.; Duarte, M.; Jurberg, I. D.; Paixão, M. W. *ACS Catal.* **2016**, *6*, 1389–1407. doi:10.1021/acscatal.5b02386
57. Yuan, Y.-q.; Majumder, S.; Yang, M.-h.; Guo, S.-r. *Tetrahedron Lett.* **2020**, *61*, 151506. doi:10.1016/j.tetlet.2019.151506
58. Crisenza, G. E. M.; Mazzarella, D.; Melchiorre, P. *J. Am. Chem. Soc.* **2020**, *142*, 5461–5476. doi:10.1021/jacs.0c01416
59. Yang, Z.; Liu, Y.; Cao, K.; Zhang, X.; Jiang, H.; Li, J. *Beilstein J. Org. Chem.* **2021**, *17*, 771–799. doi:10.3762/bjoc.17.67
60. Sumida, Y.; Ohmiya, H. *Chem. Soc. Rev.* **2021**, *50*, 6320–6332. doi:10.1039/d1cs00262g
61. Denmark, S. E.; Beutner, G. L. *Angew. Chem., Int. Ed.* **2008**, *47*, 1560–1638. doi:10.1002/anie.200604943
62. Ye, L.-W.; Zhou, J.; Tang, Y. *Chem. Soc. Rev.* **2008**, *37*, 1140. doi:10.1039/b717758e
63. Guo, H.; Fan, Y. C.; Sun, Z.; Wu, Y.; Kwon, O. *Chem. Rev.* **2018**, *118*, 10049–10293. doi:10.1021/acs.chemrev.8b00081
64. Huang, Y.; Liao, J.; Wang, W.; Liu, H.; Guo, H. *Chem. Commun.* **2020**, *56*, 15235–15281. doi:10.1039/d0cc05699e
65. Xie, C.; Smaligo, A. J.; Song, X.-R.; Kwon, O. *ACS Cent. Sci.* **2021**, *7*, 536–558. doi:10.1021/acscentsci.0c01493
66. Khong, S.; Venkatesh, T.; Kwon, O. *Asian J. Org. Chem.* **2021**, *10*, 2699–2708. doi:10.1002/ajoc.202100496



67. Wang, X.; Yu, C.; Atodiressei, I. L.; Patureau, F. W. *Org. Lett.* **2022**, *24*, 1127–1131. doi:10.1021/acs.orglett.1c04045
68. Wang, Y.-T.; Fu, M.-C.; Zhao, B.; Shang, R.; Fu, Y. *Chem. Commun.* **2020**, *56*, 2495–2498. doi:10.1039/c9cc09654j
69. Wang, H.-Y.; Zhong, L.-J.; Lv, G.-F.; Li, Y.; Li, J.-H. *Org. Biomol. Chem.* **2020**, *18*, 5589–5593. doi:10.1039/d0ob01242d
70. Wang, J.-X.; Wang, Y.-T.; Zhang, H.; Fu, M.-C. *Org. Chem. Front.* **2021**, *8*, 4466–4472. doi:10.1039/d1qo00660f
71. Chen, K.-Q.; Wang, Z.-X.; Chen, X.-Y. *Org. Lett.* **2020**, *22*, 8059–8064. doi:10.1021/acs.orglett.0c03006
72. Liu, H.-Y.; Lu, Y.; Li, Y.; Li, J.-H. *Org. Lett.* **2020**, *22*, 8819–8823. doi:10.1021/acs.orglett.0c03182
73. Liu, X.-J.; Zhou, S.-Y.; Xiao, Y.; Sun, Q.; Lu, X.; Li, Y.; Li, J.-H. *Org. Lett.* **2021**, *23*, 7839–7844. doi:10.1021/acs.orglett.1c02858
74. Wadekar, K.; Aswale, S.; Yatham, V. R. *RSC Adv.* **2020**, *10*, 16510–16514. doi:10.1039/d0ra03211e
75. Hou, T.; Peng, H.; Xin, Y.; Wang, S.; Zhu, W.; Chen, L.; Yao, Y.; Zhang, W.; Liang, S.; Wang, L. *ACS Catal.* **2020**, *10*, 5502–5510. doi:10.1021/acscatal.0c00920
76. Qu, Z.; Chen, X.; Zhong, S.; Deng, G.-J.; Huang, H. *Org. Lett.* **2021**, *23*, 5349–5353. doi:10.1021/acs.orglett.1c01654
77. Zhang, W.-K.; Li, J.-Z.; Zhang, C.-C.; Zhang, J.; Zheng, Y.-N.; Hu, Y.; Li, T.; Wei, W.-T. *Eur. J. Org. Chem.* **2022**, e202200523. doi:10.1002/ejoc.202200523
78. Takano, S.; Moriya, M.; Ogasawara, K. *J. Org. Chem.* **1991**, *56*, 5982–5984. doi:10.1021/jo00021a006
79. Greig, N. H.; Pei, X.-F.; Soncrant, T. T.; Ingram, D. K.; Brossi, A. *Med. Res. Rev.* **1995**, *15*, 3–31. doi:10.1002/med.2610150103
80. Yu, Q.-s.; Pei, X.-F.; Holloway, H. W.; Greig, N. H.; Brossi, A. *J. Med. Chem.* **1997**, *40*, 2895–2901. doi:10.1021/jm970210v
81. Nigel, H. G.; Kumar, S.; Qiansheng, Y.; Arnold, B.; Gosse, B. B.; Debomoy, K. L. *Curr. Alzheimer Res.* **2005**, *2*, 281. doi:10.2174/1567205054367829
82. Shafferman, A.; Barak, D.; Stein, D.; Kronman, C.; Velan, B.; Greig, N. H.; Ordentlich, A. *Chem.-Biol. Interact.* **2008**, *175*, 166–172. doi:10.1016/j.cbi.2008.03.013
83. Becker, R. E.; Greig, N. H. *Curr. Alzheimer Res.* **2010**, *7*, 642–651. doi:10.2174/156720510793499075
84. Suzuki, T.; Choi, J.-H.; Kawaguchi, T.; Yamashita, K.; Morita, A.; Hirai, H.; Nagai, K.; Hirose, T.; Ōmura, S.; Sunazuka, T.; Kawagishi, H. *Bioorg. Med. Chem. Lett.* **2012**, *22*, 4246–4248. doi:10.1016/j.bmcl.2012.05.021
85. Sun, Z.; Huang, H.; Wang, Q.; Huang, C.; Mao, G.; Deng, G.-J. *Org. Chem. Front.* **2022**, *9*, 3506–3514. doi:10.1039/d2qo00319h

## License and Terms

This is an open access article licensed under the terms of the Beilstein-Institut Open Access License Agreement (<https://www.beilstein-journals.org/bjoc/terms>), which is identical to the Creative Commons Attribution 4.0 International License (<https://creativecommons.org/licenses/by/4.0>). The reuse of material under this license requires that the author(s), source and license are credited. Third-party material in this article could be subject to other licenses (typically indicated in the credit line), and in this case, users are required to obtain permission from the license holder to reuse the material.

The definitive version of this article is the electronic one which can be found at:  
<https://doi.org/10.3762/bjoc.19.5>



# Practical synthesis of isocoumarins via Rh(III)-catalyzed C–H activation/annulation cascade

Qian-Ci Gao<sup>1</sup>, Yi-Fei Li<sup>1</sup>, Jun Xuan<sup>\*2</sup> and Xiao-Qiang Hu<sup>\*1</sup>

## Letter

Open Access

### Address:

<sup>1</sup>Key Laboratory of Catalysis and Energy Materials Chemistry of Ministry of Education & Hubei Key Laboratory of Catalysis and Materials Science, School of Chemistry and Materials Science, South-Central Minzu University, Wuhan 430074, People's Republic of China and <sup>2</sup>Anhui Province Key Laboratory of Chemistry for Inorganic/Organic Hybrid Functionalized Materials, College of Chemistry & Chemical Engineering, Anhui University, Hefei, Anhui 230601, People's Republic of China

### Email:

Jun Xuan<sup>\*</sup> - xuanjun@ahu.edu.cn; Xiao-Qiang Hu<sup>\*</sup> - hxq071303127@126.com

<sup>\*</sup> Corresponding author

### Keywords:

C–H activation; enaminone; iodonium ylide; isocoumarin; rhodium catalysis

*Beilstein J. Org. Chem.* **2023**, *19*, 100–106.

<https://doi.org/10.3762/bjoc.19.10>

Received: 11 November 2022

Accepted: 16 January 2023

Published: 30 January 2023

This article is part of the thematic issue "C–H bond functionalization: recent discoveries and future directions".

Guest Editor: I. Chatterjee

© 2023 Gao et al.; licensee Beilstein-Institut.

License and terms: see end of document.

## Abstract

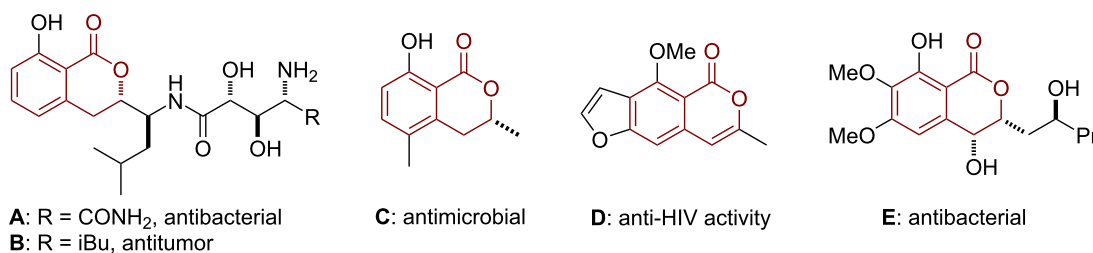
Herein, we report an unprecedented Rh(III)-catalyzed C–H activation/annulation cascade of readily available enaminones with iodonium ylides towards the convenient synthesis of isocoumarins. This coupling system proceeds in useful chemical yields (up to 93%) via a cascade C–H activation, Rh-carbenoid migratory insertion and acid-promoted intramolecular annulation. The success of gram-scale reaction and diverse functionalization of isocoumarins demonstrated the synthetic utility of this protocol.

## Introduction

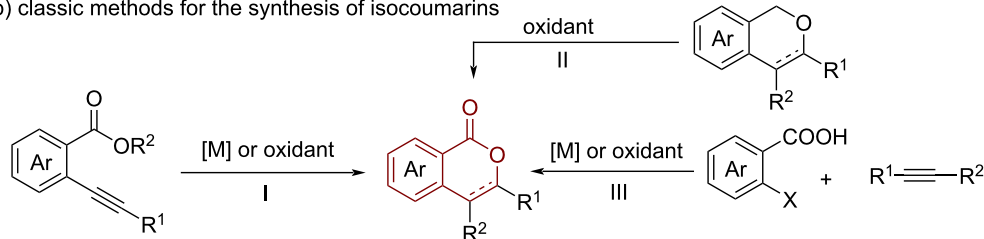
Isocoumarins are an important structural motif in many naturally occurring lactones isolated from bacterial strains, molds, and plants, exhibiting a wide range of pharmacological properties such as antibacterial, antitumor, and anti-HIV activities (Scheme 1a) [1–5]. Fascinated by their versatile properties, researchers were prompted to develop efficient methods for the synthesis of isocoumarin scaffolds. Traditional synthetic strategies including 1) intramolecular cyclization of 2-alkenyl

benzoic acids or *o*-alkynylbenzoates (Scheme 1b, I) [6–10], 2) oxidation of isochromans (Scheme 1b, II) [11,12], or 3) metal-catalyzed cross-coupling/cyclization of 1,2-difunctionalized arenes with alkynes or carbon monoxide (Scheme 1b, III) [13–16], have been widely applied for the assembly of isocoumarins over the past decades. Recently, the transition-metal-catalyzed ortho C–H activation/annulation of benzoic acids has emerged as an attractive approach towards

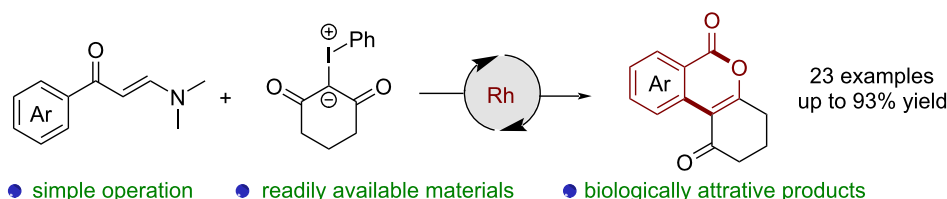
## a) representative examples of bioactive isocoumarins



## b) classic methods for the synthesis of isocoumarins



## c) this work: Rh(III)-catalyzed C–H activation/annulation cascade



**Scheme 1:** Significance of isocoumarins (a), classic methods for the synthesis of isocoumarins (b) and reaction design (c).

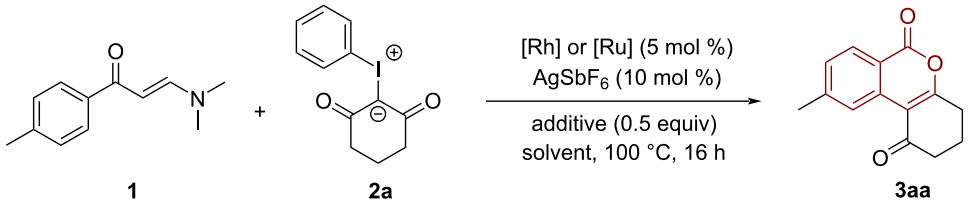
isocoumarins [17,18]. Pioneering examples relying on the Pd, Ru, and Ir-catalyzed C–H cross coupling of benzoic acids with alkenes and alkynes were realized by the groups of Miura [19], Lee [20], Ackermann [21], Zhang [22], Jiang [23], and Jegannathan [24] et al. Despite these impressive achievements, established methods often require the use of stoichiometric oxidants or harsh conditions, thus limiting their broad applicability. Consequently, it is still highly desirable to exploit innovative and convenient methods for the rapid construction of isocoumarins.

Enaminones are bench stable and easily available, which have been established as versatile synthetic building blocks for the synthesis of cyclic scaffolds [25]. In 2016, Zhu et al. reported the first example of a Rh-catalyzed C–H functionalization of enaminones with alkynes and  $\alpha$ -diazo- $\beta$ -ketoesters to access naphthalenes [26]. Very recently, the same group developed an efficient Rh(III)-catalyzed C–H cross-coupling of enaminones with diazodicarbonyls for the divergent construction of isocoumarins and naphthalenes [27]. Moreover, Loh et al. disclosed a Rh-catalyzed formal [4 + 2] cycloaddition of enaminones with diazocarbonyls [28]. Compared with highly sensitive diazo compounds, iodonium ylides are known to show

ready availability and good stability [29,30]. Our group has recently demonstrated that iodonium ylides can be used as carbene precursors in the Rh-catalyzed [4 + 2] cyclization of pyrazolidinones [31]. During the preparation of manuscript, the group of Li reported a similar Rh(III)-catalyzed [3 + 3] annulation of enaminones with iodonium ylides [32]. Inspired by the collected contributions [26–28] and based on our ongoing research in C–H activation [33–35], we recently wondered whether it might be possible to couple iodonium ylides with enaminones in a Rh(III)-catalyzed C–H activation/annulation cascade reaction for the rapid construction of isocoumarins (Scheme 1c).

## Results and Discussion

Our initial experiment was performed with enaminone **1a** and iodonium ylide **1b** in the presence of [Cp\*RhCl<sub>2</sub>]<sub>2</sub> (5 mol %) as the catalyst, AgSbF<sub>6</sub> (10 mol %) and KOAc (50 mol %) as additives in 1,2-dichloroethane (DCE) at 100 °C for 16 hours. To our delight, the desired isocoumarin **3aa** was obtained in 42% yield (Table 1, entry 1). Then, the influence of solvents has been subsequently investigated. As a result, DCE proved to be the optimal solvent, while other commonly used solvents such as toluene, dioxane, and ethanol gave inferior yields (Table 1,

**Table 1:** Optimization of the reaction conditions<sup>a</sup>.


entry	catalyst	additive	solvent	yield <sup>b</sup>
1	[Cp*RhCl <sub>2</sub> ] <sub>2</sub>	KOAc	DCE	42
2	[Cp*RhCl <sub>2</sub> ] <sub>2</sub>	KOAc	toluene	39
3	[Cp*RhCl <sub>2</sub> ] <sub>2</sub>	KOAc	dioxane	16
4	[Cp*RhCl <sub>2</sub> ] <sub>2</sub>	KOAc	EtOH	14
5	[Cp*RhCl <sub>2</sub> ] <sub>2</sub>	Cs(OPiv) <sub>2</sub>	DCE	47
6	[Cp*RhCl <sub>2</sub> ] <sub>2</sub>	Cs(OAc) <sub>2</sub>	DCE	51
7	[Cp*RhCl <sub>2</sub> ] <sub>2</sub>	K <sub>2</sub> CO <sub>3</sub>	DCE	27
8	[Cp*RhCl <sub>2</sub> ] <sub>2</sub>	AcOH	DCE	63
9 <sup>c</sup>	[Cp*RhCl <sub>2</sub> ] <sub>2</sub>	AcOH	DCE	80
10	[[Ru( <i>p</i> -cymene)Cl <sub>2</sub> ] <sub>2</sub> ]	AcOH	DCE	trace

<sup>a</sup>Standard conditions: **1a** (0.2 mmol), **2a** (0.6 mmol), catalyst (5 mol %), AgSbF<sub>6</sub> (10 mol %), additive (0.5 equiv), solvent (2.0 mL) at 100 °C for 16 h.<sup>b</sup>Isolated yields. <sup>c</sup>AcOH (5.0 equiv) was used.

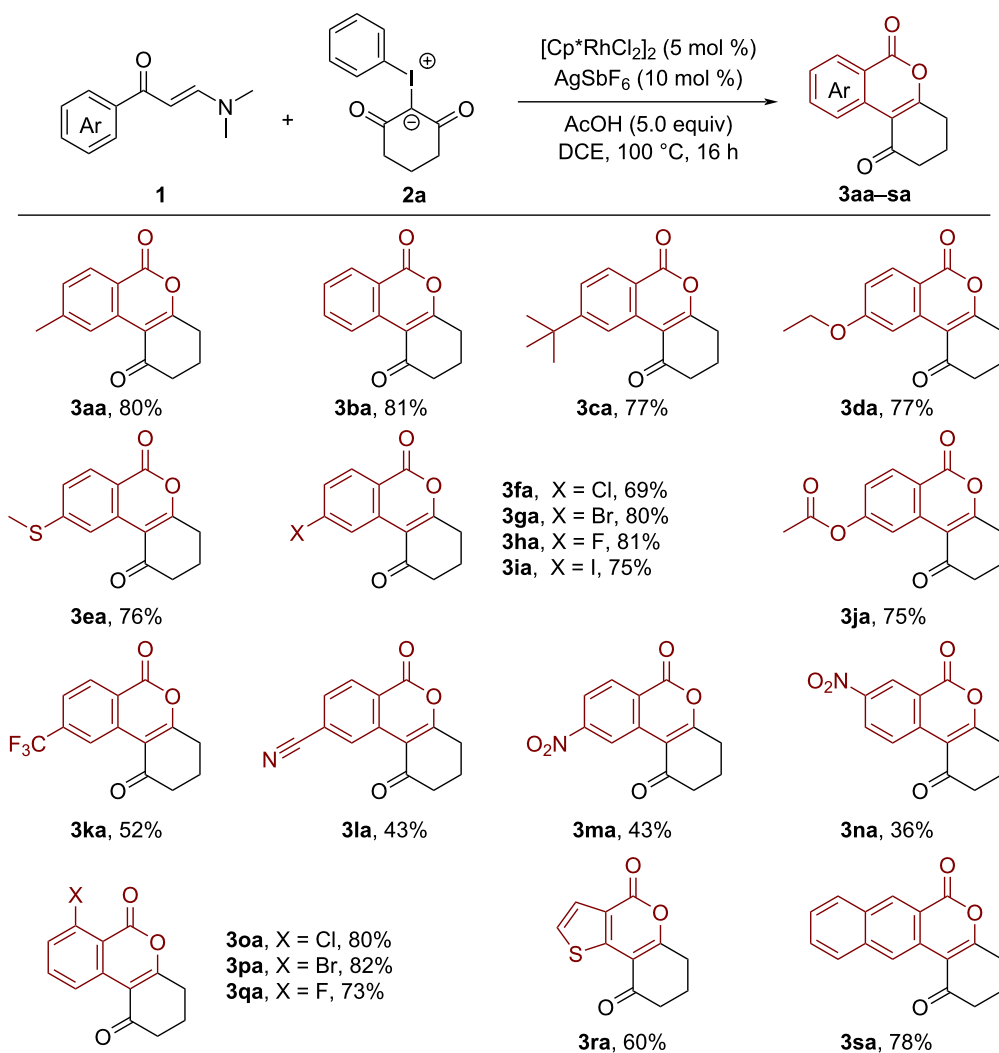
entries 2–4, 14–39%). Further screening of bases did not improve the outcome of the product, whereas 63% yield of **3aa** was obtained when acetic acid was added into the reaction system (Table 1, entry 8). Increasing the amount of acetic acid significantly improved the reaction efficiency delivering product **3aa** in 80% yield (Table 1, entry 9). The choice of a suitable catalyst was the key factor for the success of this reaction since only a trace amount of **3aa** can be obtained by using [[Ru(*p*-cymene)Cl<sub>2</sub>]<sub>2</sub>] as a catalyst (Table 1, entry 10).

With the optimal conditions in hand, we then investigated the scope of this Rh-catalyzed C–H activation/annulation cascade reaction. As shown in Scheme 2, a range of functionalized enaminones were compatible with this Rh-catalytic system, furnishing the corresponding isocoumarin products in satisfying yields. For example, enaminones bearing electron-donating (Me, OEt and *t*-Bu), as well as electron-withdrawing groups (F, Cl, Br, I, CF<sub>3</sub>, CN and NO<sub>2</sub>) at *ortho*, *meta* or *para*-positions were well tolerated in this transformation, delivering a variety of structurally diverse isocoumarins in an efficient manner (**3aa–qa**, 43–82%). It is worth mentioning that the tolerance of halogen substituents (Cl, Br and I) may open up a new opportunity for further transition-metal-catalyzed cross-coupling reactions. Sensitive groups, such as ester, trifluoromethyl and nitro substituents, were retained unchanged in the final products (**3ja**, **3ka**, **3ma**, and **3na**). Also the strongly coor-

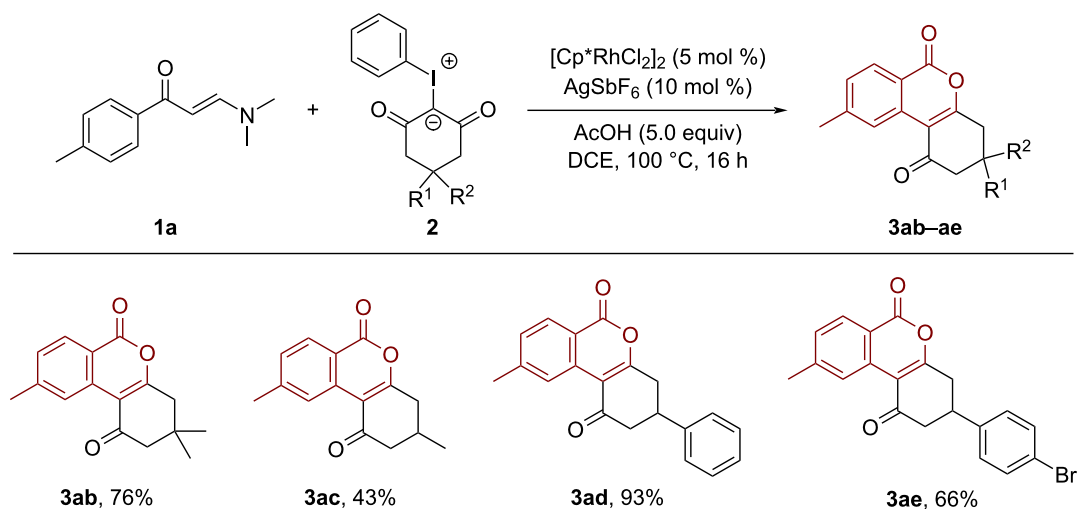
inating thioether substituent proved to be suitable for this protocol, providing the desired product **3ea** in 76% yield. Moreover, under the standard conditions, 3-thienyl and 2-naphthyl-substituted enaminones were smoothly coupled with iodonium ylide **1b** to give the expected isocoumarins **3ra** and **3sa** in 60% and 78%, respectively.

Next, we sought to test the generality of this reaction with respect to iodonium ylides. As outlined in Scheme 3, iodonium ylides featuring dimethyl, methyl, and phenyl groups underwent the current reaction efficiently, delivering the desired products **3ab–ae** in moderate to good yields (43–93%).

To demonstrate the synthetic utility of this methodology, a gram-scale synthesis of isocoumarin **3ia** was firstly performed. Under the optimal conditions, the desired product **3ia** was successfully obtained in 84% yield (1.1 g) via a simple recrystallization from the reaction mixture (Scheme 4a). In the presence of hydroxylamine hydrochloride, the carbonyl group of the ketone can be selectively converted into an oxime product **4** (Scheme 4b, 71% yield). In addition, the reaction of the isocoumarin **3ia** with *p*-toluenesulfonyl hydrazide proceeded smoothly to deliver hydrazone **5** in 66% yield (Scheme 4b, right). Of note, oxime and hydrazone compounds are versatile synthetic building blocks, which have been widely applied in transition-metal-catalyzed cross-coupling reactions and radical transformations [36–38].

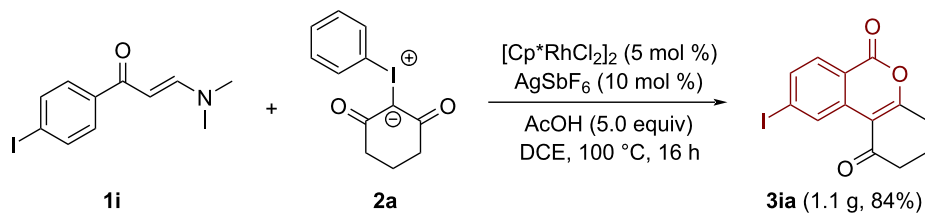
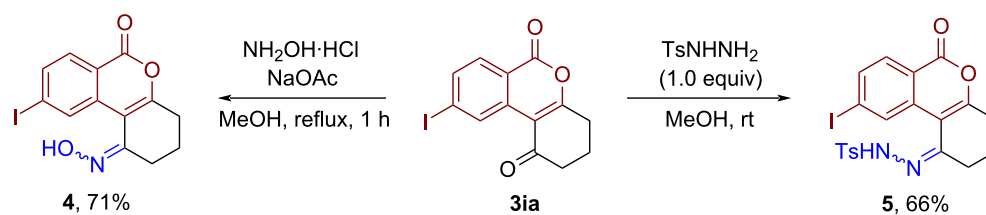


Scheme 2: Scope of enaminones.



Scheme 3: Scope of iodonium ylides.

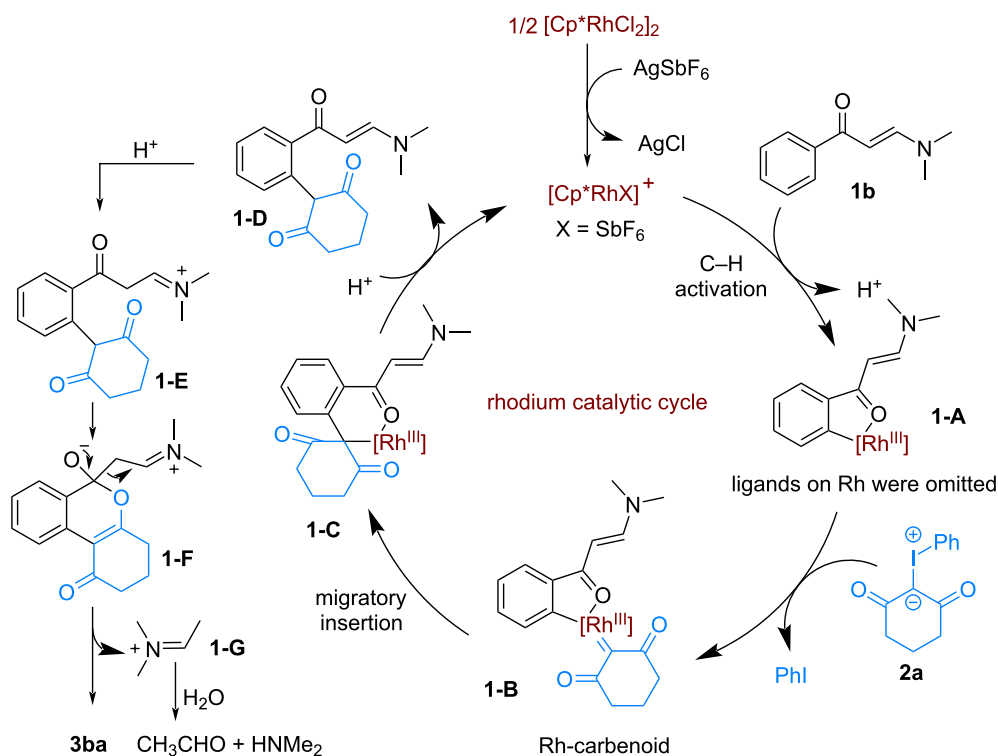
## a) gram-scale reaction

b) synthetic transformation of **3ia**

Scheme 4: Gram-scale reaction (a) and synthetic transformation (b).

Based on the literature precedents [27] and our previous work [33–35], a mechanism for this Rh-catalyzed C–H activation/annulation reaction was proposed and depicted in Scheme 5. In

the presence of  $\text{AgSbF}_6$ , dimeric  $[\text{Cp}^*\text{RhCl}_2]_2$  transforms into the active Rh catalyst. Subsequently, the oxygen atom of the enaminone is coordinated to the Rh catalyst, following by a



Scheme 5: Proposed mechanism.

Rh(III)-promoted ortho C–H activation to form a five-membered ruthenacycle **1-A**. Then, the reaction of the iodonium ylide with intermediate **1-A** generates a Rh-carbenoid intermediate **1-B**, which undergoes a rapid migratory insertion to give intermediate **1-C**. The protonation of **1-C** produces the intermediate **1-D** with the regeneration of the active Rh catalyst for the next catalytic cycle. Under acidic conditions, the further protonation of compound **1-D** delivers an imine intermediate **1-E**, which undergoes an intramolecular annulation to give **1-F**. The final isocoumarin product **3ba** can be generated from **1-F** by elimination of imine **1-G** [39]. Finally, the rapid hydrolysis of the resulting **1-G** gives rise to acetaldehyde and dimethylamine as byproducts.

## Conclusion

In summary, an efficient Rh-catalyzed C–H activation/annulation reaction of enamines with iodonium ylides has been developed. This reaction features simple operation and readily available substrates, enabling the rapid construction of biologically attractive isocoumarins in useful to good yields. The success of a gram-scale reaction and diverse functionalization of the isocoumarin products highlight the tremendous synthetic potential of this methodology in chemical synthesis and drug discovery.

## Experimental

A 10 mL screw-cap vial was charged with enaminone **1** (0.2 mmol), iodonium ylide **2** (0.6 mmol), [Cp\*RhCl<sub>2</sub>]<sub>2</sub> (6.2 mg, 5 mol %), AgSbF<sub>6</sub> (6.9 mg, 10 mol %), HOAc (60.0 mg, 1.0 mmol) and DCE (2 mL) under N<sub>2</sub> atmosphere. Then, the reaction mixture was stirred at 100 °C for 16 h. The crude product was purified by flash chromatography on silica gel (petroleum ether/ethyl acetate 5:1) directly to give the desired products **3**. (Note: a heating module was used for the preparation of isocoumarin products **3**.)

## Supporting Information

### Supporting Information File 1

Experimental and copies of spectra.

[<https://www.beilstein-journals.org/bjoc/content/supplementary/1860-5397-19-10-S1.pdf>]

## Funding

We are grateful to the National Natural Science Foundation of China (No. 21901258, 22271314, 21971001 and 21702001), the Foundation of South-Central MinZu University (YZZ19003), Hubei Provincial Natural Science Foundation, China (2021CFA022) for support of this research.

## ORCID® iDs

Jun Xuan - <https://orcid.org/0000-0003-0578-9330>

Xiao-Qiang Hu - <https://orcid.org/0000-0001-9094-2357>

## References

- Barry, R. D. *Chem. Rev.* **1964**, *64*, 229–260. doi:10.1021/cr60229a002
- Tianpanich, K.; Prachya, S.; Wiyakrutta, S.; Mahidol, C.; Ruchirawat, S.; Kittakoo, P. *J. Nat. Prod.* **2011**, *74*, 79–81. doi:10.1021/np1003752
- Chaudhary, N. K.; Pitt, J. I.; Lacey, E.; Crombie, A.; Vuong, D.; Piggott, A. M.; Karuso, P. *J. Nat. Prod.* **2018**, *81*, 1517–1526. doi:10.1021/acs.jnatprod.7b00816
- Bai, M.; Zheng, C.-J.; Huang, G.-L.; Mei, R.-Q.; Wang, B.; Luo, Y.-P.; Zheng, C.; Niu, Z.-G.; Chen, G.-Y. *J. Nat. Prod.* **2019**, *82*, 1155–1164. doi:10.1021/acs.jnatprod.8b00866
- Cai, R.; Wu, Y.; Chen, S.; Cui, H.; Liu, Z.; Li, C.; She, Z. *J. Nat. Prod.* **2018**, *81*, 1376–1383. doi:10.1021/acs.jnatprod.7b01018
- Yao, T.; Larock, R. C. *J. Org. Chem.* **2003**, *68*, 5936–5942. doi:10.1021/jo034308v
- Mallampudi, N. A.; Reddy, G. S.; Maity, S.; Mohapatra, D. K. *Org. Lett.* **2017**, *19*, 2074–2077. doi:10.1021/acs.orglett.7b00673
- Chen, B.; Ma, S. *Org. Lett.* **2013**, *15*, 3884–3887. doi:10.1021/ol401625t
- Faizi, D. J.; Issaian, A.; Davis, A. J.; Blum, S. A. *J. Am. Chem. Soc.* **2016**, *138*, 2126–2129. doi:10.1021/jacs.5b12989
- Xing, L.; Zhang, Y.; Li, B.; Du, Y. *Org. Lett.* **2019**, *21*, 1989–1993. doi:10.1021/acs.orglett.9b00047
- Finney, L. C.; Mitchell, L. J.; Moody, C. J. *Green Chem.* **2018**, *20*, 2242–2249. doi:10.1039/c7gc03741d
- Xia, Q.; Wang, Q.; Yan, C.; Dong, J.; Song, H.; Li, L.; Liu, Y.; Wang, Q.; Liu, X.; Song, H. *Chem. – Eur. J.* **2017**, *23*, 10871–10877. doi:10.1002/chem.201701755
- Bera, S.; Mondal, P.; Sarkar, D.; Pathi, V. B.; Pakrashy, S.; Datta, A.; Banerji, B. *J. Org. Chem.* **2021**, *86*, 7069–7077. doi:10.1021/acs.joc.1c00311
- Pati, B. V.; Banjare, S. K.; Das Adhikari, G. K.; Nanda, T.; Ravikumar, P. C. *Org. Lett.* **2022**, *24*, 5651–5656. doi:10.1021/acs.orglett.2c01901
- Li, Y.; Wang, Q.; Yang, X.; Xie, F.; Li, X. *Org. Lett.* **2017**, *19*, 3410–3413. doi:10.1021/acs.orglett.7b01365
- Subramanian, V.; Batchu, V. R.; Barange, D.; Pal, M. *J. Org. Chem.* **2005**, *70*, 4778–4783. doi:10.1021/jo050440e
- Luo, F. *Chin. J. Org. Chem.* **2019**, *39*, 3084. doi:10.6023/cjoc201905027
- Pichette Drapeau, M.; Gooßen, L. J. *Chem. – Eur. J.* **2016**, *22*, 18654–18677. doi:10.1002/chem.201603263
- Miura, M.; Tsuda, T.; Satoh, T.; Pivsa-Art, S.; Nomura, M. *J. Org. Chem.* **1998**, *63*, 5211–5215. doi:10.1021/jo980584b
- Nandi, D.; Ghosh, D.; Chen, S.-J.; Kuo, B.-C.; Wang, N. M.; Lee, H. M. *J. Org. Chem.* **2013**, *78*, 3445–3451. doi:10.1021/jo400174w
- Warratz, S.; Kornhaas, C.; Cajaraville, A.; Niepötter, B.; Stalke, D.; Ackermann, L. *Angew. Chem., Int. Ed.* **2015**, *54*, 5513–5517. doi:10.1002/anie.201500600
- Hong, C.; Yu, S.; Liu, Z.; Zhang, Y. *Org. Lett.* **2022**, *24*, 815–820. doi:10.1021/acs.orglett.1c03992
- Jiang, G.; Li, J.; Zhu, C.; Wu, W.; Jiang, H. *Org. Lett.* **2017**, *19*, 4440–4443. doi:10.1021/acs.orglett.7b01919
- Chinnagolla, R. K.; Jeganmohan, M. *Chem. Commun.* **2012**, *48*, 2030–2032. doi:10.1039/c2cc16916a

25. Chen, X. Y.; Zhang, X.; Wan, J.-P. *Org. Biomol. Chem.* **2022**, *20*, 2356–2369. doi:10.1039/d2ob00126h
26. Zhou, S.; Wang, J.; Wang, L.; Song, C.; Chen, K.; Zhu, J. *Angew. Chem., Int. Ed.* **2016**, *55*, 9384–9388. doi:10.1002/anie.201603943
27. Wu, W.; Wu, X.; Fan, S.; Zhu, J. *Org. Lett.* **2022**, *24*, 7850–7855. doi:10.1021/acs.orglett.2c03288
28. Zhou, S.; Yan, B.-W.; Fan, S.-X.; Tian, J.-S.; Loh, T.-P. *Org. Lett.* **2018**, *20*, 3975–3979. doi:10.1021/acs.orglett.8b01540
29. Zhao, Y.-R.; Li, L.; Xu, G.-Y.; Xuan, J. *Adv. Synth. Catal.* **2022**, *364*, 506–511. doi:10.1002/adsc.202101144
30. Jiang, Y.; Li, P.; Zhao, J.; Liu, B.; Li, X. *Org. Lett.* **2020**, *22*, 7475–7479. doi:10.1021/acs.orglett.0c02618
31. Li, R.; Hou, Y.-X.; Xu, J.-H.; Gao, Y.; Hu, X.-Q. *Org. Chem. Front.* **2022**, *9*, 2181–2186. doi:10.1039/d2qo00144f
32. Yang, Z.; Liu, C.; Lei, J.; Zhou, Y.; Gao, X.; Li, Y. *Chem. Commun.* **2022**, *58*, 13483–13486. doi:10.1039/d2cc05899e
33. Hu, X.-Q.; Liu, Z.-K.; Hou, Y.-X.; Zhang, G.; Gao, Y. *Chem. Commun.* **2021**, *57*, 1113–1116. doi:10.1039/d0cc07573f
34. Hu, X.-Q.; Liu, Z.-K.; Hou, Y.-X.; Xu, J.-H.; Gao, Y. *Org. Lett.* **2021**, *23*, 6332–6336. doi:10.1021/acs.orglett.1c02131
35. Gao, Y.; Nie, J.; Li, Y.; Li, X.; Chen, Q.; Huo, Y.; Hu, X.-Q. *Org. Lett.* **2020**, *22*, 2600–2605. doi:10.1021/acs.orglett.0c00539
36. Xia, Y.; Wang, J. *Chem. Soc. Rev.* **2017**, *46*, 2306–2362. doi:10.1039/c6cs00737f
37. Chen, J.-R.; Hu, X.-Q.; Lu, L.-Q.; Xiao, W.-J. *Chem. Soc. Rev.* **2016**, *45*, 2044–2056. doi:10.1039/c5cs00655d
38. Cai, B.; Xuan, J. *Chin. J. Org. Chem.* **2021**, *41*, 4565. doi:10.6023/cjoc202109040
39. Kumar, S.; Nunewar, S.; Kanchupalli, V. *Asian J. Org. Chem.* **2022**, *11*, e202100689. doi:10.1002/ajoc.202100689

## License and Terms

This is an open access article licensed under the terms of the Beilstein-Institut Open Access License Agreement (<https://www.beilstein-journals.org/bjoc/terms>), which is identical to the Creative Commons Attribution 4.0 International License (<https://creativecommons.org/licenses/by/4.0>). The reuse of material under this license requires that the author(s), source and license are credited. Third-party material in this article could be subject to other licenses (typically indicated in the credit line), and in this case, users are required to obtain permission from the license holder to reuse the material.

The definitive version of this article is the electronic one which can be found at:  
<https://doi.org/10.3762/bjoc.19.10>





# Transition-metal-catalyzed C–H bond activation as a sustainable strategy for the synthesis of fluorinated molecules: an overview

Louis Monsigny<sup>‡</sup>, Floriane Doche<sup>‡</sup> and Tatiana Besset<sup>\*</sup>

## Review

Open Access

### Address:

Normandie University, INSA Rouen, UNIROUEN, CNRS, COBRA (UMR 6014), 76000 Rouen, France

### Email:

Tatiana Besset<sup>\*</sup> - tatiana.besset@insa-rouen.fr

<sup>\*</sup> Corresponding author    <sup>‡</sup> Equal contributors

### Keywords:

C–H bond activation; emergent fluorinated groups; homogeneous catalysis; organofluorine chemistry; palladium; synthetic method

*Beilstein J. Org. Chem.* **2023**, *19*, 448–473.

<https://doi.org/10.3762/bjoc.19.35>

Received: 11 February 2023

Accepted: 24 March 2023

Published: 17 April 2023

This article is part of the thematic issue "C–H bond functionalization: recent discoveries and future directions".

Guest Editor: I. Chatterjee

© 2023 Monsigny et al.; licensee Beilstein-Institut.

License and terms: see end of document.

## Abstract

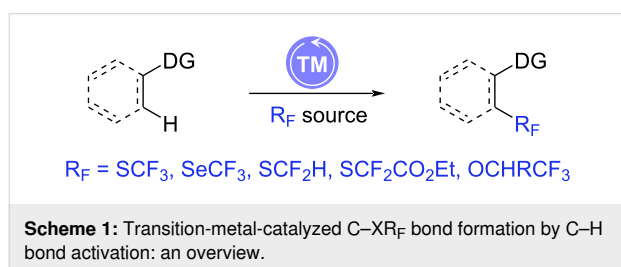
The last decade has witnessed the emergence of innovative synthetic tools for the synthesis of fluorinated molecules. Among these approaches, the transition-metal-catalyzed functionalization of various scaffolds with a panel of fluorinated groups ( $\text{XR}_\text{F}$ ,  $\text{X} = \text{S}$ ,  $\text{Se}$ ,  $\text{O}$ ) offered straightforward access to high value-added compounds. This review will highlight the main advances made in the field with the transition-metal-catalyzed functionalization of  $\text{C}(\text{sp}^2)$  and  $\text{C}(\text{sp}^3)$  centers with  $\text{SCF}_3$ ,  $\text{SeCF}_3$ , or  $\text{OCH}_2\text{CF}_3$  groups among others, by C–H bond activation. The scope and limitations of these transformations are discussed in this review.

## Introduction

Nowadays, fluorinated molecules represent an indispensable class of molecules in chemistry and in chemical biology. Thanks to the unique properties of the fluorine atom or fluorinated groups to modulate biological and physicochemical properties of the parent non-fluorinated molecules [1,2], their incorporation in various scaffolds afforded high value-added compounds as demonstrated by their numerous applications in the industrial sector such as drugs, agrochemicals, and materials. To further illustrate the ubiquity of fluorinated compounds, almost 20% of pharmaceuticals and 30–40% of agrochemicals [3–5] contain at least one fluorine atom. Because of the exceptional features of fluorinated derivatives, tremendous develop-

ments and discoveries have been made in this blossoming research area, with a high interest for fundamental research as well as the industry [6–11]. Among them [2,5,12–18], the direct functionalization of a simple C–H bond by transition-metal catalysis [19–43] became an important tool offering new retrosynthetic disconnections. In this context, a strong interest from the scientific community was shown towards the challenging synthesis of fluorinated molecules by transition-metal-catalyzed C–H bond activation [44–50], allowing the functionalization of complex molecules and even for late-stage functionalization strategy [51–53] for the synthesis of natural products [42,54–59].

The goal of this review is to highlight and discuss the recent approaches for the synthesis of fluorinated derivatives by the direct incorporation of a fluorinated group of  $\text{XR}_\text{F}$  type (e.g.,  $\text{SCF}_3$ ,  $\text{SeCF}_3$ ,  $\text{SCF}_2\text{CO}_2\text{Et}$ ,  $\text{OCH}_2\text{CF}_3$ ) by transition-metal-catalyzed C–H bond activation (Scheme 1). The review will be organized in two main parts, dedicated to the construction of a C– $\text{SCF}_2\text{R}/\text{SeCF}_3$  and C– $\text{OCH}_2\text{CF}_3$  bond. This review does not aim to be exhaustive and key examples were carefully chosen to provide the reader a nice overview. Since reviews dealing with transition-metal-catalyzed functionalization of compounds by C–H bond activation with fluorinated reagents [60–77] and vinylic, allylic or propargylic fluorinated building blocks [49] have been already reported, these reactions will not be included.



## Review

### I. Transition-metal-catalyzed directed C–chalcogen bond formation (C–S, C–Se) by C–H bond activation

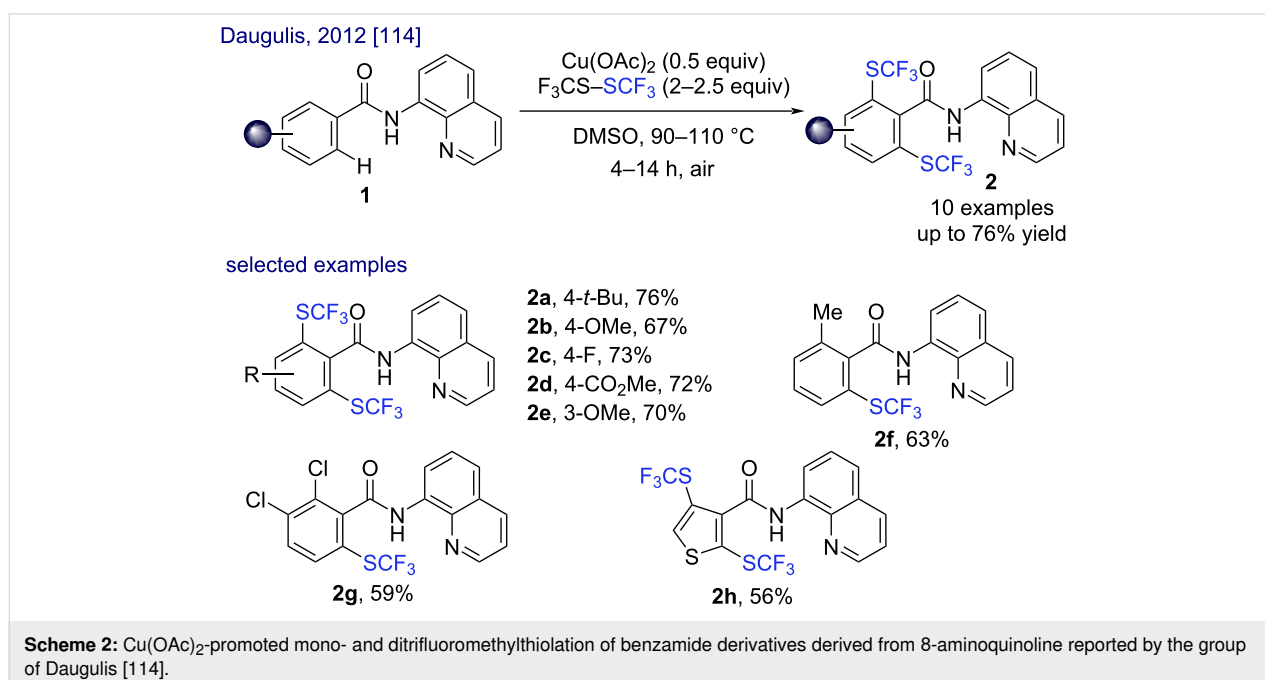
In the past decade, particular attention has been paid to the development of new methodologies for the incorporation of

sulfur-containing fluorinated groups. Although the transition-metal-catalyzed direct C–H bond functionalization appeared to be a powerful tool for the installation of C–C, C–N, or C–O bonds, the direct formation of a  $\text{C}(\text{sp}^2)\text{--SR}_\text{F}$  or a  $\text{C}(\text{sp}^3)\text{--SR}_\text{F}$  bond remains a challenging task. In this context, key players in the field have been interested in the design of original methodologies for the trifluoromethylthiolation and more recently the difluoromethylthiolation of various compounds by transition-metal catalysis [78]. Moreover, a recent interest was devoted to the trifluoromethylselenolation reaction as depicted in this section.

#### I.1) Transition-metal-catalyzed C–H trifluoromethylthiolation of aromatic $\text{C}(\text{sp}^2)$ centers

Thanks to its unique features such as an interesting lipophilicity (Hansch parameter = 1.44) [79,80] and a strong withdrawing character, the development of new methodologies for the incorporation of the  $\text{SCF}_3$  residue on various molecules has known a tremendous expansion [81–113].

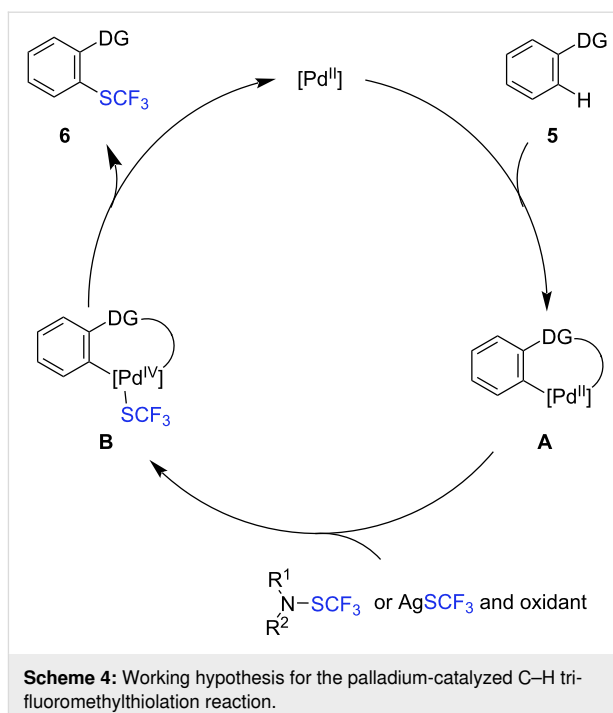
**Copper catalysis:** In 2012, Daugulis and co-workers reported the copper-promoted trifluoromethylthiolation of benzamide derivatives **1** at the *ortho*-position by C–H bond activation [114]. Indeed, using a bidentate directing group (amide derived from the 8-aminoquinoline), the mono- and difunctionalized compounds were obtained when  $\text{Cu}(\text{OAc})_2$  (0.5 equiv) and the toxic and volatile disulfide  $\text{F}_3\text{CS--SCF}_3$  were employed (Scheme 2, 10 examples, up to 76% yield). With this approach, derivatives bearing an aromatic part substituted at the *para*-position with electron-donating substituents (**1a,b**), halogens (**1c**) as well as



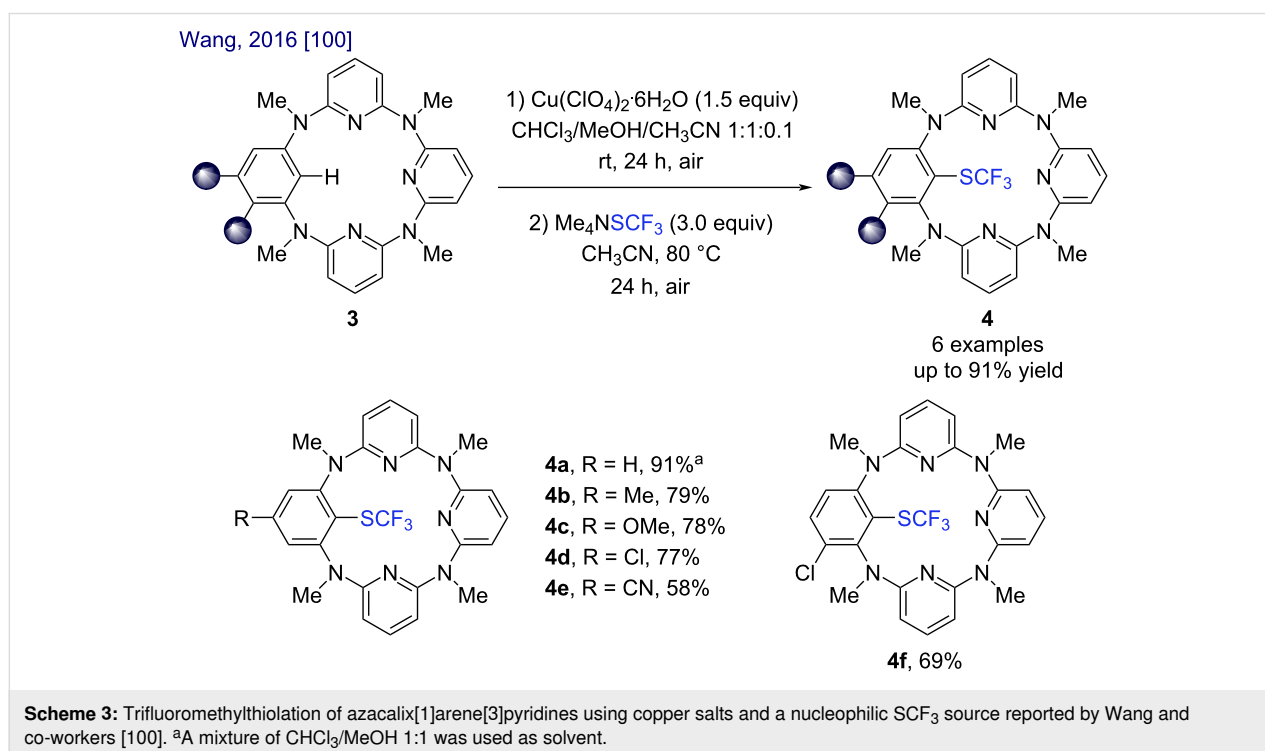
electron-withdrawing groups (**1d**) were difunctionalized in good yields. The substitution pattern on the aromatic ring did not affect the reaction efficiency, the *meta*-substituted derivative **2e** as well as the *ortho*-substituted derivative **2f** were obtained in high yields (70% and 63% yields, respectively). It should be noted that the presence of *ortho*-substituents on the aryl residue allowed the monofunctionalization to occur selectively. Also, amide **1g** bearing a disubstituted arene was successfully functionalized in 59% yield. Finally, the difunctionalized thiophene derivative **2h** was obtained in 56% yield.

In 2016, Wang's group developed another methodology for the trifluoromethylthiolation of azacalix[1]arene[3]pyridines by C–H bond activation using a complex of  $\text{Cu}(\text{ClO}_4)_2 \cdot 6\text{H}_2\text{O}$  and the shelf-stable  $\text{Me}_4\text{NSCF}_3$  [115,116] as a nucleophilic source of  $\text{SCF}_3$  (Scheme 3) [100]. Within these conditions, a set of six azacalix[1]arene[3]pyridines bearing electron-donating groups, halogens or electron-withdrawing groups were functionalized and the expected products were isolated in moderate to high yields (**4a–f**, 58–91%).

**Palladium catalysis:** Several works have been reported for the palladium-catalyzed trifluoromethylthiolation reaction of various aromatic compounds **5** by C–H bond activation and involved in most cases an electrophilic  $\text{SCF}_3$  source ( $\text{R}^1\text{R}^2\text{NSCF}_3$ ). For these transformations, the following working hypothesis was generally suggested (Scheme 4). After coordination of the palladium catalyst to a directing group, the



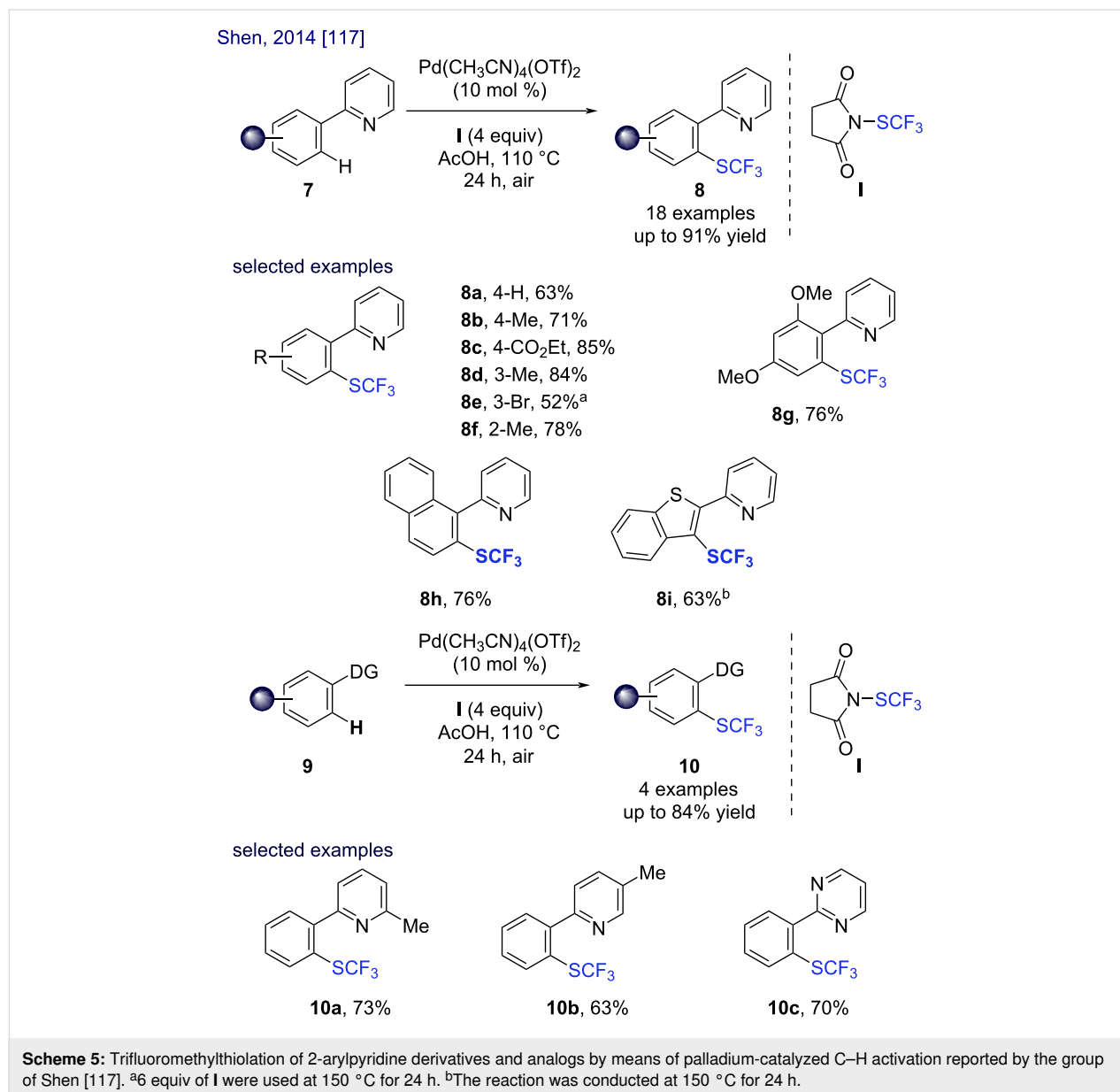
metallacycle **A** is formed. This latter undergoes an oxidative addition in the presence of an electrophilic source or an oxidation/ligand exchange in the presence of a nucleophilic source (i.e.,  $\text{AgSCF}_3$ ) and an oxidant (**B** in Scheme 4). Finally, after a reductive elimination step, the expected functionalized product **6** is obtained and the palladium catalyst is regenerated.



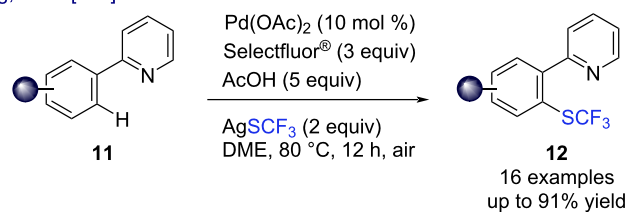
In 2014, Shen and Xu [117] developed a new methodology for the selective functionalization of 2-arylpyridine derivatives using an electrophilic  $\text{SCF}_3$  reagent, the Haas reagent **I** (Scheme 5) [118]. A broad range of 2-arylpyridine derivatives were trifluoromethylthiolated in good to high yields (18 examples, from 52 to 91% yields). The substitution pattern of the aromatic ring had no impact on the outcome of the reaction as illustrated with substrates substituted by a methyl group (**7b**, **7d**, and **7f**) at the *para*-, *meta*- and *ortho*-positions, which were readily functionalized in 71%, 84% and 78% yields, respectively. This reaction was also tolerant of a 2-naphthyl group, the palladium-catalyzed trifluoromethylthiolation afforded the corresponding product **8h** in 76% yield. Also, the 2,4-dimethoxy-substituted substrate **7g** and the benzothiophene derivative **7i** were

successfully trifluoromethylthiolated in 76% and 63% yields, respectively. This reaction proved to be compatible with the presence of an ester (**8c**) or a halogen (**8e**). Other directing groups, such as substituted pyridines (**9a** and **9b**) and pyrimidine (**9c**) turned out to be also efficient in this transformation (Scheme 5, 4 examples, up to 84% yield).

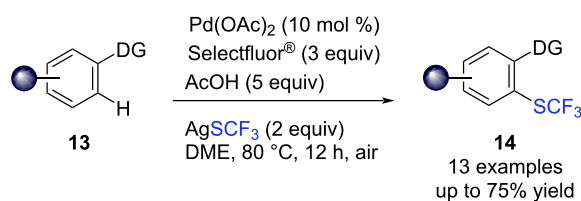
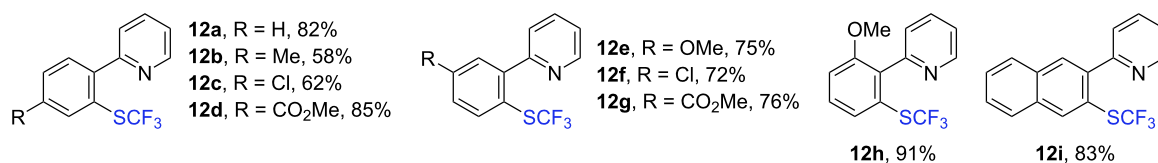
The same year, the group of Huang reported an elegant and straightforward palladium(II)-catalyzed *ortho*-selective trifluoromethylthiolation of arenes bearing various directing groups using the nucleophilic trifluoromethylthiolating source  $\text{AgSCF}_3$  in combination with Selectfluor<sup>®</sup> as oxidant (Scheme 6, 29 examples, up to 91% yield) [119]. 2-Arylpyridine derivatives bearing electron-donating groups, electron-



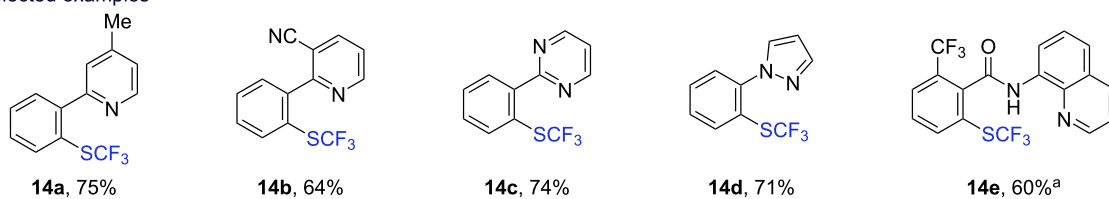
Huang, 2014 [119]



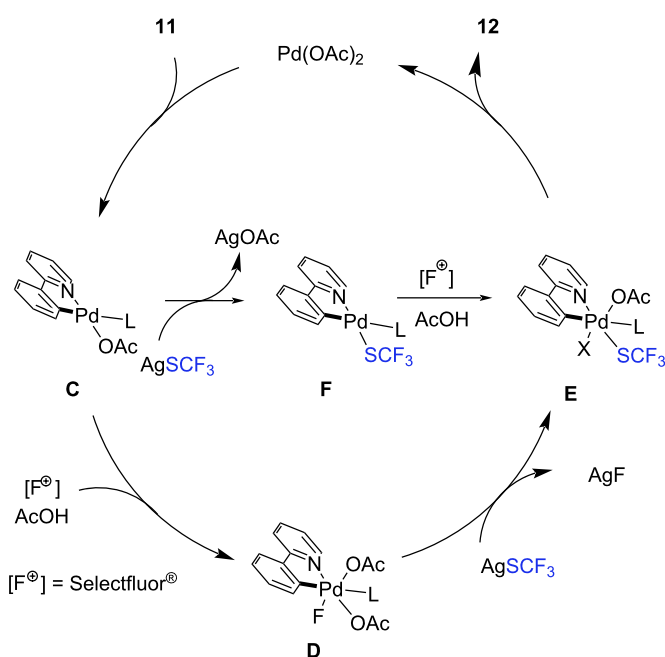
selected examples



selected examples



suggested mechanism



**Scheme 6:** C(sp<sup>2</sup>)-SCF<sub>3</sub> bond formation by Pd-catalyzed C-H bond activation using AgSCF<sub>3</sub> and Selectfluor<sup>®</sup> as reported by the group of Huang [119]. <sup>a</sup>20 equiv of Cl<sub>2</sub>CHCOOH were used instead of AcOH.

withdrawing groups or halogen at the *para*- and *meta*-positions of the aromatic ring were readily functionalized (**11a–g**, 58–85% yields). Also 2-(2-methoxyphenyl)pyridine (**11h**) and 2-(2-naphthyl)pyridine (**11i**) were found to be suitable substrates leading to the corresponding products **12h** and **12i** in 91% and 83% yields, respectively. The use of other directing groups was also suitable for this transformation such as methyl and cyano-substituted pyridines **13a,b**, pyrimidine (**13c**), pyrazole (**13d**), as well as the amide derived from 8-aminoquinoline **13e** (Scheme 6, 13 examples, up to 75% yield).

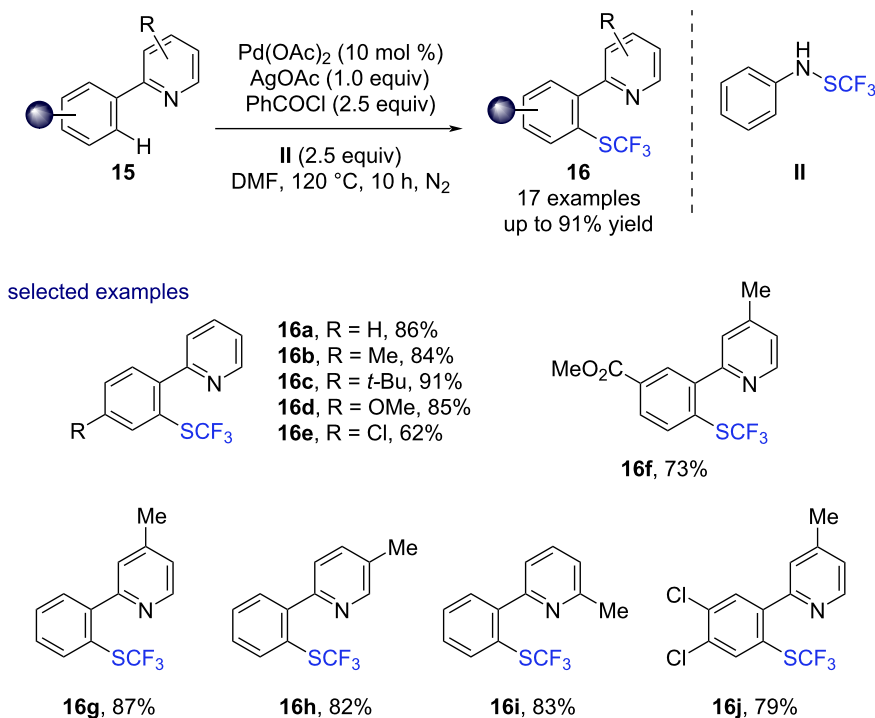
In this study, two mechanisms were reported. The first one suggested that a palladacycle **C** is formed after the irreversible chelation of the 2-phenylpyridine substrate with palladium, which is the rate-determining step (KIE = 2.7). Subsequently palladacycle **C** is oxidized by Selectfluor® to form a palladium(IV) complex **D**. After a ligand exchange with AgSCF<sub>3</sub>, the intermediate **E** is obtained, which, after reductive elimination, releases the desired product **12** and regenerates the catalyst. Alternatively, a ligand exchange with AgSCF<sub>3</sub> occurs before the oxidation step, generating the palladium(II) complex **F**. After an oxidative addition in the presence of Selectfluor®, the palladium(IV) intermediate **E** is generated. Finally, after reductive elimination step, the desired product **12** is released and

the catalyst regenerated. Note that, in this process, Selectfluor® is playing a key role. Indeed, using this electrophilic fluorinating source as oxidant generates a Pd(IV)(ppy)F(OAc)<sub>2</sub> (ppy = 2-phenylpyridine) complex as intermediate. As the competitive C–F bond formation was disfavored (slow reductive elimination step), the desired trifluoromethylthiolated product **12** is selectively afforded after a F/SCF<sub>3</sub> ligand exchange.

In 2015, Ye and Liu reported the palladium-catalyzed trifluoromethylthiolation of 2-arylpyridine derivatives using the Billard reagent **II** (Scheme 7) [120]. Unlike Shen's methodology (Scheme 5), the use of benzoyl chloride was necessary to activate the trifluoromethylthiolated reagent [120]. Unsubstituted and pyridines substituted derivatives **15** were very efficiently *ortho*-trifluoromethylthiolated (17 examples, up to 91% yield). This methodology was tolerant to electron-donating and electron-withdrawing groups as well as halogens (**16b–f**, 62–91% yields). The *meta*-substituted (**16f**) and disubstituted (**16j**) products were obtained in high yields (73% and 79%, respectively).

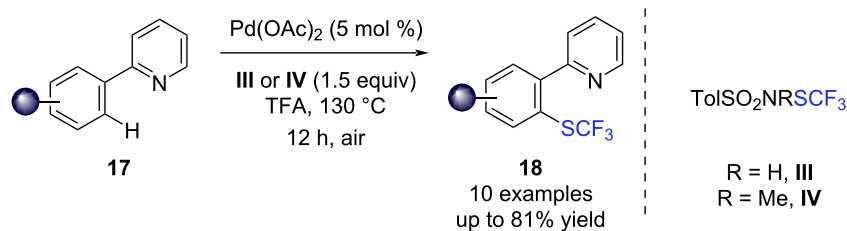
In 2018, Anbarasan and co-workers described a palladium-catalyzed trifluoromethylthiolation of arenes by C–H bond activation bearing several directing groups (Scheme 8) [121]. With

Ye and Liu, 2015 [120]

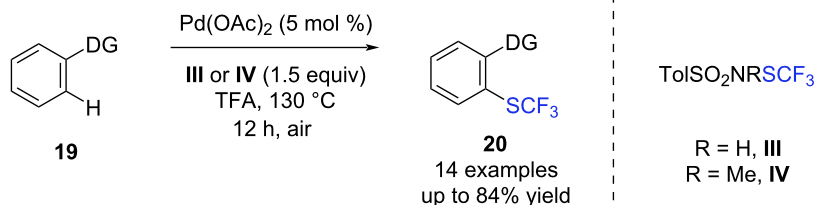


**Scheme 7:** Palladium-catalyzed *ortho*-trifluoromethylthiolation of 2-arylpyridine derivatives reported by the group of Ye and Liu [120].

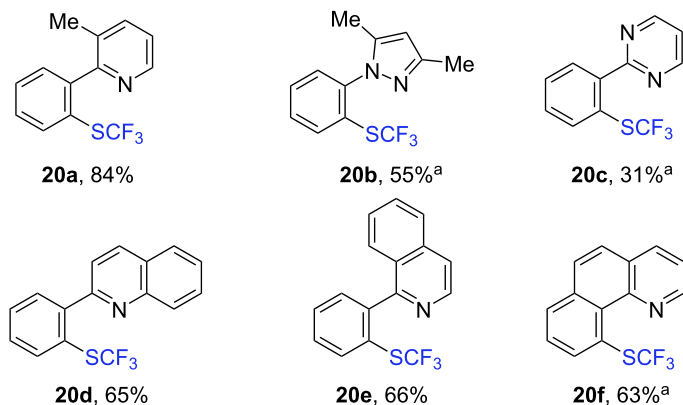
Anbarasan, 2018 [121]



selected examples



selected examples



**Scheme 8:** Palladium-catalyzed *ortho*-trifluoromethylthiolation of 2-arylpyridine and analogs reported by Anbarasan [121]. <sup>a</sup>The reaction was conducted at 120 °C using 1.1 equiv of Billard reagent **IV** (R = Me).

this methodology, the functionalization of 2-phenylpyridine derivatives was possible (10 examples, up to 81% yield) using the Billard reagents **III** or **IV** [122]. The trifluoromethylthiolation of 2-arylpyridines substituted by electron-donating groups such as methyl, methoxy or methylthio groups (**17b–d**) or by halogen (**17e**) was achieved (Scheme 8, up to 77% yield). Note that in case of disubstituted 2-(4-ethoxy-3-fluorophenyl)pyridine (**17h**), the expected product **18h** was isolated in 31% yield. Moreover, selective oxidation of the SCF<sub>3</sub> residue into the cor-

responding sulfoxide and the sulfone was possible and the corresponding products were obtained in 98% and 95% yields, respectively.

This reaction was successfully expanded to the trifluoromethylthiolation of derivatives bearing various directing groups such as substituted pyridines (4 examples, up to 84% yield, **19a**, 84% yield), substituted pyrazole derivatives (6 examples, up to 55% yield, **19b**, 55% yield), pyrimidine (**19c**,

31% yield) as well as quinoline and isoquinoline (**19d** and **19e**, 65% and 66% yields, respectively). In addition, the trifluoromethylthiolated benzo[*h*]quinoline **20f** was obtained in good yield (63%).

The same year, Besset and co-workers reported a palladium-catalyzed C(sp<sup>2</sup>)–SCF<sub>3</sub> bond formation on amides derived from 8-aminoquinoline as a cleavable directing group in the presence of the Munavalli reagent **V** (Scheme 9, 12 examples, up to 71% yield) [106]. Depending on the substitution pattern on the aromatic ring, the amides were mono- or difunctionalized. Indeed, *meta*- and *ortho*-substituted derivatives (**21a–d**) were selectively trifluoromethylthiolated while *para*-substituted substrates led to the difunctionalized products **22e** and **22f**. Within these reaction conditions, the polysubstituted derivative **21g** was also functionalized in high yield (71%).

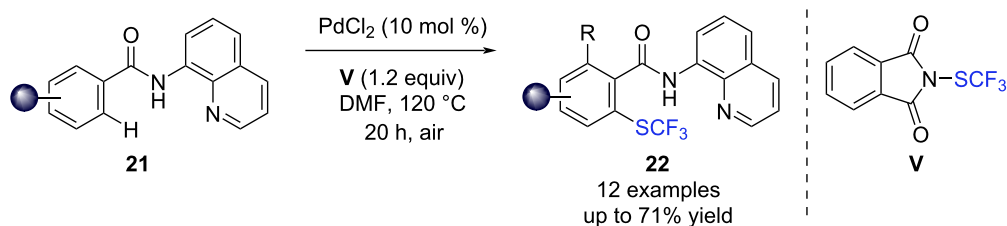
Pleasingly, other metals have been also successfully applied for the trifluoromethylthiolation of aromatic derivatives by C(sp<sup>2</sup>)–H bond activation such as Rh(III) and Co(III)-based catalysts as depicted below.

**Rhodium catalysis:** In 2015, the group of Li disclosed the Cp\*Rh(III)-catalyzed regioselective trifluoromethylthiolation of *N*-substituted indoles with (substituted) pyridines or pyrimidine as the directing groups (Scheme 10) [123]. The selective tri-

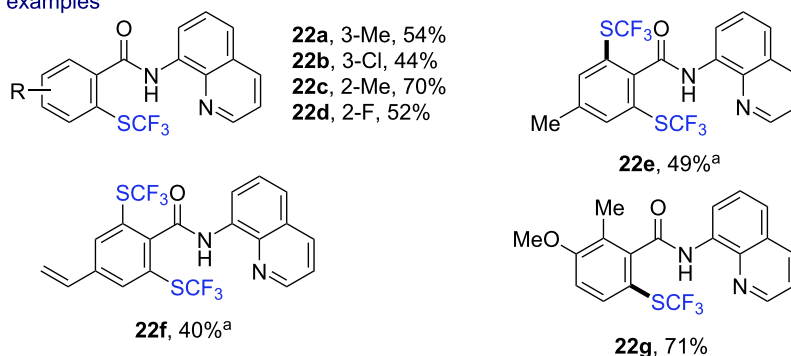
fluoromethylthiolation of indoles at the C2 position was achieved in the presence of *N*-(trifluoromethylthio)saccharine (**VI**, Shen's reagent) as both oxidant and electrophilic source (18 examples, up to 91% yield). Indoles bearing various electron-donating and electron-withdrawing groups as well as halogens at the C5-position and at the C6-position were functionalized in high yields (**24a–f**, 82–87% yields). The substitution of the indole at the C3-position did not impact the reaction and the product **24g** was obtained in 91% yield. Substituted pyridines and pyrimidine (**24h** and **24i**) were also used as directing groups (7 examples, up to 86% yield). This methodology was extended to the functionalization of other heteroaromatic derivatives (**24j**, 87% yield). It should be noted that the presence of zinc triflate, a Lewis acid, was used for the activation of the electrophilic source **VI**.

**Cobalt catalysis:** In 2017, Wang described the Cp\*Co(III)-catalyzed trifluoromethylthiolation of 2-phenylpyridine derivatives using AgSCF<sub>3</sub> (Scheme 11) [124]. This methodology allowed the functionalization of several aromatic compounds bearing a pyridine or a pyrimidine as a directing group (20 examples, up to 65% yield). The reaction proceeded smoothly with substrates bearing an electron-donating group (**25b,c**), halogen (**25d**) or withdrawing group (**25e**) and the desired SCF<sub>3</sub>-containing products were obtained in moderate to good yields. The functionalization of trisubstituted arene **25g** and

Besset, 2018 [106]



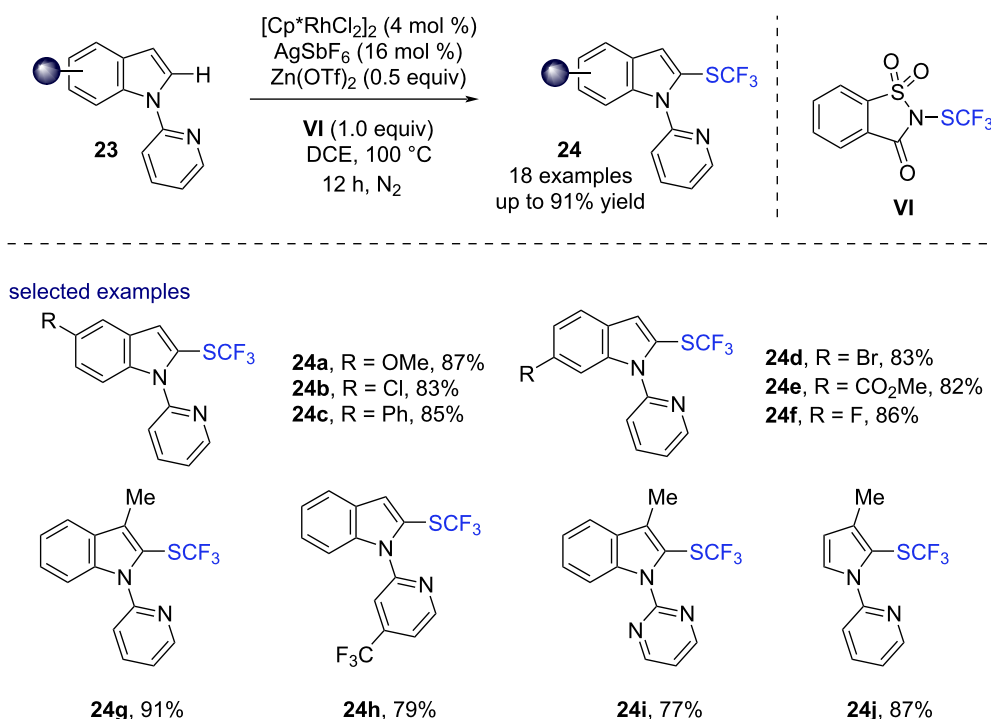
selected examples



**Scheme 9:** Mono- and difluoromethylthiolation of benzamide derivatives derived from 8-aminoquinoline using PdCl<sub>2</sub> as catalyst reported by Besset and co-workers [106]. <sup>a</sup>2.2 equiv of the fluorinated source **V** were used.



Li, 2015 [123]



**Scheme 10:** Regioselective  $\text{Cp}^*\text{Rh}(\text{III})$ -catalyzed directed trifluoromethylthiolation reported by the group of Li [123].  $\text{Cp}^*$  = pentamethylcyclopentadienyl.

heteroarene **25h** was also possible leading to the corresponding products **26g** and **26h** in moderate yields (23% and 42% yields, respectively). Regarding the reaction mechanism, the active  $\text{Co}(\text{III})$  complex **G** was obtained from the dimeric catalyst  $[\text{Cp}^*\text{CoI}_2]_2$  in the presence  $\text{AgSCF}_3$  and/or  $\text{NaOPiv}\cdot\text{H}_2\text{O}$ . Then, the reversible formation of the metallacycle **H** occurs, which after a ligand exchange in the presence of  $\text{AgSCF}_3$  leads to the formation of adduct **J**. The product **26** is released via a reductive elimination step, generating at the same time the reduced cobalt  $\text{Cp}^*\text{Co}(\text{I})$ , which is converted to the active catalyst after oxidation.

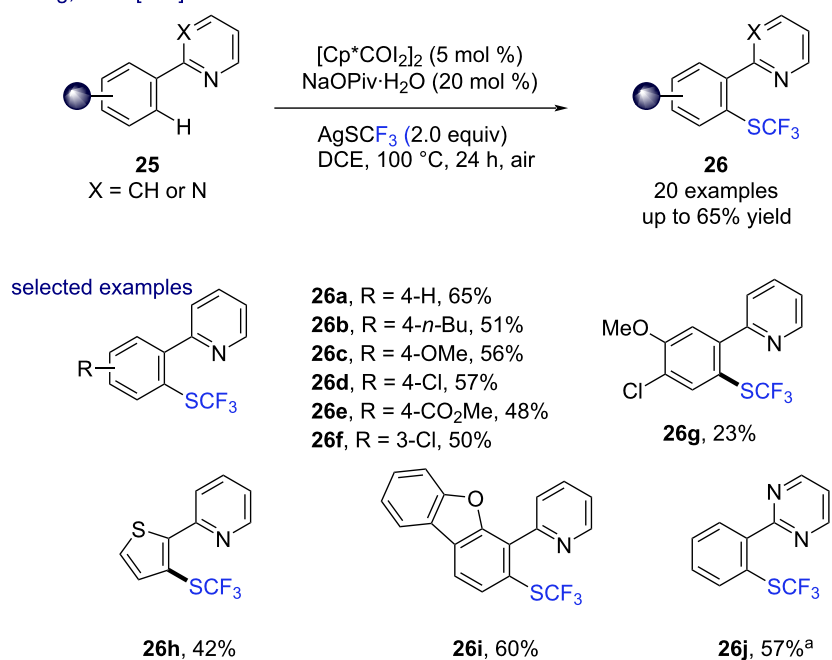
The same year, Yoshino and Matsunaga described a similar methodology, using the cobalt(III) complex  $[\text{Cp}^*\text{Co}(\text{CH}_3\text{CN})_3](\text{SbF}_6)_2$  and *N*-trifluoromethylthiodibenzenesulfonimide **VII** as electrophilic  $\text{SCF}_3$  source (Scheme 12) [125]. Under these reaction conditions, 2-arylpyridines (9 examples, up to 94% yield) or 6-arylpurines (10 examples, up to 72% yield) were *ortho*-trifluoromethylthiolated. The substitution pattern of the aryl part did not impact the outcome of the reaction. This methodology was also tolerant to a large range of functional groups (ester, halogen) as illustrated by the products **28c**, **28j**, **28d**, **28k**, and **28g**.

## 1.2) Transition-metal-catalyzed C–H trifluoromethylthiolation of vinylic $\text{C}(\text{sp}^2)$ centers

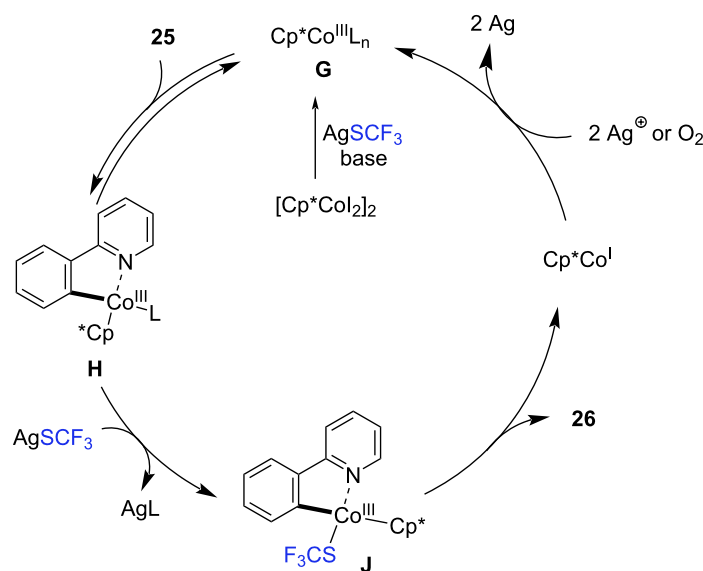
Several research groups have been interested in the development of strategies for the formation of vinylic  $\text{C}(\text{sp}^2)\text{--SCF}_3$  bonds, offering an efficient tool towards the synthesis of challenging *Z*-isomers.

**Palladium catalysis:** In 2018, Bouillon and Besset described the first example of a selective palladium-catalyzed trifluoromethylthiolation of  $\alpha$ -arylacrylamides derived from 8-aminoquinolines **29** by C–H bond activation (Scheme 13) [104]. Using the Munavalli reagent **V** as an electrophilic  $\text{SCF}_3$  source, this diastereoselective method selectively led to the formation of *Z*-isomers and turned out to be robust (not air or moisture sensitive). Under these mild reaction conditions, a panel of  $\alpha$ -(hetero)arylacrylamides were trifluoromethylthiolated in good to high yields. Acrylamides substituted at the  $\alpha$ -position by an aryl bearing an electron-donating group (OMe) or halogen (Cl) at the *para*-position were readily functionalized (**30b** and **30c**, 70% and 75% yields, respectively). The substitution of the arene with a  $\text{CF}_3$  residue at the *meta*-position or with a methoxy group at the *ortho*-position did not have any impact to the outcome of the reaction (**30e** and **30f**, 62% and 78% yields, re-

Wang, 2017 [124]



suggested mechanism

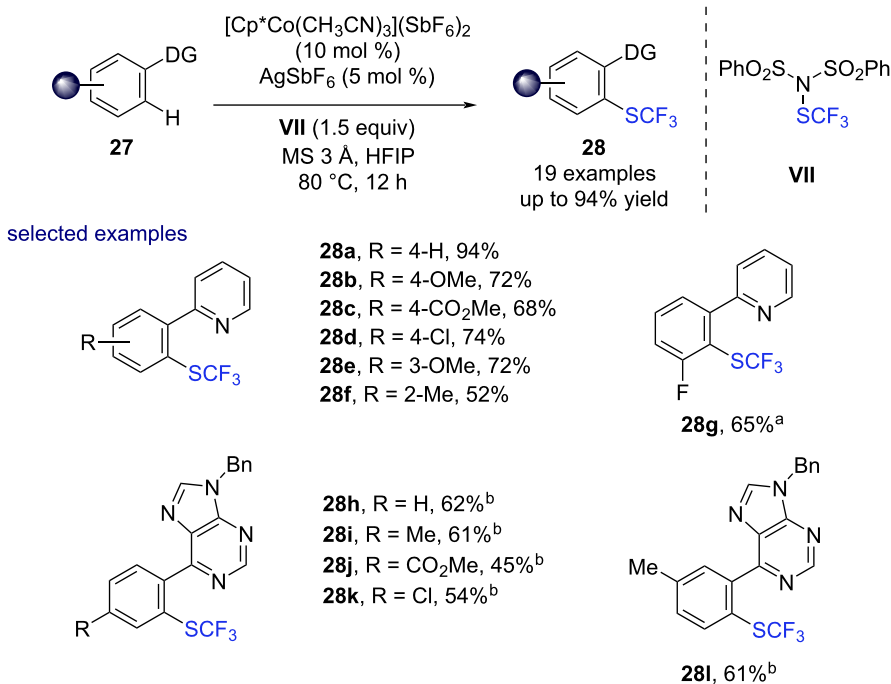


**Scheme 11:**  $\text{Cp}^*\text{Co}(\text{III})$ -catalyzed *ortho*-trifluoromethylthiolation of 2-phenylpyridine and 2-phenylpyrimidine derivatives reported by Wang and co-workers [124]. <sup>a</sup> $\text{CH}_2\text{Cl}_2$  was used as solvent.

spectively). It should be noted that acrylamides bearing a disubstituted arene (**29g,h**) and an heteroaryl (**29i**) at the  $\alpha$ -position were also suitable substrates for this reaction. Finally, acrylamides bearing a methyl group at the  $\alpha$ -position (**29j**) or the  $\alpha,\beta$ -dimethylated acrylamide (**29k**) were suitable substrates

albeit the corresponding products were obtained in 30% and 20% yields, respectively. Several mechanistic experiments revealed that the  $\text{C}(\text{sp}^2)\text{--H}$  bond activation step was reversible and represented the rate-determining step ( $\text{KIE} = 2.4$ ). First, the chelation of the palladium(II) catalyst with the bidentate

Yoshino and Matsunaga, 2017 [125]



**Scheme 12:** Cp\*Co(III)-catalyzed *ortho*-trifluoromethylthiolation of 2-phenylpyridine and 6-phenylpurine derivatives described by Yoshino and Matsunaga [125]. <sup>a</sup>Without AgSbF<sub>6</sub>. <sup>b</sup>2.0 equiv of VII, 10 mol % of AgOAc and 30 mol % of Gd(OTf)<sub>3</sub> were used instead of AgSbF<sub>6</sub>.

directing group, followed by the C(sp<sup>2</sup>)–H bond activation involving a concerted metalation–deprotonation pathway affords the metallacycle **K**. After an oxidative addition in the *N*-SCF<sub>3</sub> bond of the Munavalli reagent **V**, the palladium(IV) species **L** is obtained. Finally, the reductive elimination affords the product and regenerates the catalyst. The same year, Besset and co-workers extended this methodology to a larger class of acrylamides [106].

### I.3) Transition-metal-catalyzed trifluoromethylthiolation of aliphatic C(sp<sup>3</sup>)–H bonds

Despite the important progresses presented in the previous section, some limitations of the trifluoromethylthiolation persist. In particular, the functionalization of a C(sp<sup>3</sup>)–H bond with a trifluoromethylthiolated moiety by transition-metal-catalyzed C–H activation remains a challenging task both in terms of reactivity and selectivity.

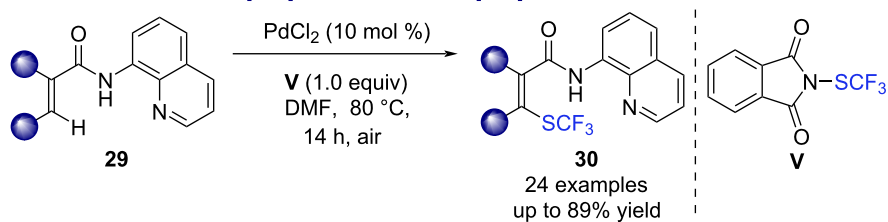
In 2015, Besset reported the first C(sp<sup>3</sup>)–SCF<sub>3</sub> bond formation of unactivated primary C(sp<sup>3</sup>) centers by transition-metal-catalyzed C–H activation with the Munavalli or the Billard reagents as the trifluoromethylthiolation source (Scheme 14) [126]. Using a bidentate directing group, this methodology allowed the functionalization of a large range of aliphatic amides with a pri-

mary β-C(sp<sup>3</sup>)–H bond (21 examples, up to 53% yield). The methodology was applied to the functionalization of a series of amides having an α-quaternary center (α,α-dialkyl (**31a**), α-alkyl,α-benzyl derivatives **31c–f**) as well as to an amide with an α-tertiary center (**31b**) and pleasingly, the presence of α-C–H bonds did not have a significant impact on the outcome of the reaction. It should be noted that this methodology afforded the products with a high regioselectivity, and no incorporation of the SCF<sub>3</sub> moiety on the benzylic or at the C5 position of the quinoline part of the directing group was observed. Note that in 2018, Besset and Lebel developed a more efficient process for the palladium-catalyzed trifluoromethylthiolation by C–H bond activation under continuous flow conditions [127].

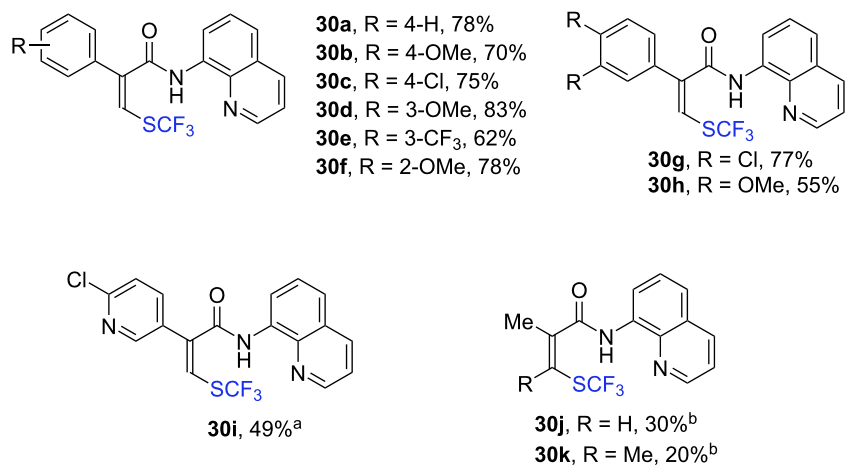
### I.4) Difluoromethylthiolation of aromatic and vinylic C(sp<sup>2</sup>)–H bonds (C–SCF<sub>2</sub>H and C–SCF<sub>2</sub>CO<sub>2</sub>Et bonds)

More recently, researchers became interested in the synthesis of molecules substituted with original and functionalized fluorinated moieties such as SCF<sub>2</sub>FG [128–136] (FG = functional group). In sharp contrast with the trifluoromethylthiolation reaction, only a handful of reports dealt with the incorporation of such high value-added fluorinated moieties onto C(sp<sup>2</sup>) centers by transition-metal-catalyzed C–H bond activation.

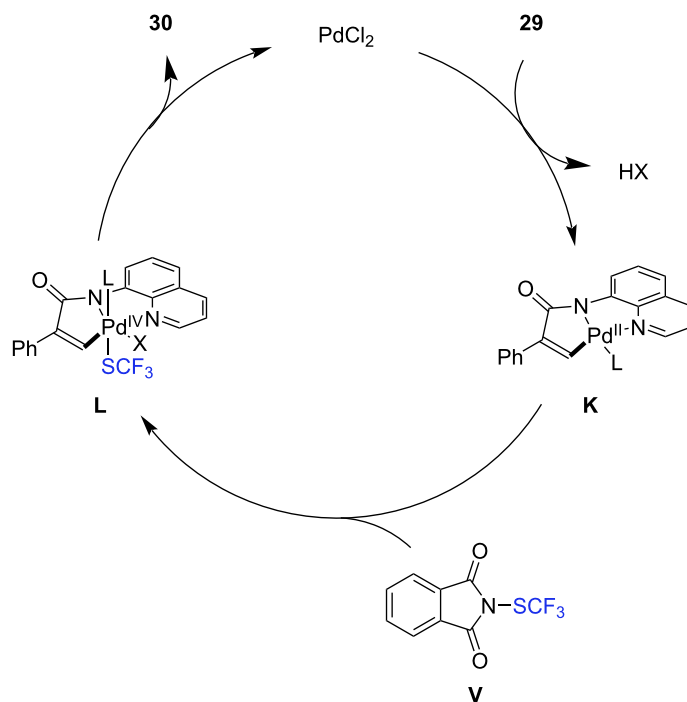
Bouillon and Besset, 2017 [104] and Besset, 2018 [106]



selected examples

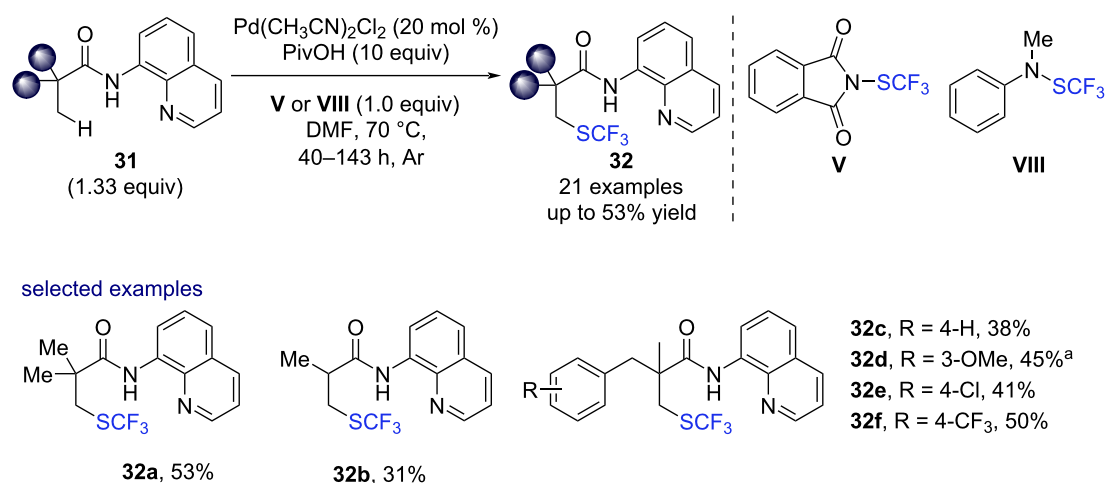


suggested mechanism



**Scheme 13:** Diastereoselective trifluoromethylthiolation of acrylamide derivatives derived from 8-aminoquinoline using  $\text{PdCl}_2$  reported by Bouillon and Besset [104,106]. <sup>a</sup>20 mol % of  $\text{PdCl}_2$  and 2.0 equiv of  $\text{SCF}_3$  source **V** were used for 36 h. <sup>b</sup>The reaction was conducted with 30 mol % of  $\text{PdCl}_2$  and 2.0 equiv of reagent **V** were used.

Besset, 2015 [126]



**Scheme 14:** C(sp<sup>3</sup>)–SCF<sub>3</sub> bond formation on aliphatic amide derivatives derived from 8-aminoquinoline by palladium-catalyzed C–H bond activation described by Besset and co-workers [126]. Product **32d** was contaminated with 10% of an inseparable impurity.

In 2022, He and Pan reported the first example of a difluoromethylthiolation achieved by transition-metal-catalyzed C–H bond activation (Scheme 15) [137]. Using the reagent **IX** and a catalytic amount of  $\text{PdCl}_2$ , they succeeded in the functionalization of acrylamides **33** derived from 8-aminoquinoline. Within these mild conditions,  $\alpha$ -arylacrylamides substituted at *para*-, *meta*-, and *ortho*-positions were readily difluoromethylthiolated (**34a–g**, 81–95% yields). This reaction was also tolerant to a large class of functional groups (halogens, cyano, trifluoromethyl), affording products **34c,d** and **34e** in high yields (86%, 89% and 81%, respectively). The  $\alpha$ -methyl-substituted acrylamide **33j** also underwent difluoromethylthiolation to give product **34j** in 81% isolated yield. The  $\alpha,\beta$ - and  $\beta$ -substituted acrylamides were functionalized in high yields (**34h,i** and **34k–m**, 71–86%). The plausible mechanism is similar as the one reported by Besset for the trifluoromethylthiolation of acrylamides derived from 8-aminoquinoline (Scheme 13).

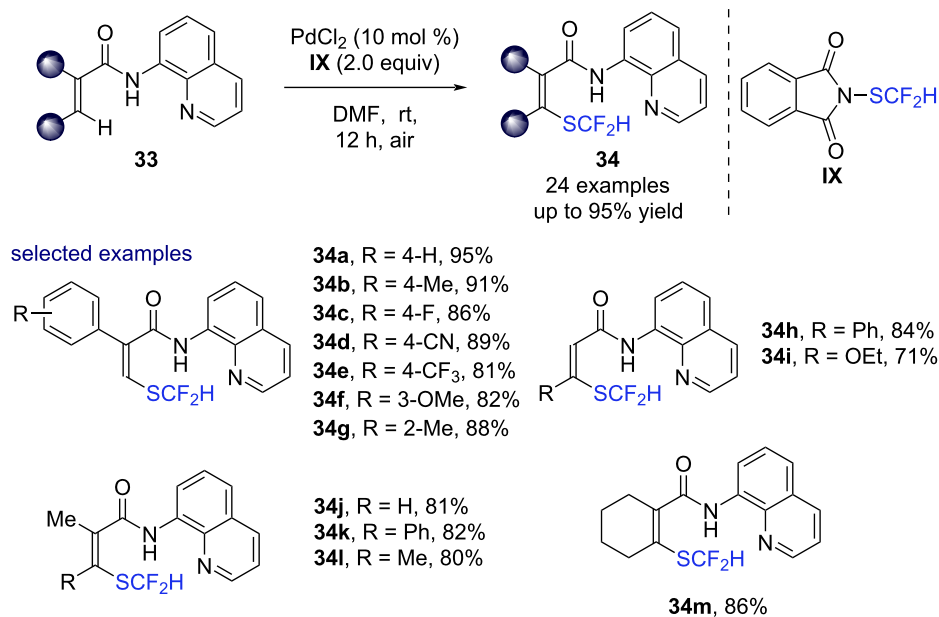
The same year, Besset and co-workers reported the first palladium-catalyzed C(sp<sup>2</sup>)–SCF<sub>2</sub>CO<sub>2</sub>Et bond formation by C–H bond activation (Scheme 16) [138]. In the presence of the electrophilic SCF<sub>2</sub>CO<sub>2</sub>Et source **X**, the methodology was successfully applied for the functionalization of 2-arylpyridine derivatives **35a–i** as well as 2-vinylpyridine derivatives **35j–m** (35 examples, up to 87% yield). The substitution pattern of the aryl substituent of the 2-phenylpyridine derivatives did not influence the reaction as for instance products **36b**, **36h**, and **36i** were obtained in good yields (70%, 63% and 61% yield, respectively). This reaction was tolerant to a broad range of functional groups such as halogens, ester, aldehyde, cyano, and nitro

(**36c–g**, 36–74% yield). It is noteworthy that a disubstituted compound **35j** and a thiophene derivative **35k** were also efficiently difluoromethylthiolated (**36j** and **36k**, 72% and 65%, respectively).  $\alpha$ -Substituted vinylpyridines with electron-donating or electron-withdrawing groups on the aromatic ring were functionalized and **36l** and **36m** were easily isolated in 73% and 81% yields, respectively. Even an  $\alpha,\beta$ -disubstituted vinylpyridine **35n** and the benzoquinoline **35o** were smoothly functionalized showing the efficiency of the approach. Of high interest, the modularity of the SCF<sub>2</sub>CO<sub>2</sub>Et was highlighted by its conversion into various other fluorinated residues (amide, carboxylic acid) and its selective oxidation into the corresponding sulfoxide and sulfone.

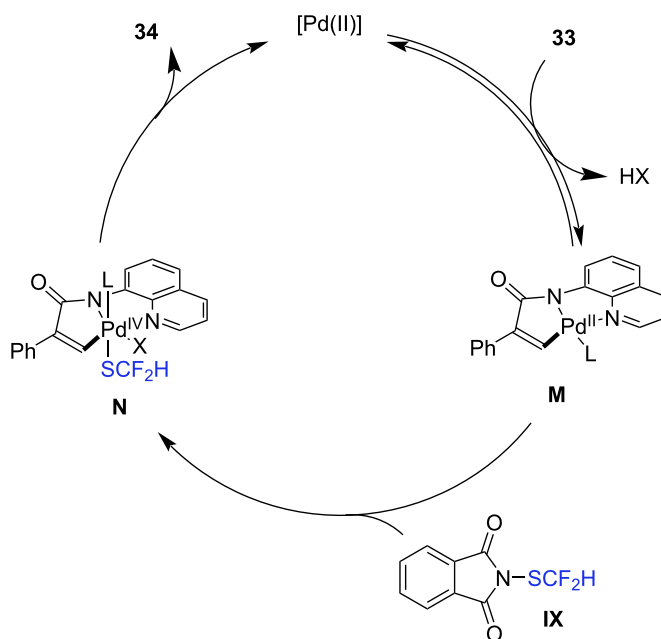
### 1.5) Trifluoromethylselenenolation of aromatic and vinylic C(sp<sup>2</sup>)–H bonds by palladium catalysis

Very recently, the palladium-catalyzed trifluoromethylselenenolation of (hetero)aromatic and olefinic derivatives has been investigated by the group of Billard using similar catalytic systems as those depicted for the trifluoromethylthiolation reactions. Indeed, using amides **37** derived from 5-methoxy-8-aminoquinoline, the functionalization of (hetero)aromatic compounds was achieved using 20 mol % of  $\text{Pd}(\text{CH}_3\text{CN})_4\text{Cl}_2$  in the presence of  $\text{ToISO}_2\text{SeCF}_3$  as the fluorinating source (14 examples, Scheme 17) [139]. Of note, when the reaction was carried out on derivatives bearing substituents at the *meta*- (**37c** and **37d**) as well as at the *para*- (**37a** and **37b**) positions, the corresponding products **38a–d** were obtained as a mixture of mono- and disubstituted trifluoromethylselenenolated derivatives with global yields ranging from 48% to 70%. When one of the *ortho*-posi-

He and Pan, 2022 [137]



suggested mechanism

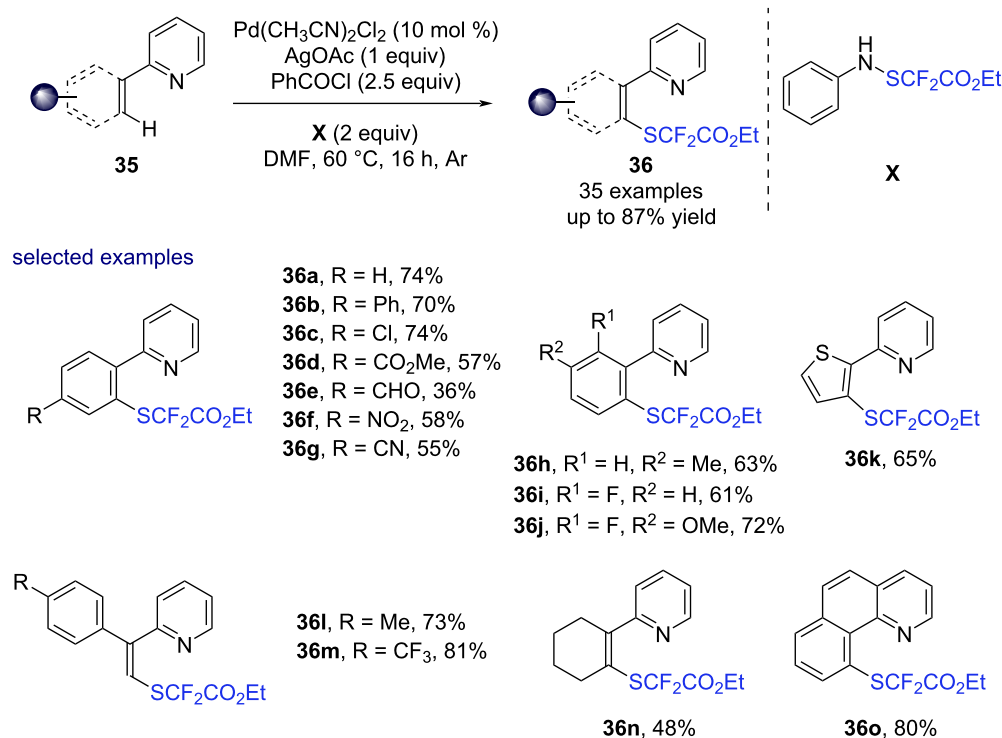
**Scheme 15:** Regio- and diastereoselective difluoromethylthiolation of acrylamides under palladium catalysis reported by He and Pan [137].

tions of the aromatic ring was substituted with a Me (**37e**), a OMe (**37f**), a Cl (**37g**) or a CF<sub>3</sub> (**37h**) group, the corresponding compounds **38e**, **38f**, **38g**, and **38h** were isolated in moderate to high yields (43% to 80%). The methodology also allowed the trifluoromethylselenolation of the furan derivative **37i**, which led to the desired product **38i** in 30% yield. A careful monitoring of the reaction unveiled the rapid formation of the

CF<sub>3</sub>SeSeCF<sub>3</sub> dimer, which could be the active trifluoromethylselenolating reagent in this transformation.

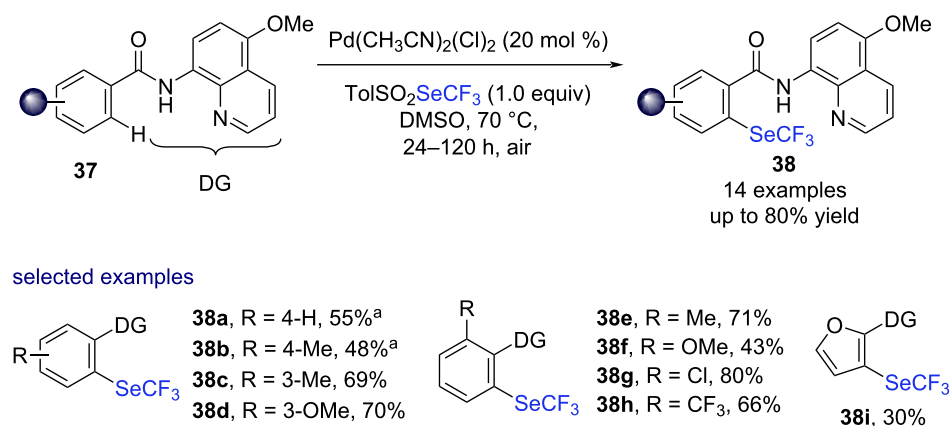
In 2022, Magnier, Billard and co-workers applied the previous methodology to the trifluoromethylselenolation of acrylamide derivatives [140]. Using the same directing group, a panel of  $\alpha$ -arylacrylamide derivatives **39a–f** was successfully functional-

Besset, 2022 [138]



**Scheme 16:** Palladium-catalyzed (ethoxycarbonyl)difluoromethylthiolation reaction of 2-(hetero)aryl and 2-( $\alpha$ -aryl-vinyl)pyridine derivatives reported by Besset [138].

Billard, 2021 [139]

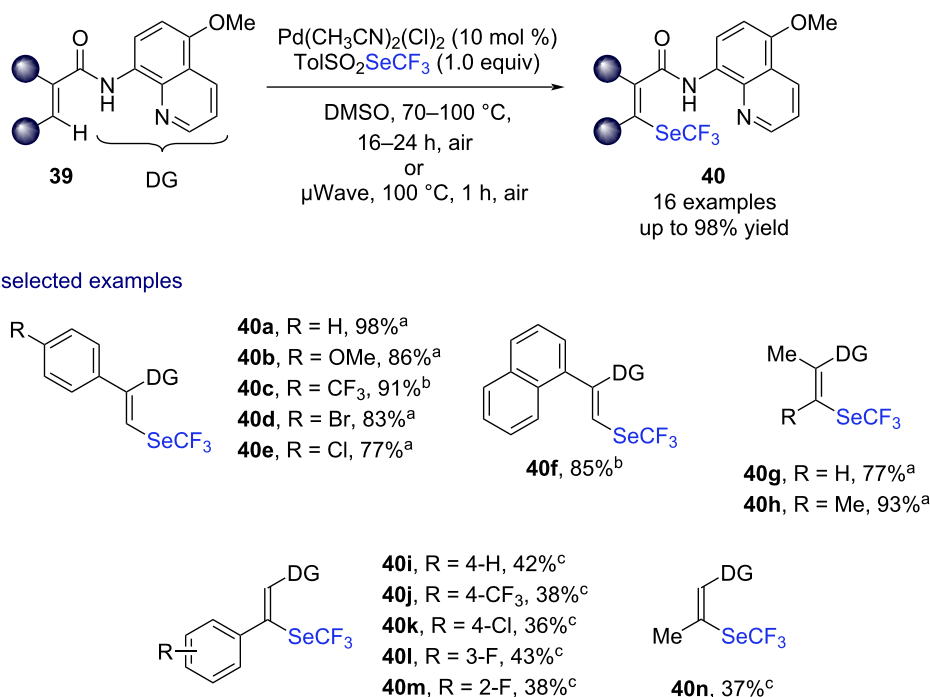


**Scheme 17:** Pd(II)-catalyzed trifluoromethylselenenolation of benzamides derived from 5-methoxy-8-aminoquinoline reported by the group of Billard [139]. <sup>a</sup>The yields given are the sum of the yields of mono- and difluoromethylselenenolated products.

ized with a high *Z*-selectivity (yields up to 98%, Scheme 18). Both, thermal reaction conditions (DMSO at 70 °C for 16 h) and microwave irradiation (100 °C using microwaves in only 1 h) turned out to be efficient in the process.  $\alpha$ -Methyl- and  $\alpha$ , $\beta$ -dimethylacrylamides **39g** and **39h** were also functionalized.

Furthermore, a series of  $\beta$ -substituted acrylamides **39i–m** with various substituents readily underwent the trifluoromethylselenenolation reaction with high selectivity in moderate yields. Finally, the  $\text{SeCF}_3$ -containing  $\beta$ -methylacrylamide **40n** was also obtained in 37% yield.

Magnier and Billard, 2022 [140]



**Scheme 18:** Pd(II)-catalyzed trifluoromethylselenenolation of acrylamide derivatives derived from 5-methoxy-8-aminoquinoline reported by the groups of Magnier and Billard [140]. <sup>a</sup>Microwave, 100 °C, 1 h. <sup>b</sup>70 °C for 16 h. <sup>c</sup>20 mol % of Pd(CH<sub>3</sub>CN)<sub>2</sub>(Cl)<sub>2</sub>, 100 °C for 24 h.

## II. Transition-metal-catalyzed fluoroalkoxylation of (hetero)arenes by C–H bond activation

### II.1) Fluoroalkoxylation of aromatic C(sp<sup>2</sup>)–H bonds by transition-metal catalysis

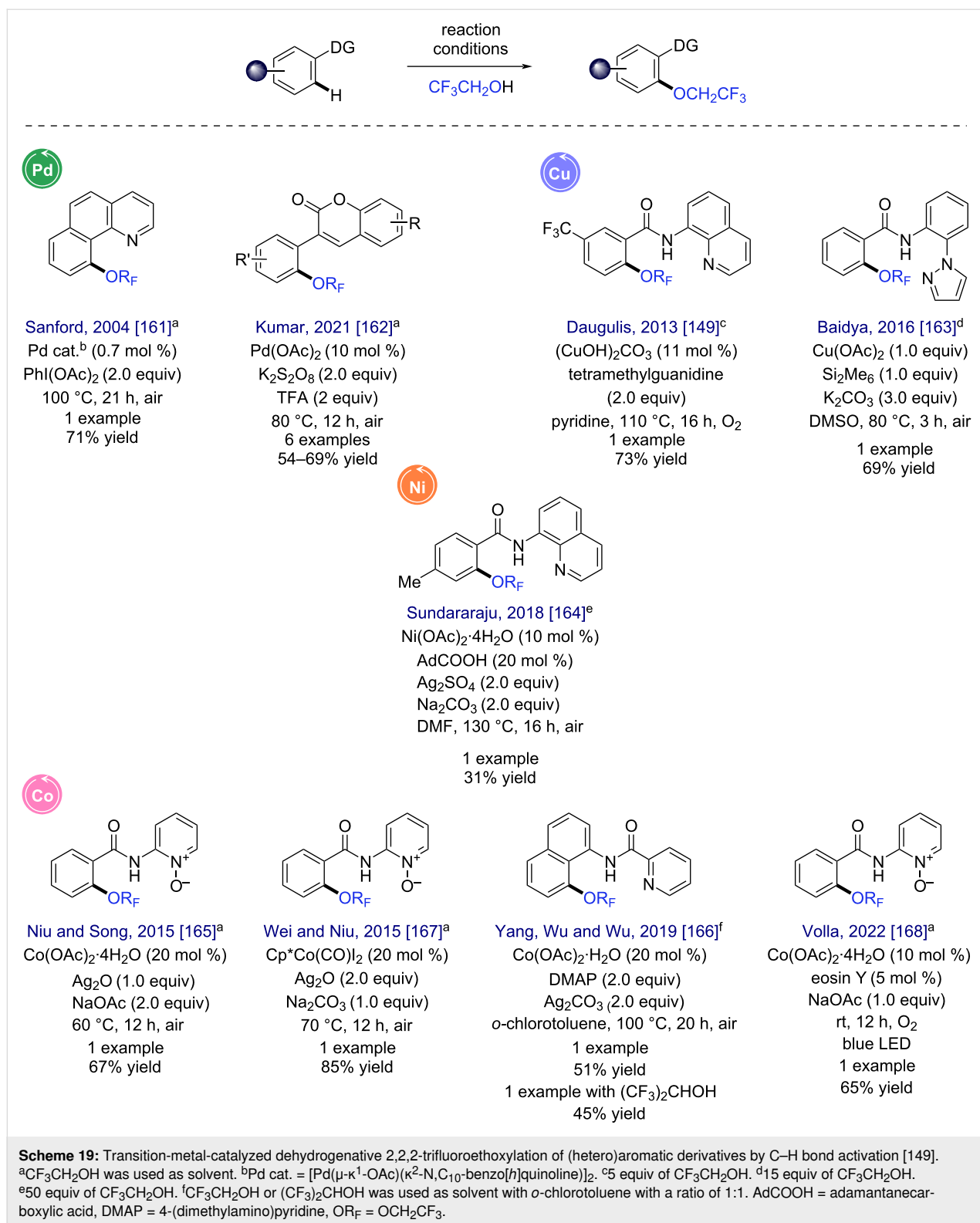
Over the last years, key advances have been made for the formation of a C(sp<sup>2</sup>)–OCHRCF<sub>3</sub> bond by transition-metal-catalyzed C–H bond activation. Indeed, fluorinated ethers [71,141–153] are key compounds, with especially molecules substituted with the 2,2,2-trifluoroethoxy moiety (OCH<sub>2</sub>CF<sub>3</sub>), an important fluorinated group found in several bioactive compounds such as flecanide [154,155] and lansoprazole [156], as flagship molecules. Although the transition-metal-catalyzed hydroxylation and alkoxylation have been studied especially under palladium catalysis [157,158], the direct dehydrogenative 2,2,2-trifluoroethoxylation of (hetero)arenes, often using 2,2,2-trifluoroethanol as a readily available, inexpensive, and green fluorination source [159,160], is still underexplored.

In 2004, Sanford and co-workers reported the dehydrogenative 2,2,2-trifluoroethoxylation of benzo[*h*]quinoline under palladium catalysis in the presence of PhI(OAc)<sub>2</sub> as oxidant (Scheme 19) [161]. Since this seminal work and in the course of their investigation towards the development of new methods for the alkoxylation of C(sp<sup>2</sup>) centers by transition-metal catalysis,

few examples of transition-metal-catalyzed dehydrogenative 2,2,2-trifluoroethoxylation reactions have been reported. In 2021, the palladium-catalyzed *ortho*-2,2,2-trifluoroethoxylation of 3-arylcoumarins was depicted by the group of Kumar (6 examples, up to 69% yield) [162]. Further developments unveiled the use of copper catalysts for such functionalization. In 2013, the group of Daugulis described the copper-catalyzed *ortho*-2,2,2-trifluoroethoxylation of a 3-trifluoromethylated benzamide derived from 8-aminoquinoline, giving the corresponding product in 73% yield [149]. The group of Baidya showed that the dehydrogenative 2,2,2-trifluoroethoxylation of benzamide with another bidentate directing group was also possible in the presence of Cu(OAc)<sub>2</sub> and hexamethyldisilane [163]. Using *N,N*- and *N,O*-bidentate directing groups, the construction of C(sp<sup>2</sup>)–OCH<sub>2</sub>CF<sub>3</sub> bonds by C–H bond activation was also reported using Ni [164] and Co catalysis [165–167]. In 2022, Volla and co-workers reported the *ortho*-2,2,2-trifluoroethoxylation of benzamide using an *N,O*-bidentate directing group by merging Co- and visible light organophotocatalysis [168].

**Palladium catalysis:** In 2017, Ji, Li and co-workers reported a thorough study on the Pd-catalyzed 2,2,2-trifluoroethoxylation of *N*-sulfonylbenzamides in the presence of PhI(OAc)<sub>2</sub> as oxidant and an excess of TFA (Scheme 20) [150]. The func-

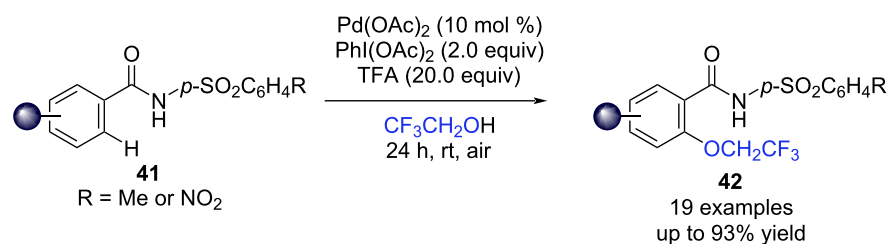




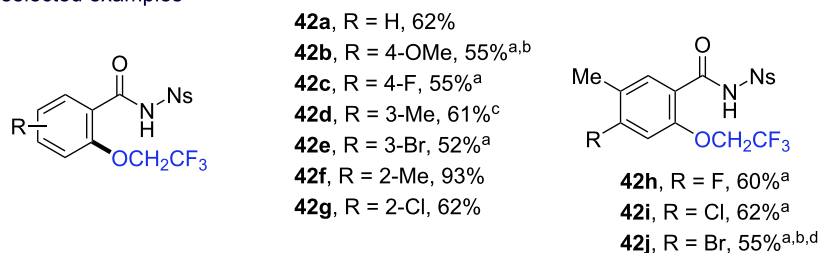
nalization of diversely substituted derivatives bearing either electron-donating groups (**41b**, **41d**, and **41f**) and electron-withdrawing groups (**41c**, **41e**, and **41g**) was achieved (19 examples, up to 93% yield). Of note, the transformation was also efficient

with disubstituted substrates such as **41h–j**. The authors suggested the following mechanism. After formation of the metal-lacycle **O**, the latter is oxidized leading to the Pd(IV) species **P**. After a ligand exchange, the intermediate **Q** is generated.

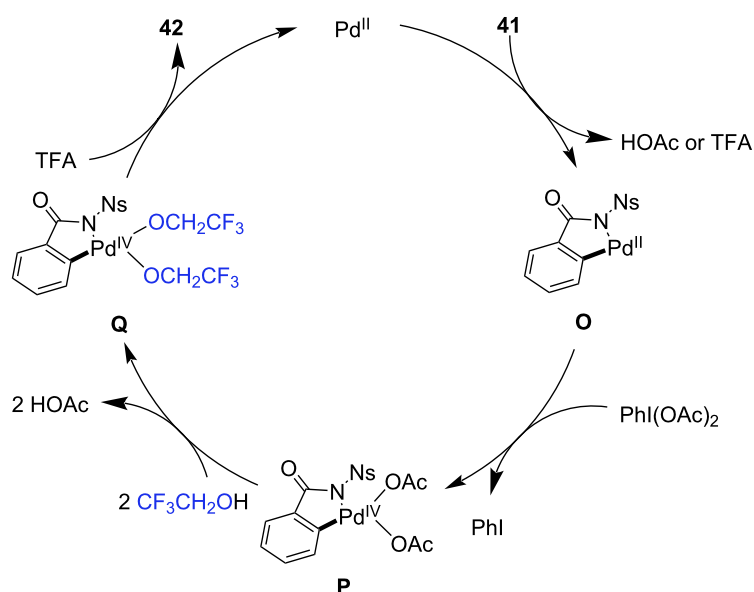
Ji and Li, 2017 [150]



selected examples



suggested mechanism



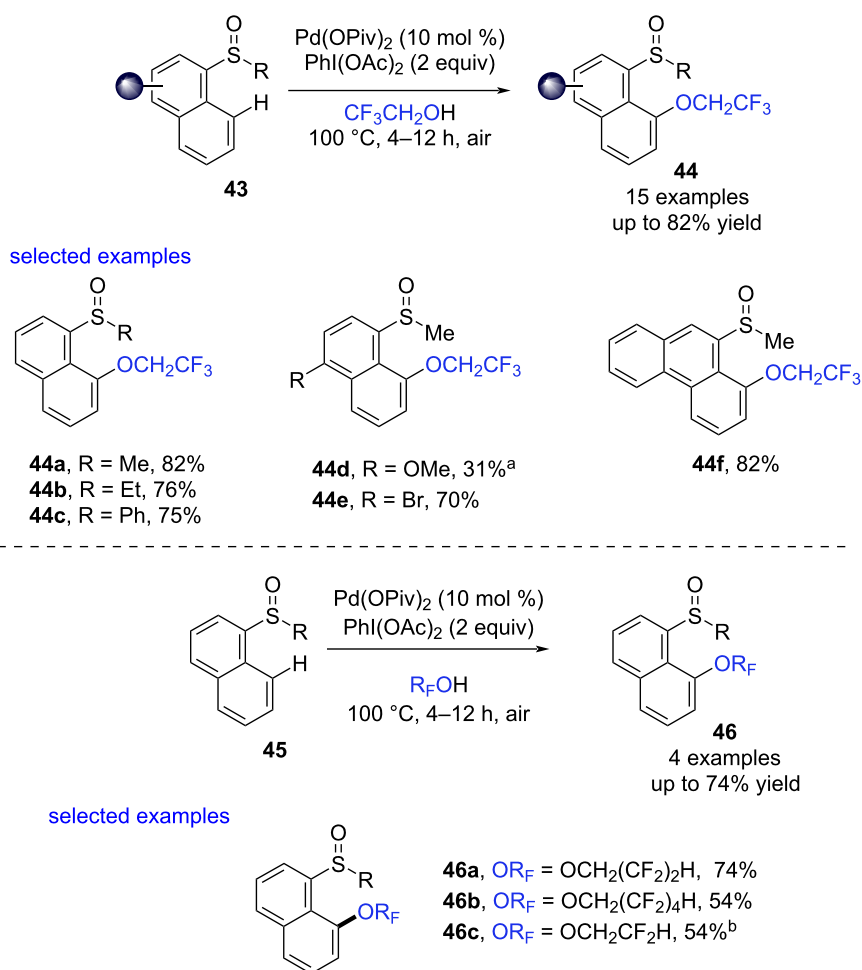
**Scheme 20:** Pd(II)-catalyzed *ortho*-2,2,2-trifluoroethoxylation of *N*-sulfonylbenzamides reported by the group of Ji and Li [150]. <sup>a</sup>50 °C. <sup>b</sup>15 equiv TFA. <sup>c</sup>5 equiv TFA. <sup>d</sup>*N*-acetylglycine (60 mol %). Ns: 4-nitrobenzenesulfonyl.

Finally, a reductive elimination step affords the expected functionalized product **42** and regenerates the catalyst.

The 2,2,2-trifluoroethoxylation reaction is not restricted to amides. In 2020, Yorimitsu and co-workers developed a methodology allowing the formation of a  $\text{C}(\text{sp}^2)\text{-OR}_\text{F}$  bond through palladium-catalyzed C–H bond activation [169]. Using  $\text{Pd}(\text{OPiv})_2$  as the catalyst in the presence of  $\text{PhI}(\text{OAc})_2$  (PIDA), the naphthalene sulfoxide **43a** was 2,2,2-trifluoroethoxylated in

82% yield (Scheme 21). The substituent of the sulfoxide part does not impact the efficiency of the reaction as illustrated by the synthesis of compounds **44b** and **44c**. The presence of an electron-donating substituent in the *para*-position of the directing group was found to be deleterious for the reaction since **44d** was obtained in 31% yield while its brominated analog **44e** was isolated in 70% yield. Mechanistic studies indicated that the C–H bond activation event was the rate-limiting step and the authors suggested a similar mechanism to the one

Yorimitsu, 2020 [169]



**Scheme 21:** Pd(II)-catalyzed selective 2,2,2-trifluoroethoxylation and other fluoroalkoxylation of naphthalene sulfoxide derivatives reported by the group of Yorimitsu [169]. <sup>a</sup>80 °C for 1 h. <sup>b</sup> $\text{R}_\text{F}\text{OH}/\text{AcOH}$  1:7.

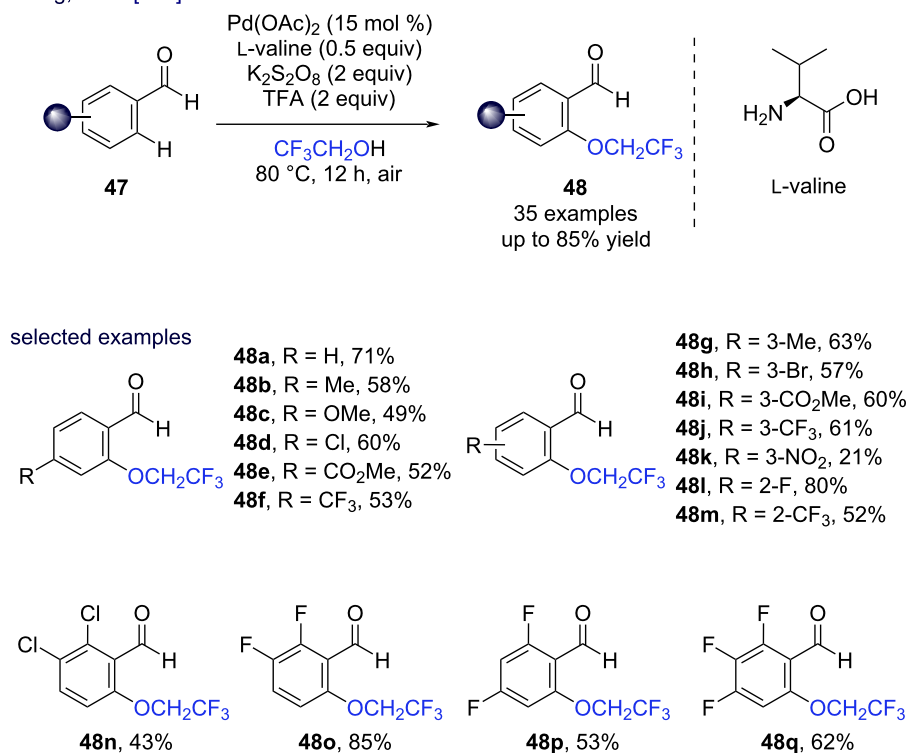
depicted in Scheme 20: formation of a palladacycle thanks to a concerted metalation deprotonation (CMD) process followed by oxidation, ligand exchange with  $\text{CF}_3\text{CH}_2\text{OH}$ , and finally, reductive elimination affording the expected product and regenerating the catalyst. Gratifyingly, the approach was applied to the incorporation of other fluorinated moieties such as  $\text{OCH}_2\text{CF}_2\text{H}$  and  $\text{OCH}_2(\text{CF}_2)_n\text{H}$  ( $n = 2$  or 4) and gave compounds **46a–c**.

Thanks to the transient directing group strategy [35,170–182], efficient methodologies for the functionalization of previously reluctant compounds such as benzaldehyde derivatives were developed, and key advances are depicted below.

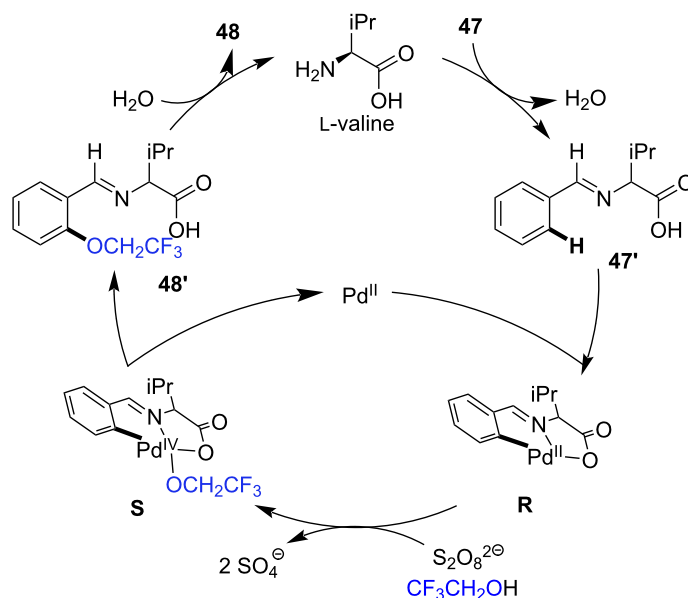
In 2021, Wang and co-workers described the selective palladium-catalyzed *ortho*-2,2,2-trifluoroethoxylation of a series of benzaldehydes (Scheme 22, 35 examples) using the amino acid

L-valine in the presence of  $\text{K}_2\text{S}_2\text{O}_8$  and TFA at 80 °C [153]. This reaction proved to be highly tolerant to various substituents including a  $\text{CF}_3$  group at the *ortho*-, *meta*- and *para*-positions (**48m**, **48j**, and **48f**, respectively), halogens (**48d**, **48h**, and **48l**), an ester moiety (**48e** and **48i**), and a methoxy group (**48c**). Note that even di- and trisubstituted benzaldehydes **47n–q** were smoothly functionalized under these conditions. The authors also suggested a plausible mechanism. The amino acid acts as an organocatalyst and first reacts with the benzaldehyde **47** to generate the transient directing group (**47'**). Then, formation of the palladacycle (species **R**) followed by its oxidation to a Pd(IV) intermediate and a ligand exchange with 2,2,2-trifluoroethanol leads to the formation of the species **S**. The latter complex **S** undergoes a reductive elimination leading to the compound **48'** along with the regeneration of the palladium catalyst. Finally, after hydrolysis of **48'**, the expected product **48** is afforded together with the organocatalyst.

Wang, 2021 [153]



suggested mechanism

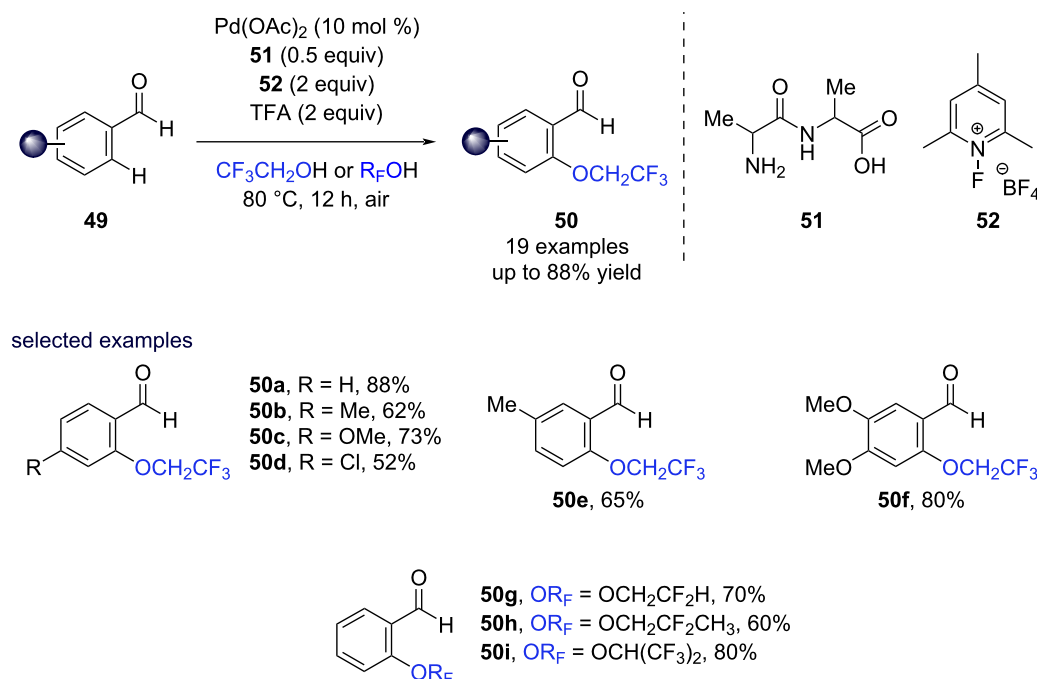


**Scheme 22:** Pd(II)-catalyzed selective *ortho*-2,2,2-trifluoroethoxylation of benzaldehyde derivatives by means of the transient directing group strategy as reported by the group of Wang [153].

Then, the group of Sun and Wang used a similar approach for the 2,2,2-trifluoroethoxylation of benzaldehydes under palladium catalysis using the amino acid **51** as organic catalyst in the

presence of the fluoropyridinium salt **52** (19 examples, up to 88% yield, Scheme 23) [183]. Pleasingly, the methodology was extended to the formation of  $\text{C}(\text{sp}^2)\text{--OR}_\text{F}$  bonds starting from

Sun and Wang, 2022 [183]



**Scheme 23:** Pd(II)-catalyzed selective *ortho*-2,2,2-trifluoroethoxylation (and other fluoroalkoxylation) of benzaldehyde derivatives via the assistance of a transient directing group reported by the group of Sun and Wang [183].

benzaldehyde ( $\text{OR}_\text{F}$  = 2,2-difluoroethoxy **50g**, 2,2-difluoropropoxy **50h**, and 1,1,1,3,3,3-hexafluoroisopropoxy **50i**).

## II.2) Fluoroalkoxylation of aliphatic $\text{C}(\text{sp}^3)\text{-H}$ bonds by transition-metal-catalysis

The functionalization of  $\text{C}(\text{sp}^3)$  centers by transition-metal-catalyzed C–H bond activation remains highly challenging [24,184–191]. In particular, the 2,2,2-trifluoroethoxylation of aliphatic derivatives is still limited to a handful of examples as illustrated by the two examples depicted in Scheme 24 [71,192]. Using a bidentate directing group (namely NHPA and CONHPIP for **53** and **55**, respectively), the groups of Chen [71] and Shi [192] independently reported the palladium-catalyzed selective 2,2,2-trifluoroethoxylation of aliphatic amines and amides at the  $\gamma$  and  $\beta$  positions, respectively, using trifluoroethanol as fluorination source in the presence of PIDA. Hence, an efficient access to the corresponding monoether derivatives **54** and **56** in 71% and 65%, respectively, were obtained.

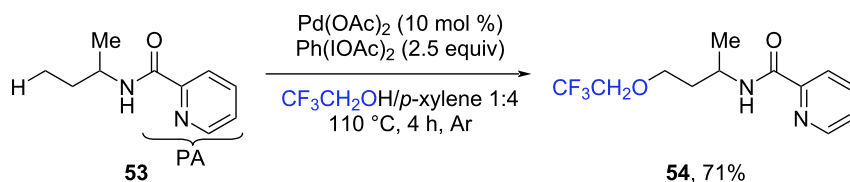
## Conclusion

In summary, this review provides an overview of the major developments made over the last years for the synthesis of fluorinated compounds by transition-metal-catalyzed C–H bond activation. This review focused on the construction of  $\text{C}(\text{sp}^2)\text{-XR}_\text{F}$  bonds and  $\text{C}(\text{sp}^3)\text{-XR}_\text{F}$  bonds with an emphasis on the trifluoro-

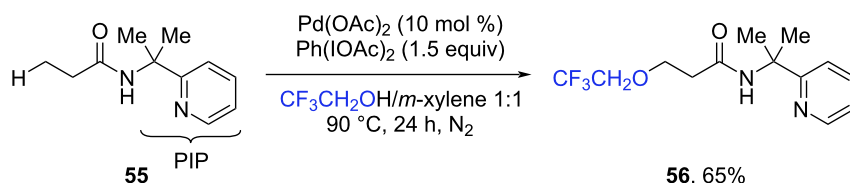
methylation reaction and transformations using emergent fluorinated residues ( $\text{SCF}_3$ ,  $\text{SeCF}_3$ ,  $\text{SCF}_2\text{H}$ ,  $\text{SCF}_2\text{CO}_2\text{Et}$  or  $\text{OCH}_2\text{CF}_3$  groups). Well-designed catalytic systems and suitable fluorinating sources were the key of success for these major developments.

Despite these advances, synthetic challenges still need to be overcome. These synthetic tools are so far still restricted to some fluorinated moieties and extension to other high value-added fluorinated residues [131,136,193–208] is of high importance. Besides, in comparison with the functionalization of  $\text{C}(\text{sp}^2)$  centers on aromatic and vinylic derivatives, transition-metal-catalyzed functionalization of  $\text{C}(\text{sp}^3)\text{-H}$  bonds remains largely underexplored to date. Furthermore, the development of enantioselective transformations allowing the synthesis of enantioenriched fluorine-containing compounds by transition-metal-catalyzed C–H bond activation will have a significant impact as for instance an access to pharmaceutically relevant derivatives. Finally, the use of abundant non-noble transition metals [209–211] in such reactions combined or not with modern technologies (photocatalysis and electrocatalysis) is still underexplored and any advances will be of high importance especially from a sustainability point of view aiming at developing greener synthetic routes towards fluorinated molecules.

Chen, 2012 [71]



Shi, 2013, [192]



**Scheme 24:** Pd(II)-catalyzed selective 2,2,2-trifluoroethoxylation of aliphatic amides using a bidentate directing group reported by the groups of Chen [71] and Shi [192].

## Funding

This work has been partially supported by University of Rouen Normandy, INSA Rouen Normandy, the Centre National de la Recherche Scientifique (CNRS), European Regional Development Fund (ERDF), Labex SynOrg (ANR-11-LABX-0029), Carnot Institute I2C, the graduate school for research XL-Chem (ANR-18-EURE-0020 XL CHEM), and Region Normandie. L.M. and T.B. thank the European Research Council (ERC) under the European Union's Horizon 2020 research and innovation program (grant agreement no. 758710). F.D. thanks Labex SynOrg (ANR-11-LABX-0029) and the Region Normandie (RIN 50% program) for a doctoral fellowship.

## ORCID® iDs

Louis Monsigny - <https://orcid.org/0000-0001-9325-1316>

Floriane Doche - <https://orcid.org/0000-0001-9317-3274>

Tatiana Besset - <https://orcid.org/0000-0003-4877-5270>

## References

- Smart, B. E. *J. Fluorine Chem.* **2001**, *109*, 3–11. doi:10.1016/s0022-1139(01)00375-x
- O'Hagan, D. *Chem. Soc. Rev.* **2008**, *37*, 308–319. doi:10.1039/b711844a
- Inoue, M.; Sumii, Y.; Shibata, N. *ACS Omega* **2020**, *5*, 10633–10640. doi:10.1021/acsomega.0c00830
- Wang, J.; Sánchez-Roselló, M.; Aceña, J. L.; del Pozo, C.; Sorochinsky, A. E.; Fustero, S.; Soloshonok, V. A.; Liu, H. *Chem. Rev.* **2014**, *114*, 2432–2506. doi:10.1021/cr4002879
- Landelle, G.; Panossian, A.; Pazenok, S.; Vors, J.-P.; Leroux, F. R. *Beilstein J. Org. Chem.* **2013**, *9*, 2476–2536. doi:10.3762/bjoc.9.287
- Purser, S.; Moore, P. R.; Swallow, S.; Gouverneur, V. *Chem. Soc. Rev.* **2008**, *37*, 320–330. doi:10.1039/b610213c
- Berger, R.; Resnati, G.; Metrangolo, P.; Weber, E.; Hulliger, J. *Chem. Soc. Rev.* **2011**, *40*, 3496–3508. doi:10.1039/c0cs00221f
- Fujiwara, T.; O'Hagan, D. *J. Fluorine Chem.* **2014**, *167*, 16–29. doi:10.1016/j.jfluchem.2014.06.014
- Ilardi, E. A.; Vitaku, E.; Njardarson, J. T. *J. Med. Chem.* **2014**, *57*, 2832–2842. doi:10.1021/jm401375q
- Gillis, E. P.; Eastman, K. J.; Hill, M. D.; Donnelly, D. J.; Meanwell, N. A. *J. Med. Chem.* **2015**, *58*, 8315–8359. doi:10.1021/acs.jmedchem.5b00258
- Zhou, Y.; Wang, J.; Gu, Z.; Wang, S.; Zhu, W.; Aceña, J. L.; Soloshonok, V. A.; Izawa, K.; Liu, H. *Chem. Rev.* **2016**, *116*, 422–518. doi:10.1021/acs.chemrev.5b00392
- Landelle, G.; Panossian, A.; Leroux, F. R. *Curr. Top. Med. Chem.* **2014**, *14*, 941–951. doi:10.2174/1568026614666140202210016
- Besset, T.; Poisson, T.; Pannecoucke, X. *Chem. – Eur. J.* **2014**, *20*, 16830–16845. doi:10.1002/chem.201404537
- Merino, E.; Nevado, C. *Chem. Soc. Rev.* **2014**, *43*, 6598–6608. doi:10.1039/c4cs00025k
- Champagne, P. A.; Desroches, J.; Hamel, J.-D.; Vandamme, M.; Paquin, J.-F. *Chem. Rev.* **2015**, *115*, 9073–9174. doi:10.1021/cr500706a
- Ni, C.; Hu, J. *Chem. Soc. Rev.* **2016**, *45*, 5441–5454. doi:10.1039/c6cs00351f
- Pan, Y. *ACS Med. Chem. Lett.* **2019**, *10*, 1016–1019. doi:10.1021/acsmchemlett.9b00235
- Nobile, E.; Castanheiro, T.; Besset, T. *Angew. Chem., Int. Ed.* **2021**, *60*, 12170–12191. doi:10.1002/anie.202009995
- Chen, X.; Engle, K. M.; Wang, D.-H.; Yu, J.-Q. *Angew. Chem., Int. Ed.* **2009**, *48*, 5094–5115. doi:10.1002/anie.200806273
- Giri, R.; Shi, B.-F.; Engle, K. M.; Maugel, N.; Yu, J.-Q. *Chem. Soc. Rev.* **2009**, *38*, 3242–3272. doi:10.1039/b816707a
- Jazzar, R.; Hitce, J.; Renaudat, A.; Sofack-Kreutzer, J.; Baudoin, O. *Chem. – Eur. J.* **2010**, *16*, 2654–2672. doi:10.1002/chem.200902374
- Lyons, T. W.; Sanford, M. S. *Chem. Rev.* **2010**, *110*, 1147–1169. doi:10.1021/cr900184e

23. Wencel-Delord, J.; Dröge, T.; Liu, F.; Glorius, F. *Chem. Soc. Rev.* **2011**, *40*, 4740–4761. doi:10.1039/c1cs15083a
24. Li, H.; Li, B.-J.; Shi, Z.-J. *Catal. Sci. Technol.* **2011**, *1*, 191–206. doi:10.1039/c0cy00076k
25. Ackermann, L. *Chem. Rev.* **2011**, *111*, 1315–1345. doi:10.1021/cr100412j
26. Kozhushkov, S. I.; Potukuchi, H. K.; Ackermann, L. *Catal. Sci. Technol.* **2013**, *3*, 562–571. doi:10.1039/c2cy20505j
27. Wang, K.; Hu, F.; Zhang, Y.; Wang, J. *Sci. China: Chem.* **2015**, *58*, 1252–1265. doi:10.1007/s11426-015-5362-5
28. Crabtree, R. H.; Lei, A. *Chem. Rev.* **2017**, *117*, 8481–8482. doi:10.1021/acs.chemrev.7b00307
29. Pototschnig, G.; Maulide, N.; Schnürch, M. *Chem. – Eur. J.* **2017**, *23*, 9206–9232. doi:10.1002/chem.201605657
30. Dong, Z.; Ren, Z.; Thompson, S. J.; Xu, Y.; Dong, G. *Chem. Rev.* **2017**, *117*, 9333–9403. doi:10.1021/acs.chemrev.6b00574
31. Sambiagio, C.; Schönbauer, D.; Blicke, R.; Dao-Huy, T.; Pototschnig, G.; Schaaf, P.; Wiesinger, T.; Zia, M. F.; Wencel-Delord, J.; Besset, T.; Maes, B. U. W.; Schnürch, M. *Chem. Soc. Rev.* **2018**, *47*, 6603–6743. doi:10.1039/c8cs00201k
32. Rej, S.; Ano, Y.; Chatani, N. *Chem. Rev.* **2020**, *120*, 1788–1887. doi:10.1021/acs.chemrev.9b00495
33. Chen, S.; Ranjan, P.; Voskressensky, L. G.; Van der Eycken, E. V.; Sharma, U. K. *Molecules* **2020**, *25*, 4970. doi:10.3390/molecules25214970
34. Lam, N. Y. S.; Wu, K.; Yu, J.-Q. *Angew. Chem., Int. Ed.* **2021**, *60*, 15767–15790. doi:10.1002/anie.202011901
35. Jacob, C.; Maes, B. U. W.; Evano, G. *Chem. – Eur. J.* **2021**, *27*, 13899–13952. doi:10.1002/chem.202101598
36. Dhawa, U.; Kaplaneris, N.; Ackermann, L. *Org. Chem. Front.* **2021**, *8*, 4886–4913. doi:10.1039/d1qo00727k
37. Dalton, T.; Faber, T.; Glorius, F. *ACS Cent. Sci.* **2021**, *7*, 245–261. doi:10.1021/acscentsci.0c01413
38. Dutta, U.; Maiti, S.; Bhattacharya, T.; Maiti, D. *Science* **2021**, *372*, 658–663. doi:10.1126/science.abd5992
39. Zhang, J.; Lu, X.; Shen, C.; Xu, L.; Ding, L.; Zhong, G. *Chem. Soc. Rev.* **2021**, *50*, 3263–3314. doi:10.1039/d0cs00447b
40. Rej, S.; Das, A.; Chatani, N. *Coord. Chem. Rev.* **2021**, *431*, 213683. doi:10.1016/j.ccr.2020.213683
41. Ahmad, M. S.; Meguellati, K. *ChemistrySelect* **2022**, *7*, e202103716. doi:10.1002/slct.202103716
42. Phukon, J.; Jyoti Borah, A.; Gogoi, S. *Asian J. Org. Chem.* **2022**, *11*, e202200581. doi:10.1002/ajoc.202200581
43. Mondal, A.; van Gemmeren, M. *Angew. Chem., Int. Ed.* **2022**, *61*, e202210825. doi:10.1002/anie.202210825
44. Petrone, D. A.; Ye, J.; Lautens, M. *Chem. Rev.* **2016**, *116*, 8003–8104. doi:10.1021/acs.chemrev.6b00089
45. Li, X.; Shi, X.; Li, X.; Shi, D. *Beilstein J. Org. Chem.* **2019**, *15*, 2213–2270. doi:10.3762/bjoc.15.218
46. Mazeh, S.; Lapuh, M. I.; Besset, T. *Chimia* **2020**, *74*, 871. doi:10.2533/chimia.2020.871
47. Egami, H. *Chem. Pharm. Bull.* **2020**, *68*, 491–511. doi:10.1248/cpb.c19-00856
48. Ruyet, L.; Besset, T. *Beilstein J. Org. Chem.* **2020**, *16*, 1051–1065. doi:10.3762/bjoc.16.92
49. Sindhe, H.; Chaudhary, B.; Chowdhury, N.; Kamble, A.; Kumar, V.; Lad, A.; Sharma, S. *Org. Chem. Front.* **2022**, *9*, 1742–1775. doi:10.1039/d1qo01544c
50. Liu, H.; Gu, Z.; Jiang, X. *Adv. Synth. Catal.* **2013**, *355*, 617–626. doi:10.1002/adsc.201200764
51. Cernak, T.; Dykstra, K. D.; Tyagarajan, S.; Vachal, P.; Krska, S. W. *Chem. Soc. Rev.* **2016**, *45*, 546–576. doi:10.1039/c5cs00628g
52. Moir, M.; Danon, J. J.; Reekie, T. A.; Kassiou, M. *Expert Opin. Drug Discovery* **2019**, *14*, 1137–1149. doi:10.1080/17460441.2019.1653850
53. Börgel, J.; Ritter, T. *Chem* **2020**, *6*, 1877–1887. doi:10.1016/j.chempr.2020.07.007
54. Chen, D. Y.-K.; Youn, S. W. *Chem. – Eur. J.* **2012**, *18*, 9452–9474. doi:10.1002/chem.201201329
55. Yamaguchi, J.; Yamaguchi, A. D.; Itami, K. *Angew. Chem., Int. Ed.* **2012**, *51*, 8960–9009. doi:10.1002/anie.201201666
56. Qiu, Y.; Gao, S. *Nat. Prod. Rep.* **2016**, *33*, 562–581. doi:10.1039/c5np00122f
57. Basu, D.; Kumar, S.; V, S. S.; Bandichhor, R. J. *Chem. Sci.* **2018**, *130*, 71. doi:10.1007/s12039-018-1468-6
58. Karimov, R. R.; Hartwig, J. F. *Angew. Chem., Int. Ed.* **2018**, *57*, 4234–4241. doi:10.1002/anie.201710330
59. Baudoin, O. *Angew. Chem., Int. Ed.* **2020**, *59*, 17798–17809. doi:10.1002/anie.202001224
60. Liang, T.; Neumann, C. N.; Ritter, T. *Angew. Chem., Int. Ed.* **2013**, *52*, 8214–8264. doi:10.1002/anie.201206566
61. Lin, A.; Huehls, C. B.; Yang, J. *Org. Chem. Front.* **2014**, *1*, 434–438. doi:10.1039/c4qo00020j
62. Li, Y.; Wu, Y.; Li, G.-S.; Wang, X.-S. *Adv. Synth. Catal.* **2014**, *356*, 1412–1418. doi:10.1002/adsc.201400101
63. Campbell, M. G.; Hoover, A. J.; Ritter, T. Transition Metal-Mediated and Metal-Catalyzed Carbon–Fluorine Bond Formation. In *Organometallic Fluorine Chemistry*; Braun, T.; Hughes, R. P., Eds.; Springer International Publishing: Cham, 2015; pp 1–53. doi:10.1007/3418\_2014\_88
64. Szpera, R.; Moseley, D. F. J.; Smith, L. B.; Sterling, A. J.; Gouverneur, V. *Angew. Chem., Int. Ed.* **2019**, *58*, 14824–14848. doi:10.1002/anie.201814457
65. McMurtrey, K. B.; Racowski, J. M.; Sanford, M. S. *Org. Lett.* **2012**, *14*, 4094–4097. doi:10.1021/ol301739f
66. Wu, T.; Cheng, J.; Chen, P.; Liu, G. *Chem. Commun.* **2013**, *49*, 8707–8709. doi:10.1039/c3cc44711a
67. Lou, S.-J.; Xu, D.-Q.; Xia, A.-B.; Wang, Y.-F.; Liu, Y.-K.; Du, X.-H.; Xu, Z.-Y. *Chem. Commun.* **2013**, *49*, 6218–6220. doi:10.1039/c3cc42220h
68. Brückl, T.; Baxter, R. D.; Ishihara, Y.; Baran, P. S. *Acc. Chem. Res.* **2012**, *45*, 826–839. doi:10.1021/ar200194b
69. Wang, X.; Truesdale, L.; Yu, J.-Q. *J. Am. Chem. Soc.* **2010**, *132*, 3648–3649. doi:10.1021/ja909522s
70. Ye, Y.; Ball, N. D.; Kampf, J. W.; Sanford, M. S. *J. Am. Chem. Soc.* **2010**, *132*, 14682–14687. doi:10.1021/ja107780w
71. Zhang, S.-Y.; He, G.; Zhao, Y.; Wright, K.; Nack, W. A.; Chen, G. *J. Am. Chem. Soc.* **2012**, *134*, 7313–7316. doi:10.1021/ja3023972
72. Zhang, L.-S.; Chen, K.; Chen, G.; Li, B.-J.; Luo, S.; Guo, Q.-Y.; Wei, J.-B.; Shi, Z.-J. *Org. Lett.* **2013**, *15*, 10–13. doi:10.1021/ol302814x
73. Miura, M.; Feng, C.-G.; Ma, S.; Yu, J.-Q. *Org. Lett.* **2013**, *15*, 5258–5261. doi:10.1021/ol402471y
74. Zou, L.; Li, P.; Wang, B.; Wang, L. *Chem. Commun.* **2019**, *55*, 3737–3740. doi:10.1039/c9cc01014a
75. Cai, S.; Chen, C.; Sun, Z.; Xi, C. *Chem. Commun.* **2013**, *49*, 4552–4554. doi:10.1039/c3cc41331d
76. Feng, C.; Loh, T.-P. *Angew. Chem., Int. Ed.* **2013**, *52*, 12414–12417. doi:10.1002/anie.201307245

77. Besset, T.; Cahard, D.; Pannecoucke, X. *J. Org. Chem.* **2014**, *79*, 413–418. doi:10.1021/jo402385g
78. Vuagnat, M.; Jubault, P.; Besset, T. Pd-Catalyzed C–Chalcogen Bond Formation (C–S, C–Se) by C–H Bond Activation. In *Handbook of CH-Functionalization*; Maiti, D., Ed.; Wiley-VCH: Germany, 2022; pp 1–25. doi:10.1002/9783527834242.chf0017
79. Leo, A.; Hansch, C.; Elkins, D. *Chem. Rev.* **1971**, *71*, 525–616. doi:10.1021/cr60274a001
80. Hansch, C.; Leo, A.; Taft, R. W. *Chem. Rev.* **1991**, *91*, 165–195. doi:10.1021/cr00002a004
81. Toulgoat, F.; Alazet, S.; Billard, T. *Eur. J. Org. Chem.* **2014**, 2415–2428. doi:10.1002/ejoc.201301857
82. Xu, X.-H.; Matsuzaki, K.; Shibata, N. *Chem. Rev.* **2015**, *115*, 731–764. doi:10.1021/cr500193b
83. Barata-Vallejo, S.; Bonesi, S.; Postigo, A. *Org. Biomol. Chem.* **2016**, *14*, 7150–7182. doi:10.1039/c6ob00763e
84. Li, M.; Guo, J.; Xue, X.-S.; Cheng, J.-P. *Org. Lett.* **2016**, *18*, 264–267. doi:10.1021/acs.orglett.5b03433
85. Zheng, H.; Huang, Y.; Weng, Z. *Tetrahedron Lett.* **2016**, *57*, 1397–1409. doi:10.1016/j.tetlet.2016.02.073
86. Boiko, V. N. *Beilstein J. Org. Chem.* **2010**, *6*, 880–921. doi:10.3762/bjoc.6.88
87. Li, X.; Zhao, J.; Zhang, L.; Hu, M.; Wang, L.; Hu, J. *Org. Lett.* **2015**, *17*, 298–301. doi:10.1021/ol5034018
88. Ye, K.-Y.; Zhang, X.; Dai, L.-X.; You, S.-L. *J. Org. Chem.* **2014**, *79*, 12106–12110. doi:10.1021/jo5019393
89. Lefebvre, Q.; Fava, E.; Nikolaienko, P.; Rueping, M. *Chem. Commun.* **2014**, *50*, 6617–6619. doi:10.1039/c4cc02060j
90. Liu, J.-B.; Xu, X.-H.; Chen, Z.-H.; Qing, F.-L. *Angew. Chem., Int. Ed.* **2015**, *54*, 897–900. doi:10.1002/anie.201409983
91. Jiang, L.; Qian, J.; Yi, W.; Lu, G.; Cai, C.; Zhang, W. *Angew. Chem., Int. Ed.* **2015**, *54*, 14965–14969. doi:10.1002/anie.201508495
92. Zheng, J.; Wang, L.; Lin, J.-H.; Xiao, J.-C.; Liang, S. H. *Angew. Chem., Int. Ed.* **2015**, *54*, 13236–13240. doi:10.1002/anie.201505446
93. Yin, G.; Kalvet, I.; Schoenebeck, F. *Angew. Chem., Int. Ed.* **2015**, *54*, 6809–6813. doi:10.1002/anie.201501617
94. Candish, L.; Pitzer, L.; Gómez-Suárez, A.; Glorius, F. *Chem. – Eur. J.* **2016**, *22*, 4753–4756. doi:10.1002/chem.201600421
95. Matheis, C.; Wagner, V.; Goossen, L. J. *Chem. – Eur. J.* **2016**, *22*, 79–82. doi:10.1002/chem.201503524
96. Jarrige, L.; Carboni, A.; Dagousset, G.; Levitre, G.; Magnier, E.; Masson, G. *Org. Lett.* **2016**, *18*, 2906–2909. doi:10.1021/acs.orglett.6b01257
97. Liu, X.; An, R.; Zhang, X.; Luo, J.; Zhao, X. *Angew. Chem., Int. Ed.* **2016**, *55*, 5846–5850. doi:10.1002/anie.201601713
98. Xiong, H.-Y.; Pannecoucke, X.; Besset, T. *Org. Chem. Front.* **2016**, *3*, 620–624. doi:10.1039/c6qo00064a
99. Yang, Y.; Xu, L.; Yu, S.; Liu, X.; Zhang, Y.; Vicić, D. A. *Chem. – Eur. J.* **2016**, *22*, 858–863. doi:10.1002/chem.201504790
100. Wang, F.; Zhao, L.; You, J.; Wang, M.-X. *Org. Chem. Front.* **2016**, *3*, 880–886. doi:10.1039/c6qo00161k
101. Bu, M.-j.; Lu, G.-p.; Cai, C. *Org. Chem. Front.* **2017**, *4*, 266–270. doi:10.1039/c6qo00622a
102. Lübecke, M.; Yuan, W.; Szabó, K. J. *Org. Lett.* **2017**, *19*, 4548–4551. doi:10.1021/acs.orglett.7b02139
103. Carbonnel, E.; Besset, T.; Poisson, T.; Labar, D.; Pannecoucke, X.; Jubault, P. *Chem. Commun.* **2017**, *53*, 5706–5709. doi:10.1039/c7cc02652h
104. Zhao, Q.; Poisson, T.; Pannecoucke, X.; Bouillon, J.-P.; Besset, T. *Org. Lett.* **2017**, *19*, 5106–5109. doi:10.1021/acs.orglett.7b02384
105. Gelat, F.; Poisson, T.; Biju, A. T.; Pannecoucke, X.; Besset, T. *Eur. J. Org. Chem.* **2018**, 3693–3696. doi:10.1002/ejoc.201800418
106. Zhao, Q.; Chen, M.-Y.; Poisson, T.; Pannecoucke, X.; Bouillon, J.-P.; Besset, T. *Eur. J. Org. Chem.* **2018**, 6167–6175. doi:10.1002/ejoc.201801071
107. Ghiazza, C.; Khrouz, L.; Monnereau, C.; Billard, T.; Tlili, A. *Chem. Commun.* **2018**, *54*, 9909–9912. doi:10.1039/c8cc05256e
108. Saravanan, P.; Anbarasan, P. *Adv. Synth. Catal.* **2018**, *360*, 2894–2899. doi:10.1002/adsc.201800366
109. Xi, C.-C.; Chen, Z.-M.; Zhang, S.-Y.; Tu, Y.-Q. *Org. Lett.* **2018**, *20*, 4227–4230. doi:10.1021/acs.orglett.8b01627
110. He, J.; Chen, C.; Fu, G. C.; Peters, J. C. *ACS Catal.* **2018**, *8*, 11741–11748. doi:10.1021/acscatal.8b04094
111. Lindberg, E.; Angerani, S.; Anzola, M.; Winssinger, N. *Nat. Commun.* **2018**, *9*, 3539. doi:10.1038/s41467-018-05916-9
112. Zhang, J.; Yang, J.-D.; Zheng, H.; Xue, X.-S.; Mayr, H.; Cheng, J.-P. *Angew. Chem., Int. Ed.* **2018**, *57*, 12690–12695. doi:10.1002/anie.201805859
113. Luo, Z.; Yang, X.; Tsui, G. C. *Org. Lett.* **2020**, *22*, 6155–6159. doi:10.1021/acs.orglett.0c02235
114. Tran, L. D.; Popov, I.; Daugulis, O. *J. Am. Chem. Soc.* **2012**, *134*, 18237–18240. doi:10.1021/ja3092278
115. Tyrre, W.; Naumann, D.; Hoge, B.; Yagupolskii, Y. L. *J. Fluorine Chem.* **2003**, *119*, 101–107. doi:10.1016/s0022-1139(02)00276-2
116. Scatollin, T.; Pu, M.; Schoenebeck, F. *Chem. – Eur. J.* **2018**, *24*, 567–571. doi:10.1002/chem.201705240
117. Xu, C.; Shen, Q. *Org. Lett.* **2014**, *16*, 2046–2049. doi:10.1021/ol5006533
118. Whitfield, S. R.; Sanford, M. S. *J. Am. Chem. Soc.* **2007**, *129*, 15142–15143. doi:10.1021/ja077866q
119. Yin, W.; Wang, Z.; Huang, Y. *Adv. Synth. Catal.* **2014**, *356*, 2998–3006. doi:10.1002/adsc.201400362
120. Xu, J.; Chen, P.; Ye, J.; Liu, G. *Acta Chim. Sin. (Chin. Ed.)* **2015**, *73*, 1294–1297. doi:10.6023/a15030211
121. Kesavan, A.; Chaitanya, M.; Anbarasan, P. *Eur. J. Org. Chem.* **2018**, 3276–3279. doi:10.1002/ejoc.201800451
122. Alazet, S.; Zimmer, L.; Billard, T. *Chem. – Eur. J.* **2014**, *20*, 8589–8593. doi:10.1002/chem.201403409
123. Wang, Q.; Xie, F.; Li, X. *J. Org. Chem.* **2015**, *80*, 8361–8366. doi:10.1021/acs.joc.5b00940
124. Liu, X.-G.; Li, Q.; Wang, H. *Adv. Synth. Catal.* **2017**, *359*, 1942–1946. doi:10.1002/adsc.201700066
125. Yoshida, M.; Kawai, K.; Tanaka, R.; Yoshino, T.; Matsunaga, S. *Chem. Commun.* **2017**, *53*, 5974–5977. doi:10.1039/c7cc03072j
126. Xiong, H.-Y.; Besset, T.; Cahard, D.; Pannecoucke, X. *J. Org. Chem.* **2015**, *80*, 4204–4212. doi:10.1021/acs.joc.5b00505
127. Bouchard, A.; Kairouz, V.; Manneveau, M.; Xiong, H.-Y.; Besset, T.; Pannecoucke, X.; Lebel, H. *J. Flow Chem.* **2019**, *9*, 9–12. doi:10.1007/s41981-018-0023-4
128. Xiong, H.-Y.; Pannecoucke, X.; Besset, T. *Chem. – Eur. J.* **2016**, *22*, 16734–16749. doi:10.1002/chem.201603438
129. Xiao, X.; Zheng, Z.-T.; Li, T.; Zheng, J.-L.; Tao, T.; Chen, L.-M.; Gu, J.-Y.; Yao, X.; Lin, J.-H.; Xiao, J.-C. *Synthesis* **2020**, *52*, 197–207. doi:10.1055/s-0039-1690714
130. Pannecoucke, X.; Besset, T. *Org. Biomol. Chem.* **2019**, *17*, 1683–1693. doi:10.1039/c8ob02995d



131. Besset, T.; Poisson, T. Extension to the SCF<sub>2</sub>H, SCH<sub>2</sub>F, and SCF<sub>2</sub>R Motifs (R = PO(OEt)<sub>2</sub>, CoO<sub>2</sub>R, R<sub>F</sub>). In *Emerging Fluorinated Motifs*; Ma, J.-A.; Cahard, D., Eds.; Wiley VCH: Germany, 2020; pp 449–475. doi:10.1002/9783527824342.ch16
132. Xiong, H.-Y.; Bayle, A.; Pannecoucke, X.; Besset, T. *Angew. Chem., Int. Ed.* **2016**, *55*, 13490–13494. doi:10.1002/anie.201607231
133. Shen, F.; Zhang, P.; Lu, L.; Shen, Q. *Org. Lett.* **2017**, *19*, 1032–1035. doi:10.1021/acs.orglett.7b00010
134. Ismailaj, E.; Glenadel, Q.; Billard, T. *Eur. J. Org. Chem.* **2017**, 1911–1914. doi:10.1002/ejoc.201700103
135. Wang, J.; Xiong, H.-Y.; Petit, E.; Bailly, L.; Pannecoucke, X.; Poisson, T.; Besset, T. *Chem. Commun.* **2019**, *55*, 8784–8787. doi:10.1039/c9cc01851d
136. Petit-Cancelier, F.; François, B.; Pannecoucke, X.; Couve-Bonnaire, S.; Besset, T. *Adv. Synth. Catal.* **2020**, *362*, 760–764. doi:10.1002/adsc.201901454
137. Xiang, T.; Liu, Y.; Xu, Q.; He, K.; Pan, F. *J. Org. Chem.* **2022**, *87*, 3135–3144. doi:10.1021/acs.joc.1c02881
138. Doche, F.; Escudero, J.; Petit-Cancelier, F.; Xiong, H.-Y.; Couve-Bonnaire, S.; Audisio, D.; Poisson, T.; Besset, T. *Chem. – Eur. J.* **2022**, *28*, e202202099. doi:10.1002/chem.202202099
139. Grollier, K.; Chefdeville, E.; Jeanneau, E.; Billard, T. *Chem. – Eur. J.* **2021**, *27*, 12910–12916. doi:10.1002/chem.202102121
140. de Zordo-Banliat, A.; Grollier, K.; Vigier, J.; Jeanneau, E.; Dagousset, G.; Pegot, B.; Magnier, E.; Billard, T. *Chem. – Eur. J.* **2022**, *28*, e202202299. doi:10.1002/chem.202202299
141. Huang, Y.; Huang, R.; Weng, Z. *Synlett* **2015**, *26*, 2327–2331. doi:10.1055/s-0035-1560054
142. Pethő, B.; Novák, Z. *Asian J. Org. Chem.* **2019**, *8*, 568–575. doi:10.1002/ajoc.201800414
143. Jeschke, P.; Baston, E.; Leroux, R. F. *Mini-Rev. Med. Chem.* **2007**, *7*, 1027–1034. doi:10.2174/138955707782110150
144. Idoux, J. P.; Madenwald, M. L.; Garcia, B. S.; Chu, D. L.; Gupton, J. T. *J. Org. Chem.* **1985**, *50*, 1876–1878. doi:10.1021/jo00211a018
145. Shen, X.; Neumann, C. N.; Kleinlein, C.; Goldberg, N. W.; Ritter, T. *Angew. Chem., Int. Ed.* **2015**, *54*, 5662–5665. doi:10.1002/anie.201500902
146. Pethő, B.; Zwillinger, M.; Csenki, J. T.; Káncz, A. E.; Krámos, B.; Müller, J.; Balogh, G. T.; Novák, Z. *Chem. – Eur. J.* **2017**, *23*, 15628–15632. doi:10.1002/chem.201704205
147. Vuluga, D.; Legros, J.; Crousse, B.; Bonnet-Delpon, D. *Eur. J. Org. Chem.* **2009**, 3513–3518. doi:10.1002/ejoc.200900303
148. Zhang, K.; Xu, X.-H.; Qing, F.-L. *J. Fluorine Chem.* **2017**, *196*, 24–31. doi:10.1016/j.jfluchem.2016.07.008
149. Roane, J.; Daugulis, O. *Org. Lett.* **2013**, *15*, 5842–5845. doi:10.1021/ol402904d
150. Yang, L.; Li, S.; Cai, L.; Ding, Y.; Fu, L.; Cai, Z.; Ji, H.; Li, G. *Org. Lett.* **2017**, *19*, 2746–2749. doi:10.1021/acs.orglett.7b01103
151. Maiti, S.; Alam, T.; Mal, P. *Asian J. Org. Chem.* **2018**, *7*, 715–719. doi:10.1002/ajoc.201800069
152. Xu, X.; Xia, C.; Li, X.; Sun, J.; Hao, L. *RSC Adv.* **2020**, *10*, 2016–2026. doi:10.1039/c9ra10194b
153. Jin, L.; Zhang, X.-L.; Guo, R.-L.; Wang, M.-Y.; Gao, Y.-R.; Wang, Y.-Q. *Org. Lett.* **2021**, *23*, 1921–1927. doi:10.1021/acs.orglett.1c00365
154. Tamargo, J.; Le Heuzey, J.-Y.; Mabo, P. *Eur. J. Clin. Pharmacol.* **2015**, *71*, 549–567. doi:10.1007/s00228-015-1832-0
155. Paolini, E.; Stronati, G.; Guerra, F.; Capucci, A. *Pharmacol. Res.* **2019**, *148*, 104443. doi:10.1016/j.phrs.2019.104443
156. Matheson, A. J.; Jarvis, B. *Drugs* **2001**, *61*, 1801–1833. doi:10.2165/00003495-200161120-00011
157. Liu, B.; Shi, B.-F. *Tetrahedron Lett.* **2015**, *56*, 15–22. doi:10.1016/j.tetlet.2014.11.039
158. Enthaler, S.; Company, A. *Chem. Soc. Rev.* **2011**, *40*, 4912–4924. doi:10.1039/c1cs15085e
159. Kauffman, G. B. *Angew. Chem., Int. Ed.* **2008**, *47*, 8155–8156. doi:10.1002/anie.200885643
160. Shuklov, I. A.; Dubrovina, N. V.; Börner, A. *Synthesis* **2007**, 2925–2943. doi:10.1055/s-2007-983902
161. Dick, A. R.; Hull, K. L.; Sanford, M. S. *J. Am. Chem. Soc.* **2004**, *126*, 2300–2301. doi:10.1021/ja031543m
162. Shinde, V. N.; Rangan, K.; Kumar, D.; Kumar, A. *J. Org. Chem.* **2021**, *86*, 9755–9770. doi:10.1021/acs.joc.1c01097
163. Selvakumar, J.; Grandhi, G. S.; Sahoo, H.; Baidya, M. *RSC Adv.* **2016**, *6*, 79361–79365. doi:10.1039/c6ra18861c
164. Rajesh, N.; Sundararaju, B. *Asian J. Org. Chem.* **2018**, *7*, 1368–1371. doi:10.1002/ajoc.201800286
165. Zhang, L.-B.; Hao, X.-Q.; Zhang, S.-K.; Liu, Z.-J.; Zheng, X.-X.; Gong, J.-F.; Niu, J.-L.; Song, M.-P. *Angew. Chem., Int. Ed.* **2015**, *54*, 272–275. doi:10.1002/anie.201409751
166. Zhang, T.; Zhu, H.; Yang, F.; Wu, Y.; Wu, Y. *Tetrahedron* **2019**, *75*, 1541–1547. doi:10.1016/j.tet.2019.02.002
167. Guo, X.-K.; Zhang, L.-B.; Wei, D.; Niu, J.-L. *Chem. Sci.* **2015**, *6*, 7059–7071. doi:10.1039/c5sc01807b
168. Kumar, S.; Nair, A. M.; Volla, C. M. R. *Chem. – Asian J.* **2022**, *17*, e202200801. doi:10.1002/asia.202200801
169. Sato, T.; Nogi, K.; Yorimitsu, H. *ChemCatChem* **2020**, *12*, 3467–3471. doi:10.1002/cctc.202000485
170. Gong, W.; Zhang, G.; Liu, T.; Giri, R.; Yu, J.-Q. *J. Am. Chem. Soc.* **2014**, *136*, 16940–16946. doi:10.1021/ja510233h
171. Sun, H.; Guimond, N.; Huang, Y. *Org. Biomol. Chem.* **2016**, *14*, 8389–8397. doi:10.1039/c6ob01258b
172. Afewerki, S.; Córdova, A. *Chem. Rev.* **2016**, *116*, 13512–13570. doi:10.1021/acs.chemrev.6b00226
173. Kim, D.-S.; Park, W.-J.; Jun, C.-H. *Chem. Rev.* **2017**, *117*, 8977–9015. doi:10.1021/acs.chemrev.6b00554
174. Zhao, Q.; Poisson, T.; Pannecoucke, X.; Besset, T. *Synthesis* **2017**, *49*, 4808–4826. doi:10.1055/s-0036-1590878
175. Gandeepan, P.; Ackermann, L. *Chem* **2018**, *4*, 199–222. doi:10.1016/j.chempr.2017.11.002
176. Bhattacharya, T.; Pimparkar, S.; Maiti, D. *RSC Adv.* **2018**, *8*, 19456–19464. doi:10.1039/c8ra03230k
177. St John-Campbell, S.; Bull, J. A. *Org. Biomol. Chem.* **2018**, *16*, 4582–4595. doi:10.1039/c8ob00926k
178. Rasheed, O. K.; Sun, B. *ChemistrySelect* **2018**, *3*, 5689–5708. doi:10.1002/slct.201801097
179. Wu, Y.; Shi, B. *Chin. J. Org. Chem.* **2020**, *40*, 3517. doi:10.6023/cjoc202003057
180. Niu, B.; Yang, K.; Lawrence, B.; Ge, H. *ChemSusChem* **2019**, *12*, 2955–2969. doi:10.1002/cssc.201900151
181. Lapuh, M. I.; Mazeh, S.; Besset, T. *ACS Catal.* **2020**, *10*, 12898–12919. doi:10.1021/acscatal.0c03317
182. Higham, J. I.; Bull, J. A. *Org. Biomol. Chem.* **2020**, *18*, 7291–7315. doi:10.1039/d0ob01587c
183. Tian, M.; Shao, L.; Su, X.; Zhou, X.; Zhang, H.; Wei, K.; Sun, R.; Wang, J. *RSC Adv.* **2022**, *12*, 18722–18727. doi:10.1039/d2ra00241h
184. Xu, Y.; Dong, G. *Chem. Sci.* **2018**, *9*, 1424–1432. doi:10.1039/c7sc04768a

185. He, C.; Whitehurst, W. G.; Gaunt, M. J. *Chem* **2019**, *5*, 1031–1058. doi:10.1016/j.chempr.2018.12.017
186. Zhang, M.; Wang, Q.; Peng, Y.; Chen, Z.; Wan, C.; Chen, J.; Zhao, Y.; Zhang, R.; Zhang, A. Q. *Chem. Commun.* **2019**, *55*, 13048–13065. doi:10.1039/c9cc06609h
187. Uttry, A.; van Gemmeren, M. *Synthesis* **2020**, *52*, 479–488. doi:10.1055/s-0039-1690720
188. Liu, B.; Romine, A. M.; Rubel, C. Z.; Engle, K. M.; Shi, B.-F. *Chem. Rev.* **2021**, *121*, 14957–15074. doi:10.1021/acs.chemrev.1c00519
189. Panda, P.; Pal, K.; Chakroborty, S. *Results Chem.* **2021**, *3*, 100154. doi:10.1016/j.rechem.2021.100154
190. Sen, S.; Das, J.; Maiti, D. *Tetrahedron Chem* **2022**, *1*, 100005. doi:10.1016/j.tchem.2022.100005
191. Xie, J.; Zhu, C. Transition Metal-Catalyzed, Directing Group-Assisted C(Sp<sup>3</sup>)–H Bond Functionalization. In *Sustainable C(sp<sup>3</sup>)–H Bond Functionalization*; Xie, J.; Zhu, C., Eds.; SpringerBriefs in Molecular Science; Springer: Berlin, Heidelberg, 2016; pp 1–23. doi:10.1007/978-3-662-49496-7\_1
192. Chen, F.-J.; Zhao, S.; Hu, F.; Chen, K.; Zhang, Q.; Zhang, S.-Q.; Shi, B.-F. *Chem. Sci.* **2013**, *4*, 4187–4192. doi:10.1039/c3sc51993g
193. Ma, J.-A.; Cahard, D., Eds. *Emerging Fluorinated Motifs: Synthesis, Properties and Applications*; Wiley-VCH: Germany, 2020; Vol. 2. doi:10.1002/9783527824342
194. Li, Y.; Yang, Y.; Xin, J.; Tang, P. *Nat. Commun.* **2020**, *11*, 755. doi:10.1038/s41467-020-14598-1
195. Duhail, T.; Bortolato, T.; Mateos, J.; Anselmi, E.; Jelier, B.; Togni, A.; Magnier, E.; Dagousset, G.; Dell'Amico, L. *Org. Lett.* **2021**, *23*, 7088–7093. doi:10.1021/acs.orglett.1c02494
196. Wang, Q.; Zhang, X.; Sorochinsky, A. E.; Butler, G.; Han, J.; Soloshonok, V. A. *Symmetry* **2021**, *13*, 2380. doi:10.3390/sym13122380
197. Barata-Vallejo, S.; Bonesi, S. M.; Postigo, A. *Chem. – Eur. J.* **2022**, *28*, e202201776. doi:10.1002/chem.202201776
198. Lee, K. N.; Lee, J. W.; Ngai, M.-Y. *Tetrahedron* **2018**, *74*, 7127–7135. doi:10.1016/j.tet.2018.09.020
199. Han, Q.; Zhao, C.; Zhang, C. *Chin. J. Org. Chem.* **2019**, *39*, 84. doi:10.6023/cjoc201808029
200. Tóth, B. L.; Kovács, S.; Sályi, G.; Novák, Z. *Angew. Chem., Int. Ed.* **2016**, *55*, 1988–1992. doi:10.1002/anie.201510555
201. Ruyet, L.; Lapuh, M. I.; Koshti, V. S.; Földesi, T.; Jubault, P.; Poisson, T.; Novák, Z.; Besset, T. *Chem. Commun.* **2021**, *57*, 6241–6244. doi:10.1039/d1cc02007b
202. Dong, L.; Feng, T.; Xiong, D.; Xu, Z.; Cheng, J.; Xu, X.; Shao, X.; Li, Z. *Org. Lett.* **2022**, *24*, 1913–1917. doi:10.1021/acs.orglett.2c00245
203. Solas, D.; Hale, R. L.; Patel, D. V. *J. Org. Chem.* **1996**, *61*, 1537–1539. doi:10.1021/jo9517508
204. Lu, Y.; Liu, C.; Chen, Q.-Y. *Curr. Org. Chem.* **2015**, *19*, 1638–1650. doi:10.2174/1385272819666150615235605
205. Rong, J.; Ni, C.; Hu, J. *Asian J. Org. Chem.* **2017**, *6*, 139–152. doi:10.1002/ajoc.201600509
206. Yerien, D. E.; Barata-Vallejo, S.; Postigo, A. *Chem. – Eur. J.* **2017**, *23*, 14676–14701. doi:10.1002/chem.201702311
207. Feng, Z.; Xiao, Y.-L.; Zhang, X. *Acc. Chem. Res.* **2018**, *51*, 2264–2278. doi:10.1021/acs.accounts.8b00230
208. Lemos, A.; Lemaire, C.; Luxen, A. *Adv. Synth. Catal.* **2019**, *361*, 1500–1537. doi:10.1002/adsc.201801121
209. Gandeepan, P.; Müller, T.; Zell, D.; Cera, G.; Warratz, S.; Ackermann, L. *Chem. Rev.* **2019**, *119*, 2192–2452. doi:10.1021/acs.chemrev.8b00507
210. Planas, O.; Peciukenas, V.; Leutzsch, M.; Nöthling, N.; Pantazis, D. A.; Cornella, J. J. *Am. Chem. Soc.* **2022**, *144*, 14489–14504. doi:10.1021/jacs.2c01072
211. Carvalho, R. L.; de Miranda, A. S.; Nunes, M. P.; Gomes, R. S.; Jardim, G. A. M.; Júnior, E. N. d. S. *Beilstein J. Org. Chem.* **2021**, *17*, 1849–1938. doi:10.3762/bjoc.17.126

## License and Terms

This is an open access article licensed under the terms of the Beilstein-Institut Open Access License Agreement (<https://www.beilstein-journals.org/bjoc/terms>), which is identical to the Creative Commons Attribution 4.0 International License (<https://creativecommons.org/licenses/by/4.0>). The reuse of material under this license requires that the author(s), source and license are credited. Third-party material in this article could be subject to other licenses (typically indicated in the credit line), and in this case, users are required to obtain permission from the license holder to reuse the material.

The definitive version of this article is the electronic one which can be found at:  
<https://doi.org/10.3762/bjoc.19.35>



# Direct C2–H alkylation of indoles driven by the photochemical activity of halogen-bonded complexes

Martina Mamone<sup>1</sup>, Giuseppe Gentile<sup>1</sup>, Jacopo Dosso<sup>1</sup>, Maurizio Prato<sup>1,2,3</sup> and Giacomo Filippini<sup>\*1</sup>

## Letter

[Open Access](#)

### Address:

<sup>1</sup>Department of Chemical and Pharmaceutical Sciences, INSTM UdR Trieste, University of Trieste, via Licio Giorgieri 1, 34127 Trieste, Italy, <sup>2</sup>Centre for Cooperative Research in Biomaterials (CIC BiomaGUNE), Basque Research and Technology Alliance (BRTA), Paseo de Miramón 194, 20014, Donostia San Sebastián, Spain and <sup>3</sup>Basque Fdn Sci, Ikerbasque, 48013 Bilbao, Spain

### Email:

Giacomo Filippini\* - gfilippini@units.it

\* Corresponding author

### Keywords:

alkylation; EDA complex; halogens; indoles; photochemistry

*Beilstein J. Org. Chem.* **2023**, *19*, 575–581.

<https://doi.org/10.3762/bjoc.19.42>

Received: 09 February 2023

Accepted: 17 April 2023

Published: 27 April 2023

This article is part of the thematic issue "C–H bond functionalization: recent discoveries and future directions".

Guest Editor: I. Chatterjee

© 2023 Mamone et al.; licensee Beilstein-Institut.

License and terms: see end of document.

## Abstract

A light-driven metal-free protocol for the synthesis of sulfone-containing indoles under mild conditions is reported. Specifically, the process is driven by the photochemical activity of halogen-bonded complexes formed upon complexation of a sacrificial donor, namely 1,4-diazabicyclo[2.2.2]octane (DABCO), with  $\alpha$ -iodosulfones. The reaction provides a variety of densely functionalized products in good yields (up to 96% yield). Mechanistic investigations are reported. These studies provide convincing evidences for the photochemical formation of reactive open-shell species.

## Findings

Direct replacement of carbon–hydrogen (C–H) bonds with new carbon–carbon (C–C) and carbon–heteroatom (C–X) bonds has been and still is a central topic in organic synthesis [1,2]. Historically, organic chemists have extensively relied on the use of noble-metal-based catalysts (e.g., Pd, Rh, Ir, among others) to achieve such type of functionalization [3–5]. However, reliance on noble metal complexes has been constantly declined over recent years due to cost, availability, and toxicity, therefore discouraged by the modern guidelines towards implemen-

tation of sustainable chemical production schemes [6]. In the last decades, organic photochemistry has become a prominent tool to guide the development of greener and more convenient synthetic protocols [7–12]. In this context, photochemical approaches based on electron donor–acceptor (EDA) complexes have been successfully exploited to drive the direct C–H functionalization of a large number of organic substrates [13–18]. In this approach, an electron acceptor substrate ("A") and a donor molecule ("D") interact to form a new aggregate defined as

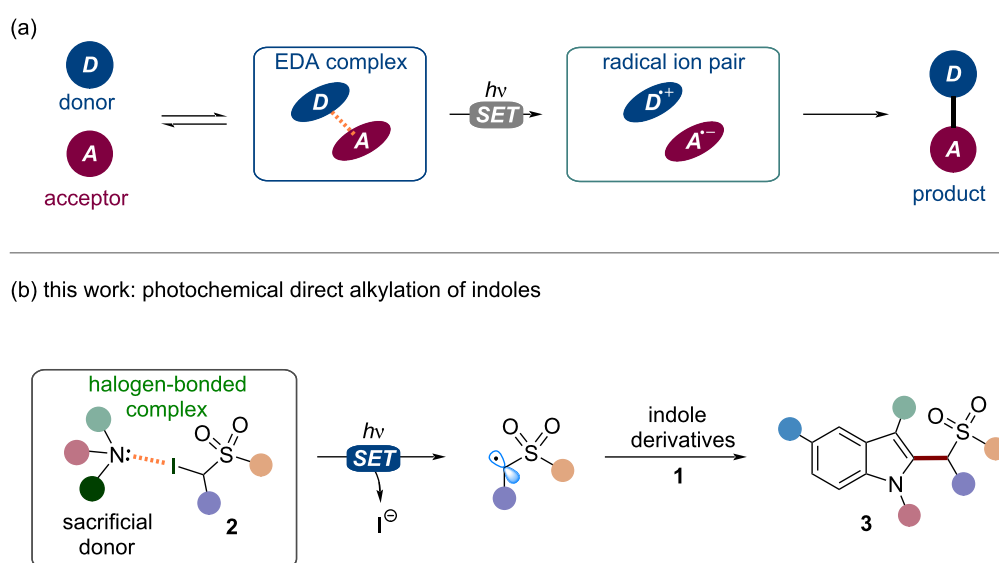
EDA complex (Figure 1a). Although the two molecular entities might not directly absorb visible light, the newly formed complex usually presents a charge transfer state which results in a bathochromic shift of the absorption towards the visible range [19,20]. Upon light irradiation, the EDA complex may undergo an intramolecular single-electron-transfer (SET) process to produce a radical ion pair ( $D^{\bullet+}$ ,  $A^{\bullet-}$ ). To avoid the occurrence of a back-electron-transfer (BET), a suitable leaving group (LG) needs to be included in one of the precursors. In this manner, reactive intermediates (e.g., radical species) may be generated in solution through the irreversible fragmentation of the substrates [15,21,22]. These intermediates eventually react to yield the final products "A–D". This approach is not limited to reagents with appropriate donor–acceptor characteristics [13,19].

Indeed, sacrificial electron donors and electron-deficient radical precursors can be used to form photoactive EDA complexes. Specifically, these aggregates can be employed to photochemically generate electrophilic radicals that can drive the functionalization of suitable electron-rich substrates [23].

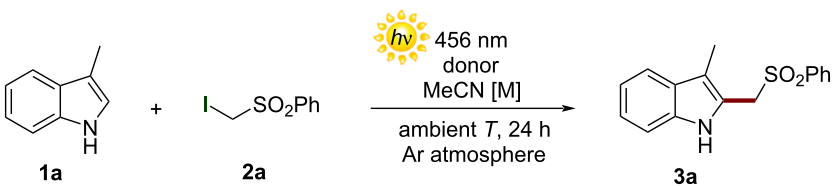
Exploiting this strategy, here we report a novel metal-free methodology for the direct homolytic aromatic substitution (HAS) reaction of indoles **1** with  $\alpha$ -iodosulfones **2** to yield the alkylated derivatives **3** (Figure 1b). Indoles play a crucial role in many natural and industrial processes. Therefore, the direct chemical manipulation of the indole system is a matter of paramount importance [24–27]. Moreover, the sulfonyl group is an extremely versatile chemical moiety which may be easily trans-

formed into different functionalities employing conventional synthetic methods. As an example, the sulfonyl group removal under simple reductive treatment may give access to important methylated compounds [12,21]. This operationally simple approach occurs at ambient temperature and under visible-light irradiation. Interestingly, this method employs 1,4-diazabicyclo[2.2.2]octane (DABCO) as sacrificial donor in the EDA complex formation with **2**. To test the feasibility of our design plan, we focused on the reaction between 3-methylindole (**1a**, 2 equiv) and  $\alpha$ -iodosulfone **2a** (Table 1).

The experiments were conducted at ambient temperature in acetonitrile (0.5 M) and under irradiation by a Kessil lamp at 456 nm. When adding 1,8-diazabicyclo[5.4.0]undec-7-ene (DBU) as sacrificial donor (1 equiv), the desired product **3a** was formed in good chemical yield (entry 1, Table 1). Control experiments were conducted to obtain more mechanistic clues (entries 2–5, Table 1). An experiment revealed how the exclusion of light completely suppressed the process, therefore establishing the photochemical nature of the transformation (entry 2, Table 1). In addition, we confirmed that DBU was essential for the reactivity, since no reaction occurred in its absence (entry 3, Table 1). Reactivity was also inhibited under an aerobic atmosphere and in the presence of 2,2,6,6-tetramethylpiperidinyl-oxyl (TEMPO). These experiments are consonant with the occurrence of a radical mechanism (entries 4 and 5, Table 1) [28]. Afterwards, the effect of the chemical nature of the sacrificial donor on the reaction was investigated (entries 6–9, Table 1). In particular, we employed 2,6-lutidine, 1,1,3,3-tetramethylguanidine (TMG), triethylamine ( $\text{NEt}_3$ ), and DABCO. Interest-



**Figure 1:** (a) Exploitation of an EDA complex in organic synthesis. (b) This work: use of halogen-bonded complexes to photochemically initiate the C–H alkylation of indoles **1** with iodosulfones **2**.

**Table 1:** Optimization of the reaction conditions and control experiments.


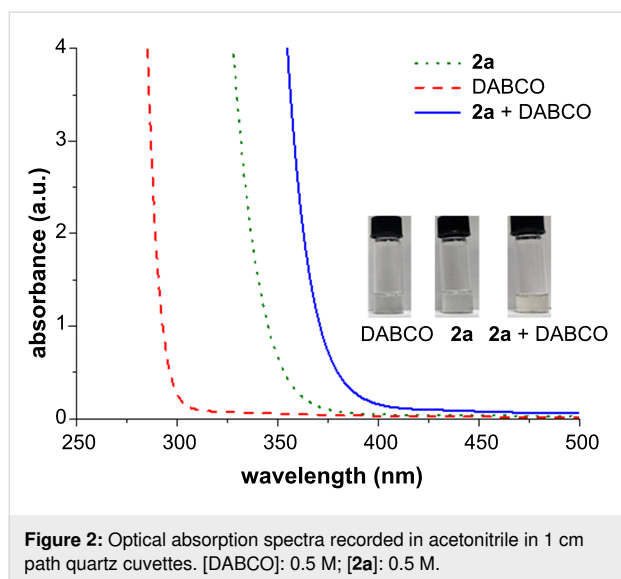
entry	donor	[M]	1a:2a:donor (equiv)	light source (nm)	yield (%) <sup>a</sup>
1 <sup>b</sup>	DBU	0.5	1:2:1	456	56
2	DBU	0.5	1:2:1	light off	0
3	–	0.5	1:2:1	456	0
4 <sup>c</sup>	DBU	0.5	1:2:1	456	0
5 <sup>d</sup>	DBU	0.5	1:2:1	456	0
6	2,6-lutidine	0.5	1:2:1	456	0
7	TMG	0.5	1:2:1	456	64
8	NEt <sub>3</sub>	0.5	1:2:1	456	64
9	DABCO	0.5	1:2:1	456	77
10	DABCO	0.25	1:2:1	456	64
11	DABCO	1.0	1:2:1	456	69
12	DABCO	0.5	1:1:1	456	65
13	DABCO	0.5	2:1:1	456	73
14	DABCO	0.5	2:1:1.5	456	95
15 <sup>e</sup>	DABCO	0.5	2:1:1.5	456	18
16 <sup>f</sup>	DABCO	0.5	2:1:1.5	456	60

<sup>a</sup>Yield determined by <sup>1</sup>H NMR spectroscopy using 1,3,5-trimethoxybenzene as the internal standard. <sup>b</sup>Conditions: indole **1a** (0.1 mmol), α-iodosulfone **2a** (0.2 mmol), acetonitrile (MeCN, 200 μL), donor (0.1 mmol), ambient temperature. <sup>c</sup>Reaction in air. <sup>d</sup>Reaction performed in the presence of 2 equiv of TEMPO. <sup>e</sup>Reaction performed in hexane as solvent. <sup>f</sup>Reaction performed in methanol as solvent.

ingly, the use of DABCO provided the best result in terms of reactivity, yielding compound **3a** in 77% yield. We also observed that either increasing or decreasing the concentration of the reaction mixture did not bring any improvement (entries 10 and 11, Table 1). Then, the ratio between the reagents was optimized. In particular, the use of **2a:1a** in a 1:1 ratio resulted in the formation of **3a** in 65% yield (entry 12, Table 1). Moreover, we found that employing an excess of **1a** (2 equiv) led to the formation of **3a** in a 73% yield (entry 13, Table 1). Due to an easier purification of product **3a** from the reaction crude by flash column chromatography, we decided to keep optimizing the transformation using the stoichiometric ratio indicated in entry 13 of Table 1. Importantly, product **3a** was obtained in excellent yield (95%) using 1.5 equivalents of DABCO (entry 14, Table 1). In addition, the use of hexane as solvent provided the desired product **3a** in low chemical yield (entry 15, Table 1). On the other hand, **3a** was obtained in moderate yield (60%) using methanol as solvent (entry 16, Table 1). To shed light on the reaction mechanism, the formation of an EDA complex between the α-iodosulfone **2a** and DABCO was investigated using both UV–vis and nuclear magnetic resonance (NMR) spectroscopy [29].

In particular, the optical absorption spectra of substrate **2a** (green dotted line), DABCO (red dotted line), and the solution containing both **2a** and DABCO (blue line) were recorded in acetonitrile (Figure 2). Specifically, it was observed that the addition of DABCO to the solution of **2a** induced a bathochromic shift of the absorption spectrum towards the visible region, thus indicating the formation of an EDA complex between these chemical species. Importantly, we also confirmed that indole **1a** and **2a** do not form a photoactive EDA complex when mixed in solution (see Figure S1 in Supporting Information File 1). To further corroborate the hypothesis of an EDA complex being at the roots of the observed reactivity, NMR studies were also performed on samples containing the α-iodosulfone **2a** and different concentrations of DABCO in deuterated acetonitrile (Figure 3).

Interestingly, a change in chemical shift of the diagnostic α-protons of **2a** was displayed upon addition of increasing amounts of DABCO, suggesting the presence of the halogen-bonding interaction [30]. More precisely, the <sup>1</sup>H NMR signal of the α-hydrogens (H<sub>α</sub>) within **2a** was found to shift to lower ppm values because the H<sub>α</sub> nuclei have been affected by higher elec-

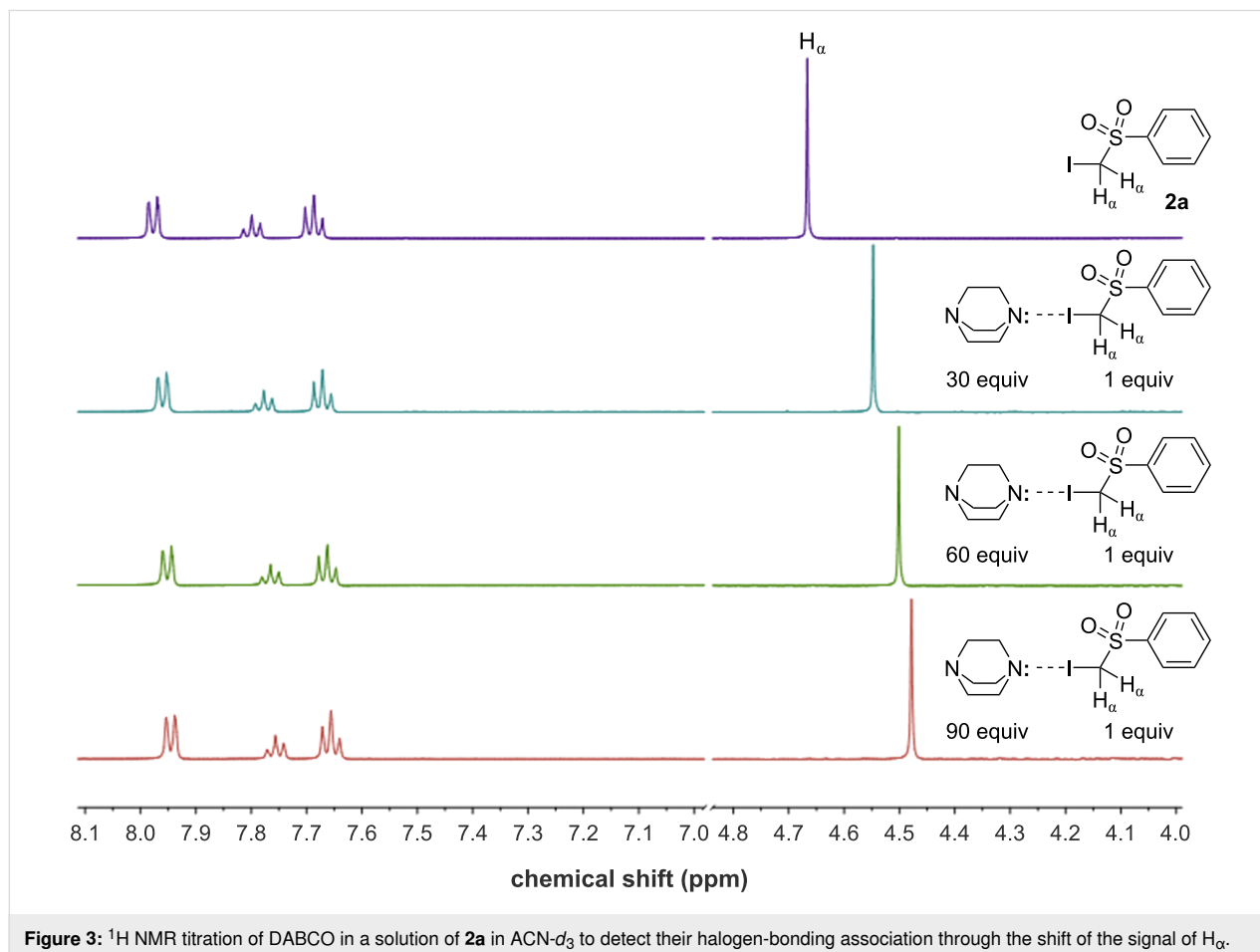


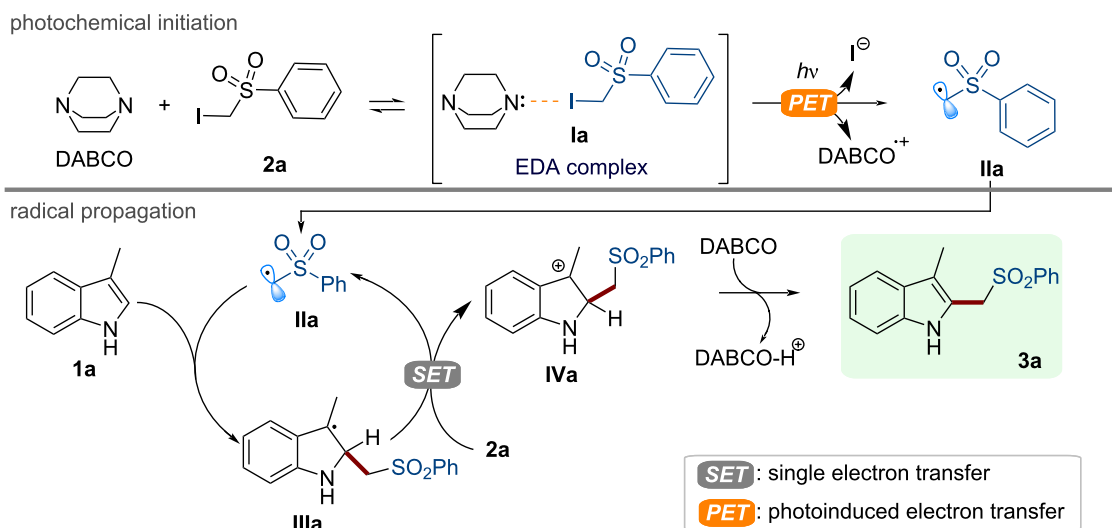
tron density caused by the formation of the halogen-bonded complex between **2a** and DABCO. To confirm that the shift of  $H_\alpha$  was indeed produced by a halogen-bonding interaction,  $^{19}\text{F}$  NMR analysis of compound **2d**, which presents a difluoro-

methylene group ( $-\text{CF}_2-$ ) in the alpha position to the iodine, was performed (see Figure S3 in Supporting Information File 1). Even in this case, an important shift of the fluorine signal was observed. Thus, from a mechanistic point of view, the reaction is driven by the formation of a halogen-bonded EDA complex (**1a**) between the sulfone **2a** and DABCO (Figure 4).

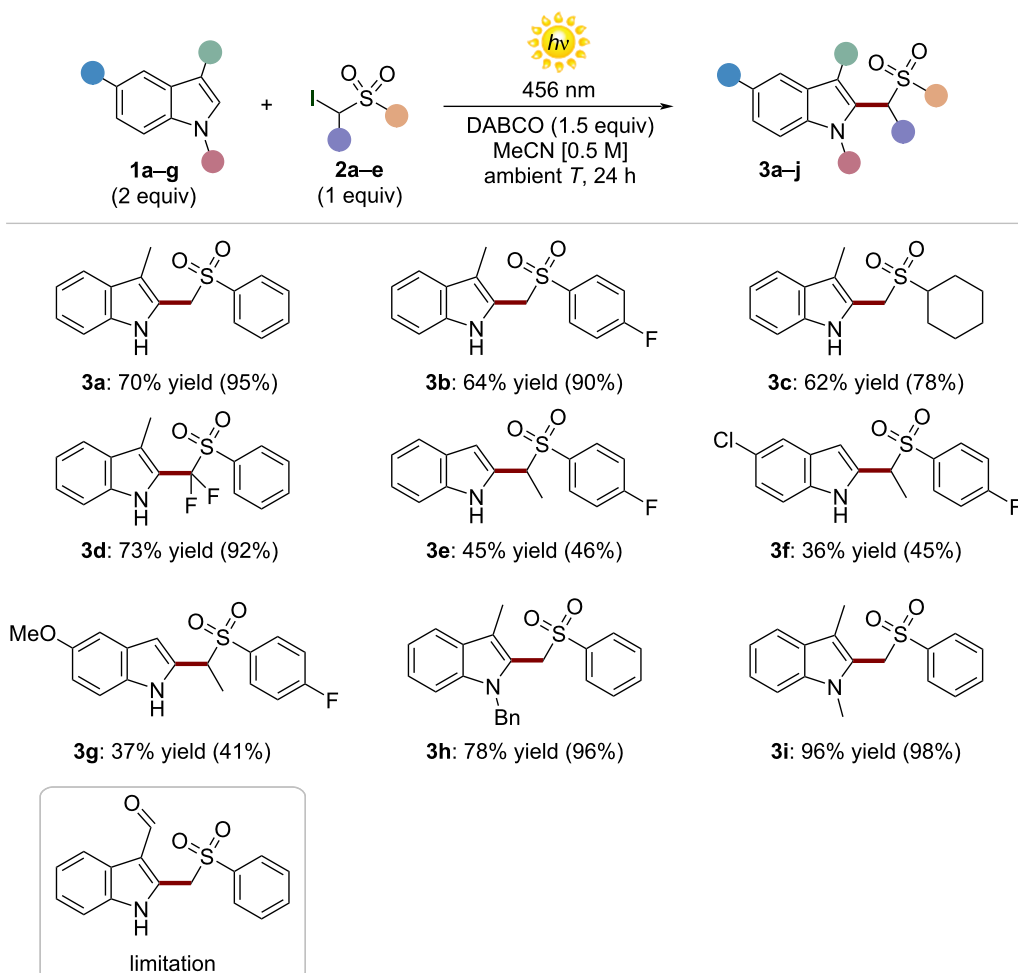
When irradiated, this photoactive aggregate led to the formation of reactive alkyl radicals (**IIa**), which may react with indole **1a** eventually yielding the product **3a** through a classical HAS pathway [31–33]. Then, we demonstrated the synthetic potential of our photochemical method (Scheme 1).

The reaction could satisfactorily tolerate a diverse set of  $\alpha$ -iodosulfones **2** to deliver the corresponding products **3a–d** from moderate to excellent yields (up to 73% yield). We found that different indoles actively participated in the photochemical alkylation, leading to the products **3e–i** (up to 96% yield). It is worth noting that derivatives **3e–g** were isolated in moderate yields as single regioisomer since the alkylation step took place exclusively in position 2 of the starting indoles. As limitation,





**Figure 4:** Proposed reaction mechanism for the photochemical alkylation of **1a** with the  $\alpha$ -iodosulfone **2a** in the presence of DABCO.



**Scheme 1:** Study of scope of the HAS reaction between indoles **1** and  $\alpha$ -iodosulfones **2**. Yields in parentheses were determined by  $^1\text{H}$  NMR analyses, using 1,3,5-trimethoxybenzene as an internal standard.

we observed that indole-3-carboxaldehyde (**1g**) was not a suitable substrate for this transformation.

## Conclusion

In conclusion, we reported a novel photochemical method for the direct C–H alkylation of indoles with  $\alpha$ -iodosulfones. This approach exploits the photochemical activity of halogen-bonded EDA complexes, formed between  $\alpha$ -iodosulfones and DABCO, that are able to produce reactive C-centered radicals under mild reaction conditions.

## Supporting Information

### Supporting Information File 1

General procedures and products characterization.

[<https://www.beilstein-journals.org/bjoc/content/supplementary/1860-5397-19-42-S1.pdf>]

## Acknowledgements

M.P. is the AXA Chair for Bionanotechnology (2016–2023).

## Funding

The authors gratefully acknowledge the University of Trieste, INSTM and the Maria de Maeztu Units of Excellence Program from the Spanish State Research Agency (Grant No. MDM-2017-0720). G.F. and J.D. kindly acknowledge FRA2022 funded by the University of Trieste. G.F. kindly acknowledges Microgrants 2021 funded by Region FVG (LR 2/2011, ART. 4). J.D. kindly acknowledges the RTDa–PON “ricerca e innovazione” 2014–2020.

## ORCID® iDs

Martina Mamone - <https://orcid.org/0000-0001-5981-1295>

Giuseppe Gentile - <https://orcid.org/0000-0002-5622-8579>

Jacopo Dosso - <https://orcid.org/0000-0003-4173-3430>

Maurizio Prato - <https://orcid.org/0000-0002-8869-8612>

Giacomo Filippini - <https://orcid.org/0000-0002-9694-3163>

## References

- Godula, K.; Sames, D. *Science* **2006**, *312*, 67–72. doi:10.1126/science.1114731
- Davies, H. M. L.; Morton, D. *J. Org. Chem.* **2016**, *81*, 343–350. doi:10.1021/acs.joc.5b02818
- Wencel-Delord, J.; Glorius, F. *Nat. Chem.* **2013**, *5*, 369–375. doi:10.1038/nchem.1607
- He, J.; Wasa, M.; Chan, K. S. L.; Shao, Q.; Yu, J.-Q. *Chem. Rev.* **2017**, *117*, 8754–8786. doi:10.1021/acs.chemrev.6b00622
- Kuhl, N.; Hopkinson, M. N.; Wencel-Delord, J.; Glorius, F. *Angew. Chem., Int. Ed.* **2012**, *51*, 10236–10254. doi:10.1002/anie.201203269
- Kar, S.; Sanderson, H.; Roy, K.; Benfenati, E.; Leszczynski, J. *Chem. Rev.* **2022**, *122*, 3637–3710. doi:10.1021/acs.chemrev.1c00631
- Bortolato, T.; Cuadros, S.; Simionato, G.; Dell'Amico, L. *Chem. Commun.* **2022**, *58*, 1263–1283. doi:10.1039/d1cc05850a
- Romero, N. A.; Nicewicz, D. A. *Chem. Rev.* **2016**, *116*, 10075–10166. doi:10.1021/acs.chemrev.6b00057
- Rosso, C.; Cuadros, S.; Barison, G.; Costa, P.; Kurbasic, M.; Bonchio, M.; Prato, M.; Dell'Amico, L.; Filippini, G. *ACS Catal.* **2022**, *12*, 4290–4295. doi:10.1021/acscatal.2c00565
- Shaw, M. H.; Twilton, J.; MacMillan, D. W. C. *J. Org. Chem.* **2016**, *81*, 6898–6926. doi:10.1021/acs.joc.6b01449
- Rosso, C.; Filippini, G.; Prato, M. *Eur. J. Org. Chem.* **2021**, 1193–1200. doi:10.1002/ejoc.202001616
- Filippini, G.; Silvi, M.; Melchiorre, P. *Angew. Chem., Int. Ed.* **2017**, *56*, 4447–4451. doi:10.1002/anie.201612045
- Crisenza, G. E. M.; Mazzarella, D.; Melchiorre, P. *J. Am. Chem. Soc.* **2020**, *142*, 5461–5476. doi:10.1021/jacs.0c01416
- Yang, Z.; Liu, Y.; Cao, K.; Zhang, X.; Jiang, H.; Li, J. *Beilstein J. Org. Chem.* **2021**, *17*, 771–799. doi:10.3762/bjoc.17.67
- Kandukuri, S. R.; Bahamonde, A.; Chatterjee, I.; Jurberg, I. D.; Escudero-Adán, E. C.; Melchiorre, P. *Angew. Chem., Int. Ed.* **2015**, *54*, 1485–1489. doi:10.1002/anie.201409529
- Arceo, E.; Jurberg, I. D.; Álvarez-Fernández, A.; Melchiorre, P. *Nat. Chem.* **2013**, *5*, 750–756. doi:10.1038/nchem.1727
- Yuan, Y.-q.; Majumder, S.; Yang, M.-h.; Guo, S.-r. *Tetrahedron Lett.* **2020**, *61*, 151506. doi:10.1016/j.tetlet.2019.151506
- Tian, Y.-M.; Hofmann, E.; Silva, W.; Pu, X.; Touraud, D.; Gschwind, R. M.; Kunz, W.; König, B. *Angew. Chem., Int. Ed.* **2023**, *62*, e202218775. doi:10.1002/anie.202218775
- Lima, C. G. S.; de M. Lima, T.; Duarte, M.; Jurberg, I. D.; Paixão, M. W. *ACS Catal.* **2016**, *6*, 1389–1407. doi:10.1021/acscatal.5b02386
- Slama-Schwock, A.; Blanchard-Desce, M.; Lehn, J.-M. *J. Phys. Chem.* **1990**, *94*, 3894–3902. doi:10.1021/j100373a007
- Cuadros, S.; Rosso, C.; Barison, G.; Costa, P.; Kurbasic, M.; Bonchio, M.; Prato, M.; Filippini, G.; Dell'Amico, L. *Org. Lett.* **2022**, *24*, 2961–2966. doi:10.1021/acs.orglett.2c00604
- Nappi, M.; Bergonzini, G.; Melchiorre, P. *Angew. Chem., Int. Ed.* **2014**, *53*, 4921–4925. doi:10.1002/anie.201402008
- Sun, X.; Wang, W.; Li, Y.; Ma, J.; Yu, S. *Org. Lett.* **2016**, *18*, 4638–4641. doi:10.1021/acs.orglett.6b02271
- Bandini, M.; Eichholzer, A. *Angew. Chem., Int. Ed.* **2009**, *48*, 9608–9644. doi:10.1002/anie.200901843
- Su, Y.-M.; Hou, Y.; Yin, F.; Xu, Y.-M.; Li, Y.; Zheng, X.; Wang, X.-S. *Org. Lett.* **2014**, *16*, 2958–2961. doi:10.1021/ol501094z
- Liu, F.; Li, P. *J. Org. Chem.* **2016**, *81*, 6972–6979. doi:10.1021/acs.joc.6b00689
- Mi, X.; Kong, Y.; Zhang, J.; Pi, C.; Cui, X. *Chin. Chem. Lett.* **2019**, *30*, 2295–2298. doi:10.1016/j.ccl.2019.09.040
- Buzzetti, L.; Crisenza, G. E. M.; Melchiorre, P. *Angew. Chem., Int. Ed.* **2019**, *58*, 3730–3747. doi:10.1002/anie.201809984
- Rosokha, S. V.; Kochi, J. K. *Acc. Chem. Res.* **2008**, *41*, 641–653. doi:10.1021/ar700256a
- Cavallo, G.; Metrangolo, P.; Milani, R.; Pilati, T.; Priimagi, A.; Resnati, G.; Terraneo, G. *Chem. Rev.* **2016**, *116*, 2478–2601. doi:10.1021/acs.chemrev.5b00484
- Metrangolo, P.; Neukirch, H.; Pilati, T.; Resnati, G. *Acc. Chem. Res.* **2005**, *38*, 386–395. doi:10.1021/ar0400995
- Bowman, W. R.; Storey, J. M. D. *Chem. Soc. Rev.* **2007**, *36*, 1803–1822. doi:10.1039/b605183a



33. Studer, A.; Bossart, M. Homolytic Aromatic Substitutions. In *Radicals in Organic Synthesis*; Renaud, P.; Sibi, M. P., Eds.; Wiley-VCH: Weinheim, Germany, 2001; Vol. 2, pp 62–80.  
doi:10.1002/9783527618293.ch29

## License and Terms

This is an open access article licensed under the terms of the Beilstein-Institut Open Access License Agreement (<https://www.beilstein-journals.org/bjoc/terms>), which is identical to the Creative Commons Attribution 4.0 International License (<https://creativecommons.org/licenses/by/4.0>). The reuse of material under this license requires that the author(s), source and license are credited. Third-party material in this article could be subject to other licenses (typically indicated in the credit line), and in this case, users are required to obtain permission from the license holder to reuse the material.

The definitive version of this article is the electronic one which can be found at:  
<https://doi.org/10.3762/bjoc.19.42>



## C3-Alkylation of furfural derivatives by continuous flow homogeneous catalysis

Grédy Kiala Kinkutu<sup>1,2</sup>, Catherine Louis<sup>2</sup>, Myriam Roy<sup>1</sup>, Juliette Blanchard<sup>\*2</sup> and Julie Oble<sup>\*1</sup>

### Full Research Paper

[Open Access](#)**Address:**

<sup>1</sup>Sorbonne Université, CNRS, Institut Parisien de Chimie Moléculaire, IPCM UMR 8232, F-75005 Paris, France and <sup>2</sup>Sorbonne Université, CNRS, Laboratoire de Réactivité de Surface, LRS UMR 7197, F-75005 Paris, France

**Email:**

Juliette Blanchard<sup>\*</sup> - [juliette.blanchard@sorbonne-universite.fr](mailto:juliette.blanchard@sorbonne-universite.fr);  
Julie Oble<sup>\*</sup> - [julie.oble@sorbonne-universite.fr](mailto:julie.oble@sorbonne-universite.fr).

\* Corresponding author

**Keywords:**

biomass; C–H activation; flow; furfural; homogeneous catalysis

*Beilstein J. Org. Chem.* **2023**, *19*, 582–592.

<https://doi.org/10.3762/bjoc.19.43>

Received: 11 February 2023

Accepted: 17 April 2023

Published: 03 May 2023

This article is part of the thematic issue "C–H bond functionalization: recent discoveries and future directions".

Guest Editor: I. Chatterjee



© 2023 Kinkutu et al.; licensee Beilstein-Institut.  
License and terms: see end of document.

## Abstract

The C3-functionalization of furfural using homogeneous ruthenium catalysts requires the preinstallation of an *ortho*-directing imine group, as well as high temperatures, which did not allow scaling up, at least under batch conditions. In order to design a safer process, we set out to develop a continuous flow process specifically for the C3-alkylation of furfural (Murai reaction). The transposition of a batch process to a continuous flow process is often costly in terms of time and reagents. Therefore, we chose to proceed in two steps: the reaction conditions were first optimized using a laboratory-built pulsed-flow system to save reagents. The optimized conditions in this pulsed-flow mode were then successfully transferred to a continuous flow reactor. In addition, the versatility of this continuous flow device allowed both steps of the reaction to be carried out, namely the formation of the imine directing group and the C3-functionalization with some vinylsilanes and norbornene.

## Introduction

The conversion of biomass derivatives into value-added products is one of the key branches of green chemistry and of the development of a sustainable chemical industry [1–4]. Furfurals, which are versatile platform molecules derived from renewable lignocellulose present in agricultural wastes [5–8], have proven to be of great importance for the preparation of value-added chemicals, biofuels, as well as monomers for materials science

[9–15]. In this context, their functionalization is fundamental to further improve their inclusion in fine organic synthesis and industrial processes. For this reason, in recent years, innovative protocols for the formation of new bonds on furfural derivatives have been developed. In particular, their direct functionalization by transition-metal-catalyzed C–H activation processes [16–18] has become a major area of interest where only a few

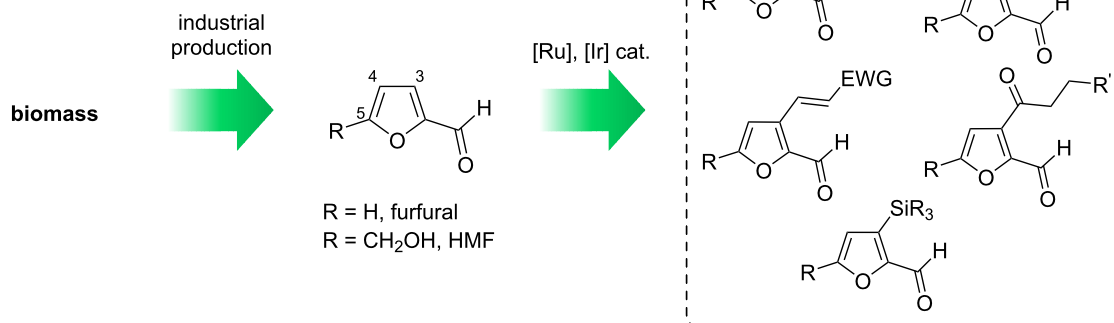
methods have been reported so far. Most examples concern functionalization at C5, which is the most reactive site. In contrast, C3-functionalizations of the formyl-furan unit via directing groups, as well as C4-functionalizations have been much less studied [19,20].

Within the framework of a large project oriented towards the selective formation of new bonds from furfural derivatives without changing the redox state of the aldehyde function, we have developed a number of directed Ru(0)-catalyzed C3-functionalizations of furfurylimines, such as alkylation [21], arylation [22], alkenylation [23] and acylation [24], as well as an Ir-catalyzed directed C3-silylation (Scheme 1a) [25]. These batch processes rely on the use of a homogeneous metal catalyst at elevated temperatures necessary to cleave the C3–H bond by oxidative addition. These experimental conditions, easily used in the laboratory, are potentially problematic for scale-up due to efficiency and safety issues (related to the high temperature). Thus, despite the synthetic interest of the molecules that

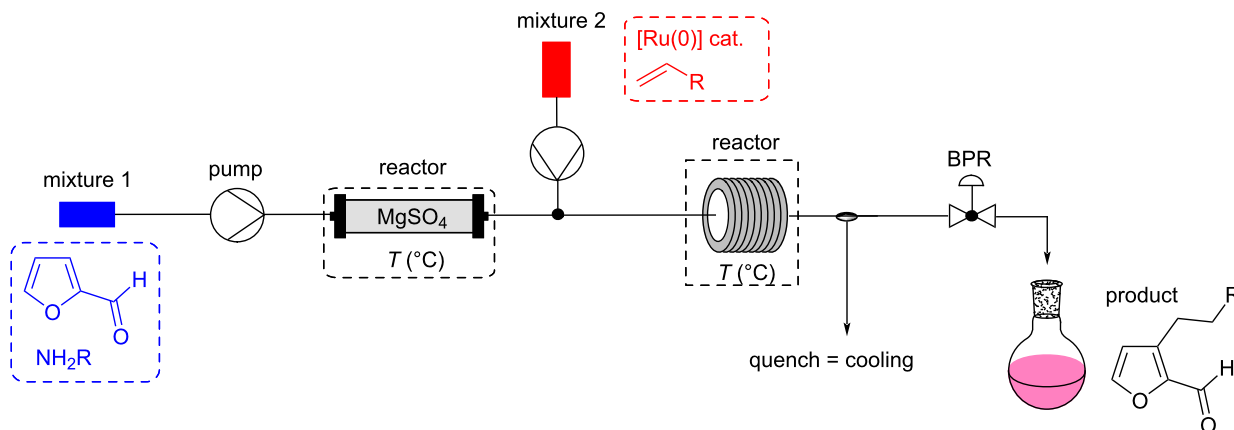
can be obtained, transfers to industry are difficult. In order to circumvent this drawback, we considered transposing these batch reactions to a flow chemistry process.

In recent years, the use of continuous flow chemistry in organic synthesis has increased dramatically and has rapidly become a routine tool for classical synthesis [26–29]. In particular, many efforts have been devoted to the development of flow alternatives for transition-metal-catalyzed cross-couplings [30] and for some C–H functionalizations [31]. Nevertheless, there are very few flow processes that have been implemented to functionalize furfurals, the scarce examples being only based on photochemical processes [32–34]. The current strong interest in continuous flow strategies is related to the modernization of flow equipment providing chemists, not only a unique control of reaction parameters, such as improved mass and heat transfer, but also reduced safety risks and increased reproducibility of the results [29,35,36]. These features should therefore allow us to scale up our directed C3-functionalizations of furfurylimines

a) C3–H-selective batch functionalizations of furfural derivatives = previous results



b) C3–H-alkylation of furfural derivatives in continuous flow = this work



**Scheme 1:** C3-Functionalization of furfural derivatives by C–H activation, a) in batch: previous works, and b) in continuous flow: this work.

under safe reaction conditions while providing products in shorter reaction times. In addition, the ability to couple multiple reactors with a flow apparatus could also enable us to perform these functionalizations directly from furfural by forming the imine in a first reactor. It should be noted that, in batch, in-situ imine formation is currently impossible with catalytic or stoichiometric amounts of amine due to decarbonylation of furfural under the reaction conditions [21]. We thus present here an adaptation of our Ru(0)-catalyzed C3-alkylation strategy of furfural derivatives to a continuous flow system (Scheme 1b).

## Results and Discussion

### First optimization with a home-made pulsed-flow setup

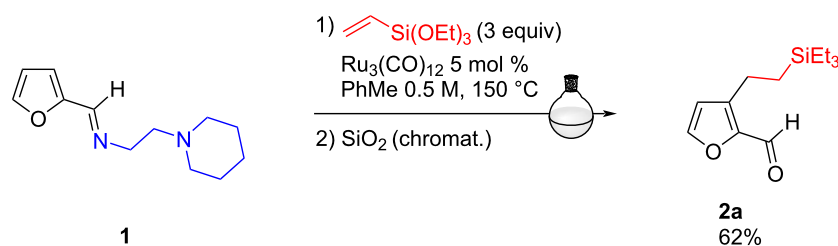
We undertook the optimization of this flow strategy for the C3-alkylation reaction (Murai reaction) [37,38] of the furfurylimine **1** bearing a removable *N,N'*-bidentate directing group. In a previous study, this starting material had proved to be the most reactive imine in batch, leading, in the presence of 5 mol % of  $[\text{Ru}_3(\text{CO})_{12}]$  and 3 equivalents of triethoxyvinylsilane in toluene at 150 °C after 5 h, to the alkylated aldehyde **2a** with 62% yield, after purification on silica gel (Scheme 2) [21,39].

The flow reactions for this first optimization were performed using a home-made setup based on an HPLC apparatus (Jasco) equipped with an injection valve (Rheodyne) comprising a 105  $\mu\text{L}$  loop into which the reaction mixture is loaded and then pushed by the solvent delivered by the HPLC pump (see Supporting Information File 1, p. S8). All the content of the loop is thus sent into the reactor. This system is coupled to a gas chromatography oven, in which the stainless-steel tubular reactor (length: 4.6 m, internal diameter of 0.8 millimeter, corresponding to a volume of 2.31 mL) is placed. The system pressure is controlled by a back-pressure regulator (BPR) to keep a pressure of about 130 bar, i.e., at a pressure much higher than that which causes the solvent (toluene) to boil in the reaction temperature range (150–200 °C). This homemade, pulsed-flow

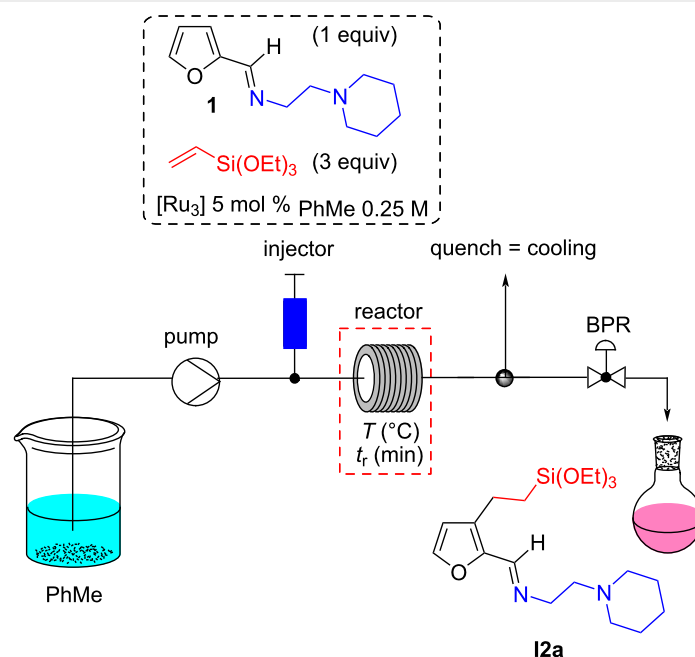
setup was used for optimizing the protocol while saving on reactants and catalyst.

Initial tests with the commercial complex  $[\text{Ru}_3(\text{CO})_{12}]$  at high temperature with different residence times provided the desired C3-alkylated imine **12a** in NMR yields ranging from 30% to 65% (Table 1, entries 1–3 and Table S1 in Supporting Information File 1, p. S10). A continuous flow system was thus found to be compatible with the realization of this type of C–H functionalization. This process led to a significant reduction of the reaction time compared to the batch, in particular by increasing the temperature to 200–250 °C, without significant losses of activity and selectivity. Unfortunately, with this catalyst, repeatability problems were detected (yield fluctuation of approximately 20%) which could be assigned to the low solubility of this catalyst in toluene. In order to overcome these problems, we synthesized triruthenium carbonyl complexes with phosphine ligand(s), namely (triethoxysilyl)ethylphosphine **L1** or triphenylphosphine [40–42]. Their synthesis, well-described in the literature, is detailed in Supporting Information File 1 (pp. S3–S6). Moreover, a kinetic study carried out in batch in the presence of the  $[\text{Ru}_3(\text{CO})_{11}(\text{L1})]$  (**comp1**),  $[\text{Ru}_3(\text{CO})_{10}(\text{L1})_2]$  (**comp2**) or  $[\text{Ru}_3(\text{CO})_9(\text{L1})_3]$  (**comp3**) catalysts allowed to show, on the one hand, the absence of solubility problems, and to discover, on the other hand, that the presence of three **L1** ligands (**comp3**) leads to a reaction rate clearly lower than that of a catalyst carrying one or two ligands (see p. S7 of Supporting Information File 1 for the reaction kinetic curves of catalysts). In addition, the catalyst with a single **L1** ligand (**comp1**) was found to be more reactive than the one with two ligands (**comp2**), and was therefore selected for further optimization. In contrast, comparison of its reaction kinetic curve with that of  $[\text{Ru}_3(\text{CO})_{12}]$  indicates that **comp1** is slightly less active than  $[\text{Ru}_3(\text{CO})_{12}]$ . Beside these three catalysts, a fourth one  $[\text{Ru}_3(\text{CO})_{11}(\text{PPh}_3)]$  **comp4**, was also used for this study.

For the continuous flow reaction, we observed, for the same residence time, a slight decrease in performance with **comp1**



**Scheme 2:** C3-alkylation of bidentate imine **1** performed in batch.

**Table 1:** Optimization of the catalyst for the alkylation reaction on the homemade pulsed-flow setup.

Entry	[Ru <sub>3</sub> ]	T [°C]	t <sub>r</sub> [min]	Conv [%] <sup>a</sup>	Yield [%] <sup>a,b</sup>
1	Ru <sub>3</sub> (CO) <sub>12</sub>	165	90	58	45
2	Ru <sub>3</sub> (CO) <sub>12</sub>	200	30	90	65
3	Ru <sub>3</sub> (CO) <sub>12</sub>	250	6	83	63 <sup>c</sup>
4	Ru <sub>3</sub> (CO) <sub>11</sub> (L1) <b>comp1</b>	200	30	66	56
5	<b>comp1</b>	200	46	79	63
6	<b>comp1</b>	200	77	95	55

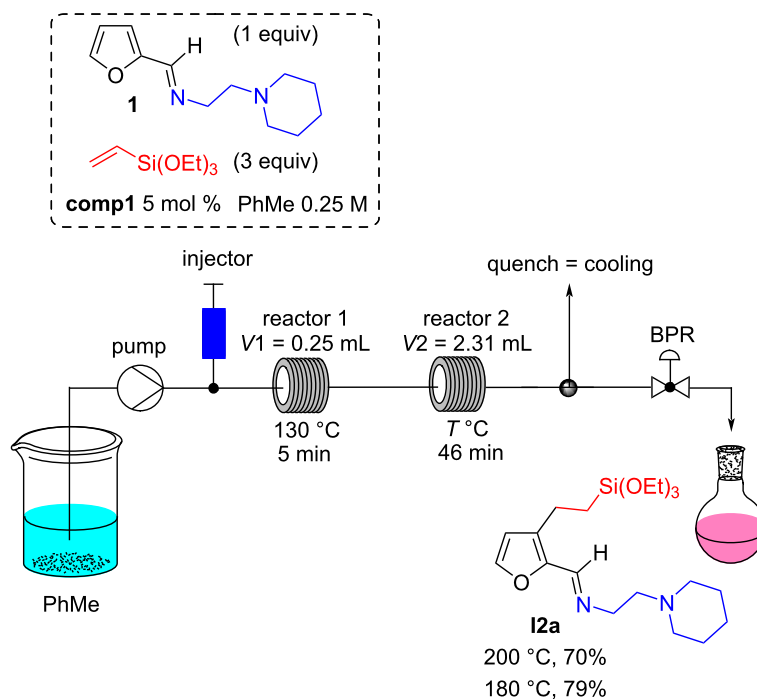
<sup>a</sup>Yields and conversions were calculated by <sup>1</sup>H NMR using *p*-dinitrobenzene as internal standard; <sup>b</sup>Non-repeatable results; <sup>c</sup>repeated four times with four different results ranging from 75% to 53%.

compared to [Ru<sub>3</sub>(CO)<sub>12</sub>] at 200 °C (Table 1, entries 3 and 4). This can be attributed, as mentioned above, to the slightly faster reaction kinetics of the [Ru<sub>3</sub>(CO)<sub>12</sub>] catalyst compared to that of **comp1**. Nevertheless, the better solubility of **comp1** in toluene allows to get around the problems of reproducibility. Moreover, increasing the residence time to 46 min resulted in 63% NMR yield of **I2a** (Table 1, entry 5), which was very similar to the results obtained with [Ru<sub>3</sub>(CO)<sub>12</sub>] in 30 min. A further increase in residence time to 77 min led to a lower yield (Table 1, entry 6), probably due to products degradation under longer heating.

In addition, we found that the **comp1** [Ru<sub>3</sub>(CO)<sub>11</sub>(L1)] was more efficient when the reaction mixture was preheated before being introduced into the reactor at 200 °C. The setup was thus modified (Scheme 3) to include a 0.8-millimeter-diameter stainless-steel preheating loop (outside the oven). An improvement in efficiency was then observed when the reaction mixture was

preheated to 130 °C for 5 min. Interestingly, only traces of product **I2a** were observed after 5 min at 130 °C, implying that the Murai reaction was indeed taking place only when passing through the second reactor. Finally, after some optimizations, the temperature in the second reactor could be lowered to 180 °C leading to an NMR yield of C3-alkylated imine **I2a** of 79% (Scheme 3).

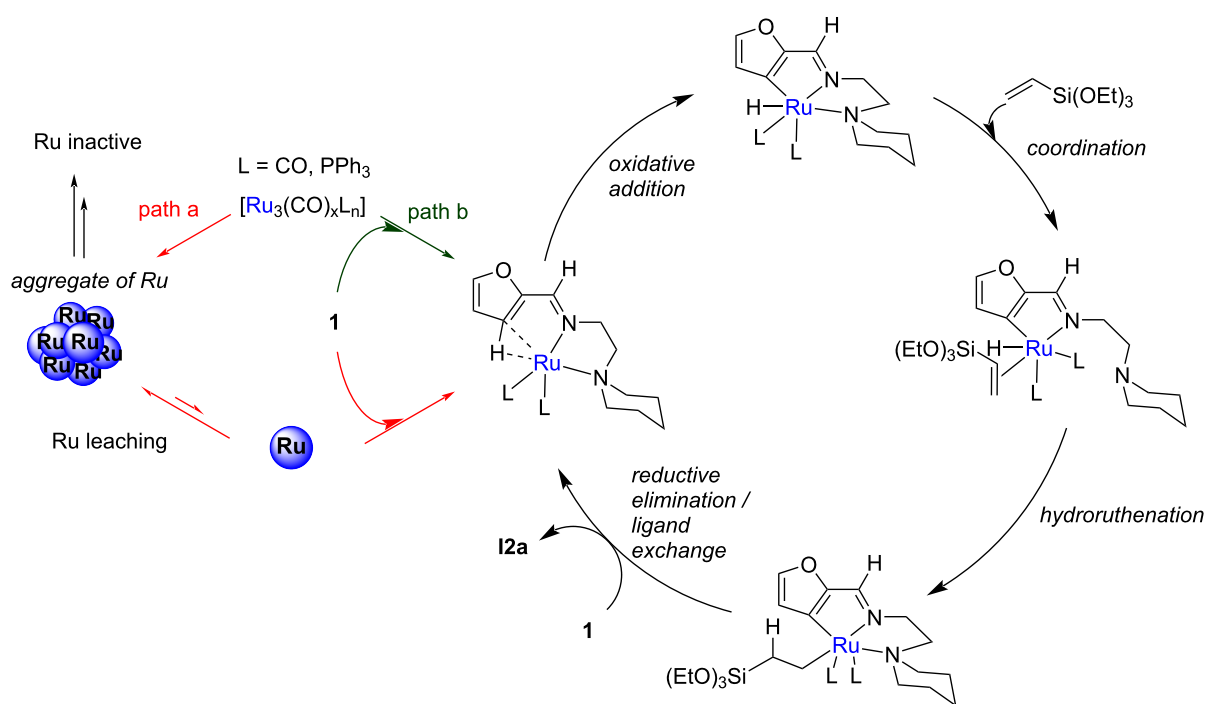
Heat transfer calculations showed us that the reaction mixture rises to the set temperatures in two seconds, and more importantly, that the inlet of reactor 2 is at room temperature after passing through the tube of 50 cm that connects the two reactors. Hence, we rationalized such a performance improvement from a chemical point of view: the [Ru<sub>3</sub>(CO)<sub>12</sub>] complex is known to thermally degrade by deligation, resulting in the formation of ruthenium aggregates [43]. We therefore propose that the active species is a mononuclear carbonyl complex in which the ruthenium is coordinated to the two nitrogen atoms of the



**Scheme 3:** Optimization of the heating for the alkylation reaction on the homemade pulsed-flow setup.

directing group (amino-imine). Preheating for 5 minutes at 130 °C would generate it from  $[\text{Ru}_3(\text{CO})_{11}(\text{L})]$ , which would therefore be more accurate to consider as a precatalyst

(Scheme 4, path b). The mononuclear complex would then initiate the alkylation reaction at 180 °C following elementary steps previously determined by DFT [21]. Conversely, a high



**Scheme 4:** Proposed reaction mechanism for the alkylation reaction with formation of ruthenium aggregates and mononuclear Ru(0) catalyst.

starting temperature would favor the formation of ruthenium aggregates, which could also generate, but less efficiently, the active catalyst (the mononuclear ruthenium(0) species) by leaching (Scheme 4, path a).

In order to detect the postulated reaction intermediate (Scheme 4) and the formation of ruthenium aggregates under reaction conditions, imine **1** was treated at 150 °C in toluene for 1 h with 0.33 equiv of **comp4** [Ru<sub>3</sub>(CO)<sub>11</sub>(PPh<sub>3</sub>)], a catalyst analogue to **comp1** but bearing a less expensive phosphine ligand (Scheme 5A). The chosen ratio of imine to catalyst was consistent with the stoichiometric amounts needed to form the postulated intermediate. The temperature of 150 °C was chosen taking into account the efficiency of the batch reaction between imine **1** and triethoxyvinylsilane (3 equiv) in the presence of 5 mol % of this catalyst at 150 °C, which leads in 5 h to the alkylated imine **I2a** with a NMR yield of 77% (conv. 100%).

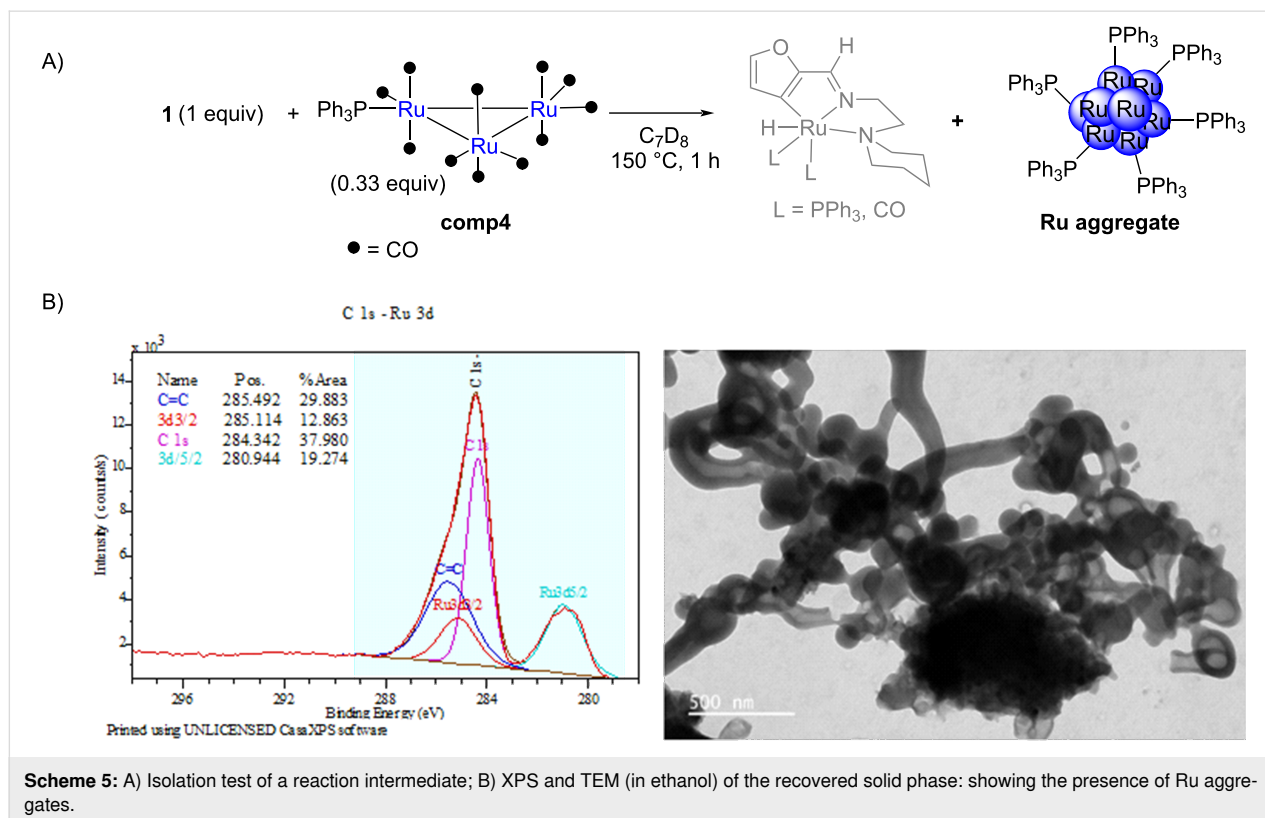
Even though the reaction intermediate we postulated on Scheme 4 could not be detected, a solid was recovered after evaporation of the solvent and precipitation in pentane. This solid displayed a <sup>31</sup>P NMR signal at 55.1 ppm (see Supporting Information File 1, p. S24), a value completely different from **comp4** (singlet at 35.06 ppm, see Supporting Information File 1, p. S20), meaning that the ruthenium trimer was no longer present. The TEM analysis of the recovered solid phase

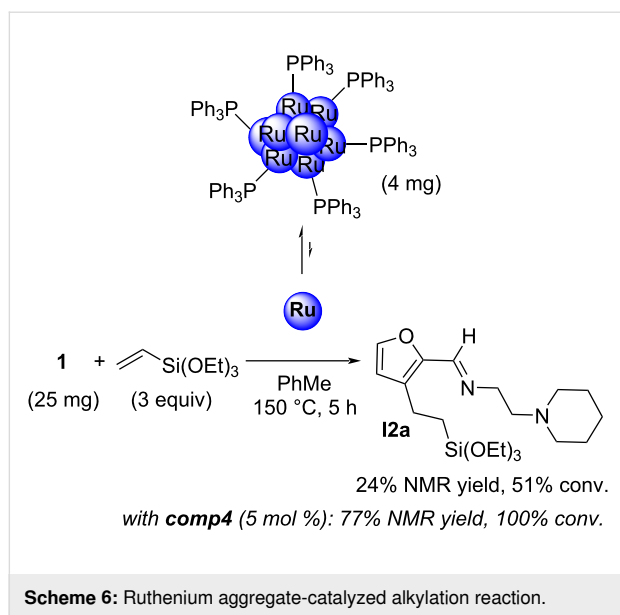
(Scheme 5B) showed the formation of large aggregates with high electron density. Moreover, ruthenium was detected by XPS analysis (Scheme 5B); the binding energy of the 3d<sub>5/2</sub> orbital was 280.94 eV, which corresponds to Ru(0). Double bonds π C=C were also detected in the sample at 285.49 eV, reflecting the presence of the PPh<sub>3</sub> groups, but no C=O double bonds could be observed (while the presence of a C=O bond was clearly observed on the XPS spectrum of **comp4** (see Supporting Information File 1, p. S6).

These Ru aggregates were also used in the reaction with furfurylimine **1** and triethoxyvinylsilane in toluene at 150 °C for 5 h (batch conditions). In this case, only 24% of **I2a** were obtained (Scheme 6), a significant decrease compared to the NMR yield of 77% with **comp4** as (pre)catalyst. These Ru(0) aggregates are therefore active, but the reaction kinetics are slower. While this observation is not a strict confirmation of our hypothesis regarding the formation of a monometallic complex, it is still consistent with it.

## Second optimization with a continuous flow chemistry system

Following these encouraging preliminary results obtained with our home-made, pulsed-flow setup, we decided to run continuous flow experiments using a commercial setup (Vapourtec E-series flow device). This equipment offers the added advan-





tage of being able to couple very simply two reaction steps, and thus to consider the direct functionalization of furfural via the in-situ formation of furfurylimine. Furthermore, as the  $[\text{Ru}_3(\text{CO})_{11}(\text{PPh}_3)]$  **comp4** catalyst showed an activity and a solubility in batch similar to **comp1**, we continued the optimization with the latter, triphenylphosphine being much cheaper than diphenyl(2-(triethoxysilyl)ethyl)phosphine.

With this setup, the flow system consisted of two mixtures: a mixture A containing furfural (0.7 M) and 2-(piperidin-1-yl)ethane-1,2-diamine (0.7 M) and a mixture B containing vinyltriethoxysilane (1.05 or 2.1 M) and the ruthenium catalyst (1 to 5 mol % with regards to furfural). The flow rates of pumps A and B being equal, the concentration of furfural in mixture A was  $\approx 0.7$  M and that of all furfural derivatives was 0.35 M in the final mixture. Mixture A was passed through a fixed bed reactor 1 filled with magnesium sulfate. The residence time depended on the intrinsic volume ( $V_i$ ) of this reactor (see Supporting Information File 1, p. S13), and was kept constant at  $\approx 18$  min. The mixture B was introduced at the outlet of the fixed bed reactor. A 1 mL stainless steel coil immersed in an oil bath at 130 °C was used as reactor 2, and was installed before the 10 mL reactor 3 (see Supporting Information File 1, pp. S12–S13 for more pictures). By also playing on the flow rate, this allowed us to have conditions close to the best ones observed during optimization on the pulsed-flow device, i.e.,  $t_{r2} = 5$  min and  $t_{r3} = 50$  min (see Table S2 in Supporting Information File 1, p. S11). Product recovery was initiated when the system reached a steady state, based on the dispersion curves provided with the apparatus (see Supporting Information File 1, p. S13). This equipment is a medium pressure system that cannot withstand pressures exceeding 10 bar. Hence, we

worked at about 7.5 bar to stay below the boiling curve of toluene in the temperature range used (180–200 °C).

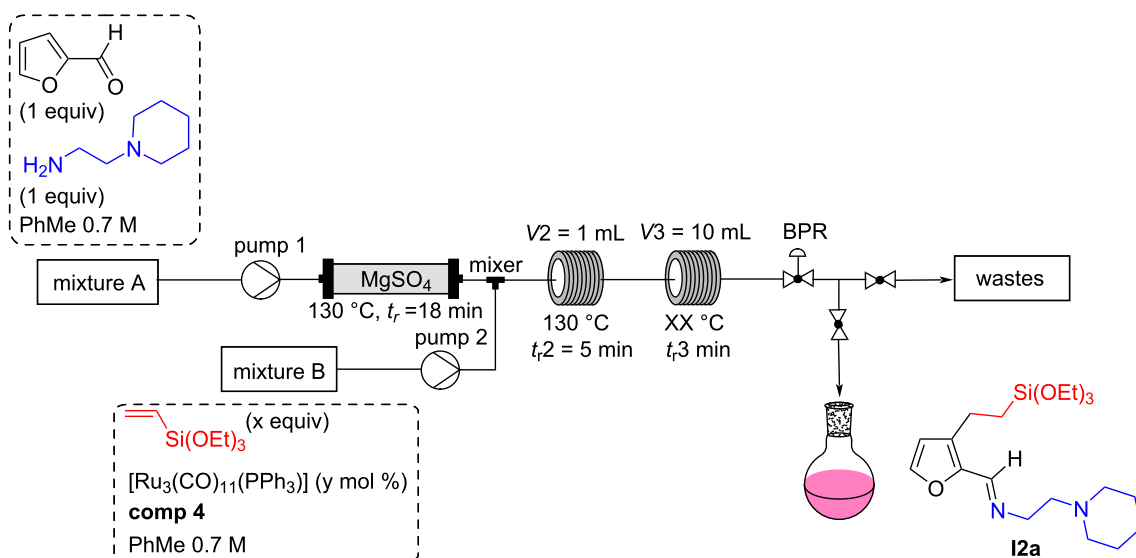
The first experiments performed with this configuration allowed us to validate our hypothesis, namely the possibility of directly functionalizing furfural by forming the imine in situ. Furthermore, the optimized conditions with the pulsed-flow device proved to be effective, as an NMR yield of 62% of the C3-alkylated imine **12a** was obtained by preheating at 130 °C for 5 min in reactor 1 (after introduction of mixture B), followed by heating at 180 °C for 45 min in reactor 2 (Table 2, entry 1). This allowed us to conclude that pressure does not have an impact on this reaction, since no noticeable difference could be reported when going from  $\approx 130$  bar to  $\approx 7.5$  bar. The catalytic loading for **comp4** could also be decreased to 1 mol % (Table 2, entries 1, 2, and 4), whereas a diminution in yield was observed when the amount of vinylsilane was decreased to 1.5 equivalents (Table 2, entry 3). The flow alkylation reaction thus appeared to be as efficient with a 1 mol % catalyst loading as with 5 mol %, in contrast to the batch conditions which required 5 mol % of the catalyst. Finally, a very slight improvement was observed by increasing the temperature to 200 °C (entry 5 compared to entry 4 in Table 2).

Finally, it is interesting to note that when the preheating was removed, the same NMR yield was measured with 1 mol % of **comp4** as catalyst (Table 2, entries 5 and 6). On the contrary, when preheating was removed with 5 mol % **comp4** (entry 1 in Table 2), a drastic decrease in yield was observed, from 62% to 44% (entry 1 vs entry 7). This allowed us to assume that such preactivation is no longer necessary with 1 mol % of **comp4**. Thus, a lower catalyst loading, i.e., a lower concentration of the catalyst in the solution, appears to prevent, or at least greatly reduce, the formation of ruthenium aggregates as observed previously, probably by simple dilution effect. As such, the preheating was suppressed for the continuation of our investigations.

## Extending the scope of the C3-alkylation of furfural in continuous flow

With the optimized conditions in hand (Table 2, entry 6), we were interested in extending the scope of this furfural alkylation reaction using a flow chemistry process to other reactants. For this, after each reaction, an aliquot of the resulting product was recovered for analysis and purification. The NMR yields were calculated on the alkylated imine before purification (based on a starting concentration of furfural of 0.35 M), and the isolated yields corresponded to the C3-alkylated aldehydes after the hydrolysis step that took place during purification. The productivity of each system is given in grams per hour (Scheme 7).



**Table 2:** Optimization of the alkylation reaction directly from furfural on the continuous flow setup.

Entry	comp4 (y mol %)	Vinylsilane (x equiv)	$t_{r3}$ [min] <sup>a</sup>	T3 [°C]	Yield [%] <sup>b</sup>
1	5	3	45	180	62
2	2.5	3	50	180	72
3	2.5	1.5	50	180	46
4	1	3	50	180	72
5	1	3	50	200	77
6 <sup>c</sup>	1	3	50	200	77
7 <sup>c</sup>	5	3	45	180	44

<sup>a</sup>A flow rate of 0.22 mL·min<sup>-1</sup> (0.11 mL·min<sup>-1</sup> for each pump), allowed us to have a residence time of 45 min in reactor 3, while a flow rate of 0.2 mL·min<sup>-1</sup> (0.1 mL·min<sup>-1</sup>), provided a residence time of 50 min in reactor 3. <sup>b</sup>Yields were calculated by <sup>1</sup>H NMR using *p*-nitrobenzene as internal standard. <sup>c</sup>Experiments performed without using the preheating loop in reactor 2.

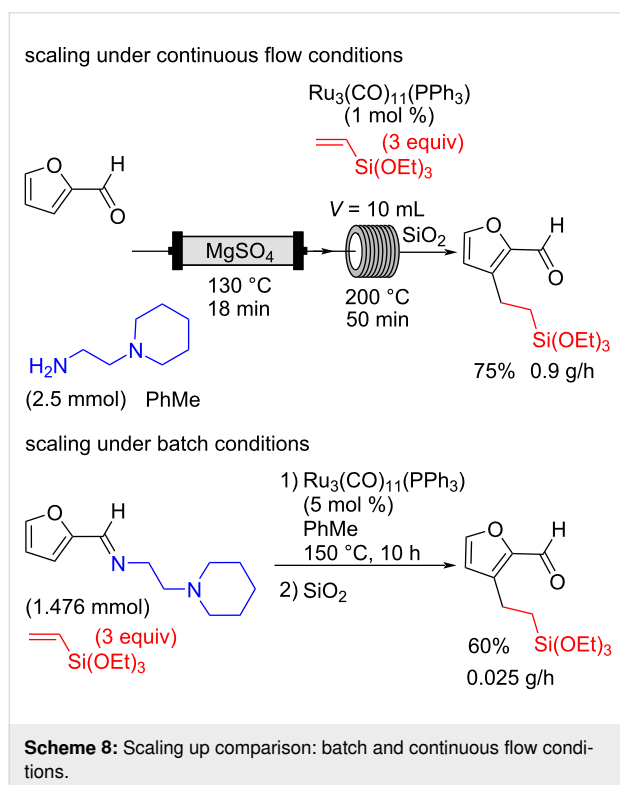
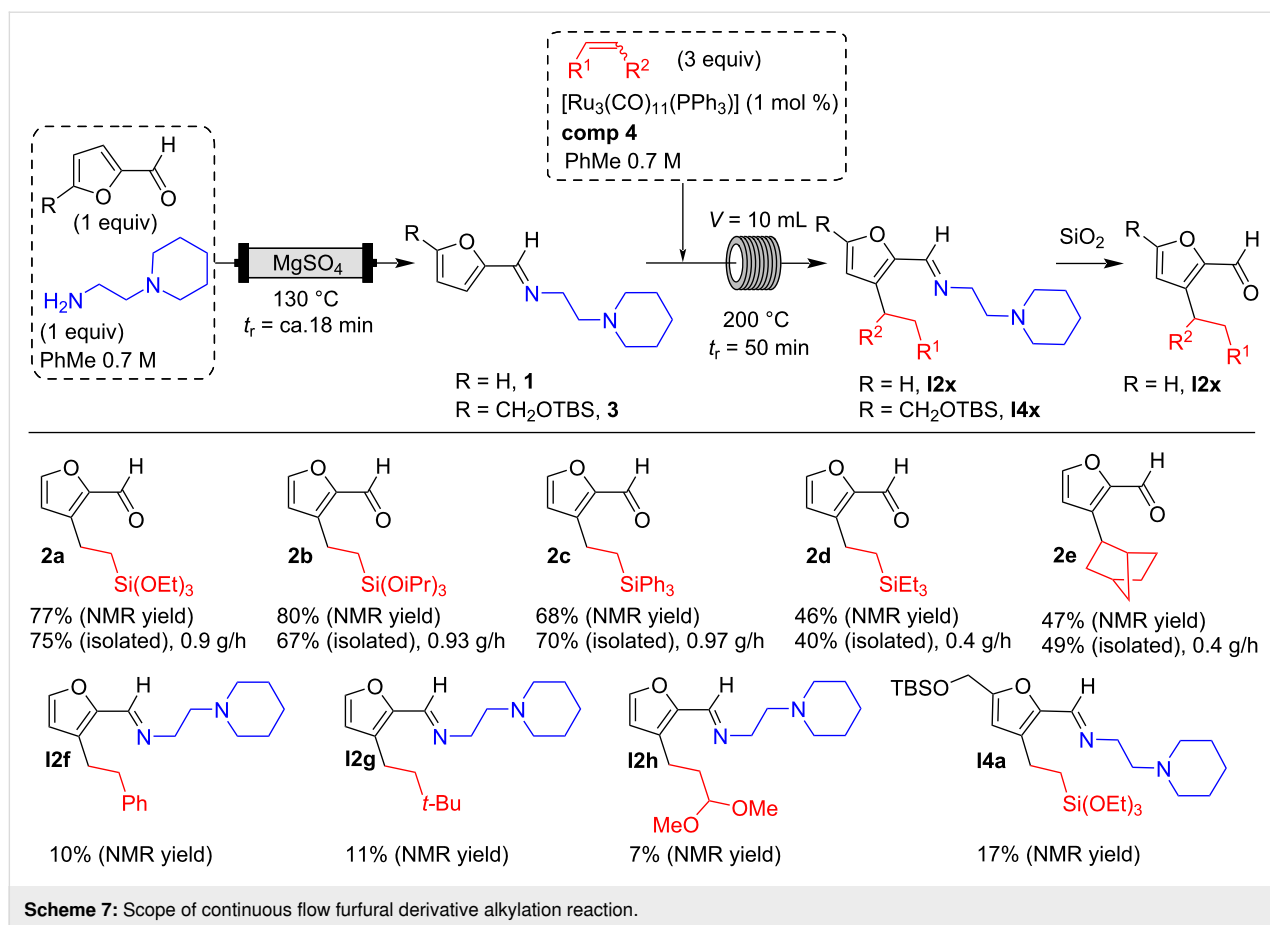
The optimized flow process conditions could be applied to a variety of vinylsilanes: trialkoxy-, triaryl-, and trialkylvinylsilanes, already used in the batch study [21]. The products **2a–e** were obtained in good yields and thus with good productivity. Alkenes without silicon in the vinyl position seemed much less reactive, such as a vinylacetal, a hindered olefin (3,3-dimethyl-1-butene), or styrene. In these cases, functionalized furfurals were not isolated. In contrast, norbornene, which has a more reactive double bond due to ring tension, gave *endo* product **2f** with an isolated yield of 49%. On the other side, disubstituted vinylsilanes proved to be ineffective, certainly because of the steric hindrance of the double bond decreasing the kinetics of the hydorruthenation step.

We also wanted to extend this alkylation reaction to a *tert*-butyldimethylsilyl (TBS)-protected 5-HMF derivative. Unfortunately, the yields obtained were very moderate. This reaction having slower kinetics could benefit from being performed at

lower temperatures and longer residence time to reduce catalyst degradation. This is unfortunately not possible to implement at the moment with our reactors.

## Conclusion

In conclusion, we have developed a method for the direct 2-step Ru-catalyzed alkylation of the C3–H bond of furfural by flow chemistry, via the preinstallation in a fixed bed reactor of an *ortho*-directing imine group that can be easily removed upon purification on silica. The reaction was found to be very efficient, with a Ru<sub>3</sub>(CO)<sub>11</sub>(PPh<sub>3</sub>) catalyst loading that could be lowered to 1 mol %, allowing for higher yields than batch conditions while requiring 5 times less catalyst. Furthermore, the interest of this flow chemistry approach lays in the scaling up of our reactions. To our great satisfaction, we could show that the productivity of the flow chemistry approach is better than the batch approach with the same catalyst (Scheme 8). This strategy represents a novel method to produce functionalized



furfurals, providing synthetically relevant building blocks on a large scale.

## Experimental

### Triphenylphosphine triruthenium undecacarbonyl (**comp4**)

Following a slightly modified procedure compared to the one reported [41], triruthenium dodecacarbonyl (1.4 g, 2.19 mmol, 1 equiv) was dissolved in freshly distilled and degassed THF (0.036 M) at 40 °C. The phosphine ligand (574.40 mg, 2.19 mmol, 1 equiv) dissolved in THF (0.11 M) was then added to the middle. The mixture was stirred at room temperature and treated dropwise with a solution of sodium benzophenone ketyl (about 0.05 equiv added) in THF (0.027 M) via a syringe until the phosphine ligand was completely consumed (monitored by TLC,  $\approx 10$  min). The solvent was then evaporated under reduced pressure. The remaining crude was purified by silica gel column chromatography using pentane as eluent, leading to 1.3 g of the desired complex as an orange solid (68% yield).  $^1\text{H}$  NMR (400 MHz,  $\text{CDCl}_3$ )  $\delta$  7.55–7.37 (m, 15H);  $^{31}\text{P}$  NMR (162 MHz,  $\text{CDCl}_3$ )  $\delta$  35.06; XPS BE Ru 3d<sub>5/2</sub> (281.58). These data are in good agreement with those reported in literature. Crystals were

grown from a solution in Et<sub>2</sub>O and identified by X-ray diffraction as a known phase of **comp4** [41].

### General procedure for C3-alkylation of furfural in continuous flow (vapourtec)

**Mixture A:** An oven-dried sealed tube equipped with a magnetic stirrer under argon, was loaded with furfural (240.20 mg, 2.50 mmol, 1 equiv), 2-(piperidin-1-yl)ethanamine (320.55 mg, 2.50 mmol, 1 equiv) and filled with dried toluene to a total volume of 3.5 mL.

**Mixture B:** An oven-dried sealed tube equipped with a magnetic stirrer, was loaded with triphenylphosphine triruthenium undecacarbonyl (1 mol % with regards to furfural) and degassed with argon. Vinyltriethoxysilane (3 equiv with regards to furfural) was then added to the middle, and the mixture was filled with dried toluene to a total volume of 3.5 mL. The mixture was stirred at room temperature to completely dissolve the catalyst.

The solution A is pumped into pump 1 (0.1 mL·min<sup>-1</sup>) and passed through the packed bed reactor which is set at 130 °C containing MgSO<sub>4</sub>. The residence time depends on the intrinsic volume (V<sub>i</sub>) of this reactor, and is kept constant at ≈18 min. The solution B is pumped through pump B (0.1 mL·min<sup>-1</sup>). The mixture of the two solutions A and B passed first through the coil reactor at 130 °C and then into a second coil reactor at the desired temperature. Product recovery is initiated when the system reaches a steady state, based on the dispersion curves given by the apparatus. After reaching the steady state an aliquot of the product was taken for <sup>1</sup>H NMR analysis using *p*-dinitrobenzene as an internal standard.

### 3-(2-(Triethoxysilyl)ethyl)furan-2-carbaldehyde (2a)

The reaction of mixture A containing furfural (240.20 mg, 2.50 mmol, 0.7 M) and 2-(piperidin-1-yl)ethanamine (320.55 mg, 2.50 mmol, 0.7 M), with mixture B containing triruthenium undecacarbonyl (22 mg, 0.025 mmol, 0.007 M) and vinyltriethoxysilane (1.43 g, 7.50 mmol, 1.07 M) was conducted by continuous flow chemistry, residence time 1 = 18 min, residence time 2 = 50 min. An aliquot of 0.5 mL of the product mixture was evaporated (93% conv., 77% NMR yield), and the crude was purified by silica gel column chromatography eluting with a mixture of cyclohexane/EtOAc 9:1 to give 38 mg of the desired product as an orange oil (75% yield). <sup>1</sup>H NMR (300 MHz, CDCl<sub>3</sub>) δ 9.76 (s, 1H), 7.54 (d, *J* = 1.7 Hz, 1H), 6.49 (d, *J* = 1.7 Hz, 1H), 3.81 (q, *J* = 7.0 Hz, 6H), 2.95–2.84 (m, 2H), 1.22 (t, *J* = 7.0 Hz, 9H), 1.01–0.90 (m, 2H). These data are in good agreement with those reported in literature [21].

## Supporting Information

### Supporting Information File 1

Experimental and copies of spectra.

[<https://www.beilstein-journals.org/bjoc/content/supplementary/1860-5397-19-43-S1.pdf>]

## Acknowledgements

The authors acknowledge MS3U of Sorbonne Université for HRMS analysis and CNRS. We also thank J. Forté for the XRD analyses (IPCM) and A. Miche for the XPS analyses (LRS).

## Funding

The authors acknowledge H2020-WIDESPREAD-05-2020-Twinning project Biomass4Synthons (B4S: grant agreement 951996) for financial support.

## ORCID® iDs

Myriam Roy - <https://orcid.org/0000-0001-9903-5067>

Juliette Blanchard - <https://orcid.org/0000-0003-1935-4207>

Julie Oble - <https://orcid.org/0000-0002-4002-255X>

## Preprint

A non-peer-reviewed version of this article has been previously published as a preprint: doi:10.26434/chemrxiv-2023-0s98h

## References

- Bozell, J. J.; Petersen, G. R. *Green Chem.* **2010**, *12*, 539–554. doi:10.1039/b922014c
- Mika, L. T.; Cséfalvay, E.; Németh, Á. *Chem. Rev.* **2018**, *118*, 505–613. doi:10.1021/acs.chemrev.7b00395
- Bender, T. A.; Dabrowski, J. A.; Gagné, M. R. *Nat. Rev. Chem.* **2018**, *2*, 35–46. doi:10.1038/s41570-018-0005-y
- Gómez Millán, G.; Hellsten, S.; Llorca, J.; Luque, R.; Sixta, H.; Balu, A. M. *ChemCatChem* **2019**, *11*, 2022–2042. doi:10.1002/cctc.201801843
- Khan, A.; Rahman, M. M.; Ramesh, M.; Khan, S.; Asiri, A. M. *Furan Derivatives: Recent Advances and Applications*; IntechOpen: London, UK, 2022. doi:10.5772/intechopen.95169
- Jaswal, A.; Singh, P. P.; Mondal, T. *Green Chem.* **2022**, *24*, 510–551. doi:10.1039/d1gc03278j
- Galkin, K. I.; Ananikov, V. P. *ChemSusChem* **2019**, *12*, 2976–2982. doi:10.1002/cssc.201900592
- Liu, B.; Zhang, Z. *ChemSusChem* **2016**, *9*, 2015–2036. doi:10.1002/cssc.201600507
- Xu, C.; Paone, E.; Rodríguez-Padrón, D.; Luque, R.; Mauriello, F. *Chem. Soc. Rev.* **2020**, *49*, 4273–4306. doi:10.1039/d0cs00041h
- Zhang, X.; Xu, S.; Li, Q.; Zhou, G.; Xia, H. *RSC Adv.* **2021**, *11*, 27042–27058. doi:10.1039/d1ra04633k
- Chen, S.; Wojcieszak, R.; Dumeignil, F.; Marceau, E.; Royer, S. *Chem. Rev.* **2018**, *118*, 11023–11117. doi:10.1021/acs.chemrev.8b00134

12. Galkin, K. I.; Ananikov, V. P. *ChemistryOpen* **2020**, *9*, 1135–1148. doi:10.1002/open.202000233
13. Kucherov, F. A.; Romashov, L. V.; Galkin, K. I.; Ananikov, V. P. *ACS Sustainable Chem. Eng.* **2018**, *6*, 8064–8092. doi:10.1021/acssuschemeng.8b00971
14. Bielski, R.; Grynkiewicz, G. *Green Chem.* **2021**, *23*, 7458–7487. doi:10.1039/d1gc02402g
15. Karlinskii, B. Y.; Ananikov, V. P. *Chem. Soc. Rev.* **2023**, *52*, 836–862. doi:10.1039/d2cs00773h
16. Dalton, T.; Faber, T.; Glorius, F. *ACS Cent. Sci.* **2021**, *7*, 245–261. doi:10.1021/acscentsci.0c01413
17. Rogge, T.; Kaplaneris, N.; Chatani, N.; Kim, J.; Chang, S.; Punji, B.; Schafer, L. L.; Musaev, D. G.; Wencel-Delord, J.; Roberts, C. A.; Sarpong, R.; Wilson, Z. E.; Brimble, M. A.; Johansson, M. J.; Ackermann, L. *Nat. Rev. Methods Primers* **2021**, *1*, 43. doi:10.1038/s43586-021-00041-2
18. Roudesly, F.; Oble, J.; Poli, G. *J. Mol. Catal. A: Chem.* **2017**, *426*, 275–296. doi:10.1016/j.molcata.2016.06.020
19. Karlinskii, B. Y.; Ananikov, V. P. *ChemSusChem* **2021**, *14*, 558–568. doi:10.1002/cssc.202002397
20. Mori, A.; Curpanen, S.; Pezzetta, C.; Perez-Luna, A.; Poli, G.; Oble, J. *Eur. J. Org. Chem.* **2022**, e202200727. doi:10.1002/ejoc.202200727
21. Pezzetta, C.; Veiros, L. F.; Oble, J.; Poli, G. *Chem. – Eur. J.* **2017**, *23*, 8385–8389. doi:10.1002/chem.201701850
22. Siopa, F.; Ramis Cladera, V.-A.; Afonso, C. A. M.; Oble, J.; Poli, G. *Eur. J. Org. Chem.* **2018**, 6101–6106. doi:10.1002/ejoc.201800767
23. Sala, R.; Kiala, G.; Veiros, L. F.; Broggini, G.; Poli, G.; Oble, J. *J. Org. Chem.* **2022**, *87*, 4640–4648. doi:10.1021/acs.joc.1c03044
24. Sala, R.; Roudesly, F.; Veiros, L. F.; Broggini, G.; Oble, J.; Poli, G. *Adv. Synth. Catal.* **2020**, *362*, 2486–2493. doi:10.1002/adsc.202000249
25. Curpanen, S.; Poli, G.; Perez-Luna, A.; Oble, J. *Asian J. Org. Chem.* **2022**, *11*, e202200199. doi:10.1002/ajoc.202200199
26. Plutschack, M. B.; Pieber, B.; Gilmore, K.; Seeberger, P. H. *Chem. Rev.* **2017**, *117*, 11796–11893. doi:10.1021/acs.chemrev.7b00183
27. Guidi, M.; Seeberger, P. H.; Gilmore, K. *Chem. Soc. Rev.* **2020**, *49*, 8910–8932. doi:10.1039/c9cs00832b
28. Gambacorta, G.; Sharley, J. S.; Baxendale, I. R. *Beilstein J. Org. Chem.* **2021**, *17*, 1181–1312. doi:10.3762/bjoc.17.90
29. Yoshida, J.-i.; Kim, H.; Nagaki, A. *ChemSusChem* **2011**, *4*, 331–340. doi:10.1002/cssc.201000271
30. Noël, T.; Buchwald, S. L. *Chem. Soc. Rev.* **2011**, *40*, 5010–5029. doi:10.1039/c1cs15075h
31. Govaerts, S.; Nyuchev, A.; Noël, T. *J. Flow Chem.* **2020**, *10*, 13–71. doi:10.1007/s41981-020-00077-7
32. Fabry, D. C.; Ho, Y. A.; Zapf, R.; Tremel, W.; Panthöfer, M.; Rueping, M.; Rehm, T. H. *Green Chem.* **2017**, *19*, 1911–1918. doi:10.1039/c7gc00497d
33. Liang, Y.-F.; Steinbock, R.; Yang, L.; Ackermann, L. *Angew. Chem., Int. Ed.* **2018**, *57*, 10625–10629. doi:10.1002/anie.201805644
34. Sharma, U. K.; Gemoets, H. P. L.; Schröder, F.; Noël, T.; Van der Eycken, E. V. *ACS Catal.* **2017**, *7*, 3818–3823. doi:10.1021/acscatal.7b00840
35. Roberge, D. M.; Ducry, L.; Bieler, N.; Cretton, P.; Zimmermann, B. *Chem. Eng. Technol.* **2005**, *28*, 318–323. doi:10.1002/ceat.200407128
36. Hessel, V. *Chem. Eng. Technol.* **2009**, *32*, 1655–1681. doi:10.1002/ceat.200900474
37. Kakiuchi, F.; Murai, S. *Acc. Chem. Res.* **2002**, *35*, 826–834. doi:10.1021/ar960318p
38. Schinkel, M.; Marek, I.; Ackermann, L. *Angew. Chem., Int. Ed.* **2013**, *52*, 3977–3980. doi:10.1002/anie.201208446
39. It should be noted that the hydrolysis of the imine occurs during the purification on silica gel.
40. Dallmann, K.; Buffon, R. *J. Mol. Catal. A: Chem.* **2002**, *185*, 187–194. doi:10.1016/s1381-1169(02)00022-5
41. Carniato, F.; Secco, A.; Gatti, G.; Marchese, L.; Sappa, E. *J. Sol-Gel Sci. Technol.* **2009**, *52*, 235–241. doi:10.1007/s10971-009-2018-y
42. bin Shawkataly, O.; Pankhi, M. A. A.; Alam, M. G.; Yeap, C. S.; Fun, H.-K. *Polyhedron* **2011**, *30*, 444–450. doi:10.1016/j.poly.2010.11.022
43. Miyajima, K.; Mafuné, F. *Chem. Phys. Lett.* **2022**, *786*, 139191. doi:10.1016/j.cplett.2021.139191

## License and Terms

This is an open access article licensed under the terms of the Beilstein-Institut Open Access License Agreement (<https://www.beilstein-journals.org/bjoc/terms>), which is identical to the Creative Commons Attribution 4.0 International License (<https://creativecommons.org/licenses/by/4.0>). The reuse of material under this license requires that the author(s), source and license are credited. Third-party material in this article could be subject to other licenses (typically indicated in the credit line), and in this case, users are required to obtain permission from the license holder to reuse the material.

The definitive version of this article is the electronic one which can be found at:  
<https://doi.org/10.3762/bjoc.19.43>



# Photocatalytic sequential C–H functionalization expediting acetoxymalonylation of imidazo heterocycles

Deepak Singh, Shyamal Pramanik and Soumitra Maity\*

## Letter

Open Access

Address:  
Department of Chemistry and Chemical Biology, Indian Institute of Technology (ISM) Dhanbad, JH 826004, India

Email:  
Soumitra Maity\* - smaity@iitism.ac.in

\* Corresponding author

Keywords:  
C–H functionalization; imidazo heterocycles; photoredox; regioselective; relay catalysis

*Beilstein J. Org. Chem.* **2023**, *19*, 666–673.  
<https://doi.org/10.3762/bjoc.19.48>

Received: 23 February 2023  
Accepted: 09 May 2023  
Published: 12 May 2023

This article is part of the thematic issue "C–H bond functionalization: recent discoveries and future directions".

Guest Editor: I. Chatterjee



© 2023 Singh et al.; licensee Beilstein-Institut.  
License and terms: see end of document.

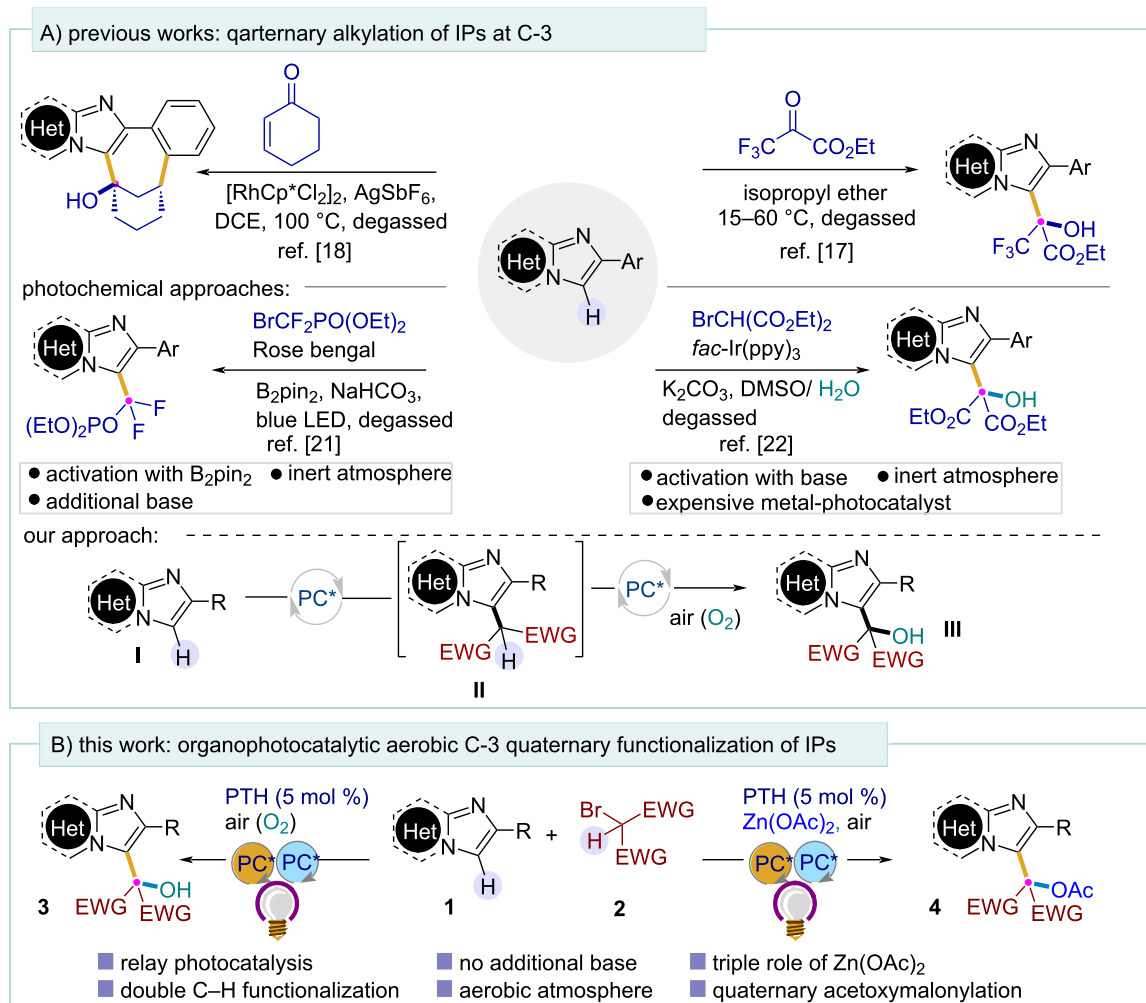
## Abstract

The importance of functionalized imidazo heterocycles has often been featured in several impactful research both from academia and industry. Herein, we report a direct C-3 acetoxymalonylation of imidazo heterocycles using relay C–H functionalization enabled by organophotocatalysis starring zinc acetate in the triple role of an activator, ion scavenger as well as an acetylating reagent. The mechanistic investigation revealed a sequential  $sp^2$  and  $sp^3$  C–H activation, followed by functionalization driven by zinc acetate coupled with the photocatalyst PTH. A variety of imidazo[1,2-*a*]pyridines and related heterocycles were explored as substrates along with several active methylene reagents, all generating the products with excellent yields and regioselectivity, thus confirming excellent functional group tolerability.

## Introduction

Among all N-fused heterocycles, imidazo[1,2-*a*]pyridines (IPs) are the prevalent moieties in several bioactive pharmaceuticals and natural products [1–4]. Moreover, due to their susceptibility towards 'excited-state intramolecular proton transfer' phenomena, IPs are also effective in optoelectronics and materials sciences [5,6]. C-3-functionalized imidazo[1,2-*a*]pyridines are particularly familiar due to their biological and medicinal attributes [7–11]. Not surprisingly, the C-3 functionalization of IPs is a continuing interest of research in the synthetic community [12–16].

Despite many successful strategies in this field, the regioselective C–H functionalization is still challenging for chemists to combine a  $C(sp^3)$  carbon of incoming functionalities and  $C(sp^2)$  carbon of the IP core. The direct C-3 alkylation of imidazopyridines using active malonates and related moieties has been achieved by different routes [17–20]. However, these reactions rely either on harsh reaction conditions or require the preactivation of substrates, which limits their synthetic efficiency. A photocatalytic quaternary C-3 alkylation has also been reported recently (Scheme 1A) [21,22]. During the course of our study,



Scheme 1: Strategies of C-3 functionalizations of IPs and present work.

the Wu group reported a solvent-controlled chemodivergent formation of C-3 ethoxycarbonylmethylated and hydroxyalkylated IPs under visible light using water or alcohol as the source of the oxygenated group under degassed conditions [22]. However, all these photochemical methods require the usage of a substantial amount of base, the preactivation with a boron complex ( $\text{B}_2\text{pin}_2$ ), and using an expensive metal-based photocatalyst [ $\text{fac-Ir}(\text{ppy})_3$ ] under inert atmosphere. We have recently demonstrated that aerial oxygen could be captured by alkyl radicals to install a keto-functionality onto alkenes in an organophotocatalytic way [23]. We aimed to extend this aerobic oxygenation approach to imidazo heterocycles **II** to install the hydroxymalonate unit onto **I** through sequential photoredox C–H functionalization.

Till date, there is no report of the direct incorporation of a quaternary hydroxyalkyl, specifically a hydroxymalonyl group at the C-3 position of IPs using air as the sole oxygen source.

Keeping in mind the progress in photochemical relay catalysis [24] and the attention paid to photocatalytic carbon-bond functionalization in the past several years [25], here we developed an organophotoredox-catalyzed C–H functionalization of imidazo[1,2-*a*]pyridines and related heterocycles with active bromomethylenes under mild conditions (Scheme 1B). Importantly, using simple  $\text{Zn}(\text{OAc})_2$  as the additive, the first photocatalytic direct acetoxymalonylation of imidazo heterocycles was developed under aerobic conditions. Here, the additive  $\text{Zn}(\text{OAc})_2$  plays a crucial triple role as activator of IPs, halide scavenger, and acetylating agent.

## Results and Discussion

### Optimization

In the quest for the optimal reaction conditions, we started our investigations with 2-phenylimidazo[1,2-*a*]pyridine (**1a**) and diethyl bromomalonate (**2a**) as model substrates. Initially, the reaction was carried out between **1a** and **2a** in dry  $\text{CH}_3\text{CN}$  as

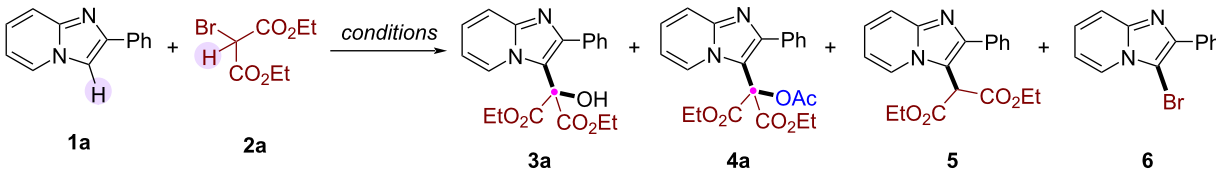
solvent under N<sub>2</sub> atmosphere using 4CzIPN as the photocatalyst. Irradiating the reaction mixture for 10 h under blue LEDs (450 nm) led to the isolation of products **5** (54%) and **6** (28%) (Table 1, entry 1). However, the same reaction, under aerobic conditions, delivered compounds **3a** (47%) and **6** (22%) (Table 1, entry 2). Keeping in mind the ability of Zn(OAc)<sub>2</sub> as a bromide ion scavenger [26], we used Zn(OAc)<sub>2</sub> (2 equiv) as an additive to prevent the formation of the bromo product **6**. While the additive successfully prevented the formation of compound **6**, we were delighted to isolate the unexpected acetylated product **4a** with a promising yield of 38% (Table 1, entry 3), reflecting the ability of Zn(OAc)<sub>2</sub> to act as an acetylating agent. While screening other organophotocatalysts, we detected no desired product **4a** (Table 1, entries 4–6) [27], except for photocatalyst 10-phenylphenothiazine (PTH) under violet LEDs which uplifted the yield up to 52% (Table 1, entry 7). Now with the optimal catalyst in hand, we screened some common solvents, out of which 1,2-DCE positively impacted the yield (Table 1, entries 8–11). However, the best result was obtained when 3.0 equiv of Zn(OAc)<sub>2</sub> was used as an additive (Table 1, entry 12). To check the viability of other acetylating agents,

Zn(OAc)<sub>2</sub> was replaced with AcOH, generating the desired product in a comparatively lower yield (Table 1, entry 13). Finally, control experiments without a catalyst (Table 1, entry 14), light (entry 15) or acetylation agent (entry 16) failed to provide the desired product **4a**, displaying the necessity of each component for developing the reaction.

## Substrate scope

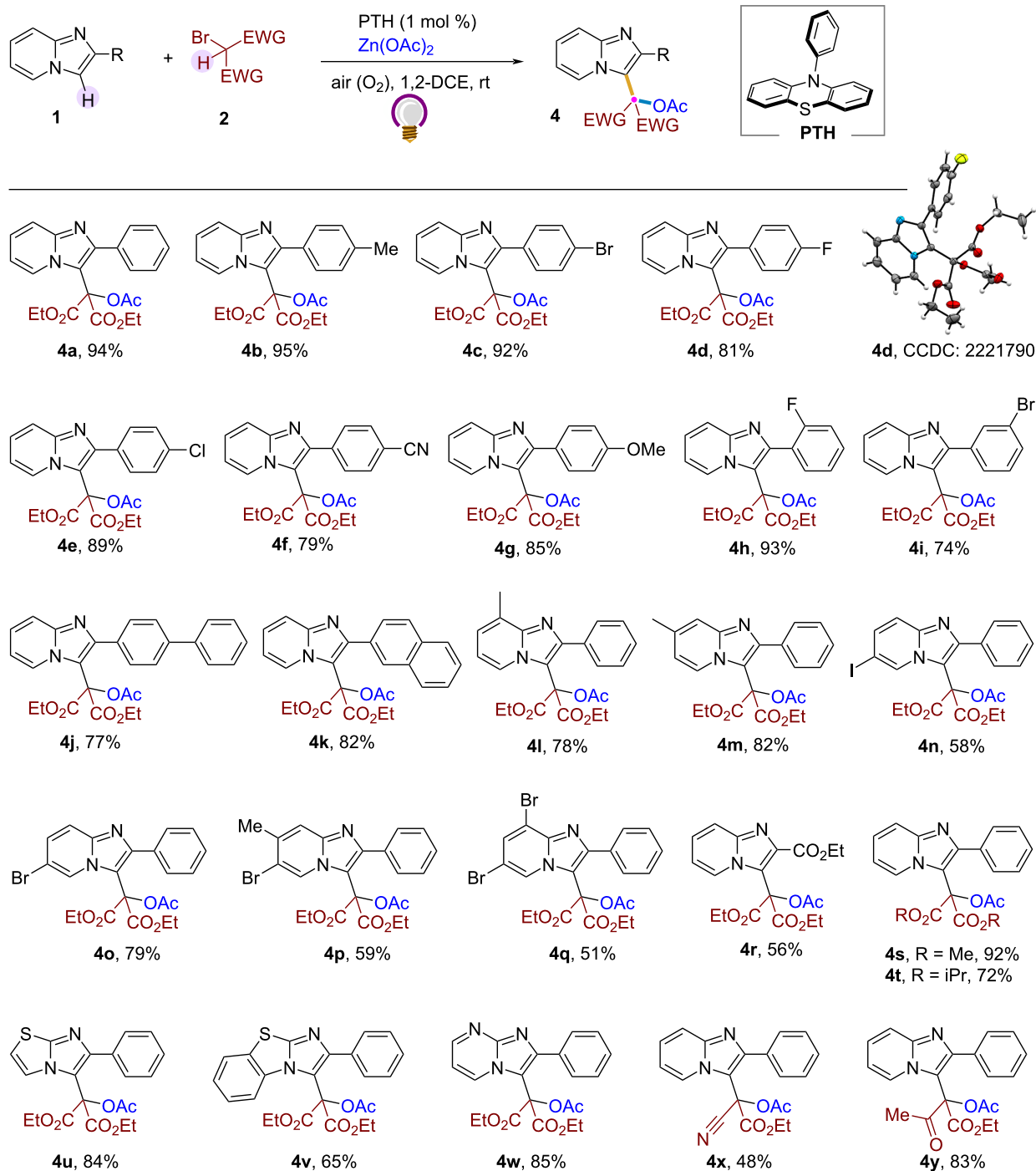
With suitable reaction conditions (Table 1, entry 12), we systematically investigated the scope of this acetoxymalonylation strategy with substrate **2a** (Scheme 2). Several imidazo[1,2-*a*]pyridines with diverse aryl substituents in the C-2 position were acetoxymalonylated, providing the desired products **4a–k** regioselectively in good to excellent yields. Reflection of electronic properties was shown by the substituents attached to the aryl ring – as electron-releasing groups (Me, OMe) showed little more reactivity than electron-withdrawing groups (CN) at the same position (**4b**, **4f**, and **4g**). Halogen-substituted IPs also followed the general reactivity trend of the respective halogens (**4c–e**). Excellent reactivity was found for *o*-F and *m*-Br-substituted IPs (**4h** and **4i**). Similarly, IPs associated with biphenyl

**Table 1:** Reaction optimization.<sup>a</sup>

				
Entry	Catalyst	Solvent	Additive	Yield (%) <sup>b</sup> <b>3a:4a:5:6</b>
1 <sup>c</sup>	4-CzIPN	CH <sub>3</sub> CN	–	0:0:54:28
2	4-CzIPN	CH <sub>3</sub> CN	–	47:0:0:22
3	4-CzIPN	CH <sub>3</sub> CN	Zn(OAc) <sub>2</sub>	0:38:0:0
4	Rose Bengal	CH <sub>3</sub> CN	Zn(OAc) <sub>2</sub>	–
5	eosin-Y	CH <sub>3</sub> CN	Zn(OAc) <sub>2</sub>	–
6	rhodamine-B	CH <sub>3</sub> CN	Zn(OAc) <sub>2</sub>	–
7 <sup>d</sup>	PTH	CH <sub>3</sub> CN	Zn(OAc) <sub>2</sub>	0:52:0:0
8	PTH	1,4-dioxane	Zn(OAc) <sub>2</sub>	0:34:0:0
9	PTH	DMF	Zn(OAc) <sub>2</sub>	0:25:0:0
10	PTH	toluene	Zn(OAc) <sub>2</sub>	0:18:0:0
11	PTH	1,2-DCE	Zn(OAc) <sub>2</sub>	0:70:0:0
<b>12<sup>e</sup></b>	<b>PTH</b>	<b>1,2-DCE</b>	<b>Zn(OAc)<sub>2</sub></b>	<b>0:94:0:0</b>
13	PTH	1,2-DCE	AcOH	0:64:0:0
14	–	1,2-DCE	Zn(OAc) <sub>2</sub>	–
15 <sup>f</sup>	PTH	1,2-DCE	Zn(OAc) <sub>2</sub>	–
16	PTH	1,2-DCE	–	57:0:0:24

<sup>a</sup>Reaction conditions: **1a** (0.2 mmol), **2a** (0.4 mmol), catalyst (5 mol %), additive (0.4 mmol) in dry solvent (2 mL) under aerobic conditions, irradiation with 12 W blue LEDs for 10 h. <sup>b</sup>Isolated yield. <sup>c</sup>Under N<sub>2</sub> atmosphere. <sup>d</sup>Irradiation with violet LEDs (λ<sub>max</sub> = 390 nm). <sup>e</sup>3.0 equiv of zinc acetate used.

<sup>f</sup>In the dark, without light source.



**Scheme 2:** Substrate scope. Conditions: unless otherwise noted, all reactions were carried out with **1** (0.2 mmol), **2** (0.4 mmol), PTH (5 mol %), Zn(OAc)<sub>2</sub> (0.6 mmol), dry 1,2-DCE (2 mL), irradiation with LEDs ( $\lambda_{\text{max}}$  = 390 nm), under air for 10 h.

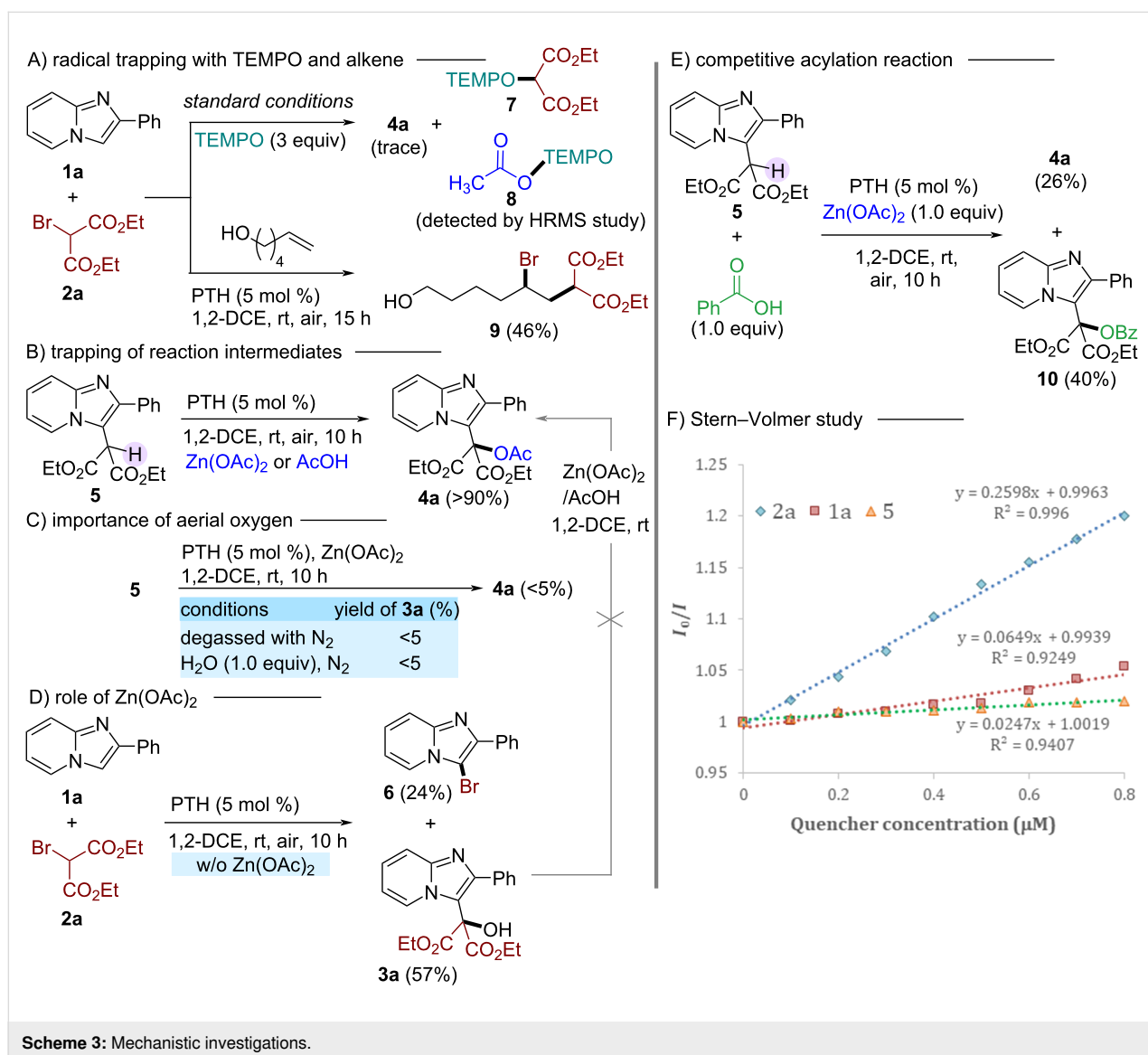
and naphthyl groups in the C-2 position were also suitable substrates giving the corresponding products **4j** and **4k** in 77% and 82% yield, respectively. However, the yield of the products varied when different groups with diverse electronic properties were present in the pyridine ring of the IP moieties (**4l–q**). With

substrates having a methyl substitution at C-7 and C-8 of the pyridine ring, the yields and regioselectivity were still excellent (**4l** and **4m**), but reduced significantly upon introducing a halogen group onto the pyridine ring. Except for the 6-bromo-substituted compound (**4o**), all other substrates having a



halogen substituent in the pyridine ring showed reduced yields (**4n**, and **4p,q**). The number of substituents also seemed to negatively affect the yield, as observed for products **4p** and **4q**, featuring two substituents each on the pyridine ring. Moreover, IPs with a non-aromatic C-2 substituent like an ester group were also included (**4r**). We also explored bromo analogues of other active methylenes such as ethyl cyanoacetate, ethyl acetoacetate, dimethyl, and diisopropyl malonates, as extension of diethyl malonate (**4s,t** and **4x,y**). Lastly, we explored a few heterocycles that resemble imidazo[1,2-*a*]pyridine to vindicate the generality of this method. Gratifyingly, 6-phenylimidazo[2,1-*b*]thiazole, 2-phenylbenzo[*d*]imidazo[2,1-*b*]thiazole, and 2-phenylimidazo[1,2-*a*]pyrimidine participated well under the standard reaction conditions, generating the corresponding acetoxy-malonated products **4u–w** in good to excellent yields.

Several control experiments were performed to gain insights into the mechanistic pathway of this reaction. Firstly, a radical scavenging experiment using the radical scavenger TEMPO was performed (Scheme 3A). Upon analyzing the reaction mixture of **1a** and **2a** under standard conditions in the presence of TEMPO, we found only a trace of the desired product **4a**. At the same time, a TEMPO-DEM adduct **7** and TEMPO-OAc adduct **8** were identified by the HRMS analysis of the crude reaction mixture, indicating the involvement of a malonyl radical and an acetyl radical in the course of the reaction (see Supporting Information File 1 for details). Additionally, when an aliphatic alkene, 5-hexen-1-ol was introduced into the reaction mixture under standard conditions without Zn(OAc)<sub>2</sub>, an ATRA product **9** was isolated, further confirming the involvement of a malonyl radical generated by the cleavage of the C–Br bond of **2a** [28]. Next, an attempt was made to identify the key interme-



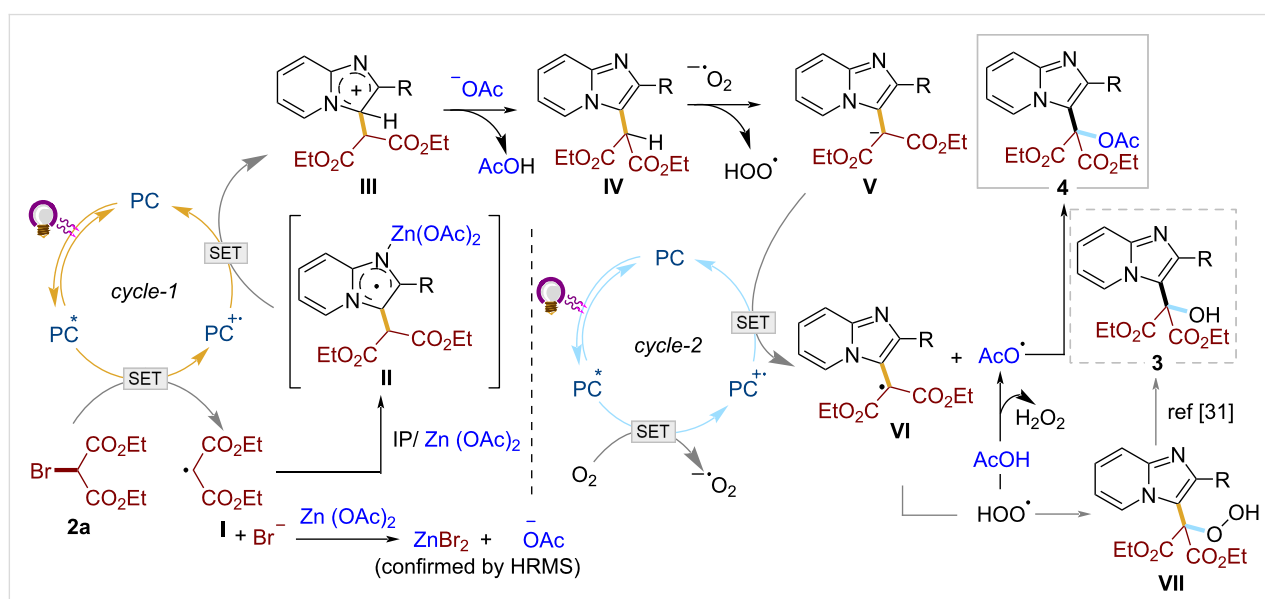
diate of the reaction (Scheme 3B). When compound **5** was subjected to the acetylation reaction individually with  $\text{Zn}(\text{OAc})_2$  and  $\text{AcOH}$  under optimized reaction conditions, the acetylated product **4a** was produced with excellent conversion (>90%). These results suggest the involvement of compound **5** as an intermediate, and  $\text{Zn}(\text{OAc})_2$  or  $\text{AcOH}$  may be effective acetylating agents via generation of acetyl radicals. Control experiments under degassed conditions with or without water only delivered a trace amount (<5%) of the desired products, indicating that aerial oxygen plays a crucial role in the second catalytic cycle for the conversion of **5** to **3a** or **4a** (Scheme 3C). To determine the role of zinc acetate, a standard reaction of **1a** and **2a** in the absence of  $\text{Zn}(\text{OAc})_2$  was conducted (Scheme 3D). The results showed the formation of hydroxymalonated product **3a** (57%) and bromo derivative **6** (24%). Notably, the hydroxymalonated product **3a** under the reaction conditions was not converted to the acetylated derivative **4a**, confirming **3a** is not the intermediate for the final product **4a**. So,  $\text{Zn}(\text{OAc})_2$  is crucial in shutting down the formation of **6** by scavenging free bromide in the reaction as  $\text{ZnBr}_2$  salt (confirmed by HRMS). In addition, an excellent yield of the final product **4a** [**4a**: 94% vs (**6**, 24% + **3a**, 57%)] with additive indicates that zinc acetate plays a crucial role in activating IP towards the photoredox coupling reaction. Shifting of protons in the  $^1\text{H}$  NMR spectrum of 2-phenylimidazo[1,2-a]pyridine (**1a**) in the presence of  $\text{Zn}(\text{OAc})_2$  in  $\text{CDCl}_3$  indicates a weak interaction of  $\text{Zn}(\text{OAc})_2$  with **1a** (see Supporting Information File 1 for details) [20,21]. Finally, the reaction of **5** with benzoic acid and zinc acetate (in a 1:1 ratio) under standard reaction protocol resulted in the competitive formation of products **4a** and **10** (Scheme 3E), indicating the susceptibility of other acids towards this method.

These results, along with the Stern–Volmer fluorescence quenching study (Scheme 3F), expressed that the photoredox reaction started with the reductive generation of a malonyl radical from bromomalonate by interaction with the photocatalyst.

Analyzing all the observations from the above mechanistic studies, we propose a plausible mechanism involving sequential activation and functionalization of  $\text{sp}^2$  and  $\text{sp}^3$  C–H bonds via relay catalysis (Scheme 4). The relay can be divided into two cycles; the first cycle (*cycle-1*) deals with the  $\text{C}(\text{sp}^2)$ –H functionalization at the C-3 position of the imidazo heterocycles, while the second cycle (*cycle-2*) is all about the  $\text{C}(\text{sp}^3)$ –H functionalization at the newly incorporated active methylene center.

*Cycle-1* is initiated with the reduction of bromomalonate **2a** by the photoexcited catalyst  $\text{PC}^*$  to malonyl radical **I**. This is followed by the Minisci-type addition of radical **I** to the imidazopyridine, preactivated by Lewis acidic  $\text{Zn}(\text{OAc})_2$  [29].  $\text{PC}^{++}$  then oxidizes the resulting radical **II** to carbocation **III** which rearomatizes by losing a proton to generate the intermediate **IV** and closing the first catalytic cycle. Meanwhile, the bromide ions in the medium undergo anion exchange with the  $\text{Zn}(\text{OAc})_2$  to release free acetate ions, along with the conversion into  $\text{ZnBr}_2$  (confirmed by HRMS). These in situ-generated free acetate ions function as a base, deprotonating carbocation **III** to produce the intermediate **IV** and  $\text{AcOH}$ .

The first step of *cycle-2* involves the oxidation of the excited photocatalyst by aerial oxygen to generate superoxide anion and



Scheme 4: Plausible reaction mechanism.

**PC<sup>+</sup>**. The superoxide anion (O<sub>2</sub><sup>•−</sup>) then captures the proton from the active methylene center of intermediate **IV** to generate the malonyl anion **V**, which undergoes single electron oxidation by **PC<sup>+</sup>** generating the malonyl radical **VI** [30,31]. Meanwhile, the hydroperoxy radical (•OOH) formed, reacts with AcOH produced in *cycle-1* to give the acetoxy radical (•OAc) and H<sub>2</sub>O<sub>2</sub>. Then, the radical recombination between AcO• and radical **VI** furnishes the desired product **4**. In the absence of the acetoxy radical (•OAc), the hydroperoxy radical (•OOH) may combine with radical **VI** to produce **VII**, which then easily converts into hydroxymalonated product **3** [31].

## Conclusion

Thus, we have reported the successful C-3 acetoxymalonylation of imidazo[1,2-*a*]pyridines and related heterocycles by an organophotocatalytic relay C–H functionalization strategy with Zn(OAc)<sub>2</sub> in the triple role of an activator, bromide scavenger, and acetylating agent. The developed method is heavy-metal free, as shown by the use of inexpensive PTH, as well as a base-free approach, and involves aerial oxygen to generate exciting derivatives, which may prove to be valuable in the field of radical chemistry research in future.

## Supporting Information

### Supporting Information File 1

Experimental section and characterization of synthesized compounds.

[<https://www.beilstein-journals.org/bjoc/content/supplementary/1860-5397-19-48-S1.pdf>]

## Funding

Financial support from SERB (CRG/2021/004140), India, is gratefully acknowledged. D.S and S.P thank IIT(ISM) and CSIR, New Delhi, for doctoral fellowships, respectively.

## ORCID® iDs

Soumitra Maity - <https://orcid.org/0000-0003-0944-8162>

## References

- Enguehard-Gueiffier, C.; Gueiffier, A. *Mini-Rev. Med. Chem.* **2007**, *7*, 888–899. doi:10.2174/138955707781662645
- Devi, N.; Singh, D.; Rawal, R. K.; Bariwal, J.; Singh, V. *Curr. Top. Med. Chem.* **2016**, *16*, 2963–2994. doi:10.2174/1568026616666160506145539
- Kishbaugh, T. L. S. *Curr. Top. Med. Chem.* **2016**, *16*, 3274–3302. doi:10.2174/1568026616666160506145141
- Sanapalli, B. K. R.; Ashames, A.; Sigalapalli, D. K.; Shaik, A. B.; Bhandare, R. R.; Yele, V. *Antibiotics (Basel, Switz.)* **2022**, *11*, 1680. doi:10.3390/antibiotics11121680
- Mutai, T.; Tomoda, H.; Ohkawa, T.; Yabe, Y.; Araki, K. *Angew. Chem., Int. Ed.* **2008**, *47*, 9522–9524. doi:10.1002/anie.200803975
- Padalkar, V. S.; Seki, S. *Chem. Soc. Rev.* **2016**, *45*, 169–202. doi:10.1039/c5cs00543d
- Deep, A.; Bhatia, R. K.; Kaur, R.; Kumar, S.; Jain, U. K.; Singh, H.; Batra, S.; Kaushik, D.; Deb, P. K. *Curr. Top. Med. Chem.* **2016**, *17*, 238–250. doi:10.2174/1568026616666160530153233
- Goel, R.; Luxami, V.; Paul, K. *Curr. Top. Med. Chem.* **2016**, *16*, 3590–3616. doi:10.2174/1568026616666160414122644
- Xi, J.-B.; Fang, Y.-F.; Frett, B.; Zhu, M.-L.; Zhu, T.; Kong, Y.-N.; Guan, F.-J.; Zhao, Y.; Zhang, X.-W.; Li, H.-y.; Ma, M.-L.; Hu, W. *Eur. J. Med. Chem.* **2017**, *126*, 1083–1106. doi:10.1016/j.ejmech.2016.12.026
- Shukla, N. M.; Salunke, D. B.; Yoo, E.; Mutz, C. A.; Balakrishna, R.; David, S. A. *Bioorg. Med. Chem.* **2012**, *20*, 5850–5863. doi:10.1016/j.bmc.2012.07.052
- Chernyak, N.; Gevorgyan, V. *Angew. Chem., Int. Ed.* **2010**, *49*, 2743–2746. doi:10.1002/anie.200907291
- Patel, O. P. S.; Nandwana, N. K.; Legoabe, L. J.; Das, B. C.; Kumar, A. *Adv. Synth. Catal.* **2020**, *362*, 4226–4255. doi:10.1002/adsc.202000633
- Ghosh, D.; Ghosh, S.; Hajra, A. *Adv. Synth. Catal.* **2021**, *363*, 5047–5071. doi:10.1002/adsc.202100981
- Tran, C.; Hamze, A. *Molecules* **2022**, *27*, 3461. doi:10.3390/molecules27113461
- Ravi, C.; Chandra Mohan, D.; Adimurthy, S. *Org. Biomol. Chem.* **2016**, *14*, 2282–2290. doi:10.1039/c5ob02475g
- Tashrif, Z.; Mohammadi-Khanaposhtani, M.; Larijani, B.; Mahdavi, M. *Eur. J. Org. Chem.* **2020**, 269–284. doi:10.1002/ejoc.201901491
- Li, K.; Zhao, X.-M.; Yang, F.-L.; Hou, X.-H.; Xu, Y.; Guo, Y.-C.; Hao, X.-Q.; Song, M.-P. *RSC Adv.* **2015**, *5*, 90478–90481. doi:10.1039/c5ra15678e
- Reddy, K. N.; Chary, D. Y.; Sridhar, B.; Reddy, B. V. S. *Org. Lett.* **2019**, *21*, 8548–8552. doi:10.1021/acs.orglett.9b03041
- Xiao, Y.; Yu, L.; Yu, Y.; Tan, Z.; Deng, W. *Tetrahedron Lett.* **2020**, *61*, 152606. doi:10.1016/j.tetlet.2020.152606
- Chaubey, N. R.; Kapdi, A. R.; Maity, B. *Synthesis* **2021**, *53*, 1524–1530. doi:10.1055/s-0040-1706103
- Singsardar, M.; Mondal, S.; Laru, S.; Hajra, A. *Org. Lett.* **2019**, *21*, 5606–5610. doi:10.1021/acs.orglett.9b01954
- Huang, M.; Wang, L.; Yang, X.; Kim, J. K.; Gong, M.; Zhang, J.; Li, Y.; Wu, Y. *Tetrahedron* **2022**, *126*, 132988. doi:10.1016/j.tet.2022.132988
- Roy Chowdhury, S.; Singh, D.; Hoque, I. U.; Maity, S. *J. Org. Chem.* **2020**, *85*, 13939–13950. doi:10.1021/acs.joc.0c01985
- Sakakibara, Y.; Murakami, K. *ACS Catal.* **2022**, *12*, 1857–1878. doi:10.1021/acscatal.1c05318
- Holmberg-Douglas, N.; Nicewicz, D. A. *Chem. Rev.* **2022**, *122*, 1925–2016. doi:10.1021/acs.chemrev.1c00311
- Samanta, A.; Pramanik, S.; Mondal, S.; Maity, S. *Chem. Commun.* **2022**, *58*, 8400–8403. doi:10.1039/d2cc002574d
- Ritu; Sharma, C.; Kumar, S.; Jain, N. *Org. Biomol. Chem.* **2020**, *18*, 2921–2928. doi:10.1039/d0ob00563k

With these catalytic systems (entries 4–6) no desired products (**3a**, **4a**, **5**, **6**) were identified; instead a new product *N*-(pyridin-2-yl)benzamide was isolated in 8–14% yield. Jain et al. recently reported that aerobic oxygen under photoredox conditions oxidatively cleave the imidazo ring of **1a** to benzamide derivatives.

28. Nguyen, J. D.; Tucker, J. W.; Konieczynska, M. D.; Stephenson, C. R. J. *J. Am. Chem. Soc.* **2011**, *133*, 4160–4163. doi:10.1021/ja108560e  
See for details for photoredox ATRA reaction between diethyl bromomalonate **2a** and 5-hexen-1-ol.
29. Dam, J.; Ismail, Z.; Kurebwa, T.; Gangat, N.; Harmse, L.; Marques, H. M.; Lemmerer, A.; Bode, M. L.; de Koning, C. B. *Eur. J. Med. Chem.* **2017**, *126*, 353–368. doi:10.1016/j.ejmech.2016.10.041
30. Katta, N.; Zhao, Q.-Q.; Mandal, T.; Reiser, O. *ACS Catal.* **2022**, *12*, 14398–14407. doi:10.1021/acscatal.2c04736
31. Xia, X.-D.; Ren, Y.-L.; Chen, J.-R.; Yu, X.-L.; Lu, L.-Q.; Zou, Y.-Q.; Wan, J.; Xiao, W.-J. *Chem. – Asian J.* **2015**, *10*, 124–128. doi:10.1002/asia.201402990

## License and Terms

This is an open access article licensed under the terms of the Beilstein-Institut Open Access License Agreement (<https://www.beilstein-journals.org/bjoc/terms>), which is identical to the Creative Commons Attribution 4.0 International License (<https://creativecommons.org/licenses/by/4.0>). The reuse of material under this license requires that the author(s), source and license are credited. Third-party material in this article could be subject to other licenses (typically indicated in the credit line), and in this case, users are required to obtain permission from the license holder to reuse the material.

The definitive version of this article is the electronic one which can be found at:  
<https://doi.org/10.3762/bjoc.19.48>



# Sulfate radical anion-induced benzylic oxidation of *N*-(arylsulfonyl)benzylamines to *N*-arylsulfonylimines

Joydev K. Laha\*, Pankaj Gupta and Amitava Hazra

## Full Research Paper

Open Access

### Address:

Department of Pharmaceutical Technology (Process Chemistry),  
National Institute of Pharmaceutical Education and Research, S. A. S.  
Nagar, Punjab 160062, India

### Email:

Joydev K. Laha\* - jlaha@niper.ac.in

\* Corresponding author

### Keywords:

arylsulfonylimine; benzylic oxidation; benzyl sulfonamide;  $K_2S_2O_8$ ;  
sulfate radical anion

Beilstein J. Org. Chem. **2023**, *19*, 771–777.

<https://doi.org/10.3762/bjoc.19.57>

Received: 28 February 2023

Accepted: 25 May 2023

Published: 05 June 2023

This article is part of the thematic issue "C–H bond functionalization: recent discoveries and future directions".

Guest Editor: I. Chatterjee



© 2023 Laha et al.; licensee Beilstein-Institut.  
License and terms: see end of document.

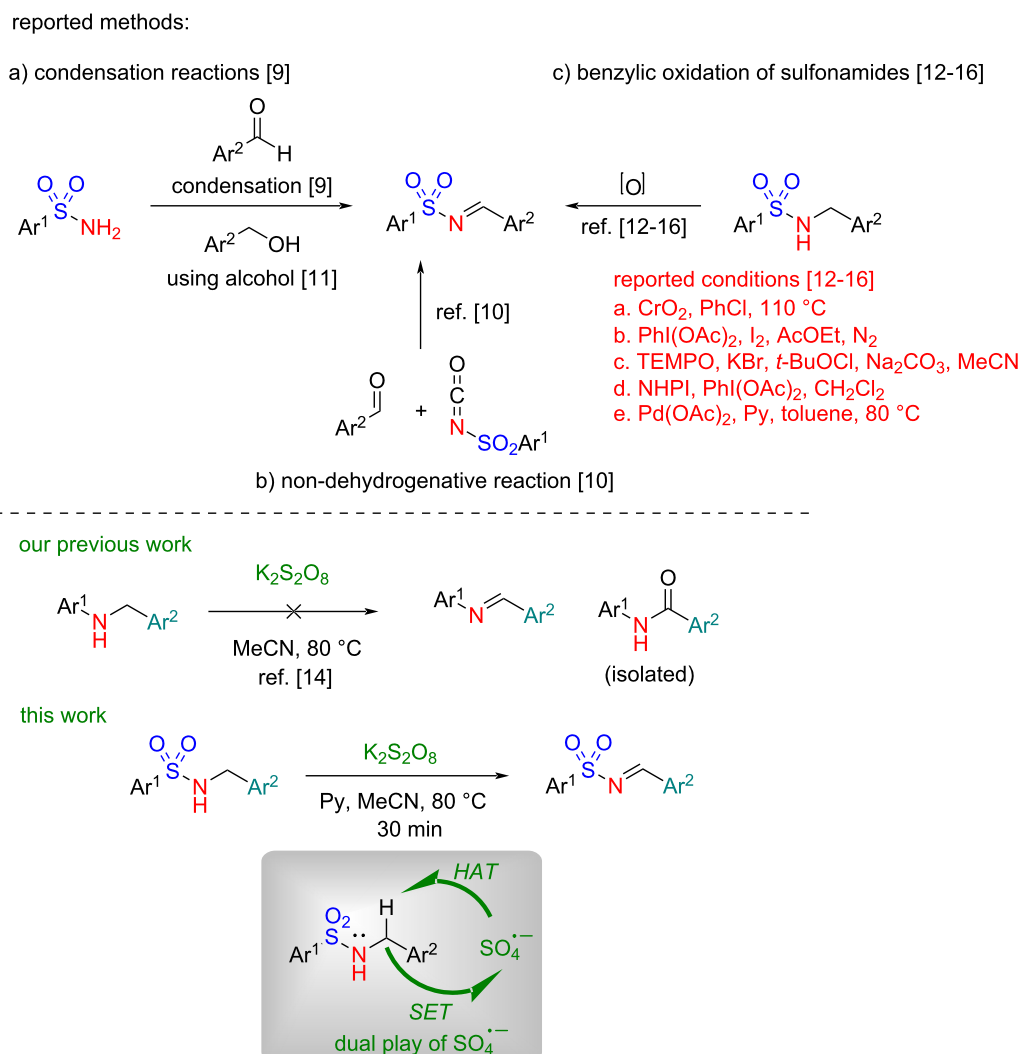
## Abstract

A mild, operationally convenient, and practical method for the synthesis of synthetically useful *N*-arylsulfonylimines from *N*-(arylsulfonyl)benzylamines using  $K_2S_2O_8$  in the presence of pyridine as a base is reported herein. In addition, a “one-pot” tandem synthesis of pharmaceutically relevant *N*-heterocycles by the reaction of *N*-arylsulfonylimines, generated in situ with *ortho*-substituted anilines is also reported. The key features of the protocol include the use of a green oxidant, a short reaction time (30 min), chromatography-free isolation, scalability, and economical, delivering *N*-arylsulfonylimines in excellent yields of up to 96%. While the oxidation of *N*-aryl(benzyl)amines to *N*-arylimines using  $K_2S_2O_8$  is reported to be problematic, the oxidation of *N*-(arylsulfonyl)benzylamines to *N*-arylsulfonylimines using  $K_2S_2O_8$  has been achieved for the first time. The dual role of the sulfate radical anion ( $SO_4^{\cdot-}$ ), including hydrogen atom abstraction (HAT) and single electron transfer (SET), is proposed to be involved in the plausible reaction mechanism.

## Introduction

Among various imine compounds [1], *N*-arylsulfonylimines are perhaps the most prominent due to their unique stability, defined reactivity, and versatility in organic synthesis [2]. Leveraging their electron-deficient nature, *N*-arylsulfonylimines are widely used in organic transformations including nucleophilic addition, cycloaddition, imino-aldol reaction, ene reactions, aza-Friedel–Crafts reactions, and C–H functionaliza-

tions ([3] and references therein), leading to the synthesis of diverse nitrogen heterocycles of pharmaceutical relevance [4]. The traditional synthetic method for the preparation of *N*-arylsulfonylimines, similar to the preparation of *N*-arylimines, is based on the condensation of aromatic aldehydes and sulfonamides (Scheme 1a) [3,5–8]. Because of the poor nucleophilicity of sulfonamides, the condensation reactions generally require



**Scheme 1:** Various synthetic approaches to *N*-arylsulfonylimines.

harsh reaction conditions involving the use of strong acids, elevated temperature, and metal catalysts. Other methods include a non-dehydrative reaction of aldehydes with isocyanate analogs ([3] and references therein) (Scheme 1b) and an oxidative reaction of primary benzylic alcohols with sulfonamides or chloramine-T ([3] and references therein), and although they are elegant, they use substrates that are not readily accessible or toxic in nature. To overcome these limitations, oxidation of *N*-(arylsulfonyl)benzylamines to *N*-arylsulfonylimines, as opposed to the traditional methods, under mild and neutral reaction conditions has been reported, although limited to a few methods. However, these methods of oxidation involving the use of  $\text{CrO}_2$  [9],  $\text{PhI}(\text{OAc})_2/\text{I}_2$  [10],  $\text{TEMPO}$  [11],  $\text{NHPI}$  [12], and metal catalysts [13], suffer from serious limitations including the use of metal catalysts, high temperature, risk of explosive hazards, production of large waste, and often low

yield (Scheme 1c). Thus, an environmentally benign method that could deliver *N*-arylsulfonylimines under mild reaction conditions is highly desirable.

Previously, we reported a tandem oxidative intramolecular cyclization of *N*-aryl(benzyl)amines, having an internal nucleophile substituted at the *ortho*-position in the aniline ring, to nitrogen heterocycles using potassium persulfate ( $\text{K}_2\text{S}_2\text{O}_8$ ) as the exclusive reagent [14]. The mechanistic study revealed that an initial oxidation to an iminium ion could be the key intermediate in the intramolecular cyclization step. In sharp contrast, when *N*-aryl(benzyl)amines that do not have an *ortho*-substituted nucleophile in aniline ring were used as the substrates in this reaction, *N*-arylimines were not isolated. Rather, an amide, in some cases, was isolated via oxidation of the benzylic methylene to a carbonyl group [14]. In the quest of a new method for

the synthesis of *N*-arylsulfonylimines, we questioned ourselves whether *N*-(arylsulfonyl)benzylamines would behave similarly as *N*-aryl(benzyl)amines under  $K_2S_2O_8$ -mediated oxidative conditions and could provide a platform for the synthesis of *N*-arylsulfonylimines.

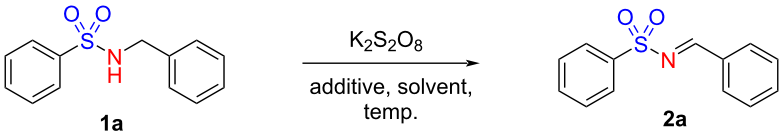
To this endeavor, we have developed a method for the synthesis of *N*-arylsulfonylimines from *N*-(arylsulfonyl)benzylamines using  $K_2S_2O_8$  in the presence of pyridine as a base. The key findings include a) requirement of a mild base for the formation *N*-arylsulfonylimines, and b) stability of *N*-arylsulfonylimines, unlike *N*-arylimines, under the oxidative conditions. Further, to demonstrate the scope and applicability of this approach, a gram-scale synthesis and a “one-pot” tandem synthesis of pharmaceutically relevant *N*-heterocycles by the reaction of in situ-generated *N*-arylsulfonylimines with various *ortho*-substituted anilines were also developed. The mechanism of the oxidation is believed to occur via hydrogen atom abstraction (HAT) followed by single electron transfer (SET) enabled by the sulfate radical anion ( $SO_4^{\cdot-}$ ).

## Results and Discussion

Initially, we investigated the reaction of *N*-benzenesulfonyl(benzyl)amine (**1a**) as a model substrate with  $K_2S_2O_8$  in MeCN at 80 °C for 12 h, conditions that were used earlier in our previous study [14]. Unfortunately, no product formation

was observed under these conditions, while substrate **1a** remained unreacted (Table 1, entry 1). When the solvent was changed to  $H_2O$ , a trace quantity of product formation was observed (Table 1, entry 2). To our surprise, when 2 equiv of pyridine were used as an additive along with the oxidant  $K_2S_2O_8$  in MeCN, the desired product *N*-benzenesulfonylimine **2a** was obtained in 90% yield (Table 1, entry 3). Subsequently, we carried out further optimization studies by changing the additive, solvent, temperature, and reaction time to obtain the best possible yield of the product **2a** (Table 1). Interestingly, when duration of the reaction was reduced to 1 h, product **2a** was obtained in 96% yield with complete conversion of substrate **1a** (Table 1, entry 4). Further shortening the reaction time to 30 min resulted in the formation of **2a** also in 96% yield (Table 1, entry 5). Lowering the temperature to 60 °C had a deleterious effect (Table 1, entry 6). Likewise, reducing the stoichiometry of pyridine to 1 equiv proved detrimental (Table 1, entry 7). Replacing pyridine with other organic and inorganic bases such as  $Et_3N$ , DBU, DABCO or  $K_2CO_3$  also gave product **2a**, however, in varying yields (Table 1, entries 8–11). While replacing the solvent MeCN with DCE delivered **2a** in 89% yield, and a dramatic reduction in the yield of **2a** was observed when  $H_2O$  was used as the solvent (Table 1, entries 12 and 13). Therefore, the conditions listed in entry 5 of Table 1 were chosen as the best conditions for further evaluating the substrate scope. Unlike the oxidation of *N*-aryl(benzyl)amines to *N*-arylimines

**Table 1:** Optimization of reaction conditions.<sup>a</sup>

					
Entry	Additive (equiv)	Solvent	Temp. (°C)	Time (h)	Yield (%) <sup>b</sup>
1	–	MeCN	80	12	n.d.
2	–	$H_2O$	80	12	trace
3	pyridine (2)	MeCN	80	12	90
4	pyridine (2)	MeCN	80	1	96
5	pyridine (2)	MeCN	80	0.5	96
6	pyridine (2)	MeCN	60	1	40
7	pyridine (1)	MeCN	80	1	80
8	$Et_3N$ (2)	MeCN	80	1	60
9	DBU (2)	MeCN	80	1	92
10	DABCO (2)	MeCN	80	1	90
11	$K_2CO_3$ (2)	MeCN	80	1	75
12	pyridine (2)	DCE	80	1	89
13	pyridine (2)	$H_2O$	80	1	20

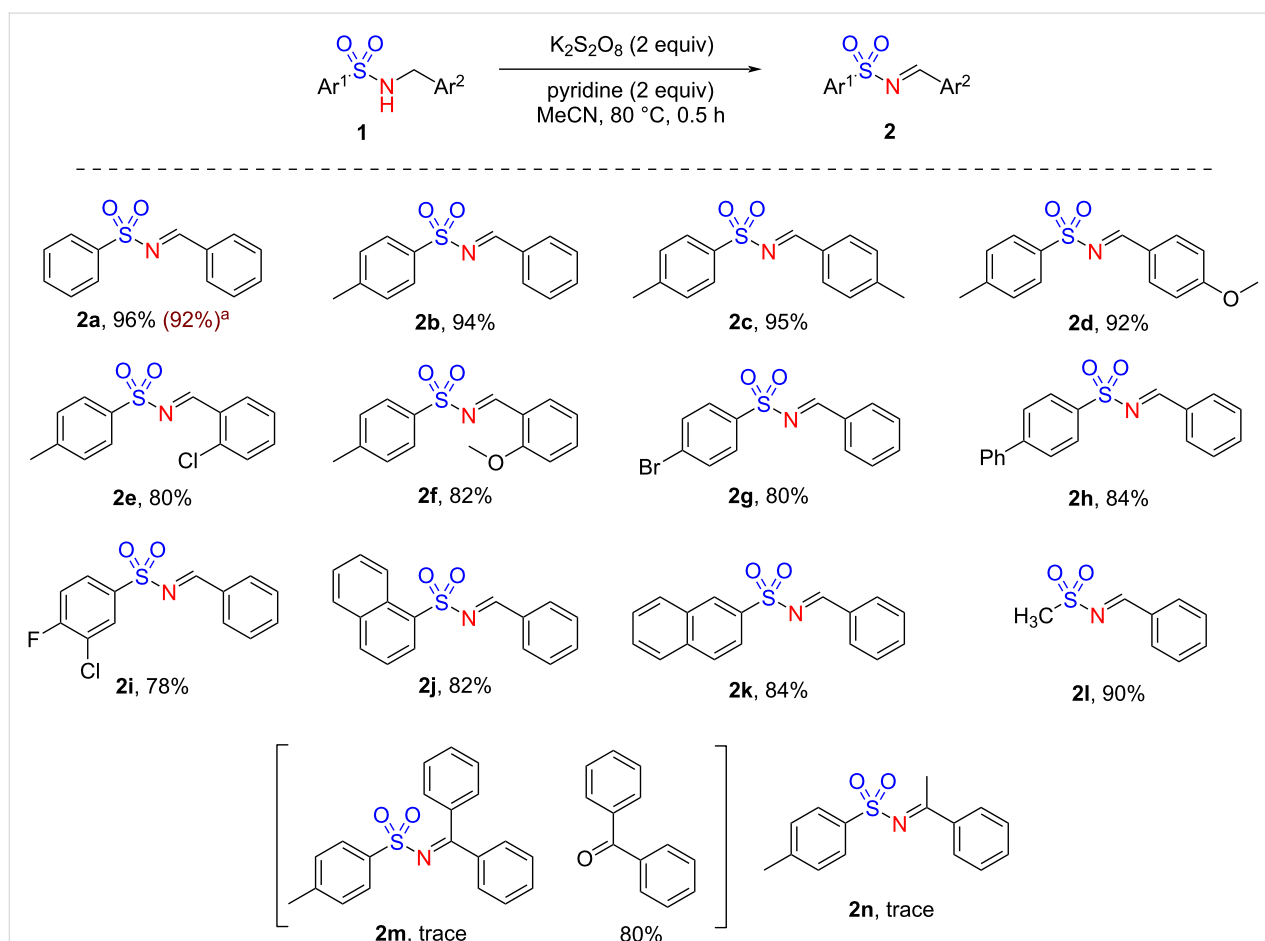
<sup>a</sup>Reaction conditions: **1a** (0.25 mmol),  $K_2S_2O_8$  (0.5 mmol), additive (0.5 mmol) in solvent (1 mL) at 80 °C for the specified period of time. n.d. = not detected. <sup>b</sup>Isolated yield.

using  $K_2S_2O_8$  in the presence or absence of a base is unsuccessful, the oxidation of *N*-arylsulfonyl(benzyl)amines **1a** to imines **2a** was achieved under the optimized conditions. Distinctly, the use of a base is the key to success in this oxidation. Perhaps more importantly, the stability of *N*-benzenesulfonylimine **2a**, unlike *N*-arylimines, under the oxidative conditions is noteworthy.

With the optimized reaction conditions in hand (Table 1, entry 5), we further investigated the substrate scope for the above transformation (Scheme 2). A limited variety of *N*-(arylsulfonyl)benzylamines **1a–m** carrying substitutions on the aromatic rings was examined. Firstly, *N*-(arylsulfonyl)benzylamines having substitution(s) on one or both rings delivered the *N*-arylsulfonylimines **2a–h** in 80–96% yield. The presence of a disubstitution in **1i** gave product **2i** in 78% yield. Replacing phenyl with naphthyl in *N*-(arylsulfonyl)benzylamines **1j** and **1k** resulted in the formation of *N*-arylsulfonylimines **2j** and **2k** also in very good yield (82–84%). Interestingly, when the arylsulfonyl group was replaced by methylsulfonyl, as in substrate **1l**,

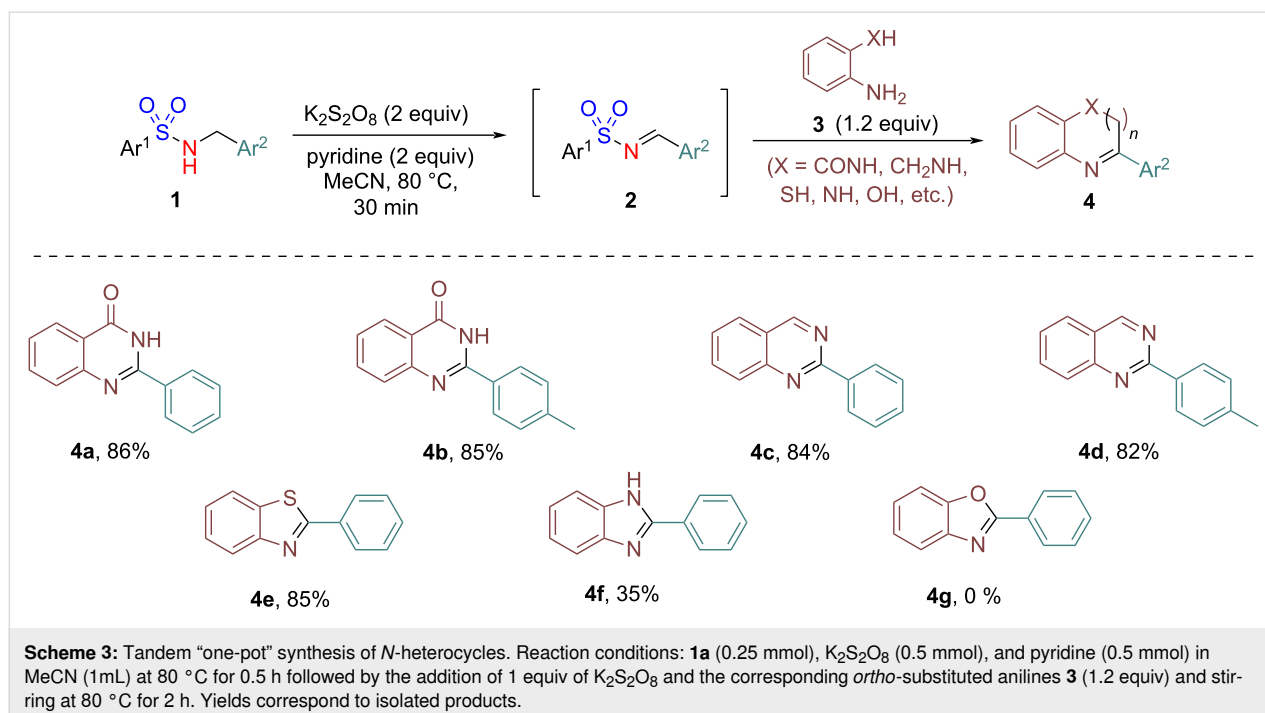
the desired *N*-sulfonylimine **2l** was obtained in 90% yield under the optimized reaction conditions. However, an attempted synthesis of *N*-arylsulfonylketimines was unsuccessful. Thus, *N*-(arylsulfonyl)benzylamine **1m** having a phenyl substituent at the benzylic position gave benzophenone in 80% yield with a trace of *N*-benzenesulfonylketimine **2m** under the optimized reaction conditions. Likewise, *N*-(arylsulfonyl)benzylamine **1n** having a methyl group present at the benzylic position gave product **2n** only in a trace quantity. To demonstrate further the scalability of the developed protocol, we carried out a gram-scale synthesis of **2a** from **1a** under the optimized reaction conditions. A complete conversion of substrate **1a** was observed within 2 h under the optimized reaction conditions giving the product with an isolated yield of 92%.

Furthermore, to demonstrate the synthetic utility of the developed protocol, a tandem “one-pot” synthesis of *N*-heterocycles was successfully executed (Scheme 3). Thus, exposition of substrates **1** under the optimized reaction conditions followed by the addition of *ortho*-substituted anilines **3** and



**Scheme 2:** Substrate scope for the synthesis of *N*-arylsulfonylimines. Reaction conditions: **1a** (0.25 mmol),  $K_2S_2O_8$  (0.5 mmol), pyridine (0.5 mmol) in MeCN (1 mL) at 80 °C for 0.5 h. Yields refer to isolated compounds. <sup>a</sup>Gram-scale synthesis (**1a**, 5 mmol).





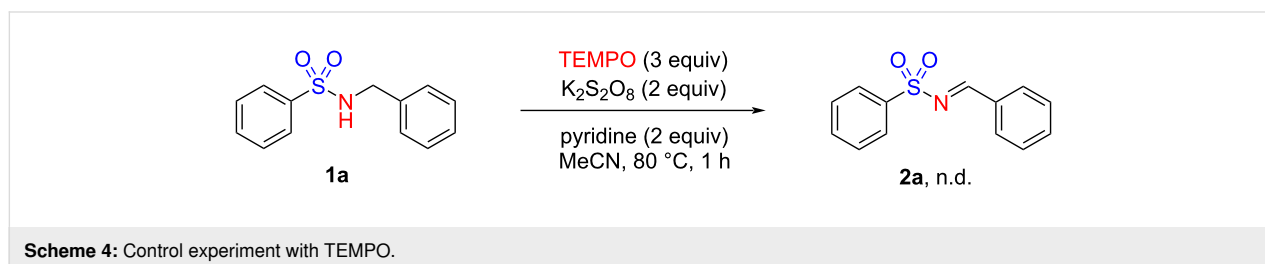
$K_2S_2O_8$  (1 equiv) and heating the reaction mixture at 80 °C for 2 h furnished the desired *N*-heterocycles **4**. Thus, treatment of substrate **1a** under the standard conditions, followed by reaction of the intermediate *N*-benzenesulfonylimine **2a** with 2-aminobenzamide in one-pot gave 2-phenylquinazolin-4(3*H*)-one (**4a**) in 86% yield. Similarly, the reaction of the intermediate product **2c** and 2-aminobenzamide gave 2-(*p*-tolyl)quinazolin-4(3*H*)-one (**4b**) in 85% yield.

Furthermore, when various other *ortho*-substituted aniline derivatives such as 2-aminobenzylamine, 2-aminothiophenol, and *o*-phenylenediamine are reacted with imine **2a** in a similar manner, the corresponding *N*-heterocycles **4c–f** were obtained in good to moderate yield. However, the reaction with 2-aminophenol did not give the corresponding cyclized product **4g**. This could be possibly due to the poor nucleophilicity of the *ortho*-OH group in 2-aminophenol thereby restricting the intramolecular nucleophilic addition and as a result the corresponding cyclized product is not formed. The synthesis of these nitrogen heterocycles signifies the innate ability of in situ-generated

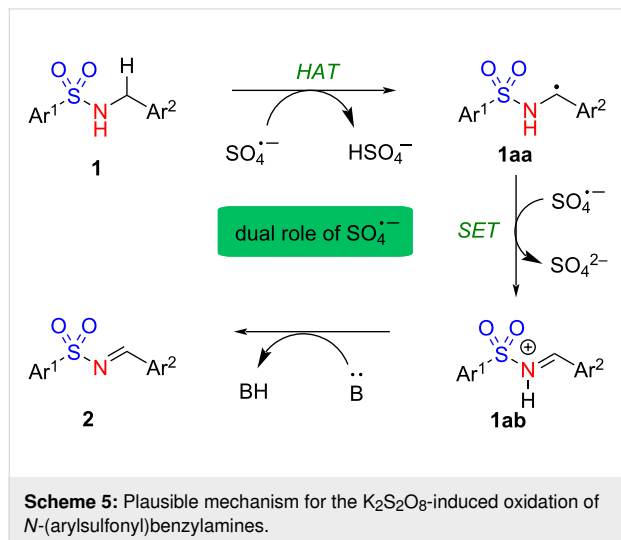
*N*-arylsulfonylimines in a variety of reactions with various *ortho*-substituted anilines without the need for pre-isolation or purification.

Next, in order to determine whether the reaction proceeds via a radical pathway, we performed a control experiment. When substrate **1a** was treated with the radical scavenger TEMPO under the optimized reaction conditions, the formation of product **2a** was completely suppressed (Scheme 4). This confirms that the reaction proceeds via a radical pathway.

Based on the literature [15,16], our previous experience [14,17,18], and current understanding, a plausible mechanism for the benzylic oxidation is depicted in Scheme 5. Initially, a sulfate radical anion ( $SO_4^{\cdot-}$ ) is generated by homolytic cleavage of the peroxy linkage under heating conditions [17]. The hydrogen atom is abstracted from the benzylic position of **1** by  $SO_4^{\cdot-}$ , generating benzylic radical **1aa** [14–16]. A single electron transfer (SET) could subsequently occur from **1aa** to form the reactive species **1ab**. Finally, the base abstracts the activated



NH proton to produce imine **2**. The dual role of  $\text{SO}_4^{\cdot-}$  involving HAT and SET is proposed in this plausible mechanism, which requires further investigation.



Similarly, a plausible mechanism for the one-pot synthesis of *N*-heterocycles is shown in Scheme 6. Initially, the *N*-arylsulfonylimine **2**, generated in situ from the corresponding *N*-(arylsulfonyl)benzylamine **1**, undergoes transimination with the *ortho*-substituted aniline **3** to form imine **3ab** via **3aa**. Subsequent intramolecular nucleophilic addition in imine **3ab** produces intermediate **3ac**, which upon oxidation delivers the desired *N*-heterocycle **4**.

## Conclusion

In conclusion, we have developed a complementary approach to the currently available methods for the oxidation of *N*-(arylsulfonyl)benzylamines to *N*-arylsulfonylimines using  $\text{K}_2\text{S}_2\text{O}_8$  and

pyridine as a base. While *N*-arylimines are difficult to prepare by the oxidation of *N*-aryl(benzyl)amines using  $\text{K}_2\text{S}_2\text{O}_8$ , *N*-arylsulfonylimines are successfully prepared and are quite stable under the oxidative conditions. In addition, we demonstrated a “one-pot” tandem synthesis of pharmaceutically relevant *N*-heterocycles through the reaction of in situ-generated *N*-arylsulfonylimines with *ortho*-substituted anilines. The key features including the use of a green oxidant, a short reaction time, chromatography-free isolation, and scalability mark a distinction from the contemporary methods. Although we propose a dual role for  $\text{SO}_4^{\cdot-}$  involving both hydrogen atom abstraction (HAT) and single electron transfer (SET), further investigation of the mechanism would enrich our understanding of persulfate-mediated oxidative reactions.

## Supporting Information

### Supporting Information File 1

General procedures, product characterization, and copies of  $^1\text{H}$  NMR and  $^{13}\text{C}$  NMR spectra of all compounds.

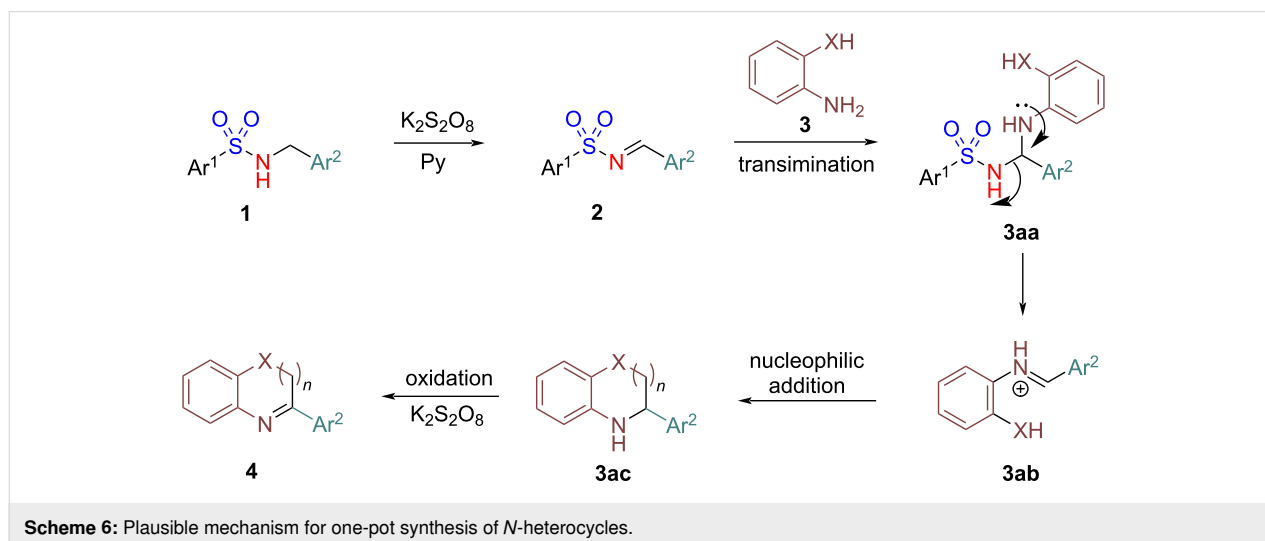
[<https://www.beilstein-journals.org/bjoc/content/supplementary/1860-5397-19-57-S1.pdf>]

## Acknowledgements

The authors acknowledge NIPER S.A.S. Nagar for providing excellent research facilities.

## Funding

We greatly appreciate the generous financial support from the Science & Engineering Research Board (SERB) of DST, New Delhi (award number CRG/2020/000462). PG thanks the DST INSPIRE (IF180484) for a research fellowship.



## ORCID® iDs

Joydev K. Laha - <https://orcid.org/0000-0003-0481-5891>Pankaj Gupta - <https://orcid.org/0000-0002-0004-077X>Amitava Hazra - <https://orcid.org/0000-0003-1129-7025>

## References

1. Belowich, M. E.; Stoddart, J. F. *Chem. Soc. Rev.* **2012**, *41*, 2003–2024. doi:10.1039/c2cs15305j
2. Weinreb, S. M. *Top. Curr. Chem.* **1997**, *190*, 131–184. doi:10.1007/bfb0119248
3. Hopkins, M. D.; Scott, K. A.; DeMier, B. C.; Morgan, H. R.; Macgruder, J. A.; Lamar, A. A. *Org. Biomol. Chem.* **2017**, *15*, 9209–9216. doi:10.1039/c7ob02120h
4. Laha, J. K.; Satyanarayana Tummalapalli, K. S.; Jethava, K. P. *Org. Biomol. Chem.* **2016**, *14*, 2473–2479. doi:10.1039/c5ob02670a
5. Jennings, W. B.; Lovely, C. J. *Tetrahedron* **1991**, *47*, 5561–5568. doi:10.1016/s0040-4020(01)80987-x
6. Verrier, C.; Carret, S.; Poisson, J.-F. *ACS Sustainable Chem. Eng.* **2018**, *6*, 8563–8569. doi:10.1021/acssuschemeng.8b00864
7. Boger, D. L.; Corbett, W. L. *J. Org. Chem.* **1992**, *57*, 4777–4780. doi:10.1021/jo00043a047
8. Liu, Y.; Lin, L.; Han, Y.; Liu, Y. *Chin. J. Org. Chem.* **2020**, *40*, 4216. doi:10.6023/cjoc202004053 and references cited therein.
9. Smith, E. M. Preparation of sulfonyl imine compounds. Australian Pat. Appl. AU7206601A, Feb 5, 2002.
10. Fan, R.; Pu, D.; Wen, F.; Wu, J. *J. Org. Chem.* **2007**, *72*, 8994–8997. doi:10.1021/jo7016982
11. Moriyama, K.; Kuramochi, M.; Fujii, K.; Morita, T.; Togo, H. *Angew. Chem.* **2016**, *128*, 14766–14771. doi:10.1002/ange.201607223
12. Wang, J.; Yi, W.-J. *Molecules* **2019**, *24*, 3771. doi:10.3390/molecules24203771
13. Wang, J.-R.; Fu, Y.; Zhang, B.-B.; Cui, X.; Liu, L.; Guo, Q.-X. *Tetrahedron Lett.* **2006**, *47*, 8293–8297. doi:10.1016/j.tetlet.2006.09.088
14. Laha, J. K.; Tummalapalli, K. S. S.; Nair, A.; Patel, N. J. *Org. Chem.* **2015**, *80*, 11351–11359. doi:10.1021/acs.joc.5b01872
15. Ueda, M.; Kamikawa, K.; Fukuyama, T.; Wang, Y.-T.; Wu, Y.-K.; Ryu, I. *Angew. Chem.* **2021**, *133*, 3587–3592. doi:10.1002/ange.202011992
16. Zhang, H.; Wang, S.; Wang, X.; Wang, P.; Yi, H.; Zhang, H.; Lei, A. *Green Chem.* **2022**, *24*, 147–151. doi:10.1039/d1gc03896f
17. Mandal, S.; Bera, T.; Dubey, G.; Saha, J.; Laha, J. K. *ACS Catal.* **2018**, *8*, 5085–5144. doi:10.1021/acscatal.8b00743
18. Gupta, P.; Laha, J. K. Development of Synthetic Approaches to Biaryl Sultams via C–H Functionalization. *Handbook of CH-Functionalization*; Wiley-VCH: Weinheim, Germany, 2002; pp 1–24. doi:10.1002/9783527834242.chf0117

## License and Terms

This is an open access article licensed under the terms of the Beilstein-Institut Open Access License Agreement (<https://www.beilstein-journals.org/bjoc/terms>), which is identical to the Creative Commons Attribution 4.0 International License (<https://creativecommons.org/licenses/by/4.0>). The reuse of material under this license requires that the author(s), source and license are credited. Third-party material in this article could be subject to other licenses (typically indicated in the credit line), and in this case, users are required to obtain permission from the license holder to reuse the material.

The definitive version of this article is the electronic one which can be found at:  
<https://doi.org/10.3762/bjoc.19.57>



# Pyridine C(sp<sup>2</sup>)-H bond functionalization under transition-metal and rare earth metal catalysis

Haritha Sindhe<sup>1</sup>, Malladi Mounika Reddy<sup>2</sup>, Karthikeyan Rajkumar<sup>2</sup>, Akshay Kamble<sup>1</sup>, Amardeep Singh<sup>2</sup>, Anand Kumar<sup>2</sup> and Satyasheel Sharma<sup>\*2</sup>

## Review

[Open Access](#)

### Address:

<sup>1</sup>Department of Medicinal Chemistry, National Institute of Pharmaceutical Education and Research - Ahmedabad, Gandhinagar, Gujarat, 382355, India and <sup>2</sup>Department of Natural Products, National Institute of Pharmaceutical Education and Research - Ahmedabad, Gandhinagar, Gujarat, 382355, India

### Email:

Satyasheel Sharma<sup>\*</sup> - sharma.satyasheel@gmail.com

<sup>\*</sup> Corresponding author

### Keywords:

C-H functionalization; heterocycles; pyridine; rare earth metal; transition-metal-catalyzed

*Beilstein J. Org. Chem.* **2023**, *19*, 820–863.

<https://doi.org/10.3762/bjoc.19.62>

Received: 13 February 2023

Accepted: 16 May 2023

Published: 12 June 2023

This article is part of the thematic issue "C–H bond functionalization: recent discoveries and future directions".

Guest Editor: I. Chatterjee



© 2023 Sindhe et al.; licensee Beilstein-Institut.  
License and terms: see end of document.

## Abstract

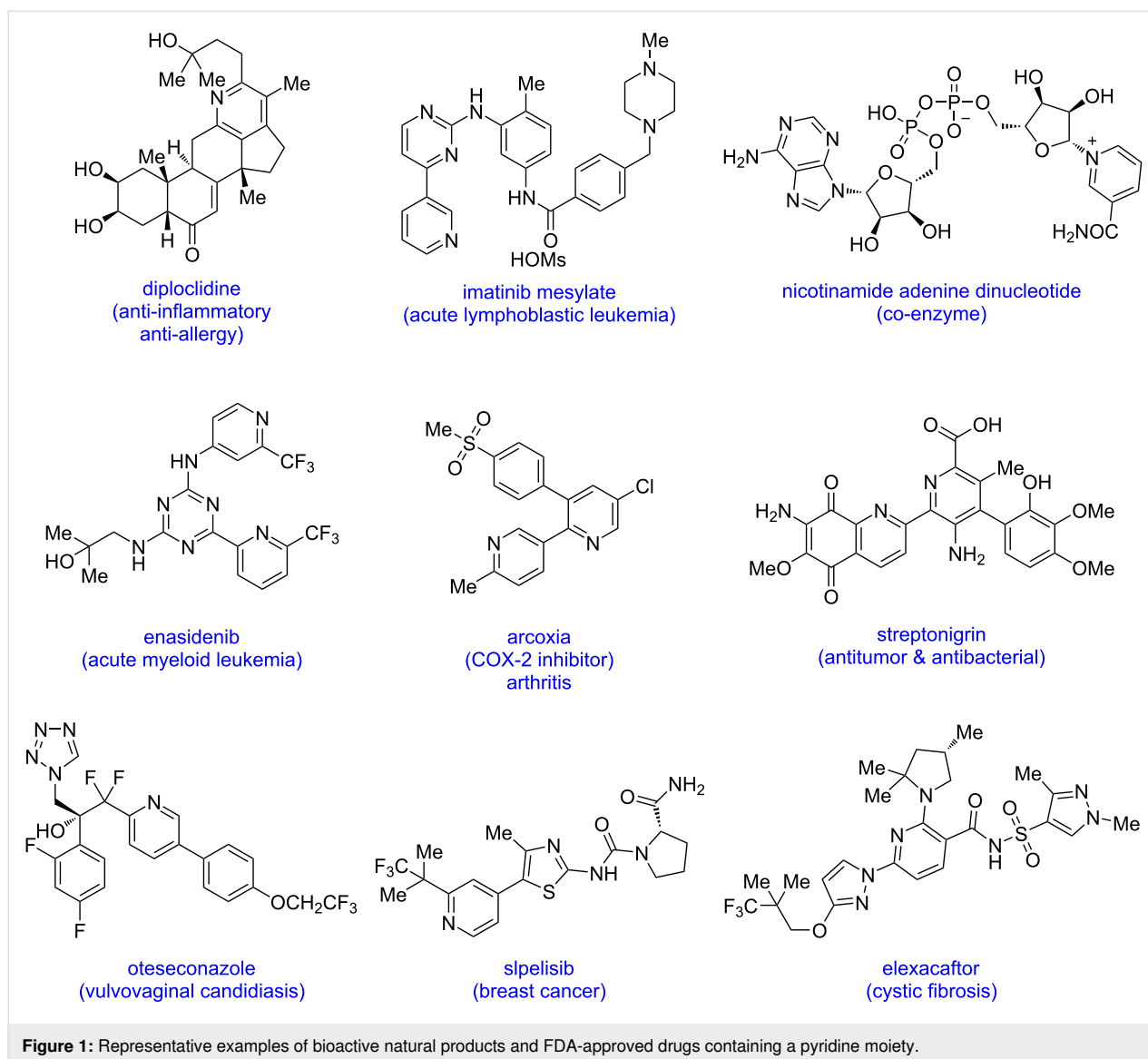
Pyridine is a crucial heterocyclic scaffold that is widely found in organic chemistry, medicines, natural products, and functional materials. In spite of the discovery of several methods for the synthesis of functionalized pyridines or their integration into an organic molecule, new methodologies for the direct functionalization of pyridine scaffolds have been developed during the past two decades. In addition, transition-metal-catalyzed C–H functionalization and rare earth metal-catalyzed reactions have flourished over the past two decades in the development of functionalized organic molecules of concern. In this review, we discuss recent achievements in the transition-metal and rare earth metal-catalyzed C–H bond functionalization of pyridine and look into the mechanisms involved.

## Introduction

Pyridine, one of the most important azaheterocyclic scaffolds, is found in a diverse range of bioactive natural products, pharmaceuticals, and functional materials [1–10]. Due to its different characteristics such as basicity, stability, water solubility, small molecular size, and ability to form hydrogen bonds, pyridine continues to be a suitable moiety in organic synthesis. In addition, it has been observed that pyridine rings serve as

bioisostere for aromatic rings, amines, amides, and N-containing heterocycles. Due to the aforementioned qualities, numerous U.S. FDA-approved medications have pyridine scaffolds in their molecules (Figure 1).

In this context, the synthesis of the pyridine motif is always there in trend. Many pyridine syntheses have relied on the con-



**Figure 1:** Representative examples of bioactive natural products and FDA-approved drugs containing a pyridine moiety.

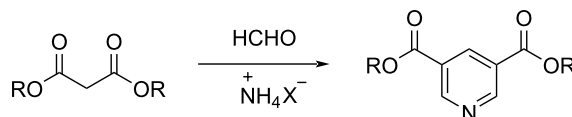
densation of carbonyl compounds and amines for a very long time [11]. The classical methods for the synthesis of functionalized pyridine include the Hantzsch pyridine synthesis and the Bohlmann–Rahtz synthesis (Scheme 1a and b). Furthermore, alternative methodologies are being developed for the synthesis of functionalized pyridines or its integration into an organic molecule [12–20]. Although classical organic synthesis is incredibly effective, it frequently requires the prefunctionalization of substrates and involves stoichiometric waste.

The challenges associated with the functionalization of pyridine are based on the low reactivity of the pyridine ring system for undergoing substitution reactions. This is attributed to the electron-deficient nature of the ring system due to the presence of the  $sp^2$ -hybridized nitrogen atom. In addition, the lone pair electrons of the nitrogen atom interact with Lewis acids instead

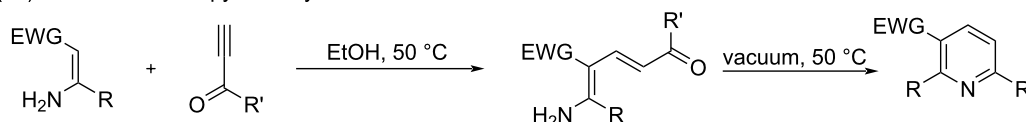
of the  $\pi$ -electrons of the ring system thus resulting to its reduced reactivity for electrophilic aromatic substitution reactions, such as a Friedel–Crafts reaction [21–23]. Hence, it is challenging to functionalize a C–H bond in pyridine with traditional chemical transformations. On the other hand, intriguing developments have been made for the functionalization of inert C–H bonds in organic synthesis during the past two decades. In this regard, the transition-metal-catalyzed C–H functionalization has made its way towards the synthesis and functionalization of various complex organic molecules [24–31]. In addition, rare earth metal-catalyzed C–H functionalization reactions have been known for a few decades, however, they received growing interest only recently [32–34]. Thus, diversely functionalized pyridines have been synthesized via C–H activation under transition-metal and rare earth metal catalysis, including C–H alkylation, alkenylation, arylation, heteroarylation, borylation, etc.

## (1) synthesis of functionalized pyridines: classical approaches for functionalized pyridine

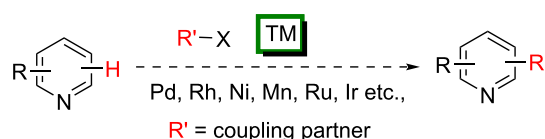
## (1a) Hantzsch pyridine synthesis



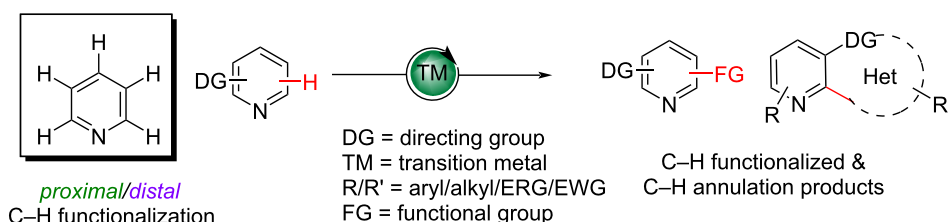
## (1b) Bohlmann-Rahtz pyridine synthesis



## (2) synthesis of functionalized pyridines: traditional cross-coupling reactions



## transition-metal-catalyzed C–H functionalization of pyridine



Scheme 1: Classical and traditional methods for the synthesis of functionalized pyridines.

Recently, metal-free approaches have also been developed for the C–H functionalization of N-heterocycles [35–39]. However, due to the vastness of reports on C–H functionalizations of N-heterocycles, in this review we have summarized recent progress (from year 2010 to 2023) in the C–H functionalization of the pyridine ring only. Herein, we discuss transition-metal as well as rare earth metal-catalyzed directed and undirected, proximal as well as distal pyridine C(sp<sup>2</sup>)–H bond functionalizations in detail under different types of reactions. Further, this review excludes the use of pyridine as a directing group for C–H functionalizations and the C–H functionalization of fused pyridines.

## Review

## C–H Alkylation of pyridine

The C–H bond is the backbone of an organic molecule and the conversion of a C–H bond to a C–X bond (X = carbon or heteroatom) forms the basis in organic synthesis. The functionalization of C–H bonds is challenging due to a large kinetic barrier for C–H bond cleavage and also achieving selectivity is difficult due to its ubiquitous nature [40]. The metal-catalyzed

C–H bond functionalization is a good strategy for synthesizing highly functionalized organic frameworks. In this context, the C–H alkylation is one of the most important C–C bond-formation reactions [41–45]. On the other hand, a metal-catalyzed functionalization of arene/heteroarene C–H bonds to the corresponding C–C bonds is an area of great interest and has been well studied [46,47]. Pyridine, being an important heterocyclic scaffold, various studies have been conducted for the C(sp<sup>2</sup>)–H alkylation of the pyridine ring. In this part, we describe pyridine C–H alkylation reactions sub-sectioning based on the position of the alkylation reported.

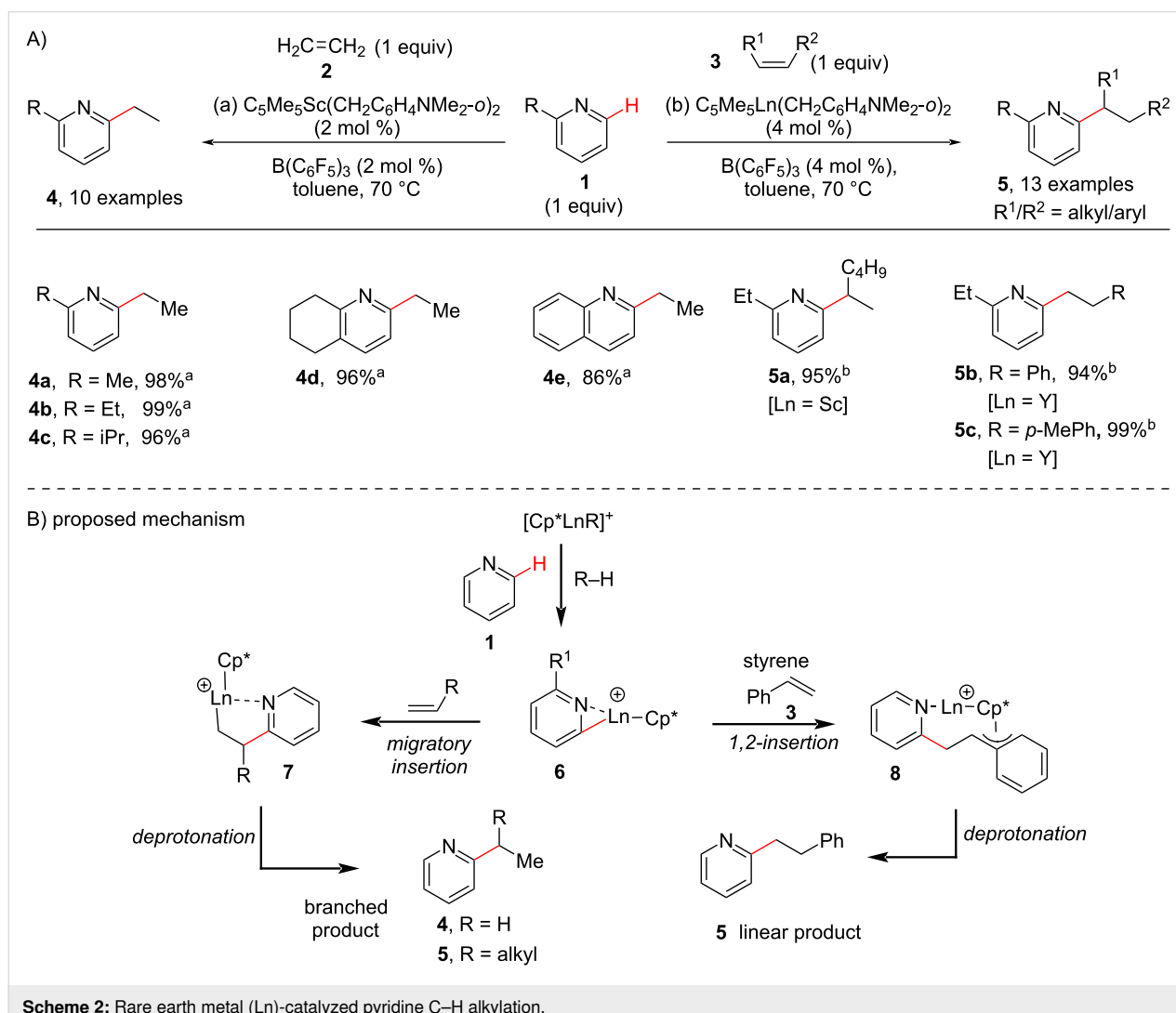
*ortho*-C–H Alkylation

Inspired by the pioneering work of Jordan and co-workers [48] on the *ortho*-selective C–H alkylation of 2-picoline with propene using a cationic zirconium complex under a H<sub>2</sub> atmosphere in 1989 and the work done by Bergman and Ellmann [49] in 2010 for the *ortho*-C–H alkylation of pyridines under Rh(I) catalysis at high temperature, in 2011 Hou and Guan reported an atom economical method for the selective *ortho*-alkylation of pyridines by C–H

addition to olefins under cationic half-sandwich rare-earth catalysis [50]. They carried out the reaction in the presence of dialkyl complexes of scandium (Sc) or yttrium (Y) such as  $(C_5Me_5)Ln(CH_2C_6H_4NMe_2-o)_2$  ( $Ln = Sc, Y$ ) in combination with  $B(C_6F_5)_3$  as an activator. The method demonstrated a wide substrate scope of both pyridines and olefins including  $\alpha$ -olefins, styrenes, and conjugated dienes. The yttrium complex was found to be superior as compared to the scandium complex for the alkylation reaction of bulkier 2-*tert*-butylpyridine with ethylene. In addition, the yttrium catalyst was also found to have a higher catalytic activity for the *ortho*-alkylation of pyridines with styrenes to give the linear alkylated products (**5b,c**, Scheme 2). Further, the authors proposed that the C–H bond activation could be the rate limiting step based on kinetic isotope experiments (KIE). The proposed mechanism involves the coordination of pyridine to the metal center of the cationic catalyst and  $B(C_6F_5)_3$  promotes the *ortho*-C–H activation (deprotonation) of pyridine to afford pyridyl species **6**. Next, the

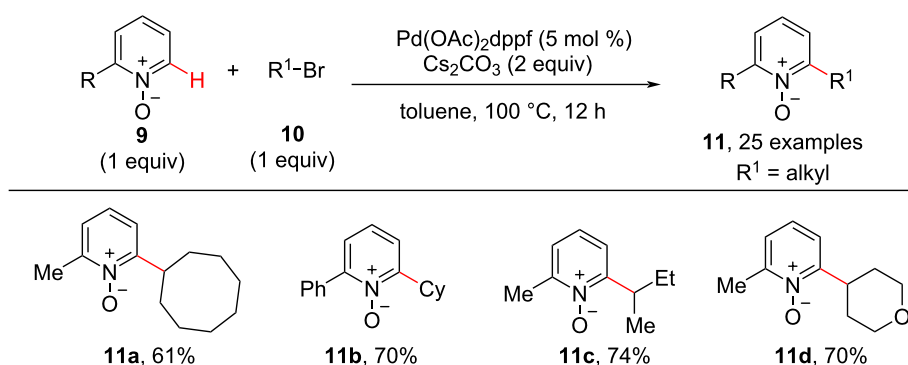
2,1-migratory insertion of alkene **2** into the metal–pyridyl bond in **6** gives the intermediate **7**, which on subsequent deprotonation gives the branched alkylated product **4**. Whereas, in case of styrene **3** a 1,2-insertion takes place possibly due to the formation of the stable benzallylic species **8**, which on deprotonation gives the linear alkylated product **5**.

The C–H activation/C–C cross-coupling reaction with 1° alkyl electrophiles has been known in the past, however, the C–H alkylation with nonactivated secondary (2°) alkyl electrophiles and tertiary alkyl electrophiles was little known. In this context, in 2013, Fu and co-workers came across an unexpected finding with Pd-catalyzed C–H activation/C–C cross-coupling of pyridine *N*-oxides with nonactivated secondary (2°) alkyl bromides [51]. The cross-coupling is difficult to achieve as the Pd-catalyzed  $S_N2$  process is sensitive towards the steric bulk of the secondary or tertiary alkyl electrophiles. The optimized conditions for the *ortho*-alkylation of pyridine *N*-oxides **9** with nonactivat-

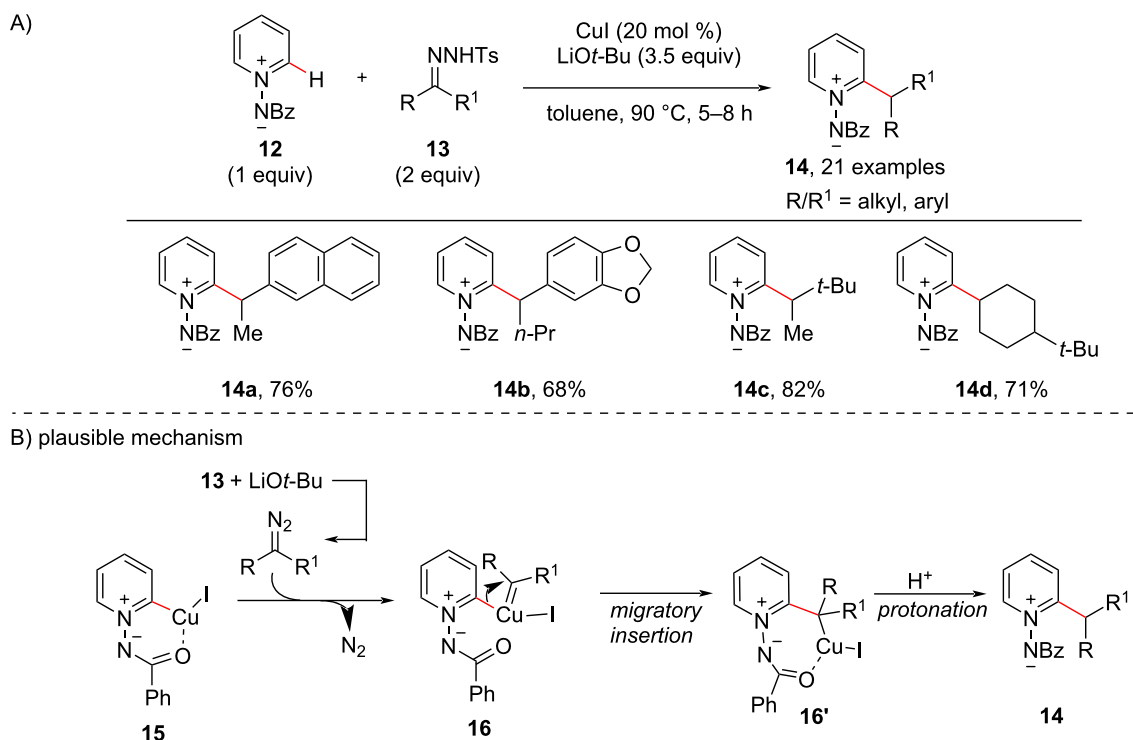


ed secondary (2°) alkyl bromides **10** required 5 mol % of the Pd(OAc)<sub>2</sub>dppf catalyst, Cs<sub>2</sub>CO<sub>3</sub> (2.0 equiv) as base in toluene at 100 °C as shown in Scheme 3. Under these conditions, the reaction provided diverse 2-alkylpyridine derivatives **11** in moderate to good yields starting from both cyclic and acyclic alkyl bromides. The findings of the reaction's stereochemistry and observations made during some cyclization or ring-opening reactions indicated that the C–H alkylation may proceed through a radical-type mechanism. Next, in 2013, Wang and co-workers [52] reported a protocol using CuI (10 mol %) as inexpensive catalyst and LiOt-Bu (3.5 equiv) as the base for the C–H alkylation of *N*-iminopyridinium ylides **12** with *N*-tosylhy-

drazones **13** showing good substrate scope for both coupling partners (Scheme 4). A substituent on the aromatic ring of the tosylhydrazones did not significantly affect the C–H alkylation reaction and the reaction also proceeded well with hydrazones **13** obtained from aliphatic aldehydes or ketones. Based on mechanistic experiments and DFT calculations, the reaction presumably proceeds via a Cu–carbene migratory insertion (Scheme 4b). In the presence of CuI and the base the initial direct C–H activation of the ylide **12** gives the copper pyridinium ylide **15**. The latter reacts with the diazo compound formed through reaction of hydrazone **13** with the base to give the copper–carbene species **16**. Then, the intermediate **16**



**Scheme 3:** Pd-catalyzed C–H alkylation of pyridine *N*-oxide.



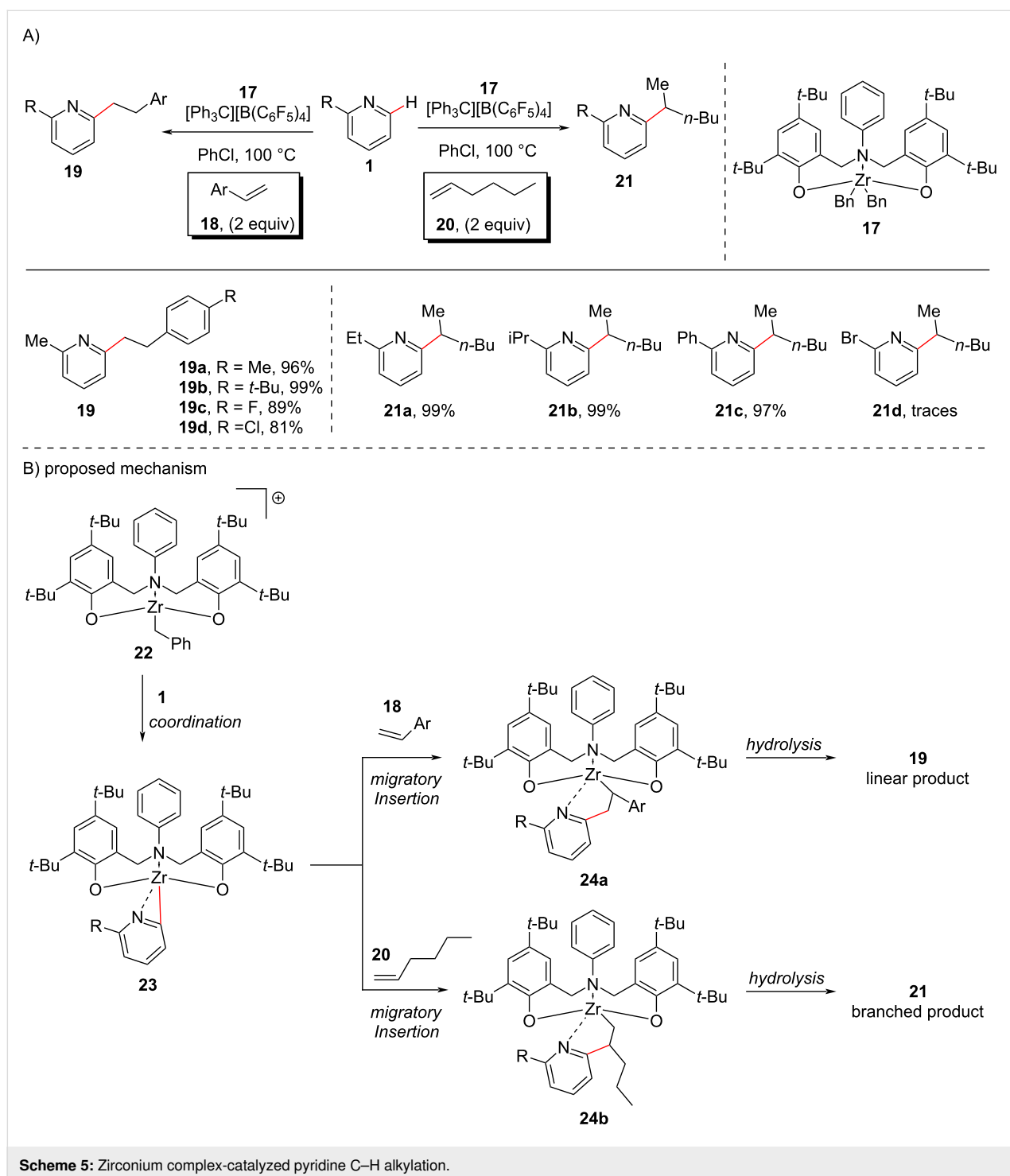
**Scheme 4:** CuI-catalyzed C–H alkylation of *N*-iminopyridinium ylides with tosylhydrazones (A) and a plausible reaction mechanism (B).



undergoes a Cu–carbene migratory insertion giving intermediate **16'**, which upon protonation gives the desired alkylated product **14**.

Later, in the year 2018, Yao and co-workers [53] developed the first example of a group 4 metal-based catalyst protocol for the C–H alkylation of pyridine **1** with alkenes **18** and **20** as cou-

pling partners. They demonstrated that the reaction in the presence of cationic zirconium complexes derived from zirconium dibenzyl complexes bearing tridentate [ONO]-type amine-bridged bis(phenolato) ligands and  $[\text{Ph}_3\text{C}][\text{B}(\text{C}_6\text{F}_5)_4]$  (Scheme 5), gave rise to *ortho*-selective C–H alkylated pyridines **19** and **21**. It was observed that the cationic Zr complexes provided good transformations, probably due to good



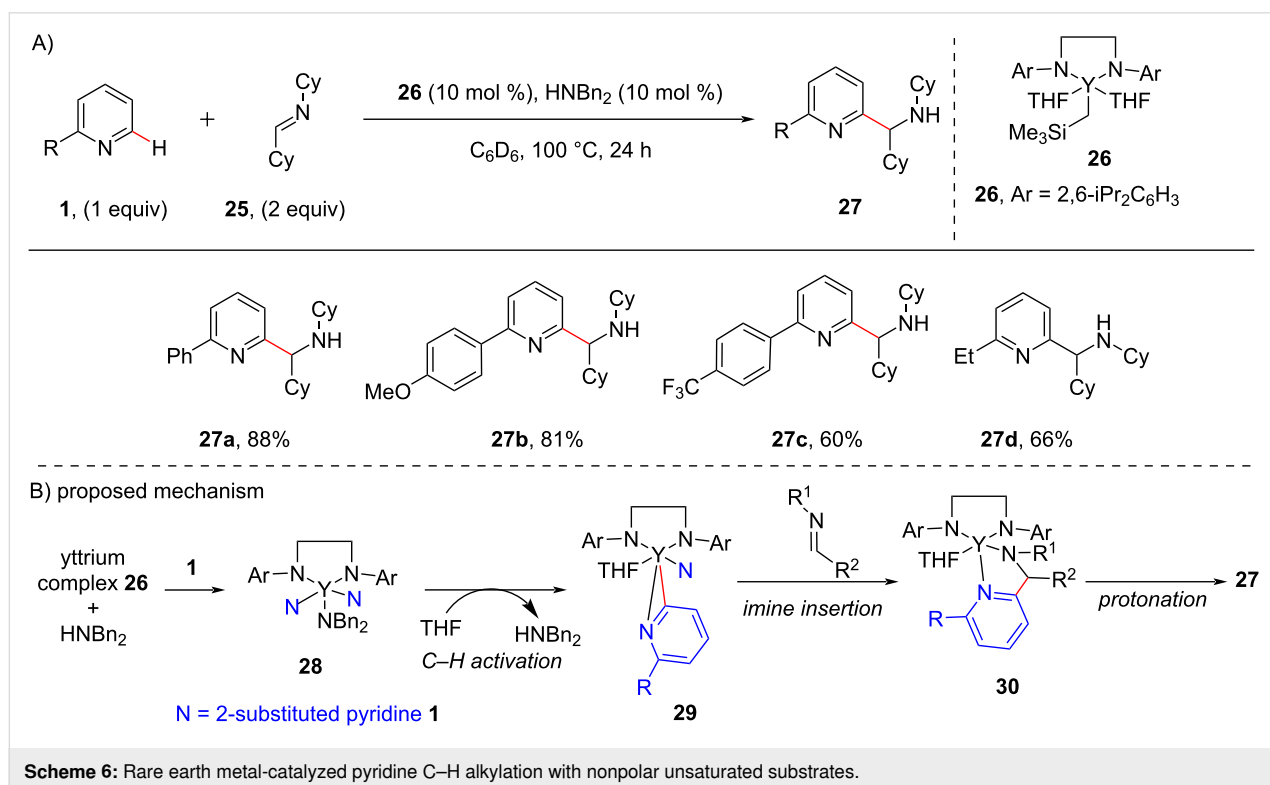
accessibility of the coordination site and an increased Lewis acidity of the metal center. The authors also demonstrated that this catalytic system also catalyzes the alkylation of benzylic C–H bonds ( $C(sp^3)$ –H) of various dialkylpyridines with alkenes. It is to be noted that the ligands' backbones were found to be crucial for the regioselectivity of the addition to benzylic  $C(sp^3)$ –H bonds, as *N*-arylamine-bridged bis(phenolato) Zr complexes provided branched products whereas *N*-alkylamine-bridged bis(phenolato) Zr complexes provided the linear addition products. The proposed mechanism (Scheme 5b) involves the initial formation of Zr complex **22** through the reaction of neutral Zr complex **17** with  $[Ph_3C][B(C_6F_5)_4]$ , which on coordination with the pyridine resulted in the formation of the 3-membered zirconacyclic intermediate **23**. The migratory insertion of the alkene into the metal–C bond of **23** gives the intermediate **24a** on reaction with styrene **18** and intermediate **24b** in the presence of alkene **20**. The intermediates **24a** and **24b** then undergo further hydrolysis to give the desired linear products **19** and branched products **21**, respectively.

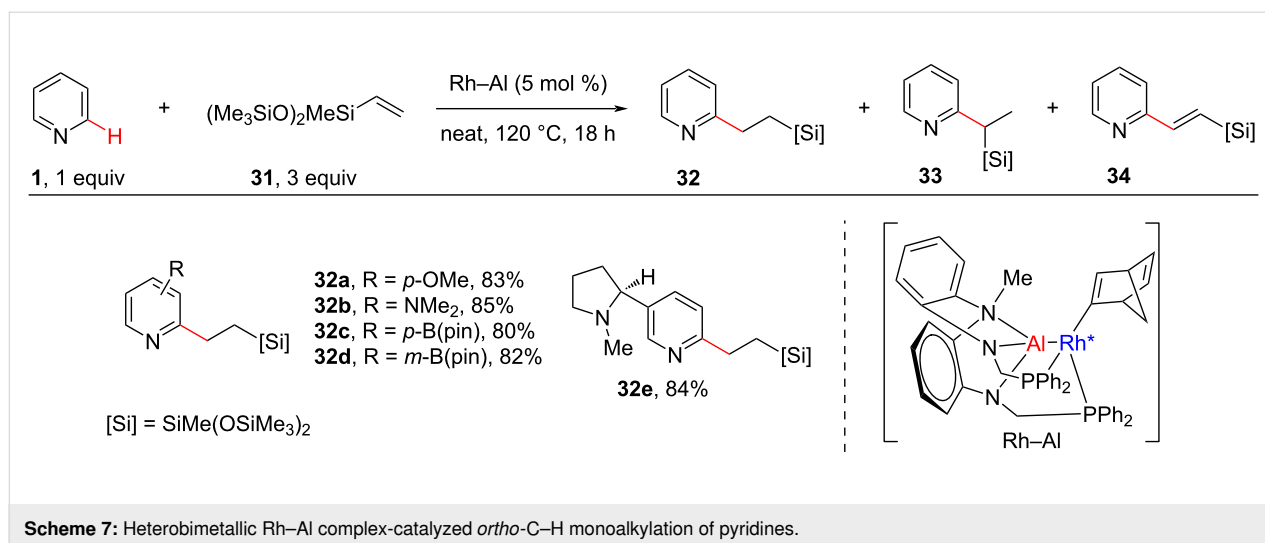
In the same year, Tsurugi and Mashima reported the use of rare earth metal complexes for the insertion of nonpolar unsaturated substrates ( $C=N$ ) into the *ortho*-C–H bond of pyridine derivatives [54]. They carried out the C–H aminoalkylation of pyridines **1** using yttrium complex **26** with nonactivated imines **25** (Scheme 6). The authors also demonstrated the enantioselective aminoalkylation, using chiral diamines as ligands. The

introduction of chiral diamines in the metal complex produced the aminoalkylated products enantioselectivity with good ratio of enantiomeric excess. The plausible mechanism involves the formation of (dibenzylamido)yttrium complex **28** by the reaction of yttrium complex **26** with  $HNBn_2$ . Then  $\sigma$ -bond metathesis between the Y–N bond of **28** and the *ortho*-C–H bond of pyridine gives  $\eta^2$ -pyridyl species **29** which on imine insertion produces species **30**. Subsequent protonation then provides the aminoalkylated product **27** (Scheme 6b).

The selective C–H monoalkylation of pyridines with alkenes is a challenging task. Most *ortho*-C–H alkylation reactions have been achieved starting from C2-substituted pyridines. There are a few studies reported for the selective C–H monoalkylation of unsubstituted pyridines, which, however, displayed limited substrate scope [55,56]. In this regard, in 2021, Nakao and co-workers [57] reported a selective C2-monoalkylation of 2,6-unsubstituted pyridines with alkenes **31** using a hetero-bimetallic Rh–Al catalyst. The reaction provided the linear product **32** with aliphatic alkenes **31**, whereas vinylarenes produced the branched product **33** and also alkenylated products **34**. The reaction gave excellent yields of the *ortho*-alkylated products with good functional group tolerance (Scheme 7).

The C–H functionalization of pyridines through action of different catalyst systems including transition metals and rare earth metals has been described and some other organometallic

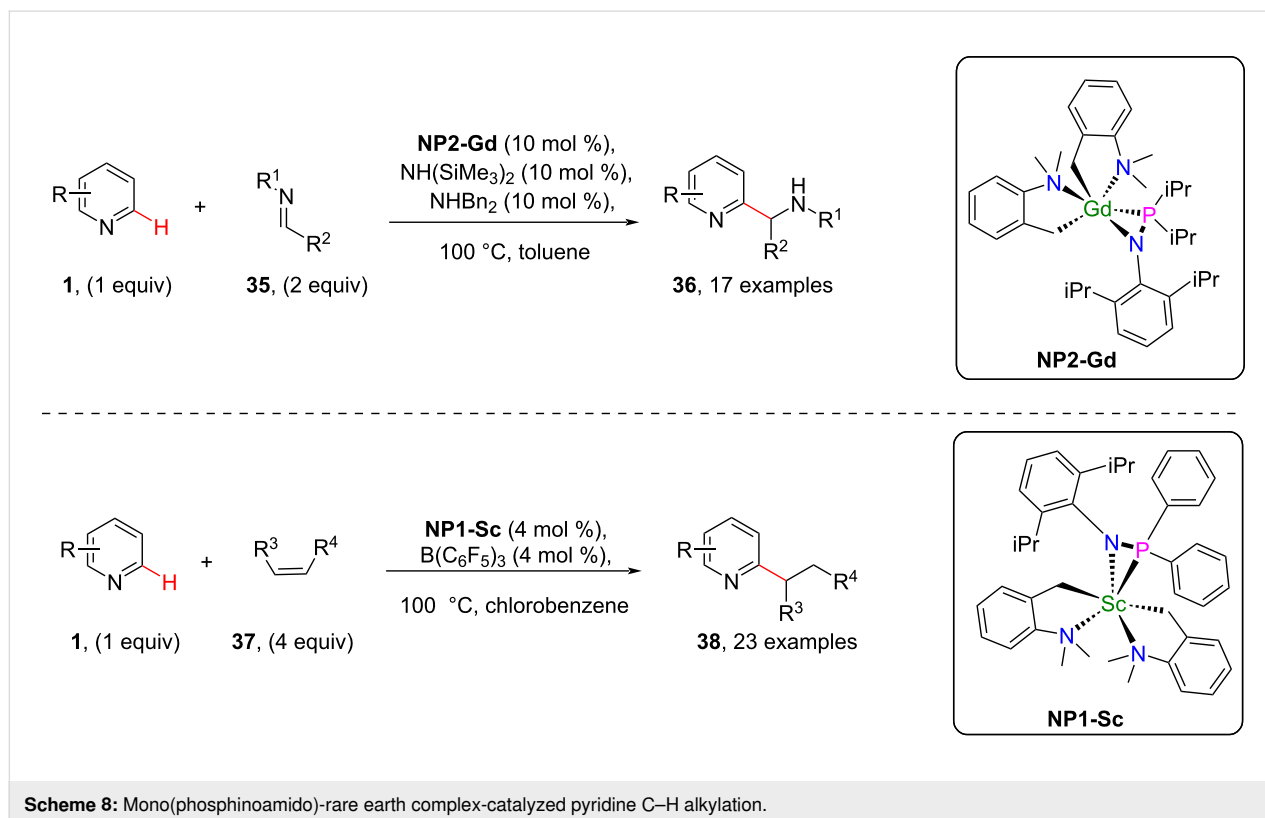




systems also were shown to have catalytic reactivity. Adopting this catalytic reactivity of organometallics and also the special bidentate nature of phosphinoamide ligands, in 2021, Chen and group [58] described the catalytic *ortho*-C(sp<sup>2</sup>)-H functionalization of pyridines with polar imines **35** and nonpolar alkenes **37** by using mono(phosphinoamido)-ligated rare earth complexes (**NP2-Gd** and **NP1-Sc**) as shown in Scheme 8. Complex **NP2-Gd** was found to be effective in the functionalization of pyridines with imines providing various *ortho*-aminoalkylated

products **36** whereas *ortho*-alkylated pyridine derivatives **38** were obtained when using **NP1-Sc** as the catalyst (Scheme 8).

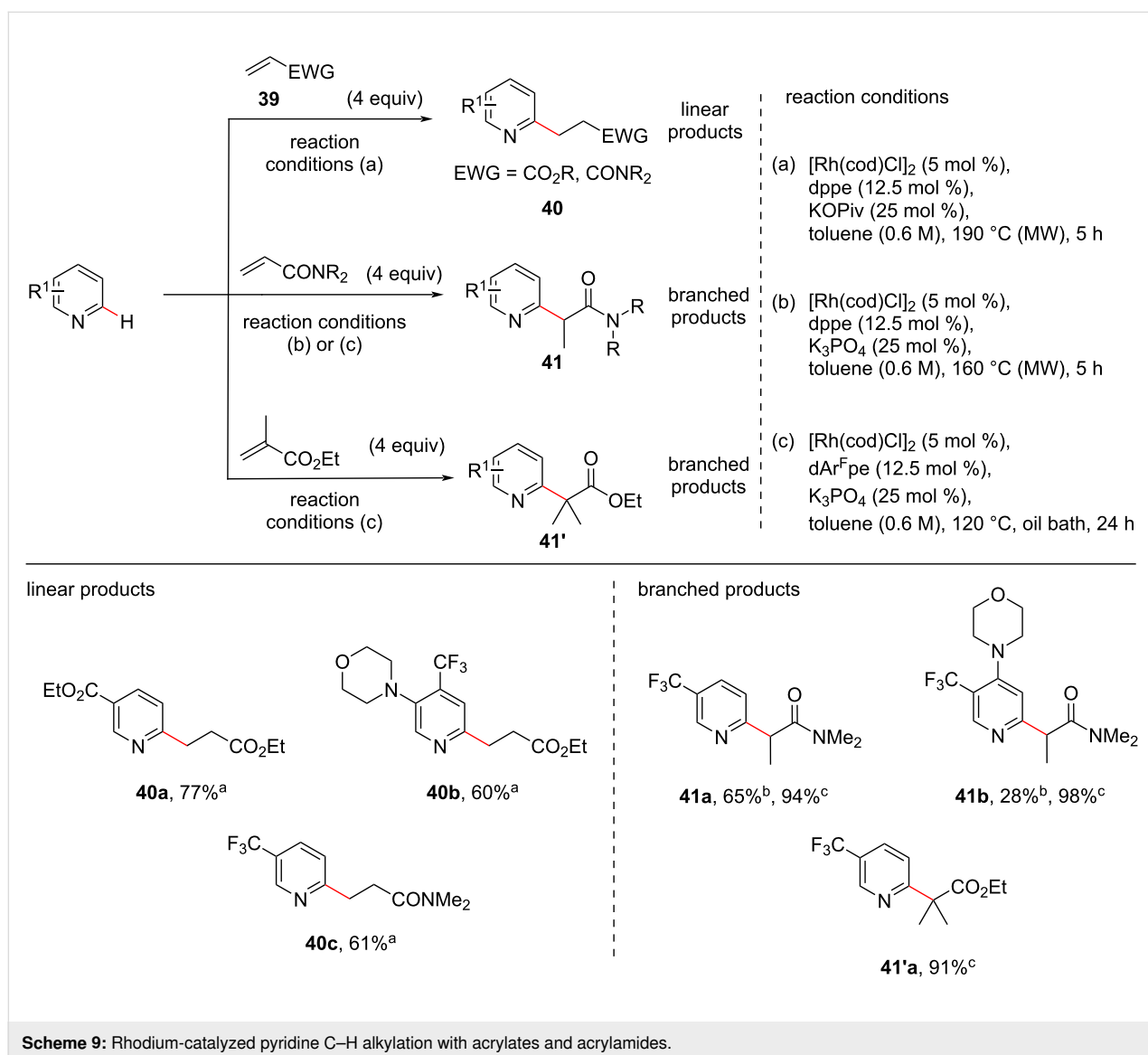
Attributing to the strong coordination of unsubstituted pyridine with Rh(I) catalysts, C–H alkylations of pyridine lacking *ortho*-blocking groups is a challenge. In this context, a regioselective alkylation of *ortho*-unsubstituted or substituted unactivated pyridines with acrylates and acrylamides under Rh(I) catalysis has been demonstrated by Ellman and co-workers [59]. The



authors observed that in the presence of  $[\text{Rh}(\text{cod})\text{Cl}]_2$  as catalyst, dppe as ligand, and potassium pivalate (KOPIv) as base, linear C–H-alkylated products **40** were obtained from both acrylates and acrylamides in moderate to high yields (Scheme 9, reaction conditions a). However, when  $\text{K}_3\text{PO}_4$  was employed as the base under otherwise identical conditions, the authors observed a switch in regioselectivity and branched products **41** were obtained with acrylamides as coupling partners (Scheme 9, reaction conditions b). Thus, the authors demonstrated a switch in regioselectivity (linear/branched) which was controlled exclusively by the base used. During further investigations the authors found that the use of ligand dArFpe at reduced reaction temperature resulted in a significant increase in the yield of the branched alkylated product **41** (Scheme 9, reaction conditions c) compared to using the ligand dppe (Scheme 9, reaction conditions b). Moreover, when ethyl meth-

acrylate was used as the coupling partner under the reaction conditions c, branched alkylated products **41'** were obtained selectively in high yields (Scheme 9). A high functional group tolerance was observed in both linear and branched alkylated products.

It is known that the strong coordination of the nitrogen atom in pyridine rings with metals inhibits the metal–chiral ligand coordination, thus making the C–H alkylation of pyridine substrates challenging. In addition, transition-metal-catalyzed enantioselective C–H alkylation reactions of pyridine still remain a great challenge. In this regard, in 2022, Ye and co-workers [60] reported for the first time an enantioselective C-2 alkylation of pyridine using a chiral phosphine oxide-ligated Ni–Al bimetallic catalyst system and the protocol was found effective for a wide range of pyridines including unsubstituted pyridines,

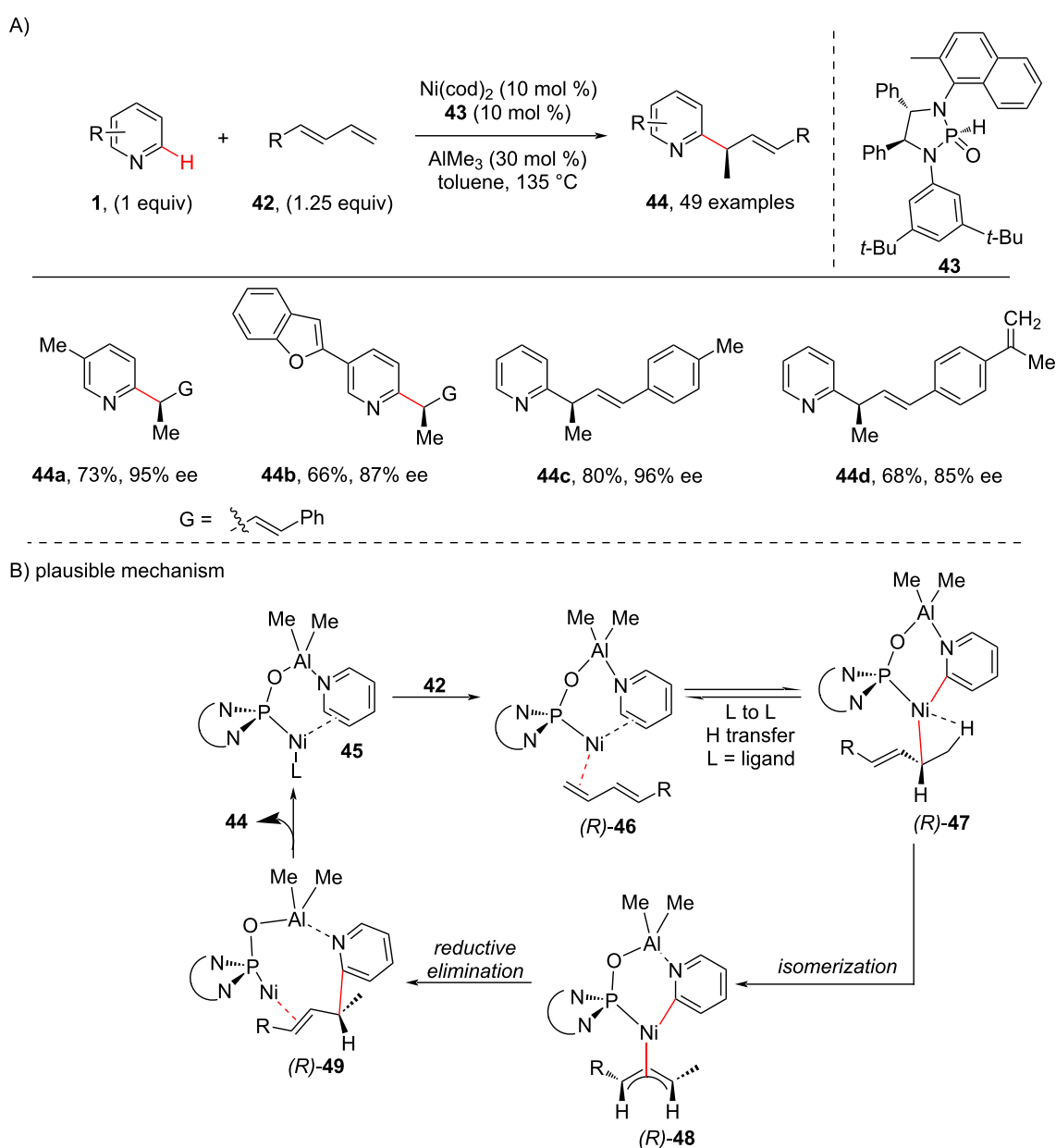


C2, C3 and C4-substituted pyridines and complex pyridines containing bioactive molecules (Scheme 10). To attain enantioselectivity a chiral phosphine oxide (**43**)-ligated Ni–Al bimetallic catalyst was used that was critical in improving the reactivity and controlling the selectivity of the reaction. Further, based on deuterium labelling experiments, KIE studies, and DFT calculation, a plausible mechanism (Scheme 10b) has been proposed. Initially, a reversible ligand-to-ligand H-transfer process occurs for C–H activation between the intermediates **46** and **47**. Next, isomerization of the  $\eta^1$ -allyl complex **47** forms the  $\eta^3$ -allylic nickel complex **48**, which on reductive elimina-

tion delivers the desired product **44** via the intermediate **49** (Scheme 10b). It was proposed that the enantioselectivity was mainly due to the C–C reductive elimination of the *R*-pathway, which is lower in energy than the *S*-pathway.

### Remote C–H alkylation

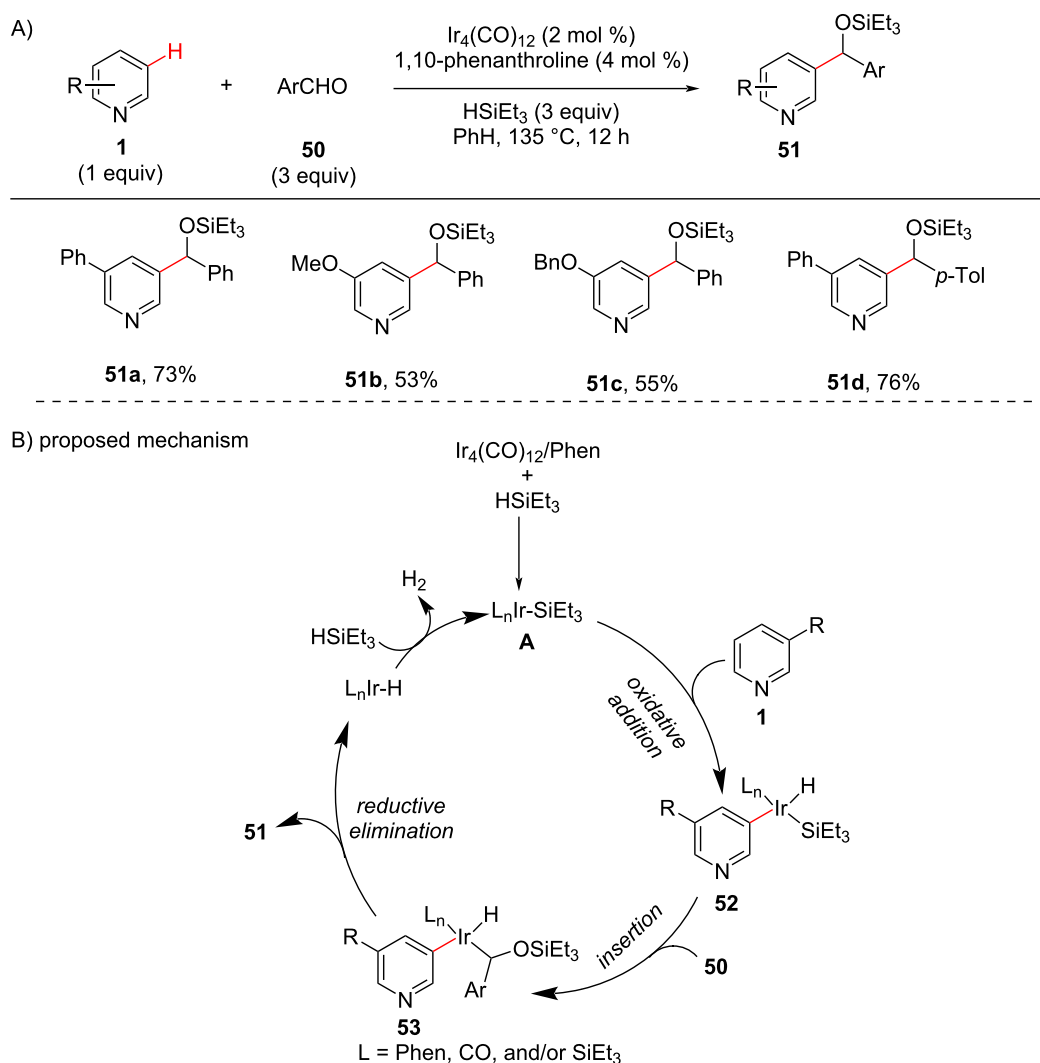
Several remarkable studies have been reported for proximal C–H functionalizations in pyridine substrates under different catalytic systems. However, the intermolecular undirected distal C–H functionalization in pyridine remained unstudied. In these circumstances, the distal C–H alkylation by addition of the pyri-



**Scheme 10:** Ni–Al bimetallic system-catalyzed pyridine C–H alkylation.

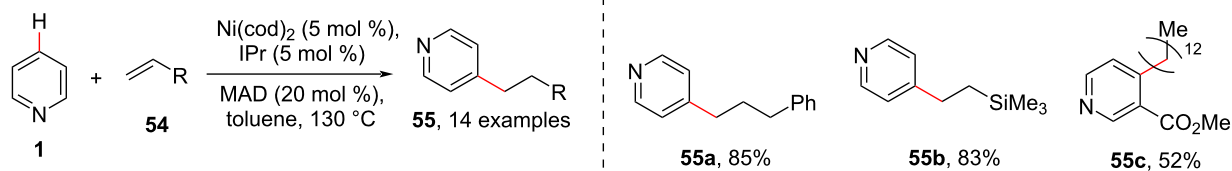
dine C–H bond to an aldehyde **50** under iridium catalysis was achieved by Shi [61] in 2010 through an unusual *meta*-selectivity for the first time (Scheme 11a). To achieve *meta*-selectivity, the group has screened various transition metals and revealed that a silyl-iridium complex promoted the addition of *meta*-pyridyl C–H bonds to aldehydes **50** which resulted in C3-alkylated pyridines **51**. Based on the reactions performed for the catalytic activity of the silyl-iridium complex, the authors proposed a catalytic mechanism (Scheme 11b). The mechanism involves the initial formation of the active silyl-iridium catalyst **A** which through oxidative addition of **1** gives the silyl-iridium complex **52**. The insertion of aldehyde **50** into the Ir–Si bond of **52** provides the pyridyl alkyl iridium species **53** that finally by C–C formation via reductive elimination furnishes the desired products **51** along with the formation of an iridium hydride species (Scheme 11b).

A direct selective C4-alkylation of pyridine has been reported by the groups of Hiyama [62] (Scheme 12a) and Zhang [63] (Scheme 12c) in 2010 and 2020, respectively. The Hiyama group developed a C-4-selective alkylation of pyridines using a Ni/Lewis acid cooperative catalytic system in combination with a bulky N-heterocyclic carbene ligand and (2,6-*t*-Bu<sub>2</sub>-4-Me-C<sub>6</sub>H<sub>2</sub>O)<sub>2</sub>AlMe (MAD) as the Lewis acid which allowed the direct C-4 alkylation of pyridines **1** (Scheme 12a). With the optimized reaction conditions in hand the group also screened the alkene and pyridine substrate scope which resulted C4-alkylated products **55** in moderate to high yields. A possible mechanistic cycle (Scheme 12b) was also proposed, comprising an initial formation of  $\eta^2$ -arenenickel species **56A**, which undergoes oxidative addition to the C(4)–H bond of pyridine to form intermediate **56B**. Next, coordination and migratory insertion of the alkene provides the intermediate **57** which on subsequent re-

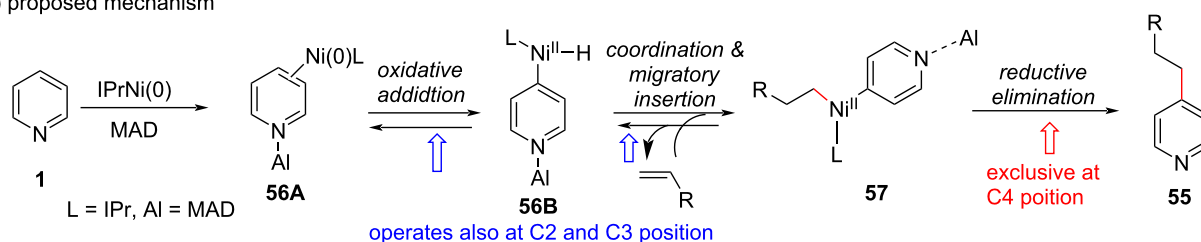


**Scheme 11:** Iridium-catalyzed pyridine C–H alkylation.

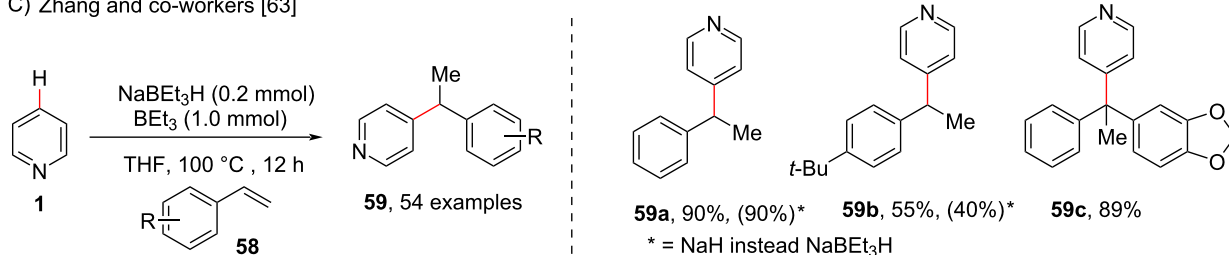
## A) Hiyama and co-workers [62]



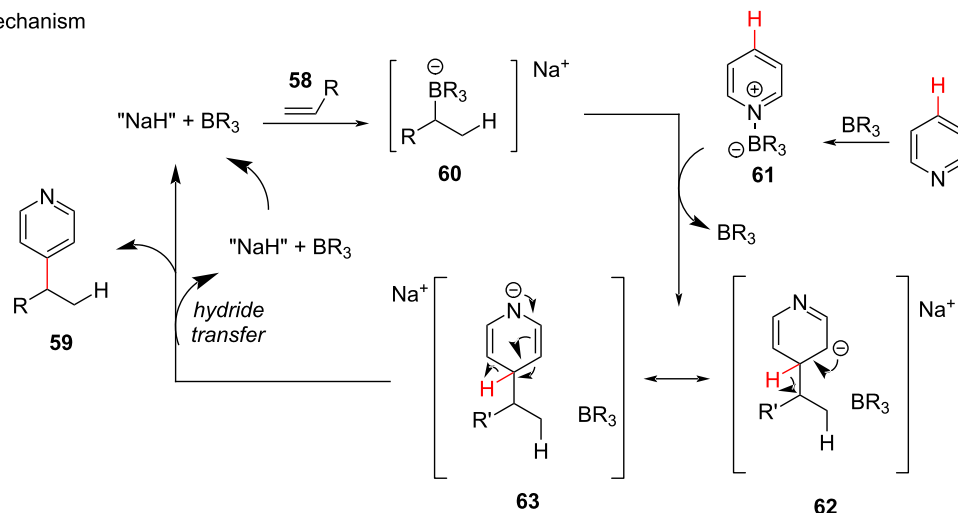
## B) proposed mechanism



## C) Zhang and co-workers [63]



## D) proposed mechanism

Scheme 12: *para*-C(sp<sup>2</sup>)-H Alkylation of pyridines with alkenes.

ductive elimination furnishes the C4-alkylated products **55**. Based on the deuterium exchange experiment, the author suggested that the steps involved in the catalytic cycle from **56A** to **57** are reversible in nature, which may activate the C2 or C3 position as well. However, the reductive elimination at the C4-position was suggested to be irreversible in nature and does not take place at the C2 and C3 position. On the other hand, the

Zhang group reported the C4 alkylation of pyridines using alkenes **58** catalyzed by an organoborohydride ( $\text{NaBEt}_3\text{H}$ ) and aided by organoboranes (Scheme 12c). The proposed mechanism (Scheme 12d) involves the formation of the organoborate intermediate **60** from alkene **58** in the presence of the  $\text{NaBEt}_3\text{H}$  catalyst and the organoborane. Next, the organoborane-activated pyridine species **61** undergoes an addition reaction regio-

selectively at the C4 position of the organoborate intermediate **60** delivering the  $\alpha^H$ -adduct intermediates **62** and **63**. Subsequently, hydride elimination with the help of the organoborane gave the desired alkylated product **59** and regenerates the hydride catalyst.

Further enantioselective pyridine C–H alkylation reactions are very scarcely reported which specifically include the intramolecular C–H alkylation of pyridine with alkenes at the C3 or C4 positions. Hence, very recently in 2022, Shi and co-workers [64] adopted an intermolecular process and reported the enantioselective *para*-alkylation of pyridines with styrenes **64** using a Ni–Al bimetallic system and NHC ligand **65** through intermolecular hydroarylation with high levels of enantio- and regioselectivity in the alkylated products **66** (Scheme 13). Also, the authors performed DFT studies revealing the reaction mechanism and supported that the interaction of the NHC aryl part with *trans*-styrene was highly important for the reaction to proceed and for the enantiocontrolled formation of the products.

## Alkenylation

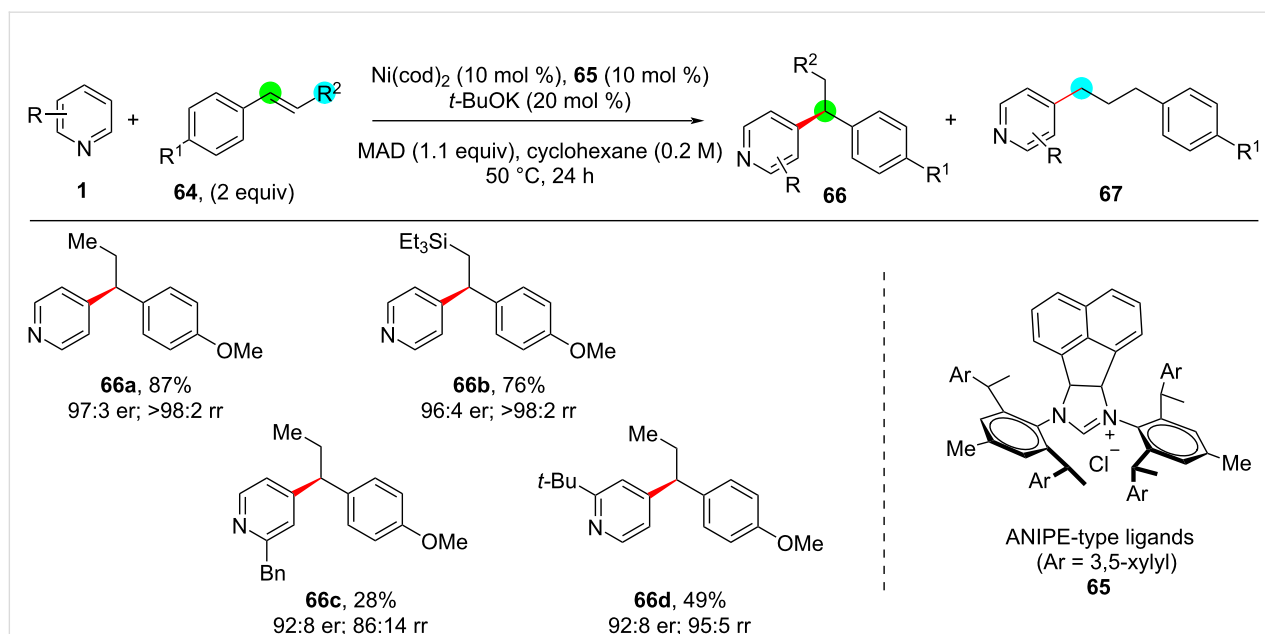
The C–H alkenylation is another important C–C bond-forming reaction. Olefinated organic molecules like vinylarenes play a significant role as key intermediates in organic synthesis and are also present in various natural products as well as drug molecules [65–68]. Though there are traditional methods available for C–H olefinations they suffer from some disadvantages such as for example requiring prefunctionalized substrates as in case of the Heck cross-coupling [69,70]. However, researchers have

developed various methods for the transition-metal-catalyzed C(sp<sup>2</sup>)–H olefination using various types of alkenes as coupling partners [71–73]. This part of the review covers reports for the alkenylation of pyridine with terminal alkynes, acrylates, allenes, and alkynes as coupling partners achieving the functionalized C(sp<sup>2</sup>)–H-olefinated pyridine frameworks via metal catalysis.

### *ortho*-C–H Alkenylation

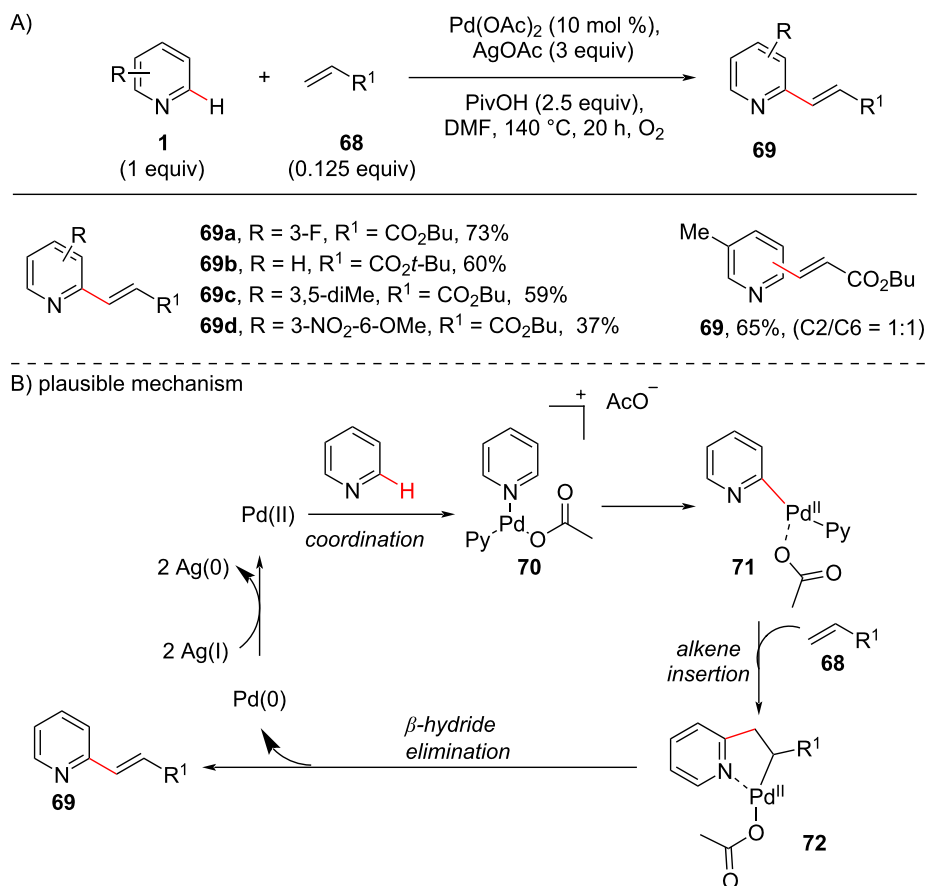
In 2012, Huang and co-workers [74] disclosed a ligand-free oxidative cross-coupling reaction of pyridine with acrylates, acrylamides, and styrenes (Scheme 14). Their preliminary investigation provided both C2 and C3-olefinated products, with the C2-selective product **69** as the major product (Scheme 14a). With the optimized conditions of Pd(OAc)<sub>2</sub> (10 mol %), AgOAc (3 equiv), PivOH (2.5 equiv) in DMF, the method showed wide substrate scope and good yields. Based on the experimental findings the authors proposed a catalytic cycle (Scheme 14b) which commences with the coordination of Pd(II) with the pyridine nitrogen to provide intermediate **70**. A strong *trans*-effect results in the C–H cleavage for the formation of Pd(II) species **71**. Subsequently, insertion of alkene **68** provides the cyclic Pd(II) intermediate **72** which undergoes  $\beta$ -hydride elimination to produce the desired product **69**.

In the same year, Ramana and Goriya [75] proposed an unexpected C-6 (C-2)-propenylation reaction of pyridine in the presence of allyl bromide (**73**) and a Ru catalyst using 2-arylpyridines (Scheme 15). Earlier reports described the

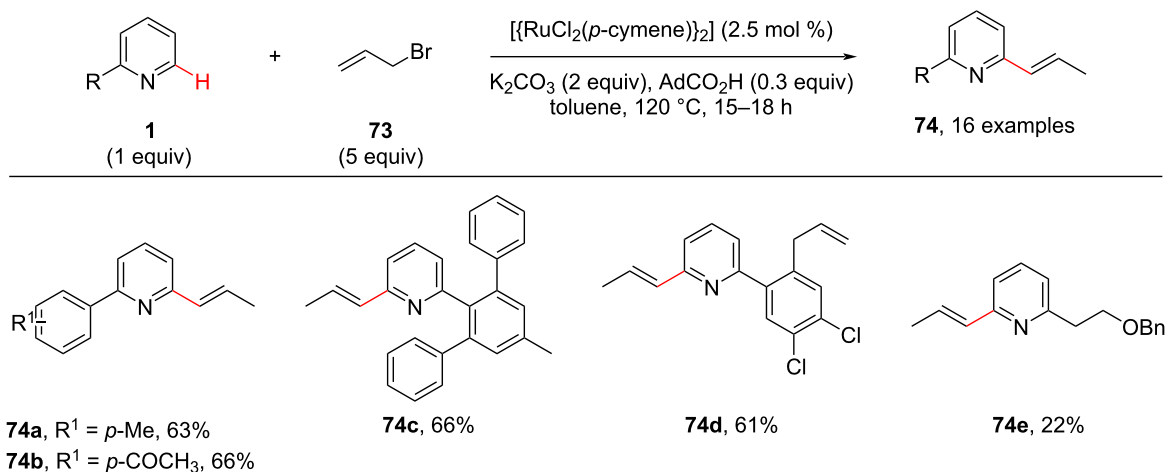


**Scheme 13:** Enantioselective pyridine C–H alkylation.





Scheme 14: Pd-catalyzed C2-olefination of pyridines.



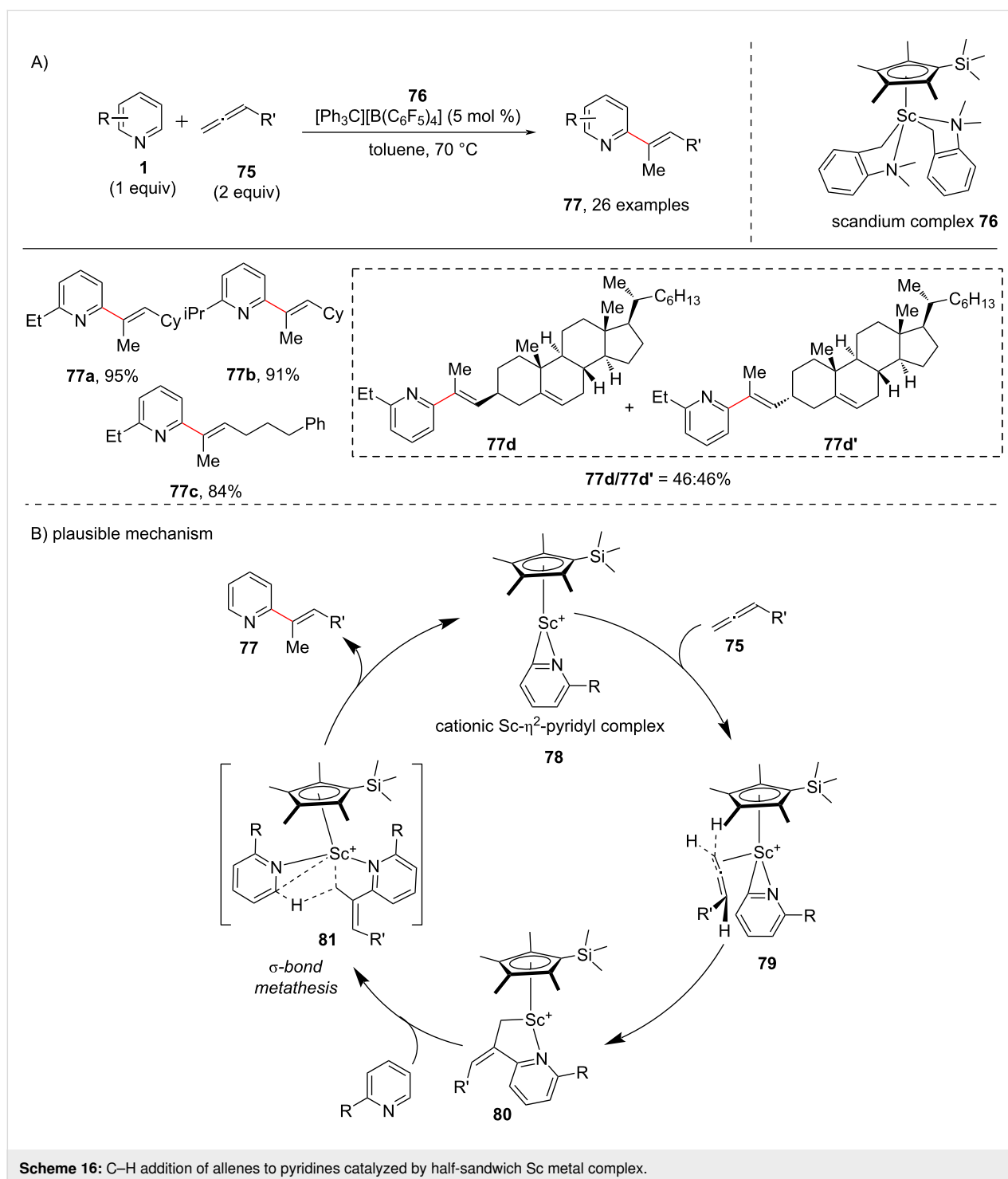
Scheme 15: Ru-catalyzed C-6 (C-2)-propenylation of 2-arylated pyridines.

propenylation took place on the *ortho*-position of the phenyl ring [76,77], whereas this group achieved the propenylation of the pyridine moiety. The authors screened different allyl halides

and Ru complexes as catalysts. With the optimized conditions in hand, diverse 2-arylated pyridines were screened resulting in the corresponding products **74** in good yields.

Allene, a cumulated diene and an important building block in organic synthesis has versatile biological properties and is also an important subunit in various natural products and pharmaceutical compounds [78]. Allenes have been applied as useful substrates for the alkenylation of organic molecules [79]. There are various reports for the C–H alkenylation of aromatic C–H bonds using allenenes [80]. To this end, Hou and group in

2015 [81] demonstrated the C–H allenylation of pyridines with excellent substrate scope using a scandium catalyst (Scheme 16). A vast number of pyridines and allenenes were studied as substrates to provide the C2-alkenylated pyridines in good to high yields. Based on the mechanistic experiments a possible catalytic cycle has been proposed (Scheme 16b). The half-sandwich scandium complex **76** along with the

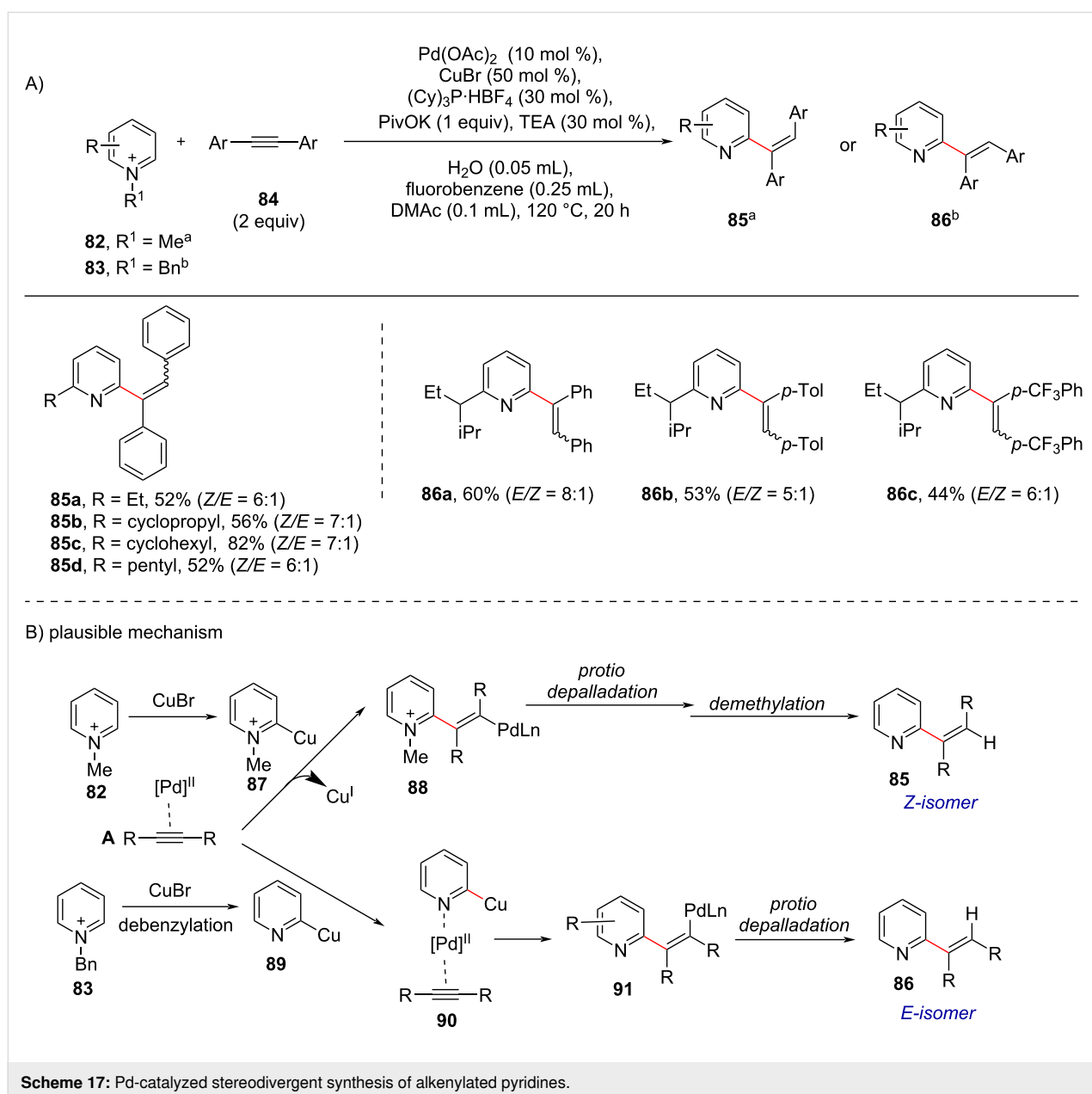


tetrakis(pentafluorophenyl)borate and pyridine forms a cationic Sc-pyridyl complex **78**, which after addition of allene **75**, forms a transient pentacyclic intermediate **80** via intermediate **79**. Next, another molecule of pyridine adds to intermediate **80** to furnish the transient complex **81** which undergoes  $\sigma$ -bond metathesis to give the product **77** and regenerating **78** (Scheme 16b).

While speaking regarding the alkenylation, the geometrical isomerism, i.e., the stereoselectivity between the *cis*- and *trans*-alkenylation, has not been considered so far. Except lately, in 2020, Chen and group [82] reported a Pd/Cu-catalyzed regio- and stereoselective synthesis of C2-alkenylated pyridines

starting from internal alkynes **84** and pyridinium salts in a stereodivergent manner (Scheme 17a). The interesting part of this work was the switching of the alkene configuration of the products by modifying the substituents on the nitrogen of the pyridinium salts. Further, the method showed a wide substrate scope for both the *Z*- and *E*-alkenylated products in which *Z*-selectivity was achieved when *N*-methylpyridinium salts were used and *E*-selectivity when *N*-benzylpyridinium salts were used.

In the proposed mechanism (Scheme 17b) the *E*- and *Z*-isomers can be assessed through point at which dealkylation occurs, i.e., if it occurs as last step the *Z*-isomer **85** is obtained and if it



takes place at an early stage, *E*-isomer **86** predominates (Scheme 17b). The proposed mechanism involves the initial formation of  $\pi$ -complex **A** via activation of the alkyne by Pd. Then, in case of *N*-methylpyridinium salt **82**, in presence of CuBr the pyridine–Cu(I) complex **87** is formed through C–H activation that further undergoes nucleophilic attack to the coordinated alkyne in a *trans*-manner to give Pd(II)–alkenyl intermediate **88**. Then, the intermediate **88** undergoes protio-depalladation and demethylation to yield the *Z*-isomer **85** (Scheme 17b). In case of *N*-benzylpyridinium salts **83**, first debenzilation occurs to form 2-pyridyl–Cu(I) species **89** in the presence of CuBr which then coordinates to the Pd center of  $\pi$ -complex **A** via the lone electron pair of the pyridine nitrogen to give **90** which further attacks the  $\pi$ -bond in a *cis*-manner to give intermediate **91**. After protio-depalladation the *E*-isomer **86** is obtained as major product (Scheme 17b).

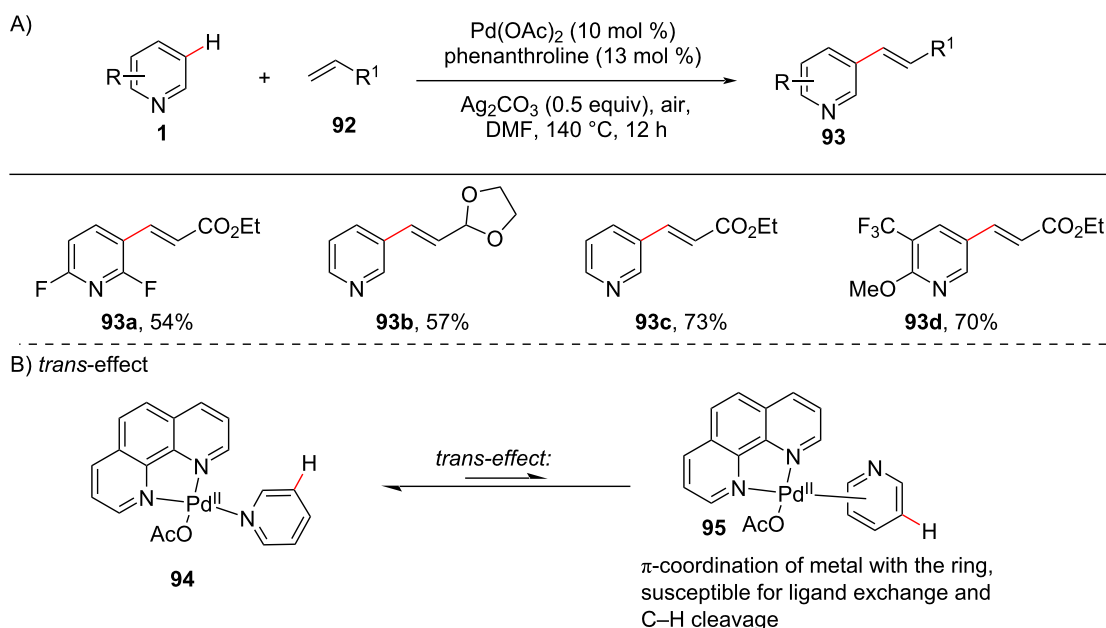
### Remote alkenylation

In 2011, a study for weakening the strong coordination of the pyridyl *N*-atom with Pd in the presence of a bidentate ligand was reported by Yu and co-workers [83]. They showcased the C3-selective olefination of pyridines using 1,10-phenanthroline, a bis-dentate ligand that weakens the coordination of the Pd catalyst with the pyridyl *N*-atom through the *trans*-effect (Scheme 18). The *trans*-effect is the switching of the metal coordination between the  $\pi$ -ring system and the hetero-(nitrogen) atom of pyridine [84,85]. In comparison to coordination with nitrogen, which is strong in nature, the coordination

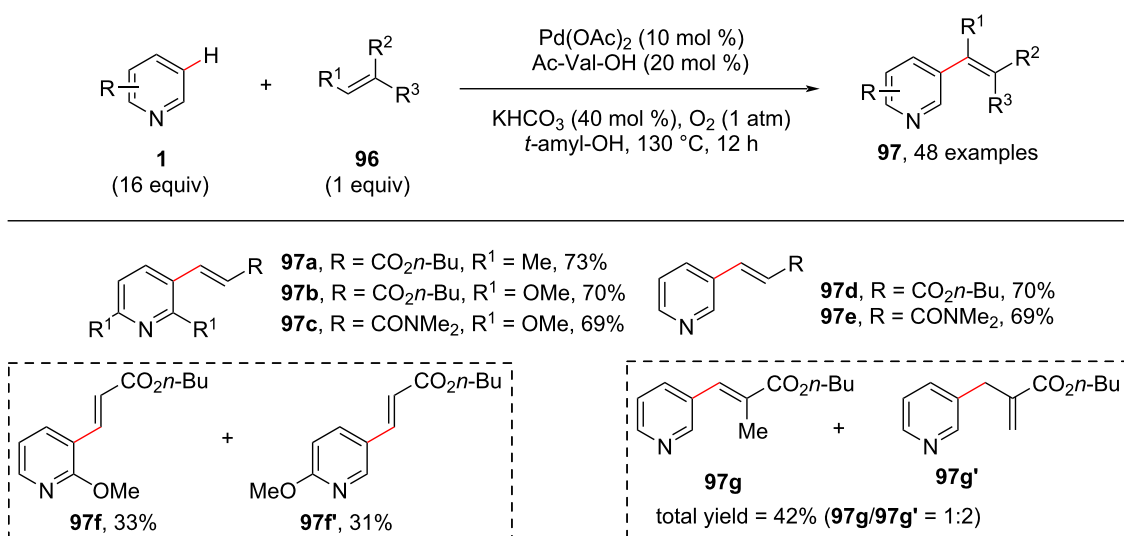
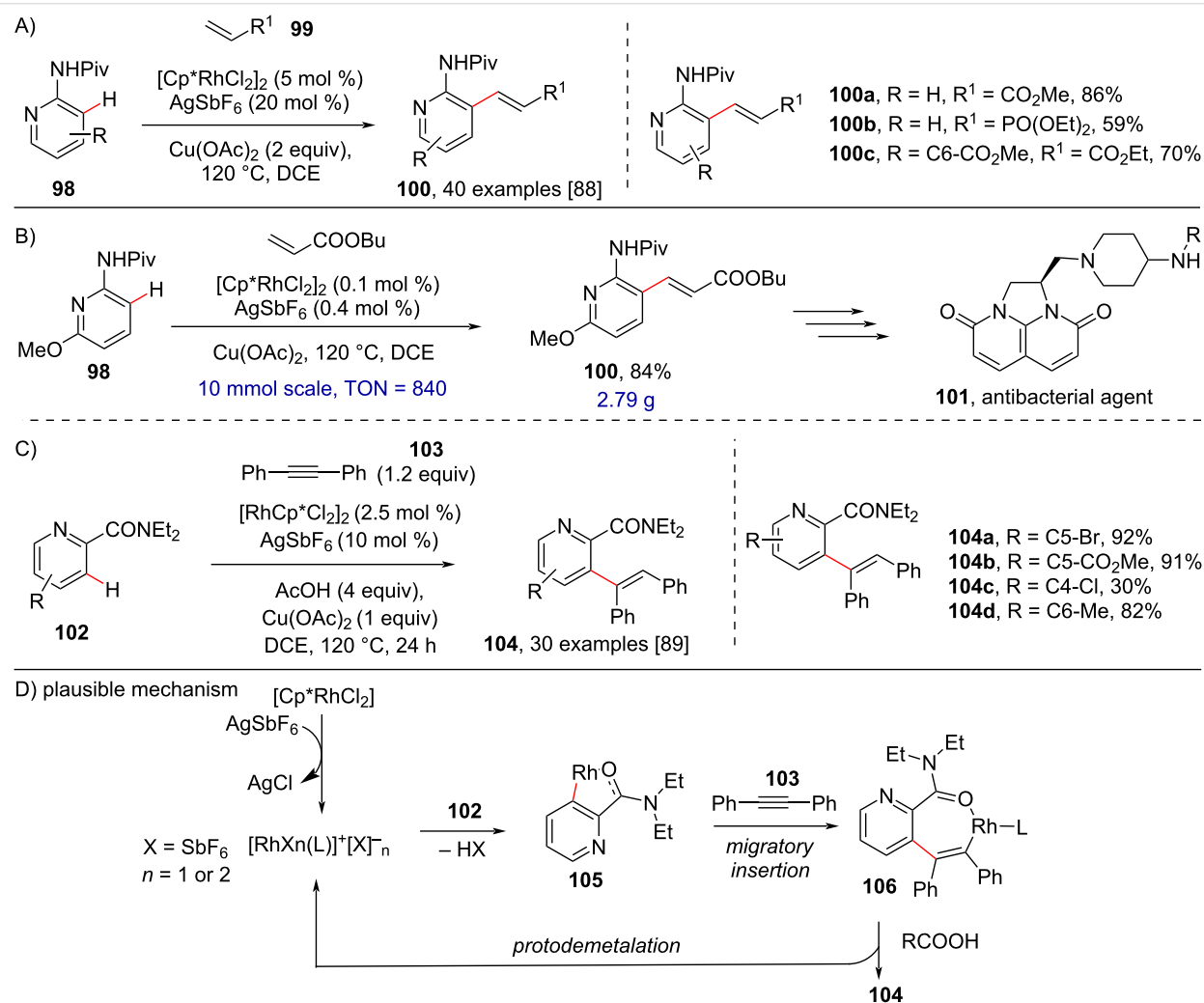
with the ring is weaker and cleavable. The usage of a bidentate ligand will enhance the *trans*-effect and shift the coordination towards the ring (Scheme 18b).

There are numerous studies reported for directing group or chelate-assisted metal-catalyzed C–H functionalization reactions. However, non-chelate-assisted or undirected C–H functionalizations under ligand-controlled conditions are underexplored. Hence, differentiating from this co-coordinative model, in 2013, Zeng and co-workers [86] reported the MPAA (mono-*N*-protected amino acids) ligand-promoted non-chelate-assisted C–H activation via Pd-catalyzed dehydrogenative Heck reactions on pyridines with simple alkenes **96**, leading to the C3-alkenylated products **97** (Scheme 19). The reaction was based on the previous reports of using of the MPAA ligands in the Pd-catalyzed oxidative cross-coupling reactions discovered by Yu et al. [87]. When 2-methoxypyridine was screened, the reaction resulted in a mixture of C3- and C5-selective C–H functionalized products **97f** and **97f'** in a regioisomeric ratio of nearly 1:1. Further, during the substrate scope study, when 1,1'-disubstituted butyl methacrylate was used as coupling partner a mixture of **97g** and the isomeric product **97g'** was observed in 42% yield.

Further, Shi and co-workers reported the rhodium-catalyzed directed C–H olefination of pyridines using different directing groups in 2013 [88] (Scheme 20a) and 2014 [89] (Scheme 20c), respectively. In the former study, under optimized conditions of



**Scheme 18:** Pd-catalyzed ligand-promoted selective C3-olefination of pyridines.

Scheme 19: Mono-*N*-protected amino acids in Pd-catalyzed C3-alkenylation of pyridines.

Scheme 20: Amide-directed and rhodium-catalyzed C3-alkenylation of pyridines.

[RhCp\*Cl<sub>2</sub>]<sub>2</sub> (5 mol %), AgSbF<sub>6</sub> (20 mol %) in DCE at 120 °C, Cu(OAc)<sub>2</sub> was found crucial for the transformation in comparison to other additives and showed good substrate scope while unactivated alkenes like styrene resulted in no reaction. Also, the authors successfully applied the developed protocol to a multigram-scale synthesis of compound **101**, a tricyclic imidazophthalidinone derivative having antibacterial properties, with low catalyst loading (0.1 mol %) (Scheme 20b). Later, in 2014, the same authors, using an amide as directing group (DG), developed a protocol for the regioselective C3-alkenylation of pyridines through *syn*-addition of alkynes, displaying broad substrate scope and high yields (Scheme 20c). Based on literature reports and experimental studies, a possible mechanism (Scheme 20d) was proposed in which coordination of the DG **102** to the rhodium cationic species followed by *ortho*-metalation and migratory insertion of **103** into the Rh–C bond of **105** provides a seven-membered rhodacyclic intermediate **106**. The protonation at the Rh–C bond of intermediate **106** in the presence of RCOOH furnishes hydroarylation product **104**.

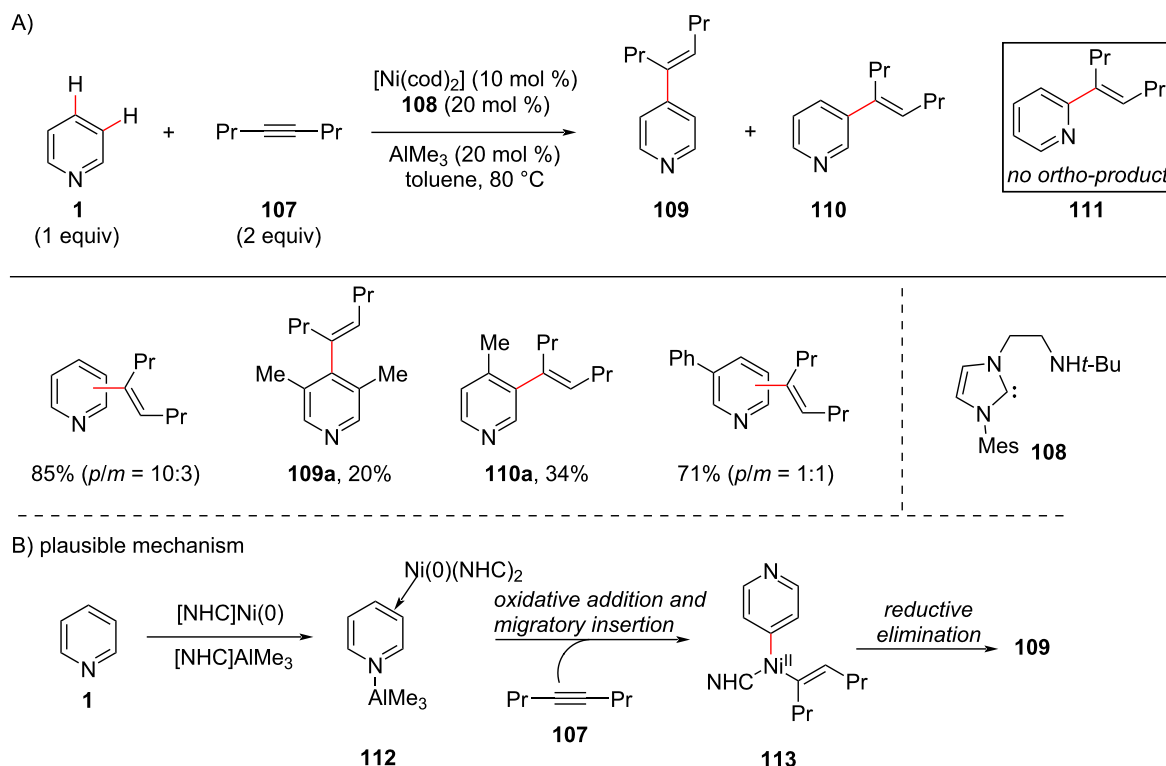
Nitrogen heterocyclic carbenes (NHCs) are of central importance in organometallic chemistry and in organic synthesis.

Also, metal–NHC complexes have wide application in catalysis and various organic transformations and a range of metal–NHCs served as catalysts. In 2010, using NHC ligands, Yap and co-workers [90] developed a method for the direct *para* and *meta*-C–H alkenylation of pyridines with 4-octyne (**107**) using a nickel Lewis acid catalyst with amino pendant linked NHC complex (Scheme 21). In addition, the authors were able to isolate the bimetallic intermediate structure  $\eta^2, \eta^1$ -pyridine–Ni(0)–Al(III) complex **112**, as a support for their mechanism for the *para*-C–H functionalization. They further investigated the scope and limitations of the dual catalyst Ni–AlMe<sub>3</sub> and also the sensitivity of the reaction towards the steric environment on the pyridine ring. The complex **112** undergoes oxidative addition followed by an alkyne insertion reaction to give intermediate **113**, which after reductive elimination provides the alkenylated product **109** (Scheme 21b).

## Arylation

### C-2 Arylation

Owing to the remarkable role of aromatic C–H arylation reactions in organic synthesis abundant methods have been reported for aromatic C–H arylations using different arylating coupling partners, such as for instance, aryl halides. In 2014,



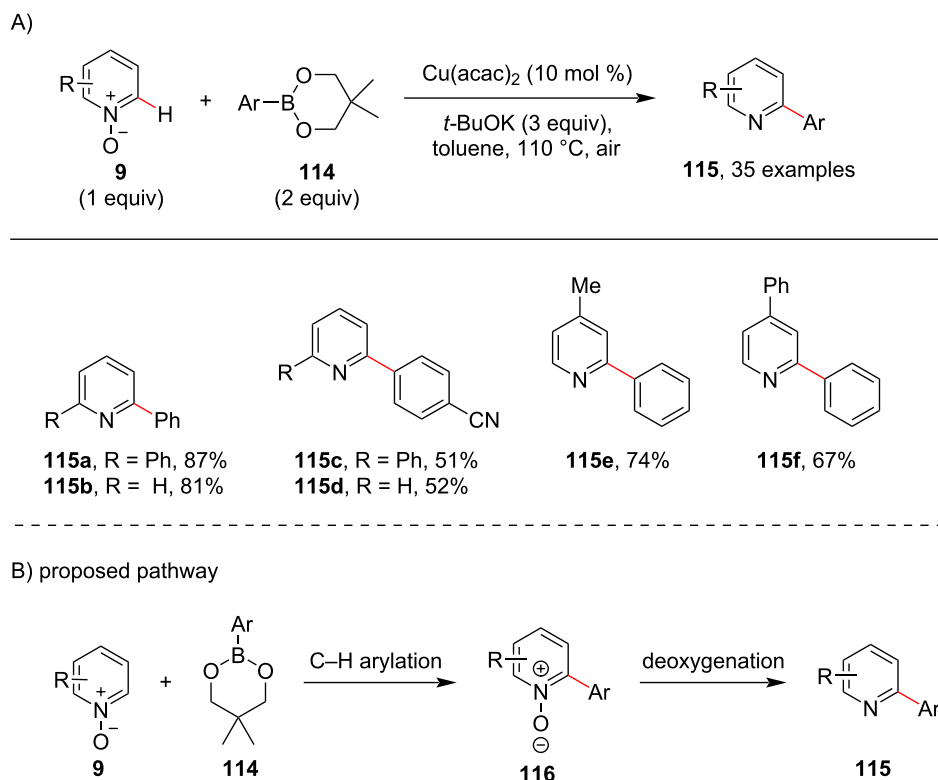
**Scheme 21:** Bimetallic Ni–Al-catalyzed *para*-selective alkenylation of pyridine.

using organoboron coupling partners, Wu and co-workers [91] reported a protocol for the Cu-catalyzed C–H arylation of pyridine *N*-oxides **9** with arylboronic esters **114** and prepared C2-arylated pyridines **115** in moderate to good yields (Scheme 22). By using an inexpensive Cu catalyst, the method allows for the simple and practical synthesis of 2-arylpyridines. The reaction starts with the formation of arylated pyridine *N*-oxide **116** by reaction of pyridine *N*-oxide **9** with the arylboronic ester **114** in the presence of Cu catalyst and base which is followed by deoxygenation to furnish the desired product **115** (Scheme 22b).

In 2015, a palladium-catalyzed cross dehydrogenative coupling of pyridine *N*-oxides with toluene for the regioselective arylation and benzylation of pyridine *N*-oxide was reported by Khan and co-workers [92] (Scheme 23). The authors have shown toluene **117** when used as benzyl and aryl source remained intact under the reaction conditions without any further oxidation. Different oxidants resulted in different products such as the monoarylated product **118** formed in the presence of TBHP as oxidant and the benzylated product **119** was obtained when potassium persulfate was used. Interestingly, aza-fluorene *N*-oxide **119b** was formed during benzylation of

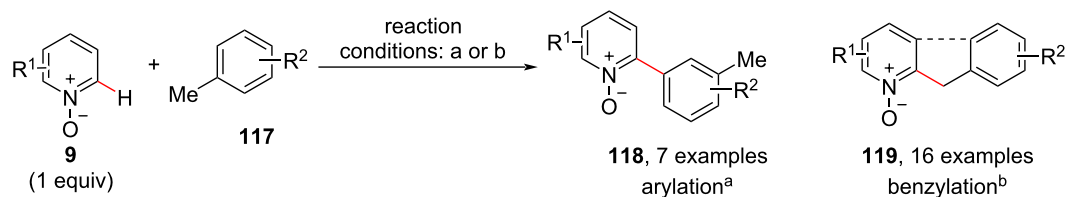
2-ethylpyridine *N*-oxide. A possible mechanism has also been reported (Scheme 23b). Electrophilic palladation at the C2-position of pyridine *N*-oxide **9** provides intermediate **120**. The radical intermediate **121** is generated in situ by H-atom abstraction from toluene **117** by sulfate radical anion. Coordination of intermediate **120** and **121** leads to complex **122** which undergoes reductive elimination to provide product **119**. 2-Ethyl-substituted pyridine *N*-oxides may undergo a dual C–H activation due to the buttressing effect of the ethyl group to produce azafluorene *N*-oxide **119b**.

In 2016, Wei and co-workers [93] reported the arylation of pyridine *N*-oxides **9** employing potassium (hetero)aryltrifluoroborates **126** as coupling partner using palladium acetate and TBAI (Scheme 24). Electron-withdrawing and donating groups on the pyridine *N*-oxide **9** resulted in the corresponding C2-arylated products **127** in good to excellent yields with high site selectivity. A catalytic mechanism was proposed in which the electrophilic C–H palladation of pyridine *N*-oxide **9** occurs preferentially at the C-2 position leading to heterocoupling intermediate **128**. Subsequent transmetalation provides the arylpalladium intermediate **129** which after reductive elimination furnishes the desired product **127**.

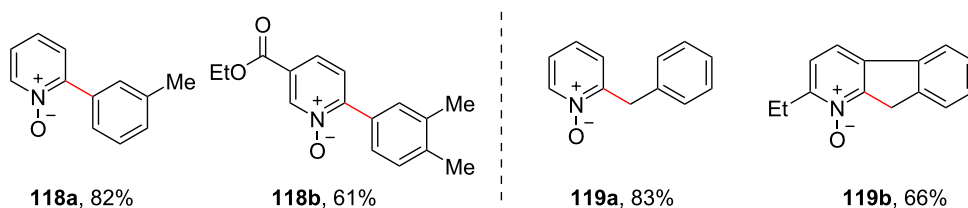


**Scheme 22:** Arylboronic ester-assisted pyridine direct C–H arylation.

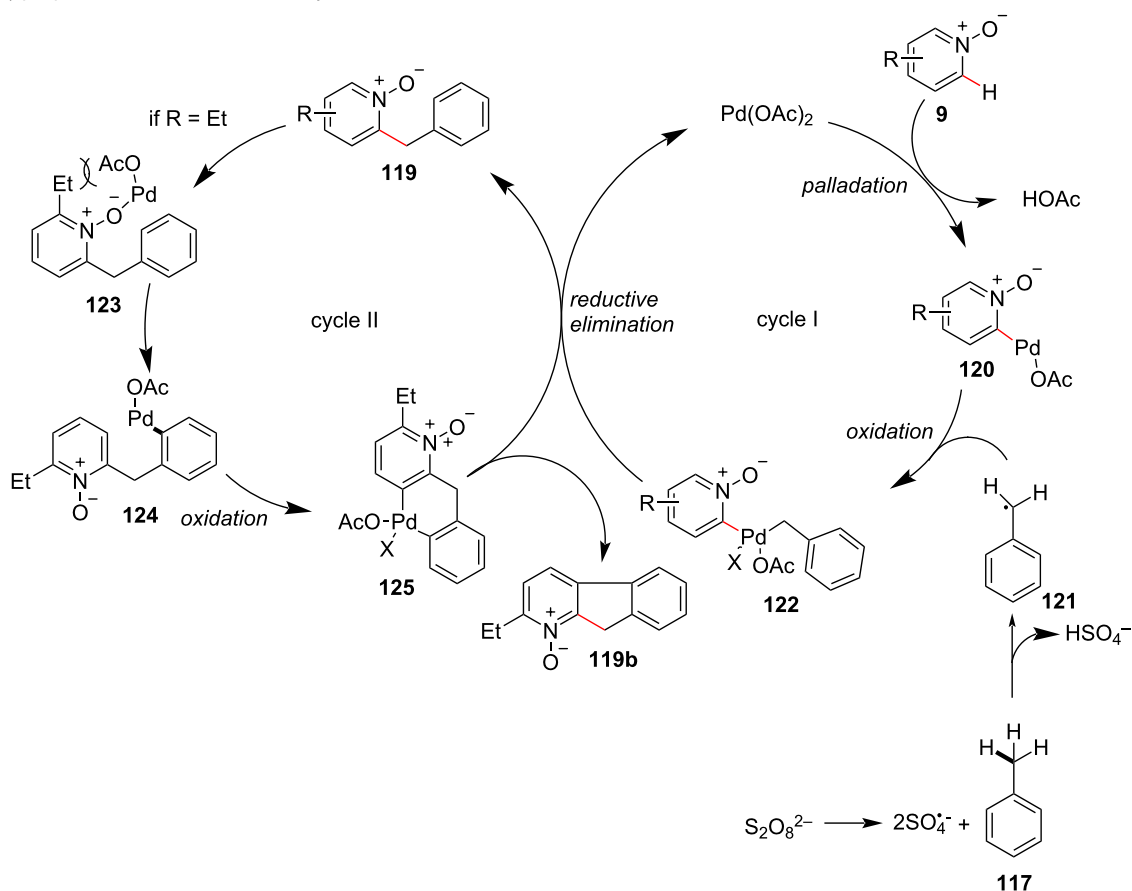
A)



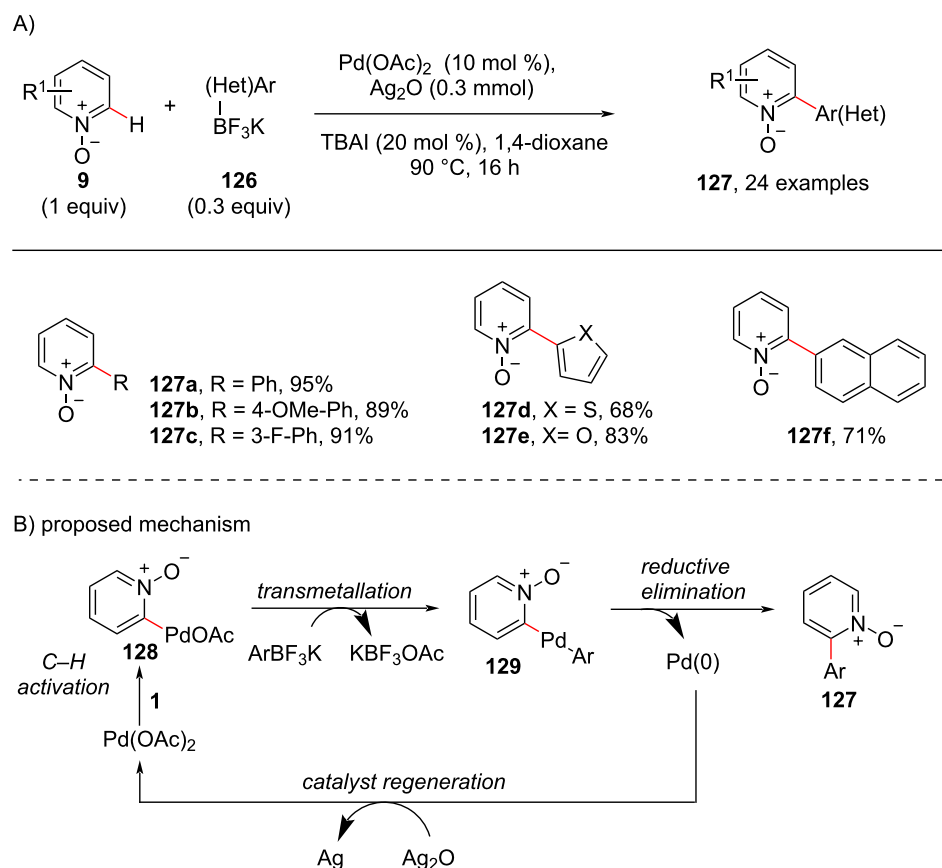
reaction conditions:

(a) toluene (2 mL),  $\text{Pd}(\text{OAc})_2$  (3 mol %), TBHP (2 equiv),  $\text{Cu}(\text{OAc})_2 \cdot \text{H}_2\text{O}$  (0.5 equiv), 120 °C, 18 h(b) toluene (20 equiv),  $\text{Pd}(\text{OAc})_2$  (3 mol %),  $\text{K}_2\text{S}_2\text{O}_8$  (0.75 equiv), 120 °C, 18 h

B) proposed mechanism for benzylation

**Scheme 23:** Pd-catalyzed C–H arylation/benzylation with toluene.





**Scheme 24:** Pd-catalyzed pyridine C–H arylation with potassium aryl- and heteroaryltrifluoroborates.

In 2017, Chen and group [94] developed a protocol for the C2,C6-arylation of pyridine under Pd catalysis (Scheme 25). In their study, *N*-alkylpyridinium salts were used as a directing group, facilitating the C–H arylation of pyridine. Dimethyl sulfate was used as a good *N*-methylating agent, which acts as transient activator. The group performed HRMS and KIE studies and proposed a catalytic cycle (Scheme 25b). The oxidative addition of ArBr **130** to the in situ-formed Pd(0) species gives species **132** followed by transmetalation with CuI pyridyl species **133** generated from the reaction of Cu<sub>2</sub>O with the methylated pyridine to afford intermediate **134** that on reductive elimination results in salt **135**. Subsequent demethylation of **135** gives monoarylated product **136** or the intermediate **135** reenters the catalytic cycle to produce the diarylated *N*-methylpyridinium species, which again undergoes demethylation to produce product **131**.

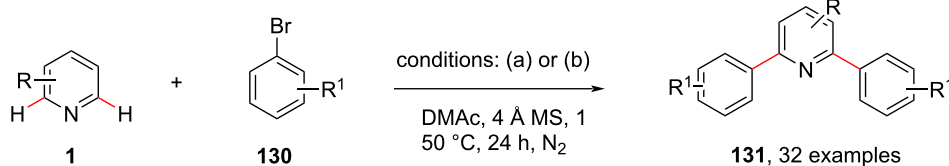
### C-3 Arylation

In 2011 and 2013, the groups Yu [95] and Tan [96], reported a ligand-assisted distal arylation selectively taking place at the *meta*-position in pyridine. Both groups used Pd(OAc)<sub>2</sub> as cata-

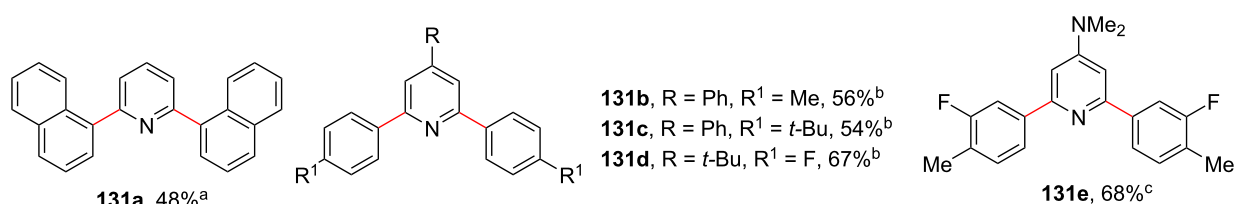
lyst with 1,10-phenanthroline as ligand. The group of Yu used aryl halides **137** as coupling partner, whereas the group of Tan utilized aryl tosylates **142** as coupling partner (Scheme 26). The Yu group also applied the developed protocol for the synthesis of the drug molecule preclamol (**139**, Scheme 26b). The presumed catalytic cycle (Scheme 26c) involved the coordination of Pd(II) to the pyridine nitrogen to give *N*-bound pyridine substrate **A** followed by the formation of Pd(II) intermediate (**B**) involving the  $\pi$ -system of pyridine, which initiates the activation of the C(3)–H of pyridine to form aryl–Pd(II) species **140** via intermediate **C**. Subsequently, oxidative addition takes place in the presence of the aryl halide to give the Pd(IV) complex **141** followed by reductive elimination furnishing 3-arylpiperidines **138**.

Almost at the same time, Yu and co-workers reported the selective Pd(0)/PR<sub>3</sub>-catalyzed C3 or C4-arylation of nicotinic and isonicotinic acids using amide as a directing group (Scheme 27) [97]. This method provides a way for arylated nicotinic acid derivatives which serve as building blocks for biologically important molecules. This was the first report for a directing group-

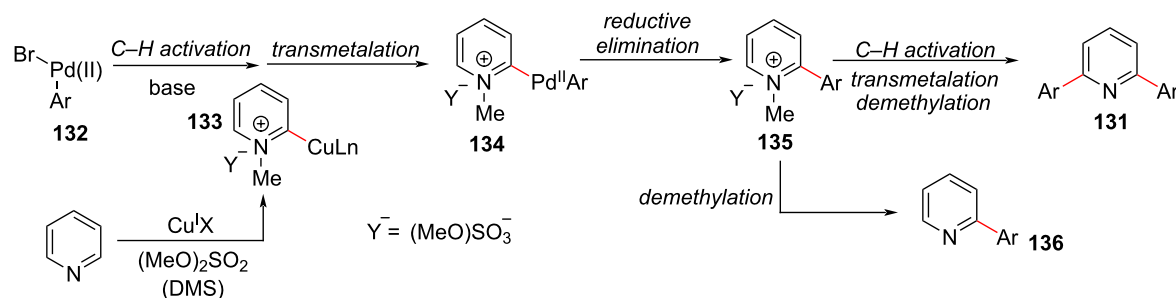
A)



- a) **1** (0.75 mmol), **130** (0.5 mmol), PdCl<sub>2</sub> (5 mol %), PPh<sub>3</sub> (10 mol %), DMS (0.8 equiv), Cu<sub>2</sub>O (0.75 equiv), K<sub>2</sub>CO<sub>3</sub> (2 equiv)  
 b) **1** (0.125 mmol), **130** (0.375 mmol), PdCl<sub>2</sub> (10 mol %), PPh<sub>3</sub> (20 mol %), DMS (1.6 equiv), Cu<sub>2</sub>O (1.5 equiv), K<sub>2</sub>CO<sub>3</sub> (2 equiv)  
 c) **1** (0.5 mmol), **130** (1.5 mmol), PdCl<sub>2</sub> (5 mol %), PPh<sub>3</sub> (10 mol %), DMS (0.8 equiv), Cu<sub>2</sub>O (0.5 equiv), K<sub>2</sub>CO<sub>3</sub> (4 equiv)



B) plausible mechanism

**Scheme 25:** Transient activator strategy in pyridine C–H biarylation.

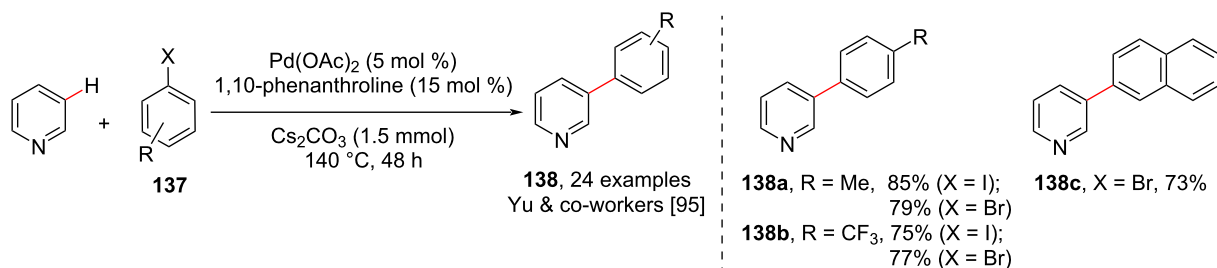
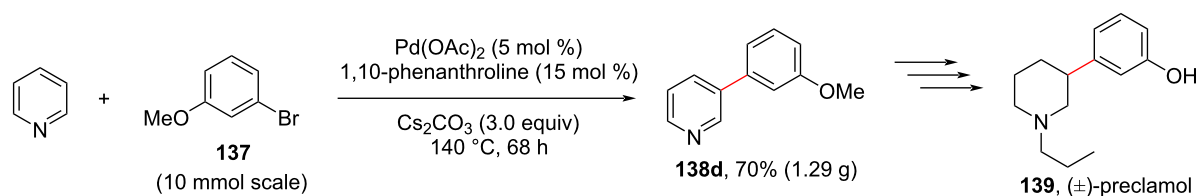
assisted C3/C4-arylation of pyridines. The authors screened various *N*-arylamide directing groups **144** out of which *N*-phenylamide was found to be the better directing group. Then, the authors screened various nicotinic and isonicotinic acids which afforded the desired products **145** and **146** in good yields generating a library of isonicotinic and nicotinic acid derivatives.

Another inexpensive and non-toxic iron-catalyzed C–H arylation of pyridines has been reported by DeBeof and co-workers [98]. Using the imine in **147** as directing group, afforded the arylated pyridine products **150** in good to high yields (Scheme 28). In this reaction, Grignard reagent **148** was used as arylation source in excess amount as the reagent underwent homocoupling leading to the formation of biaryl systems under the reaction conditions. 1,2-Dichloro-2-methylpropane (**149**) was found to be an effective oxidant under the reaction condi-

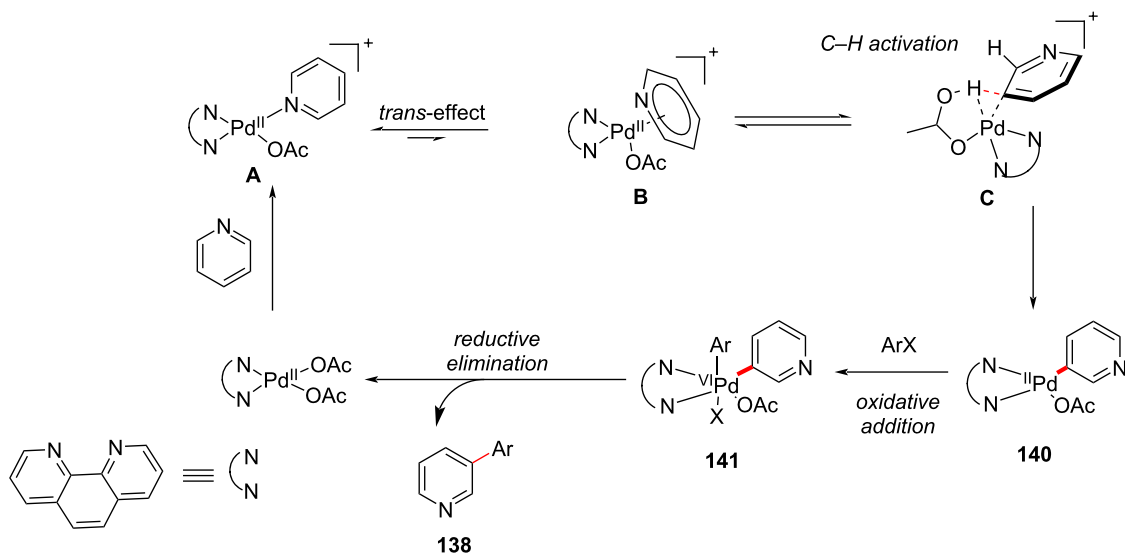
tions. Also, the additive KF was employed in order to minimize the oxidative iron-catalyzed homocoupling of **148**. An imine directing group at the *para*-position in pyridine **147** lead to activated *ortho*-position products **150** within 15 minutes. The imine group of the products can further be hydrolyzed to get the corresponding ketones.

In 2018, Albéniz and group [99] reported the direct C3-arylation of pyridines with the help of bipy-6-OH as coordinating ligand under palladium catalysis (Scheme 29). In most of the cases the arylated pyridines **152** were obtained as mixtures of *ortho*-/*meta*-/*para*-substitution, however, the authors found that the yield of the *meta* (C-3)-arylated pyridines were drastically higher, thereby showcasing the regioselectivity of the reaction. The chelating anionic ligand acted as base in the catalytic cycle, allowing for the oxidative addition of the arene to the Pd complex. The proposed mechanism (Scheme 29b) involves the oxi-

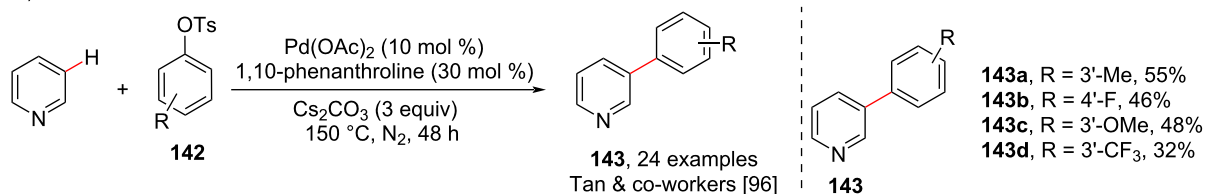
A)

B) synthesis of ( $\pm$ )-preclamol

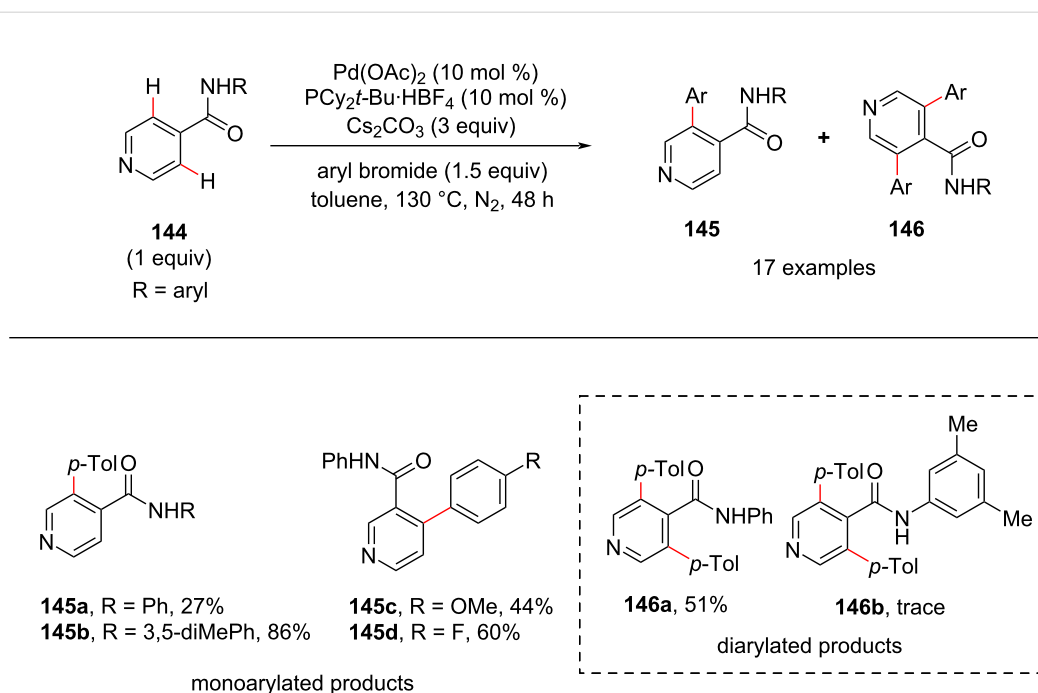
C) plausible mechanism



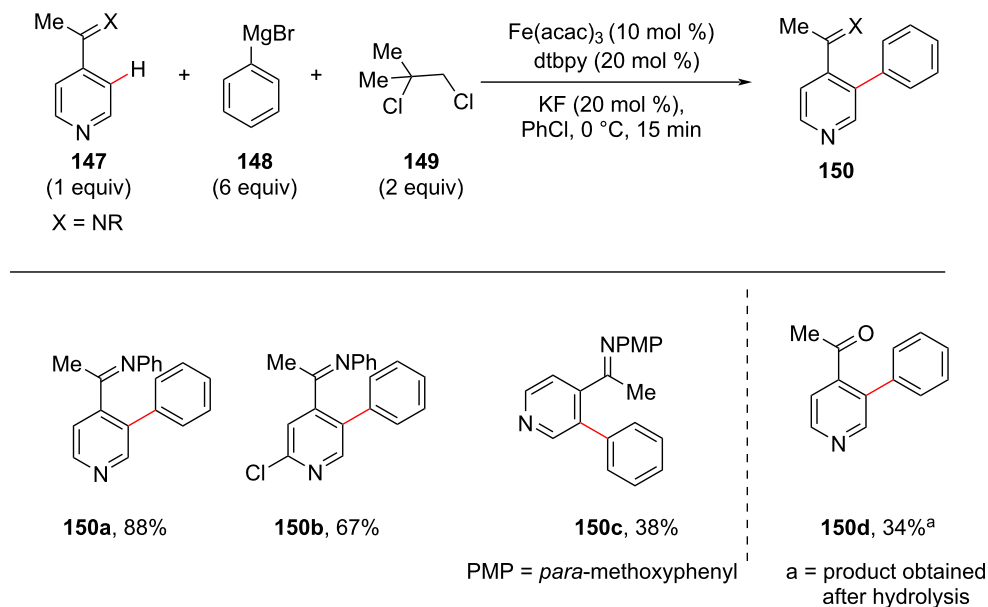
D)



Scheme 26: Ligand-promoted C3-arylation of pyridine.



Scheme 27: Pd-catalyzed arylation of nicotinic and isonicotinic acids.



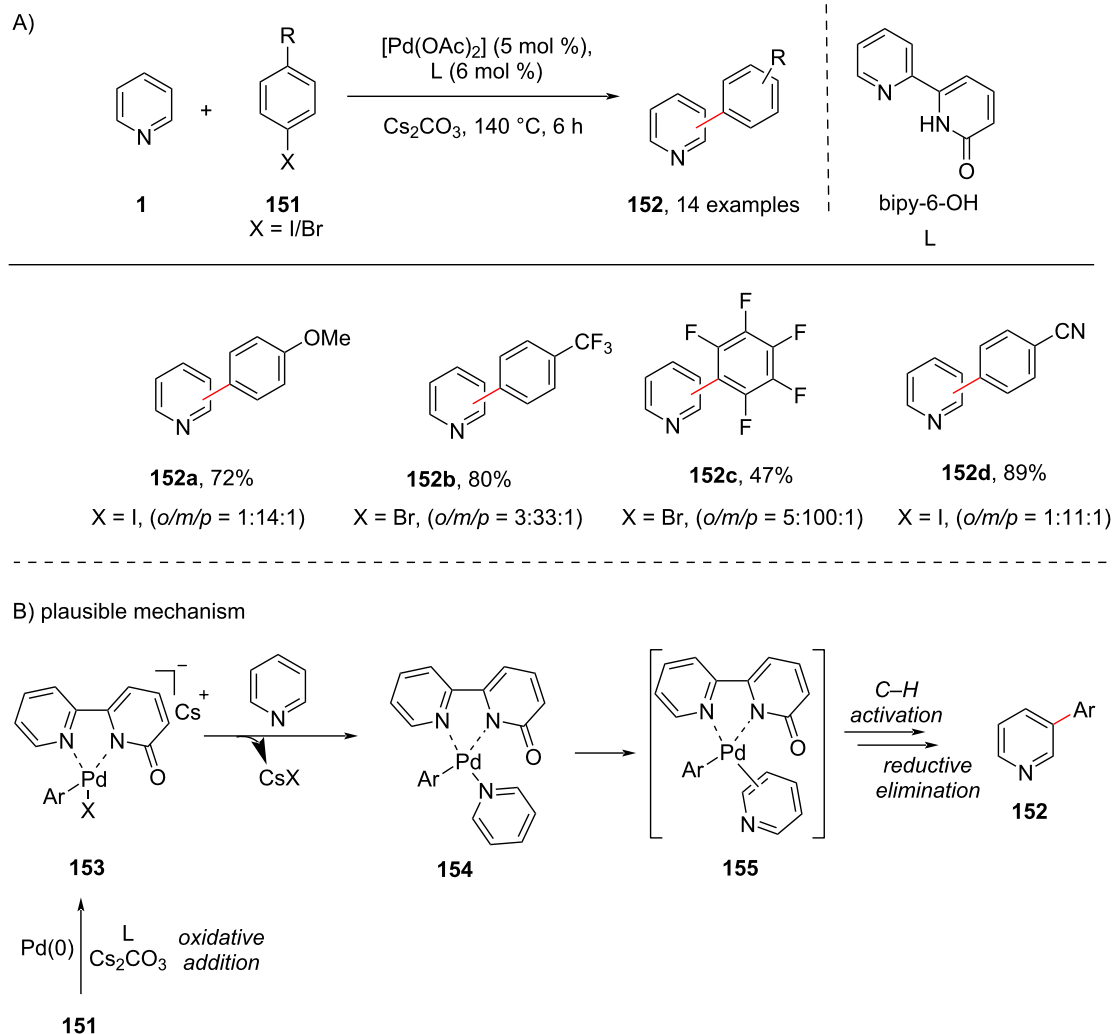
Scheme 28: Iron-catalyzed and imine-directed C–H arylation of pyridines.

dative addition of the aryl halide to the Pd(0) complex in the presence of base ligand to afford **153**. Subsequently, the substitution of the halide by pyridine **1** provides the intermediate **154** which undergoes C–H activation followed by reductive elimination to furnish the C3-arylated product **152**.

## Heteroarylation

### C-2 Heteroarylation

Heteroaryl groups are a common core in natural products and pharmaceuticals. In addition, the heterodiaryl systems widely occur in biologically important organic molecules, dyes,



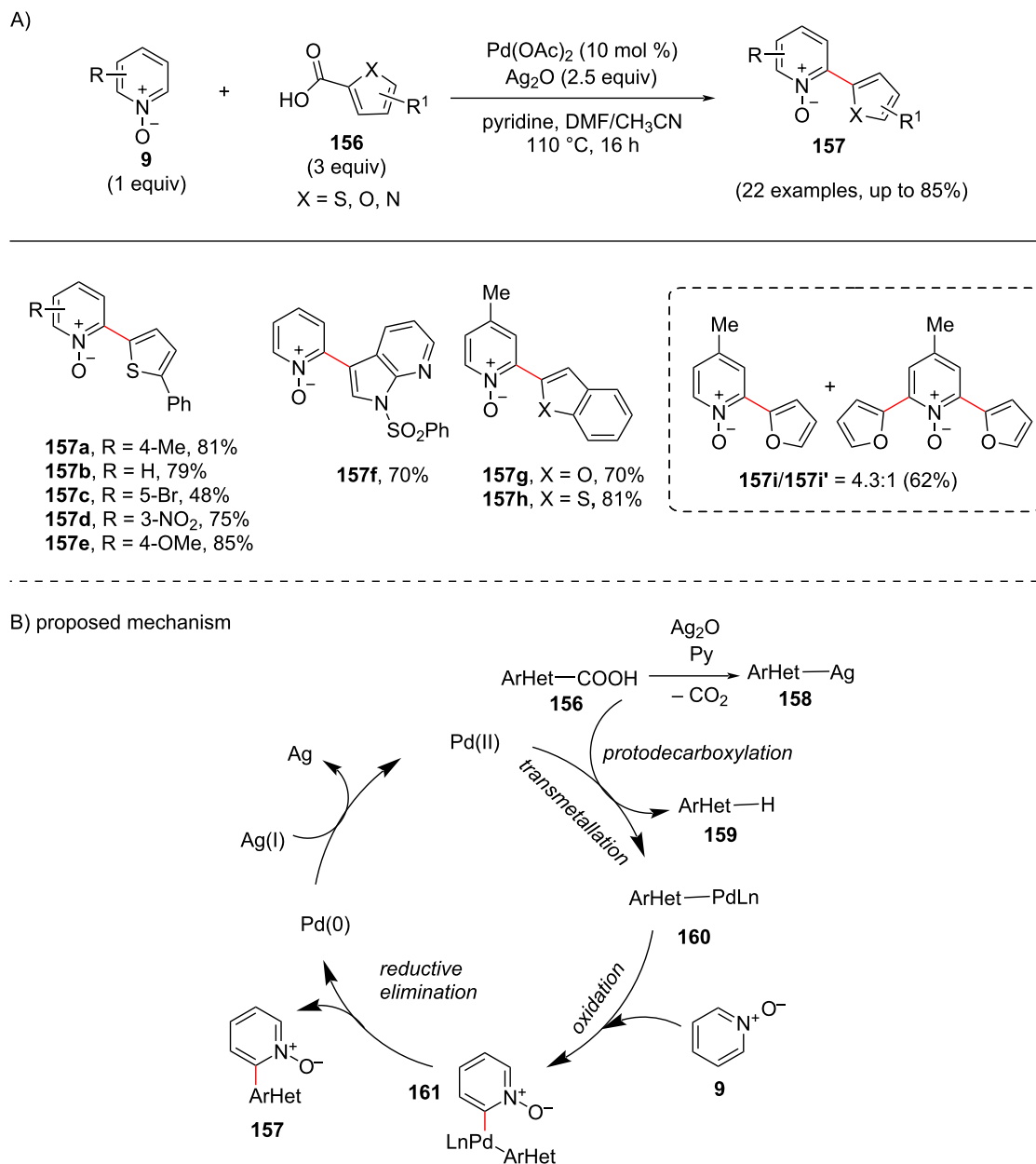
**Scheme 29:** Pd–(bipy-6-OH) cooperative system-mediated direct pyridine C3-arylation.

fragrances, advanced materials, and agrochemicals as well. Thus, the functionalization of the pyridine core with a heterocycle is a desirable transformation in organic synthesis. Manickam and co-workers [100] carried out a palladium-catalyzed decarboxylative *ortho*-(hetero)arylation of pyridine *N*-oxides **9** with heteroarylcarboxylic acids **156** (Scheme 30). The reaction showed good compatibility with various functional groups. The proposed mechanism (Scheme 30b) involves the silver-catalyzed decarboxylation of heteroaryl acid **156** followed by transmetalation providing palladium intermediate **160**. Further, C–H activation of pyridine *N*-oxide **9** provides intermediate **161** which upon reductive elimination furnishes the desired product **157** and regeneration of Pd(0) (Scheme 30b).

Later in 2014, Kuang and co-workers [101] developed a highly efficient and regioselective oxidative cross-coupling of pyri-

dine *N*-oxides **9** with five-membered heterocycles **162** and **163** through a two-fold C–H activation under palladium catalysis. Silver carbonate and 2,6-lutidine were found to be an effective base and ligand, respectively, for providing the desired products **164** and **165** in good yields (Scheme 31).

In 2015, an economic route for copper-catalyzed biaryl coupling of azine(pyridine)-*N*-oxides **9** with oxazoles **166** was reported by Miura and group [102]. Although their work majorly covered quinoline *N*-oxide substrates, they also investigated three pyridine substrates in the reaction leading to the corresponding products in moderate yields (Scheme 32). The *N*-oxide plays a role as an activator and is subsequently eliminated via deoxygenative elimination furnishing the C-2-functionalized pyridines **167**. The reaction mechanism (Scheme 32b) involves the initial C–H-cupration of **166** producing an oxazolyl–copper intermediate **168**. Nucleophilic addition fol-



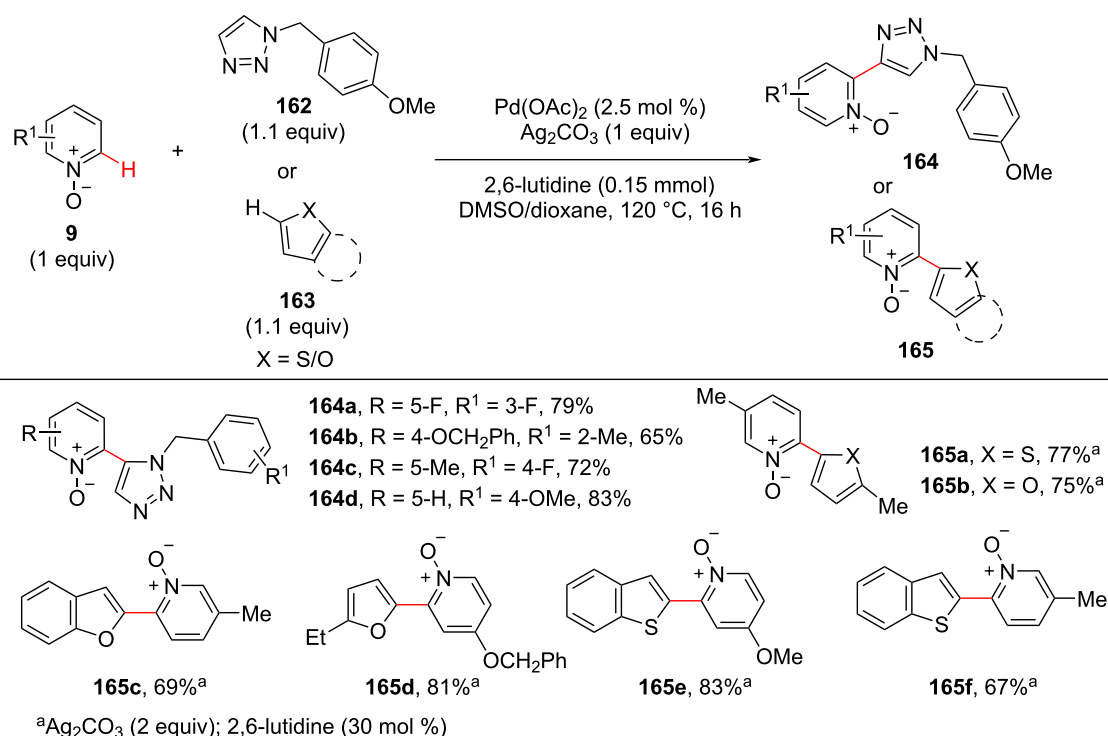
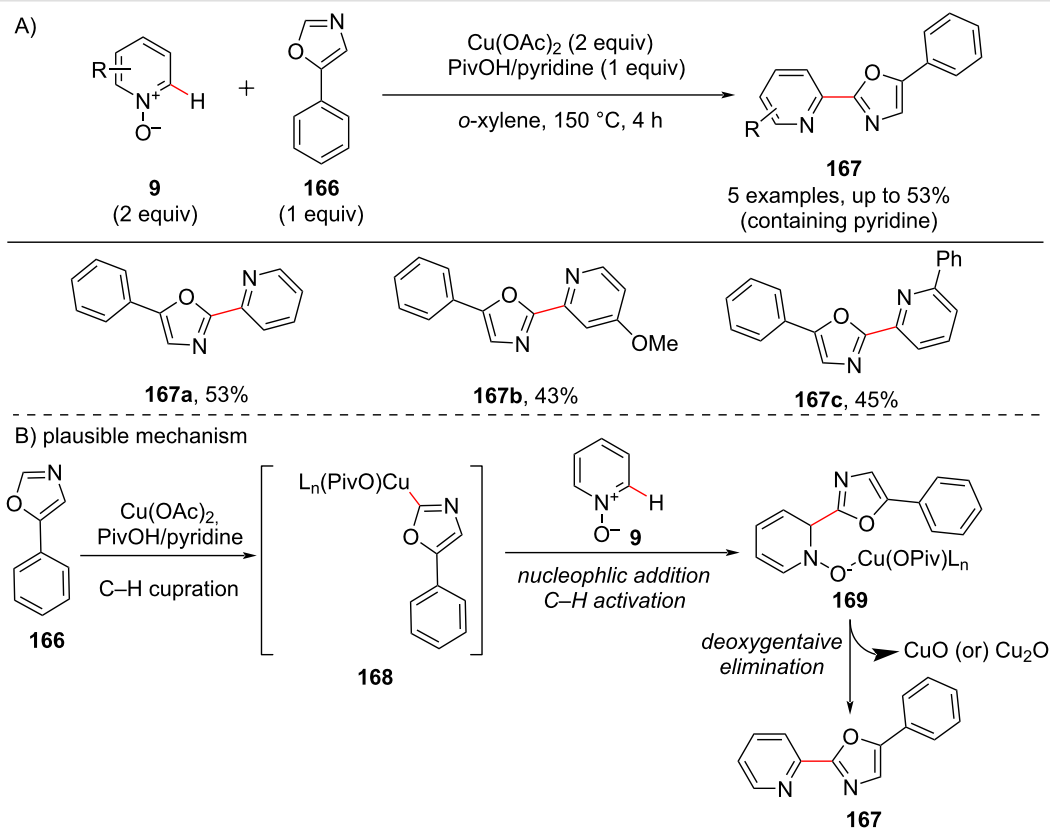
**Scheme 30:** Pd-catalyzed pyridine *N*-oxide C–H arylation with heteroarylcarboxylic acids.

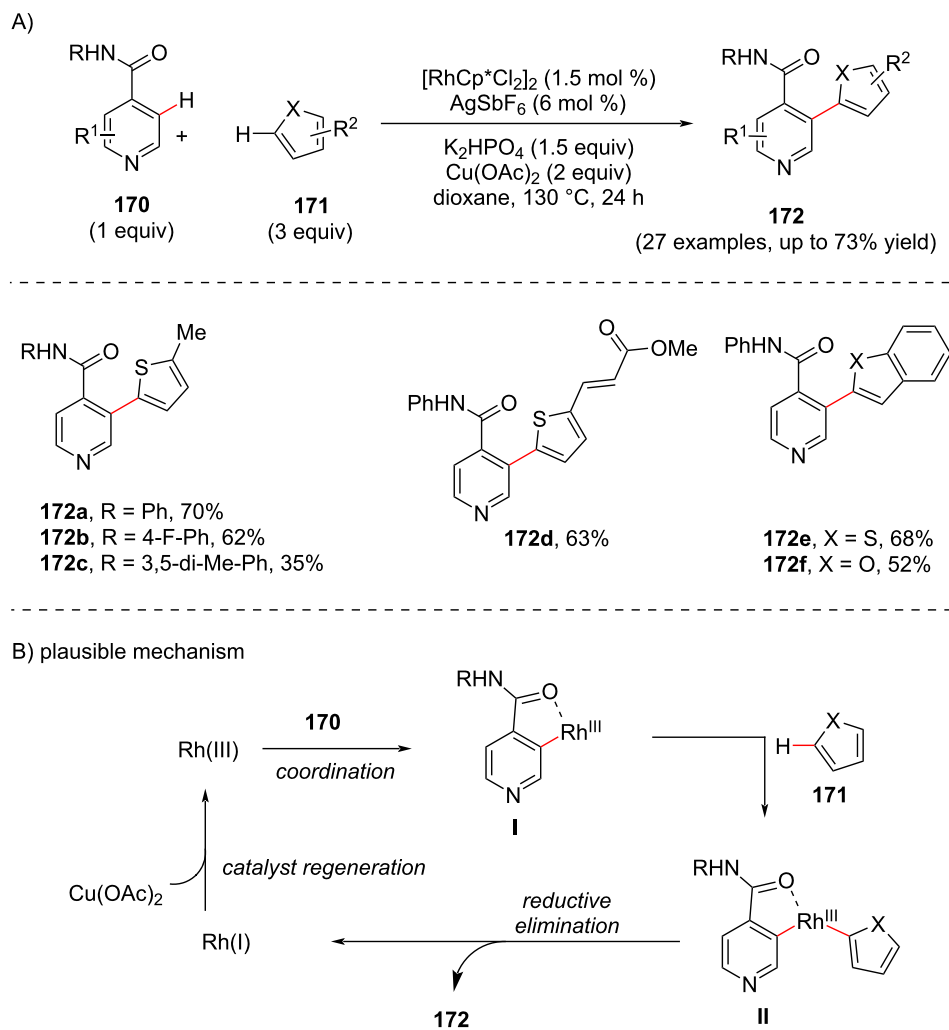
lowed by C–H activation of **9** provides the hydroxy copper species **169**, which on deoxygenative elimination furnishes the desired product **167**.

### C-3 Heteroarylation

In 2013, Su and co-workers [103] developed a catalytic methodology for the distal heteroarylation of pyridines **170** via Rh(III)-catalyzed dehydrogenative cross-coupling showcasing a good substrate scope (Scheme 33). Initially, their investigation involved evaluating the reaction between *N*-phenylisonicotin-

amide **170** and 2-methylthiophene **171** which resulted in the desired product **172**. The plausible mechanism (Scheme 33b) starts with the initial coordination of the pyridine directing group **170** with rhodium providing a five-membered rhodacyclic intermediate **I** which further forms the aryl–rhodium(III) complex **II** by reaction with **171**. Subsequently, this intermediate undergoes reductive elimination from the rhodium(III) center to furnish the desired *ortho*-C–H-arylated product **172** releasing a Rh(I) species. The Rh(III) species is regenerated in the presence of the copper salt.

Scheme 31: Pd-catalyzed C–H cross-coupling of pyridine *N*-oxides with five-membered heterocycles.Scheme 32: Cu-catalyzed dehydrative biaryl coupling of azine(pyridine) *N*-oxides and oxazoles.



**Scheme 33:** Rh(III)-catalyzed cross dehydrogenative C3-heteroarylation of pyridines.

In another case of C3-(hetero)arylation, Yu and group [104] using palladium for C–H activation of pyridine with phenanthroline as a ligand developed a method in 2016 (Scheme 34). The authors achieved both arylation and heteroarylation at the C-3-position in pyridine and showcased the formation of bipyridines **174**. The mechanism is depicted in Scheme 34b, where the complex **A** undergoes C3–H activation to provide intermediate **176** which similarly undergoes one more step of C–H activation to provide the bi(hetero)arene–Pd(II) species **177** which undergoes reductive elimination furnishing the desired products **174/175**.

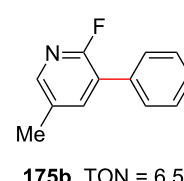
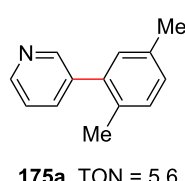
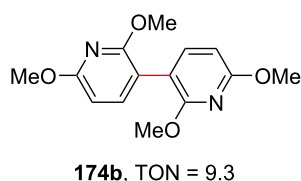
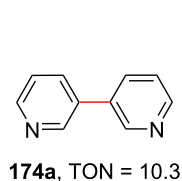
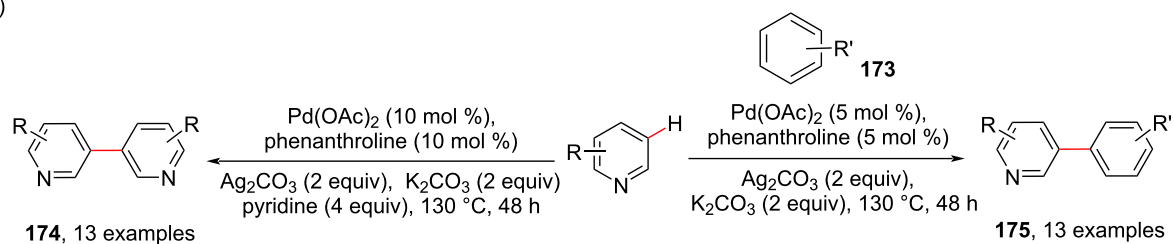
### C–H Annulation of pyridine to fused heterocycles

Annulation reactions in organic synthesis have achieved great attention toward the construction of various carbocycles and

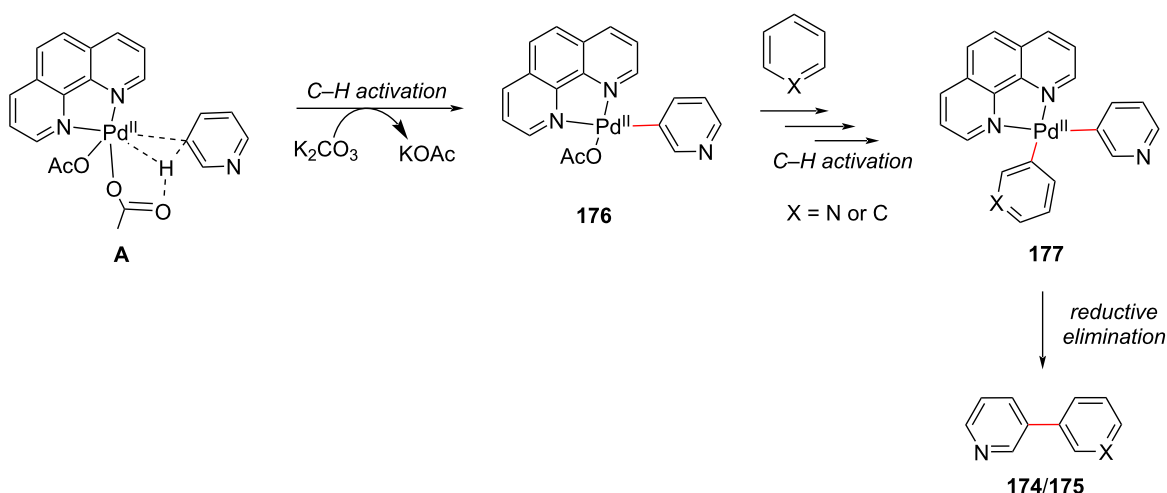
heterocycles. These annulations can be either intermolecular or intramolecular and various substrates have been studied resulting in diverse products. Pyridine has been also reported for the construction of pyridine-fused heterocycles via C(sp<sup>2</sup>)–H functionalization and further annulation. In this aspect, considering the use of pyridines for the formation of quinolines and isoquinolines, an oxidant-dependent rhodium-catalyzed C–H annulation of pyridines with alkynes was reported by Li and co-workers [105] in 2011 for the direct synthesis of quinolines **180** and isoquinolines **181** involving a two-fold C–H activation of pyridine at the C2 and C3 position (Scheme 35a). Further, during optimization when silver additives like Ag<sub>2</sub>CO<sub>3</sub>, Ag<sub>2</sub>O, and AgOAc were used the reaction resulted in the formation of isoquinoline derivative **181**. In addition, the reaction showed high regioselectivity in the presence of unsymmetrical alkynes **179**. Different directing groups **178** were employed resulting in



A)



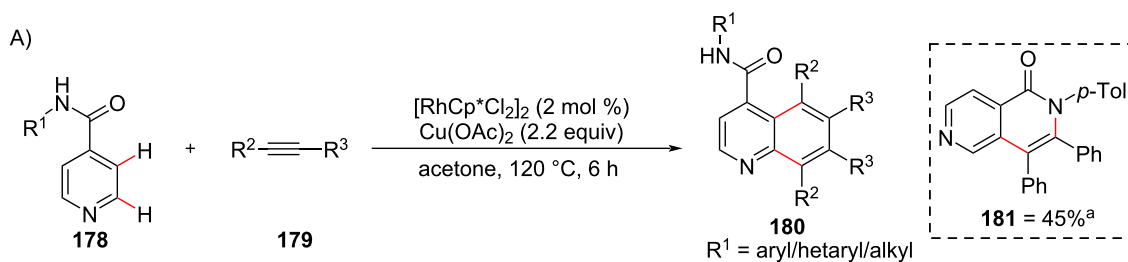
B) plausible mechanism

**Scheme 34:** Pd-catalyzed C3-selective arylation of pyridines.

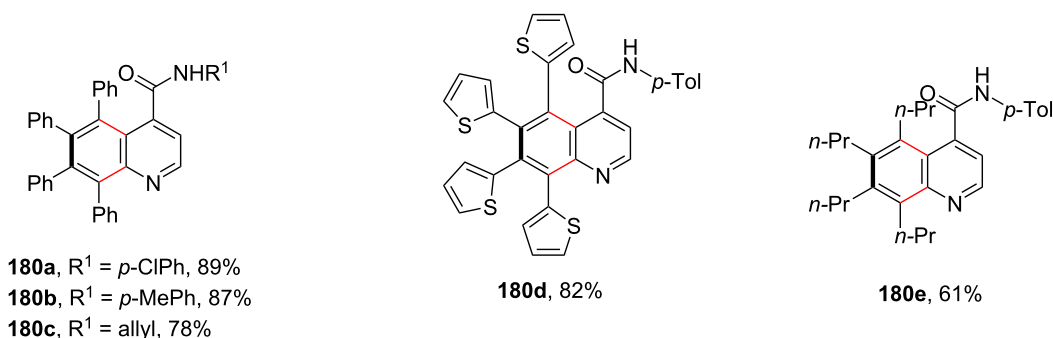
diversified products **180**. The proposed mechanism (Scheme 35b) involves coordination of rhodium with isonicotinamide **178** and subsequent *ortho*-C–H activation generating the five-membered rhodacycle **183**. Next, first alkyne **179** insertion results in the five-membered rhodacycle **184** which is followed by a second regioselective insertion of alkyne **179** into the Rh–C bond of **184** providing the seven-membered cyclic intermediate **185**. Further reductive elimination furnishes the quinoline product **180** and a Rh(I) species, with the latter being oxidized by Cu(II) to complete the catalytic cycle.

Next, considering the role of N-heterocyclic carbene (NHC) ligands acting as directing group as well as functionalizing unit

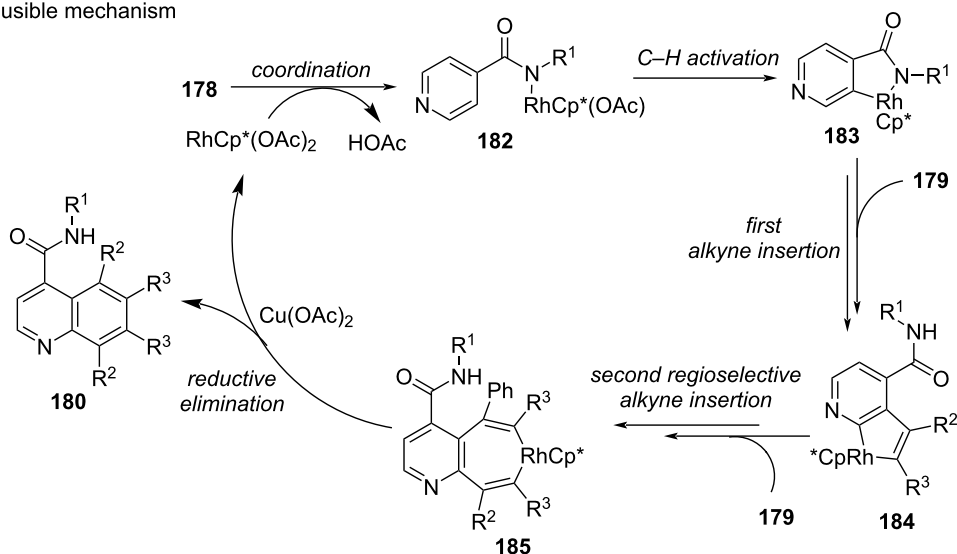
in arene C–H functionalization reactions with alkynes, Choudhury and group [106] in 2015 developed a protocol for the intermolecular C–H annulation of NHC-substituted pyridines with a variety of internal alkynes **187** under rhodium catalysis for the synthesis of annulated and highly decorated pyridines **188** (Scheme 36). The authors used the N-heterocyclic carbene ligand as directing group to prepare imidazo[1,2-*a*][1,6]naphthyridine motifs **188** as desired products. Based on the experimental results and annulation chemistry a catalytic mechanism has been proposed (Scheme 36b) that involves the C3 hydrogen of pyridine undergoing a cyclorhodation with the catalyst in the presence of NaOAc, directed by in-built NHC ligand coordination to provide intermediate **189**. The further coordination of



$a = [\text{RhCp}^*\text{Cl}_2]_2$  (2 mol %),  $\text{Ag}_2\text{CO}_3$  (1.1 equiv), acetone, 120 °C, 6 h (24 examples, up to 90%)



B) plausible mechanism

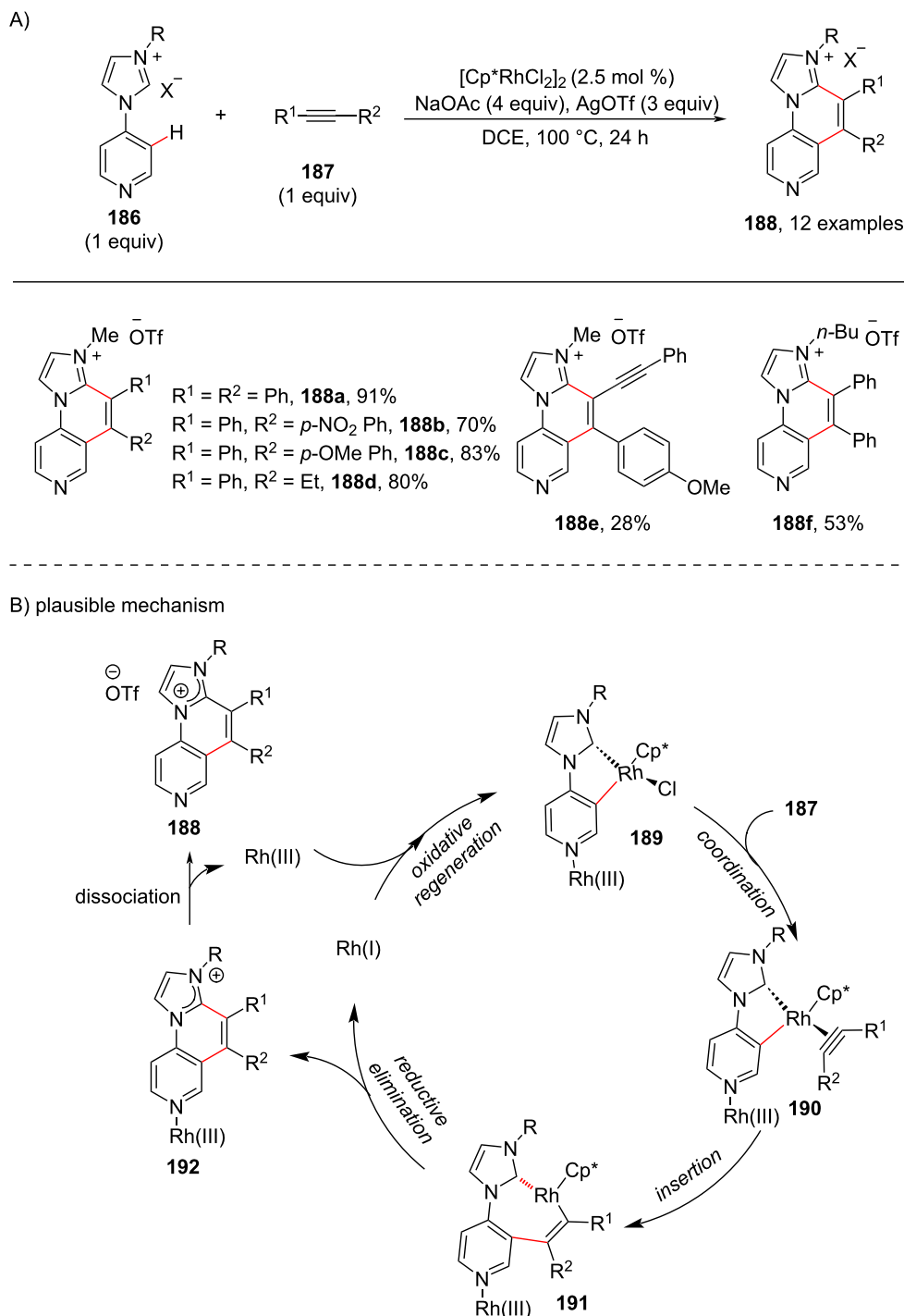


**Scheme 35:** Rhodium-catalyzed oxidative C–H annulation of pyridines to quinolines.

**189** with the alkyne **187** results in intermediate **190** and subsequent insertion provides rhodacycle intermediate **191** which undergoes reductive elimination to furnish the product **188** via dissociation of intermediate **192** along with oxidative regeneration of **189** (Scheme 36b).

In 2019, using NHC ligands, a protocol for the regio- and enantioselective C–H cyclization of pyridines was reported by Shi

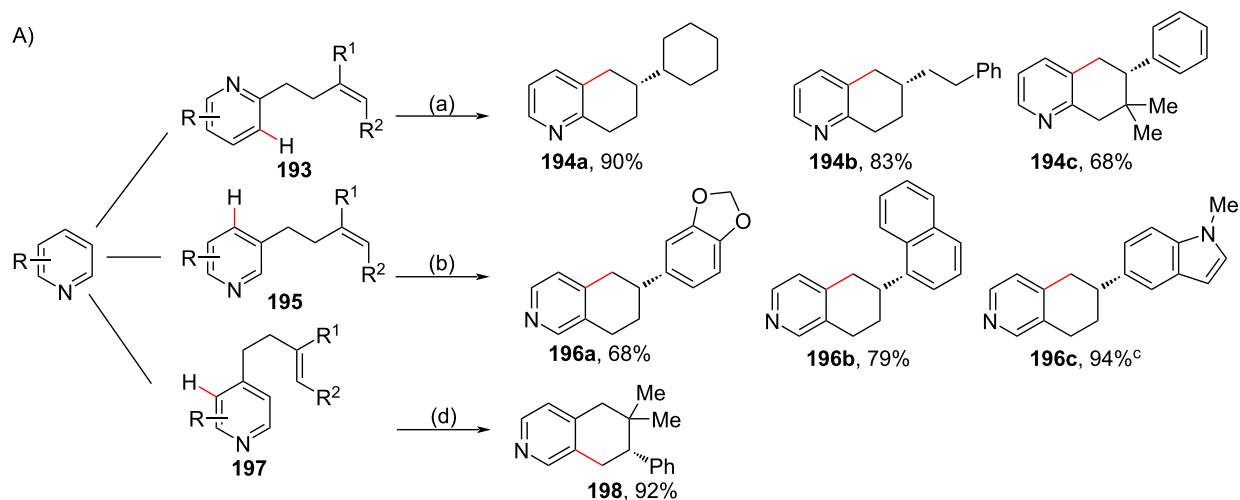
and co-workers [107] toward the direct asymmetric pyridine C–H alkylation (Scheme 37). The authors found that alkene-tethered C2 pyridine **193**, C3 pyridine **195** and C4 pyridine **197** can undergo *endo*-cyclization reactions in the presence of  $\text{Ni}(\text{cod})_2$ , a chiral NHC ligand, and MAD as Lewis acid to afford optically active 5,6,7,8-tetrahydroquinolines **194** and 5,6,7,8-tetrahydroisoquinolines **196** and **198**. The *endo*-selective annulation approach was compatible with various tethered



**Scheme 36:** Rhodium-catalyzed and NHC-directed C–H annulation of pyridine.

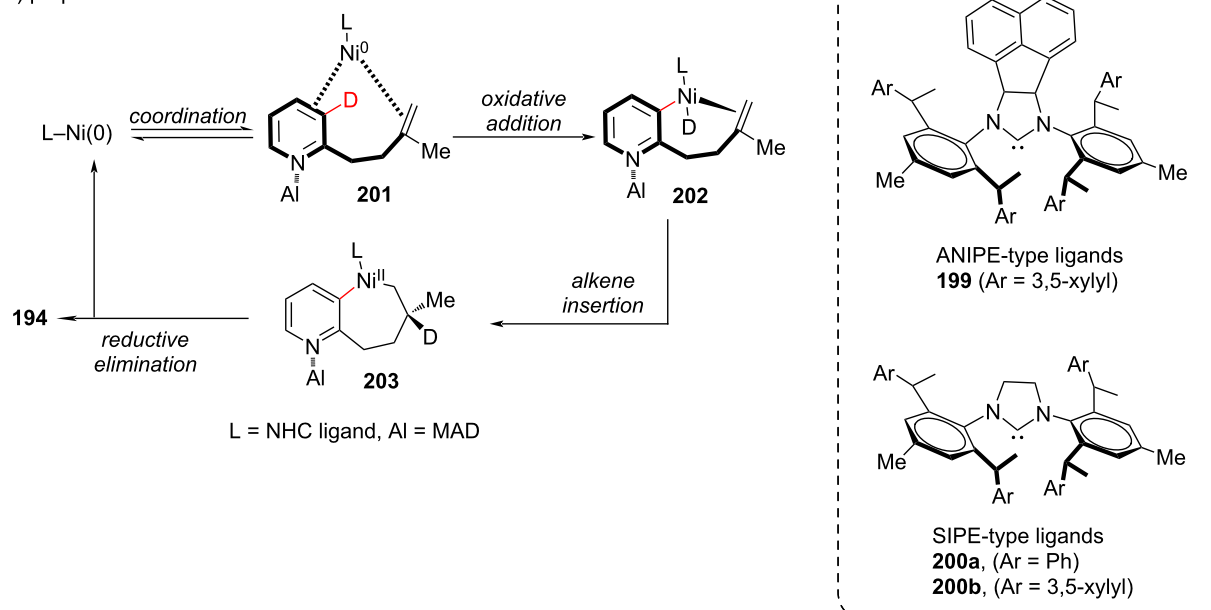
alkenes, such as 1,1-disubstituted alkenes, styrene, diene, trisubstituted alkene and enamines. To get insights into the mechanism the authors conducted additional experiments including deuterium labelling reactions and proposed the mechanism depicted in Scheme 37b. Initially, the sterically bulky additive

MAD coordinates to the pyridine nitrogen, which pushes the tethered alkene close to the nickel center subsequently providing the intermediate **201**. Then, the C–D bond on cleavage via oxidative addition of Ni(0) forms the Ni–D species **202** which after anti-Markovnikov hydronickeleation of the alkene provides



- a) Ni(cod)<sub>2</sub> (5 mol %), **200a**/HCl (5 mol %), NaOt-Bu (10 mol %), MAD (1.2 equiv), *n*-heptane, 80 °C, 24 h  
 b) Ni(cod)<sub>2</sub> (5 mol %), **200a**/HCl (5 mol %), NaOt-Bu (10 mol %), MAD (1.2 equiv), CPME (0.5 M), 80 °C, 24 h  
 c) Ni(cod)<sub>2</sub> (10 mol %), **200b**/HCl (10 mol %), NaOt-Bu (20 mol %), MAD (1.2 equiv), CPME (0.5 M), 120 °C, 48 h  
 d) Ni(cod)<sub>2</sub> (10 mol %), **199**/HCl (10 mol %), NaOt-Bu (20 mol %), MAD (1.2 equiv), CPME (0.5 M), 80 °C, 48 h

B) proposed mechanism



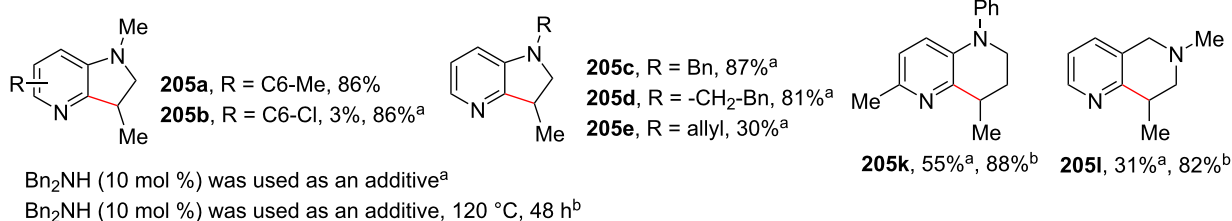
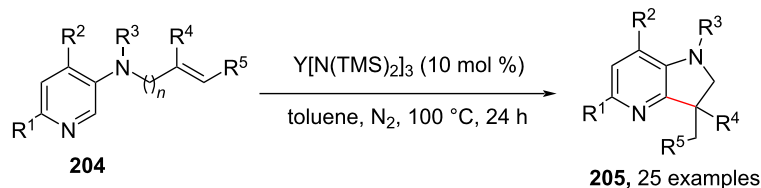
**Scheme 37:** Ni/NHC-catalyzed regio- and enantioselective C–H cyclization of pyridines.

the seven-membered cyclic intermediate **203**. Subsequent reductive elimination furnishes the endo-annulated product **194** (Scheme 37b).

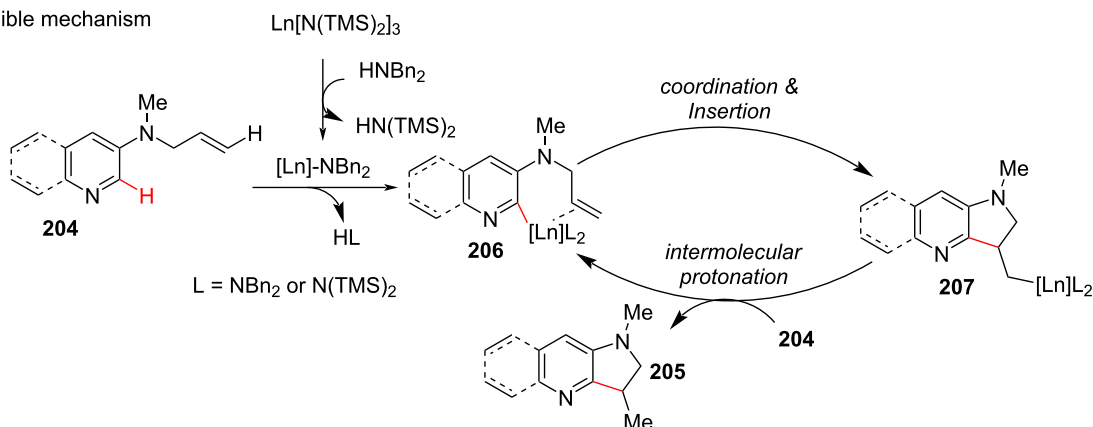
Out of various pyridine-fused heterocyclic hybrids, azaindolines are important scaffolds in natural products and pharmaceuticals serving different biological activities. Hence, looking at the importance of azaindolines in drug discovery a protocol of rare earth metal-catalyzed intramolecular insertion of the pyri-

dine C–H bond into unactivated vinyl C–H bonds has been developed by Chen and co-workers [108] (Scheme 38). Using this protocol azaindolines **205** were accessed in moderate to excellent yields and also naphthyridine derivatives (**205k** and **205l**) were synthesized. In the proposed mechanism, the initial deprotonation of HNBn<sub>2</sub> by Ln[N(TMS)<sub>2</sub>]<sub>3</sub> provided the lanthanide amide. Activation of the vinyl-substituted pyridin-3-amine **204** by the lanthanide amide gives a lanthanide–pyridine complex **206**. Then, coordination and sequential insertion of C=C into

A)



B) plausible mechanism

**Scheme 38:** Rare earth metal-catalyzed intramolecular C–H cyclization of pyridine to azaindolines.

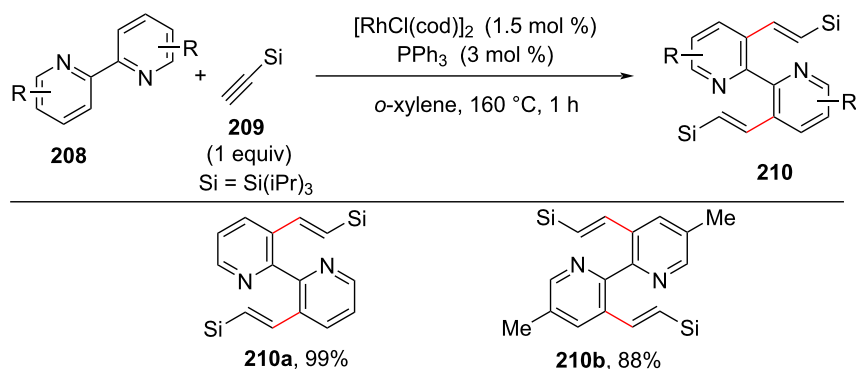
the Ln–pyridine bond of **206** provided intermediate **207**, which undergoes intermolecular protonation with **204** to afford the desired product **205** and regenerating the lanthanide species (Scheme 38b).

### C(sp<sup>2</sup>)–H Functionalization of pyridine rings in bipyridine systems

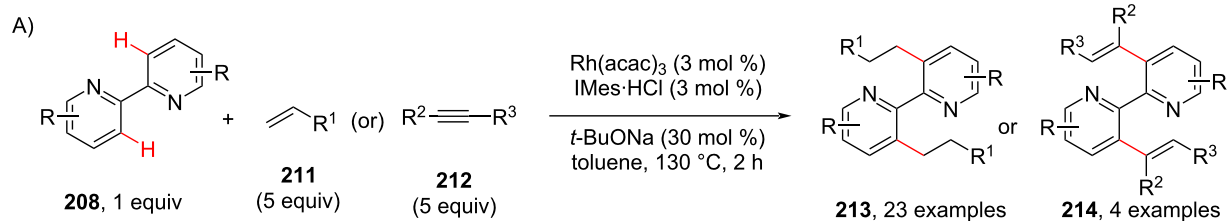
The functionalization and synthesis of bipyridine derivatives is of great interest and importance in synthetic chemistry. These compounds are well-studied for their roles as chelating ligands in transition-metal-catalyzed reactions, coordination chemistry including materials science [109,110]. The challenge associated with the C–H functionalization of bidentate molecules is the finding strategy in the subduing the high activation barrier of rollover cyclometallation pathway. In this section we discuss the C(sp<sup>2</sup>)–H functionalization of the pyridine ring in bipyridine ring systems. In early 2009 Miura and co-workers [111] reported the rhodium-catalyzed regioselective reaction of aryl-*N*-heterocycles and aromatic imines with terminal silylacetylenes **209** to synthesize C–H-alkenylated products **210**. The terminal silylacetylenes were employed as effective substrates for cata-

lytic cross-dimerization reactions. The reaction was performed in the presence of  $[RhCl(cod)]_2$  (3 mol %), taking  $PPh_3$  or  $(4-ClC_3H_4)_3P$  as the ligand at 160 °C, for about 48 h (Scheme 39). This work provides an effective way for preparing C–H-alkenylated bipyridines **210**.

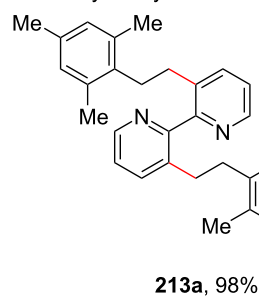
In 2012, a hydroarylation of alkenes **211** and alkynes **212** with 2,2'-bipyridines **208** and 2,2'-biquinolines was reported by Chang and co-workers [112] in the presence of  $Rh(acac)_3$  as catalyst, IMes-HCl (3 mol %) as ligand and *t*-BuONa (30 mol %) in toluene for 2 h (Scheme 40). The authors demonstrated theoretically and mechanistically the important role of the NHC ligand in the resultant catalyst  $Rh(NHC)$  for the hydroarylation of alkenes and alkynes with chelating 2,2'-bipyridine and 2,2'-biquinoline molecules. The experimental studies revealed that the *trans*-effect of the NHC ligand in the complex assisting in the reduced energy barrier of a rollover cyclometallation pathway and results in selective and efficient hydroarylation of the alkenes and alkynes. This was the first report for the role of a “rollover” cyclometallation pathway catalytically leading to double C–H bond functionalization of chelating mol-



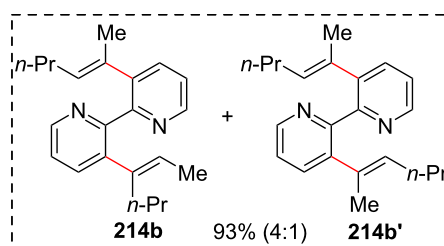
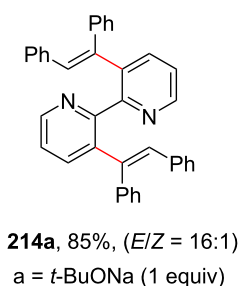
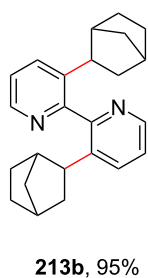
**Scheme 39:** Rh-catalyzed alkenylation of bipyridine with terminal silylacetylenes.



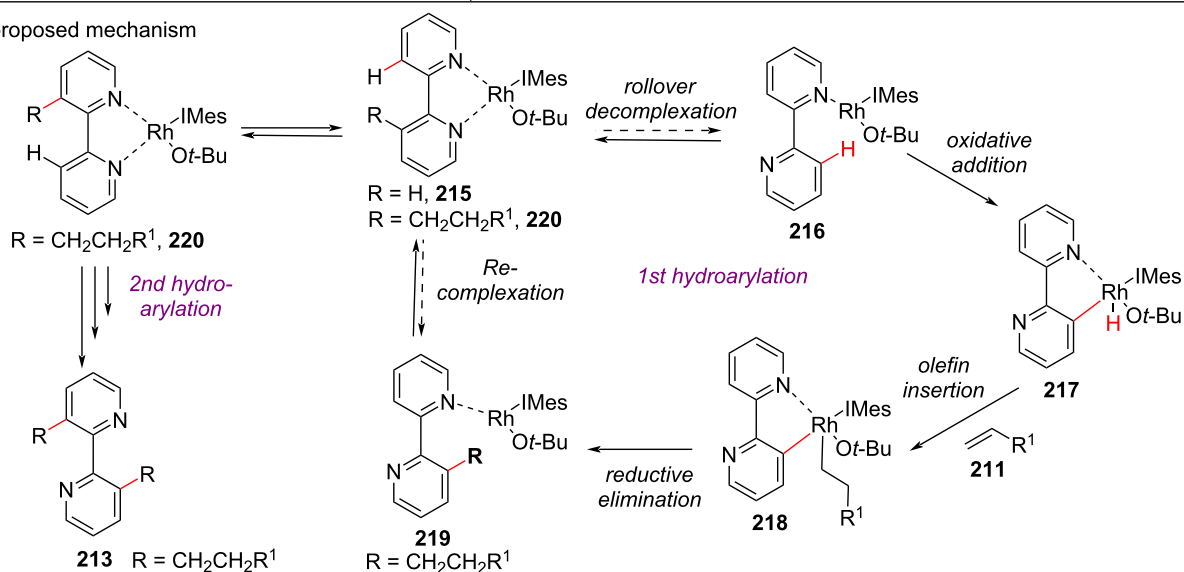
alkene hydroarylation



alkyne hydroarylation<sup>a</sup>



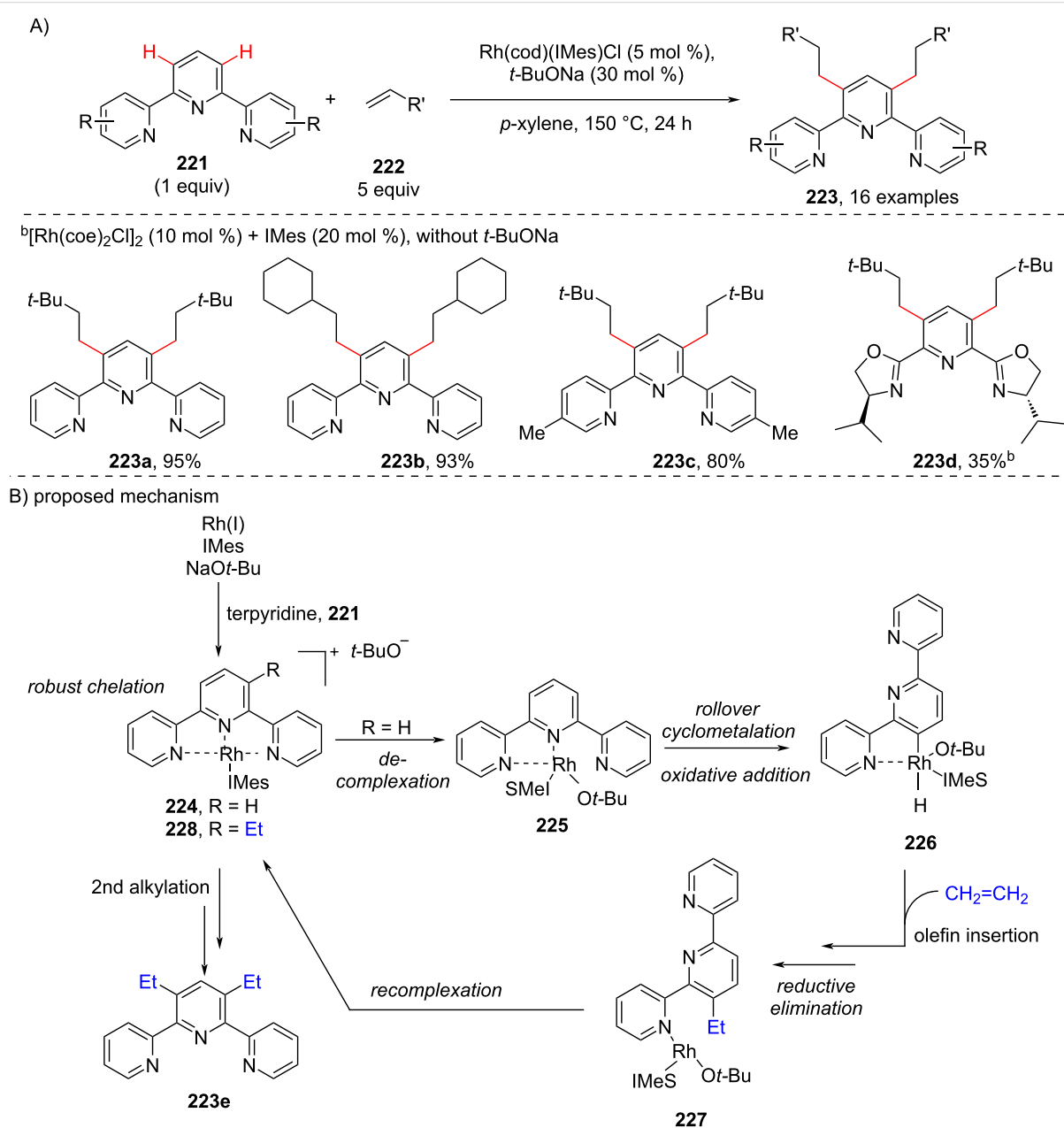
B) proposed mechanism



**Scheme 40:** Rollover cyclometallation in Rh-catalyzed pyridine C–H functionalization.

ecules under action of a Rh(NHC) system. Based on the computational studies and experimental data, the proposed mechanism (Scheme 40b) describes that the Rh(I) complex ligated to *tert*-butoxide and NHC (IMes·HCl) **215** is a catalytically active species. The Rh–hydride species **217** is formed after oxidative addition via C–H bond cleavage followed by olefin insertion to form intermediate **218**, which on subsequent reductive elimination results in the formation of monoalkylated bipyridine **219**. This intermediate reenters into another cycle of hydroarylation by starting as bidentate complex **220** and finally furnishing the desired bishydroarylated product **213** (Scheme 40b).

Next, a protocol for the selective and catalytic C–H functionalization of *N,N,N*-tridentate chelating compounds using a rollover cyclometallation strategy was reported by the same group in 2016 [113]. The reaction involves the Rh-catalyzed alkylation of 2,2':6',2''-terpyridine **221** with 3,3-dimethyl-1-butene coupled in the presence of a catalytic amount of *t*-BuONa providing the mono- and dialkylated products in low combined yields. The alkylation of terpyridines with aliphatic olefins **222** afforded only anti-Markonikov linear products **223** (Scheme 41). The authors also expanded their study to tridentate heteroarenes. Delightfully, they observed the dialkylated



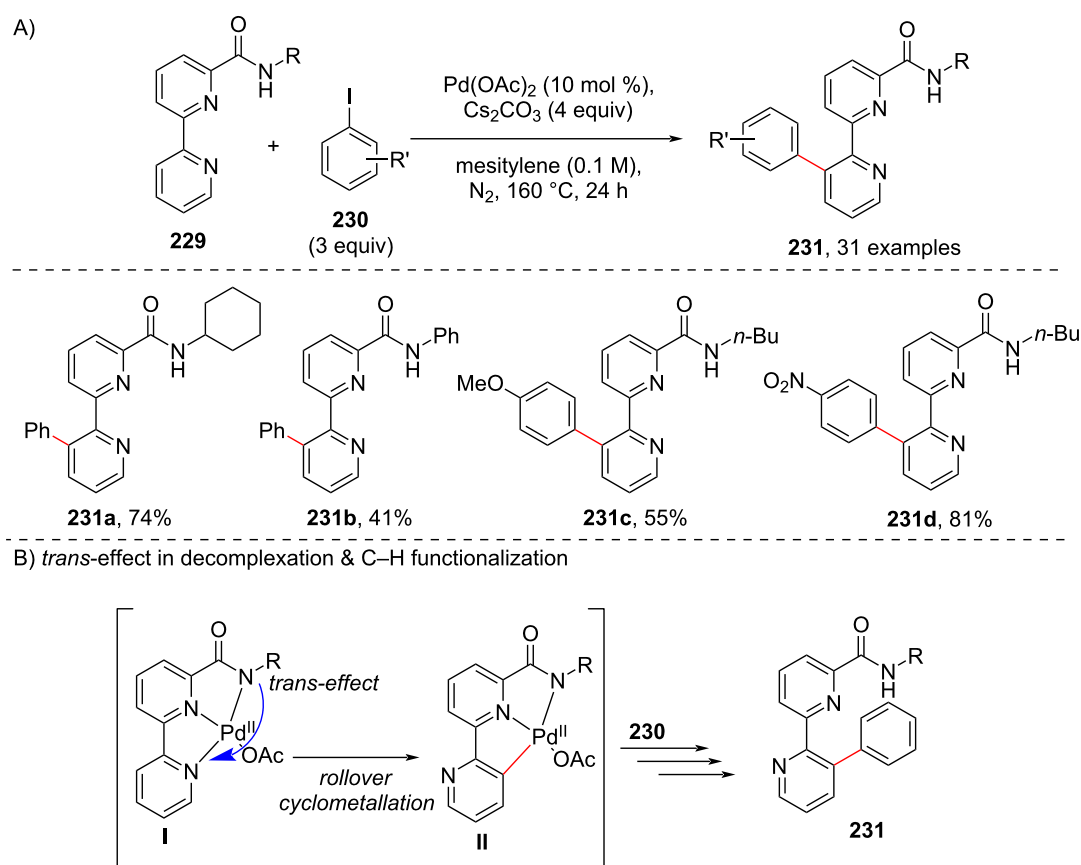
**Scheme 41:** Rollover pathway in Rh-catalyzed C–H functionalization of *N,N,N*-tridentate chelating compounds.

products **223** in good yields. The plausible reaction mechanism (Scheme 41b) was explained by the formation of a cationic Rh–terpyridine complex **224** generated from terpyridine **221** and a Rh(NHC) species formed from the Rh(I) precursor and the NHC in the presence of an external base and successive decomplexation of **224** provides complex **225**. The latter undergoes an initial key rollover cyclometallation followed by oxidative addition leading to the metal–hydride intermediate **226** which on olefin insertion and subsequent reductive elimination resulted in the monoalkylated rhoda complex **227**. Complex **227** then undergoes recomplexation to form **228** and enters the subsequent catalytic cycle furnishing the bisalkylated product **223**.

In 2018, Cheng and co-workers [114] reported a straight forward approach to 3'-aryl-2,2'-bipyridine-6-carboxamide derivatives **231** with exclusive selectivity starting from 2,2'-bipyridine-6-carboxamides **229** under Pd catalysis (Scheme 42). The arylation reaction of *N*-butyl-2,2'-bipyridine-6-carboxamide with iodobenzene **230** in the presence of Pd(OAc)<sub>2</sub> as catalyst, Cs<sub>2</sub>CO<sub>3</sub> as a base in DMSO at 160 °C furnished the desired products **231** (Scheme 42). It was found that non-polar

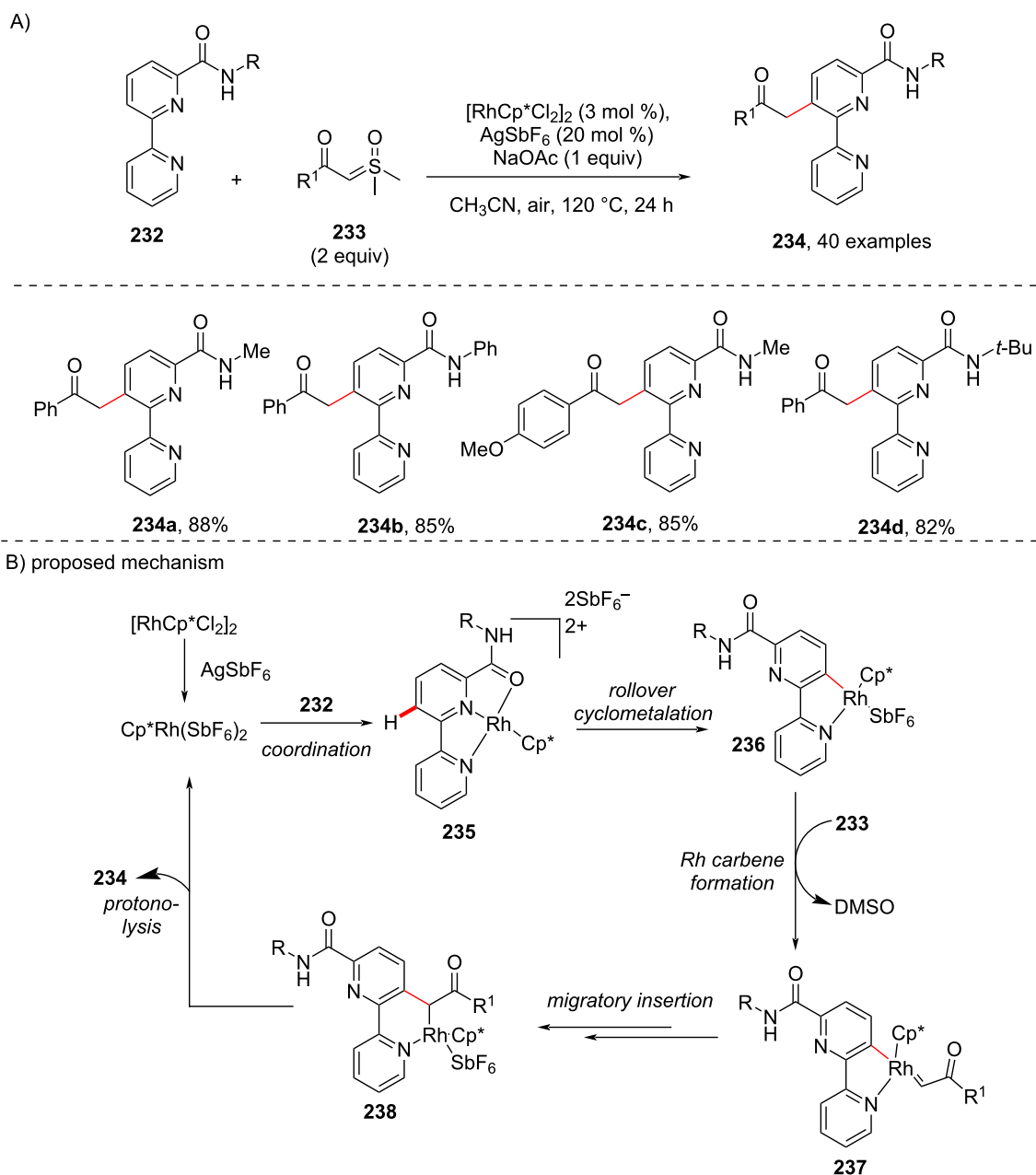
solvents resulted in good yields of the products **231**. It is reported that 2,2'-bipyridine-6-carboxamides **229** can bind to the transition metal, such as Pd(II), to form stable *N,N,N*-chelates **I** (Scheme 42b). The amide moiety of the *N,N,N*-chelates **I** exerts a strong *trans*-effect which weakens the Pd(II)–pyridyl bond *trans* to the amide anion, thus, allowing the decomplexation to afford complex **II** which is key intermediate for furnishing the desired C–H functionalization product (Scheme 42b).

In 2019, Cheng and co-workers reported an approach for the C3-selective acylmethylation of [2,2'']-bipyridine]-6-carboxamides **232** with sulfoxonium ylides **233** in the presence of a Rh(III) catalyst (Scheme 43) [115]. Sterically hindered amide directing groups were also well tolerated under the optimal conditions. A H/D exchange reaction exclusively at the C3-position suggested C–H-bond cleavage is reversible. The catalytic cycle involves the coordination of the carboxamide **232** with the Rh(III) species affording Rh(III) complex **235**, which on rollover cyclometallation gives the complex **236**. The addition of sulfoxonium ylide **233** to the intermediate complex **236** generates the Rh–carbene complex **237** with the release of DMSO and further migratory insertion of complex **237** and subsequent



**Scheme 42:** Pd-catalyzed rollover pathway in bipyridine-6-carboxamides C–H arylation.



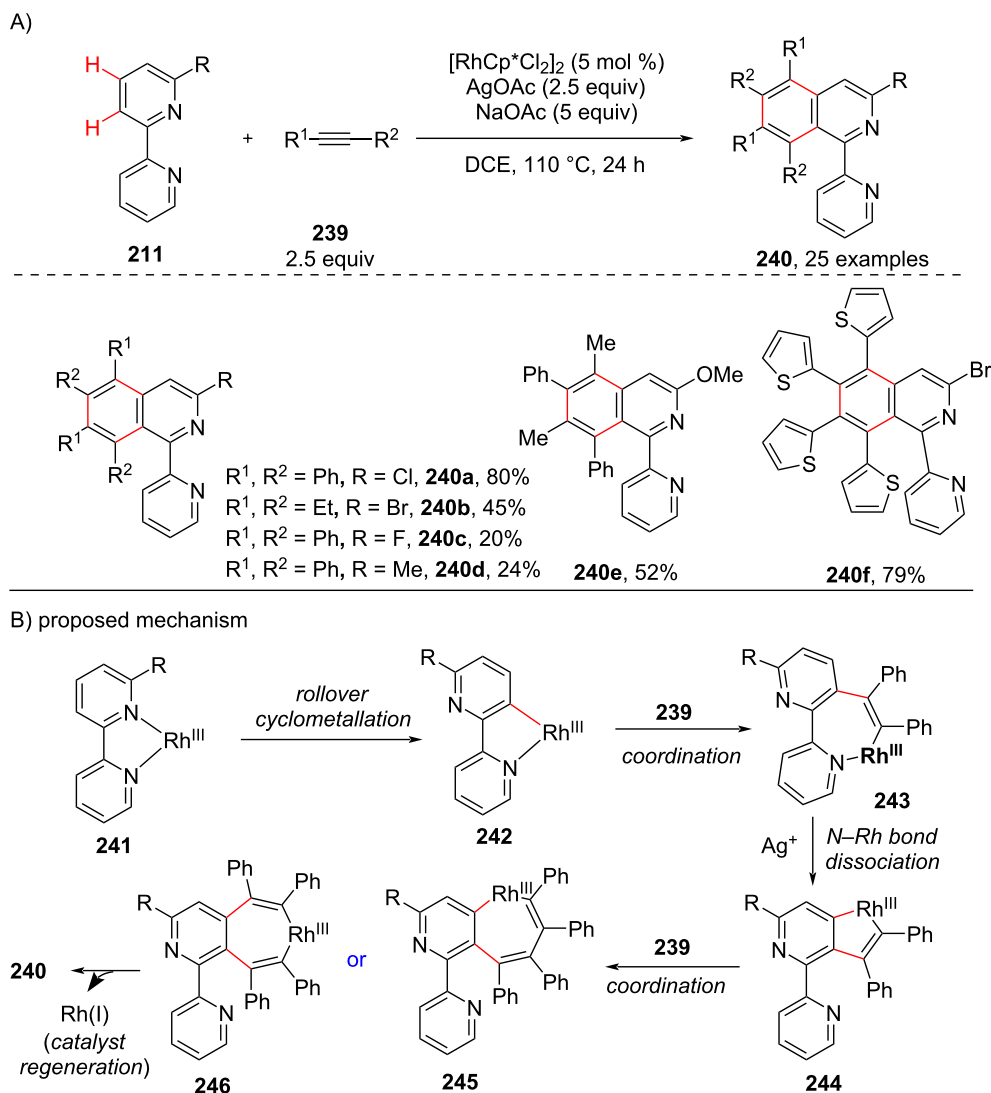


**Scheme 43:** Rh-catalyzed C3-acylmethylation of bipyrindine-6-carboxamides with sulfoxonium ylides.

protonolysis furnishes the acylmethylated product **234** (Scheme 43b).

Recently, in 2020, Zhu and co-workers [116], developed a novel annulation reaction of bipyrindine systems **211** with alkynes **239** via a Rh(III)-catalyzed dual C–H functionalization. The authors have initiated their studies with 6-bromo-2,2'-bipyrindine as their model substrate and with diphenylacetylene as coupling partner. The optimized conditions included [RhCp<sup>\*</sup>Cl<sub>2</sub>]<sub>2</sub> (5 mol %), AgOAc (2.5 equiv), NaOAc (5 equiv)

in DCE, at 110 °C for 24 h to obtain the annulated product **240** (Scheme 44). The proposed mechanism (Scheme 44b) involves the formation of Rh(III) complex **241** by coordination of the bipyrindine with rhodium and complex **241** via a rollover cyclometallation process gives the intermediate **242**. It was suggested that the substitution at the 6 position of the bipyrindine ring system facilitates the rollover cyclometallation process by weakening the Rh–N bond. Next, intermediate **242** coordinates with alkyne **239** to give the seven-membered rhodacycle **243**. The excess Ag<sup>+</sup> help in the dissociation of the N–Rh bond in



**Scheme 44:** Rh-catalyzed C–H functionalization of bipyridines with alkynes.

complex **243** and give the five-membered rhodacyclic intermediate **244** which again coordinates with the alkyne **239** furnishing another seven-membered rhodacyclic intermediate **245** or **246**. Finally, reductive elimination delivers the desired product **240**.

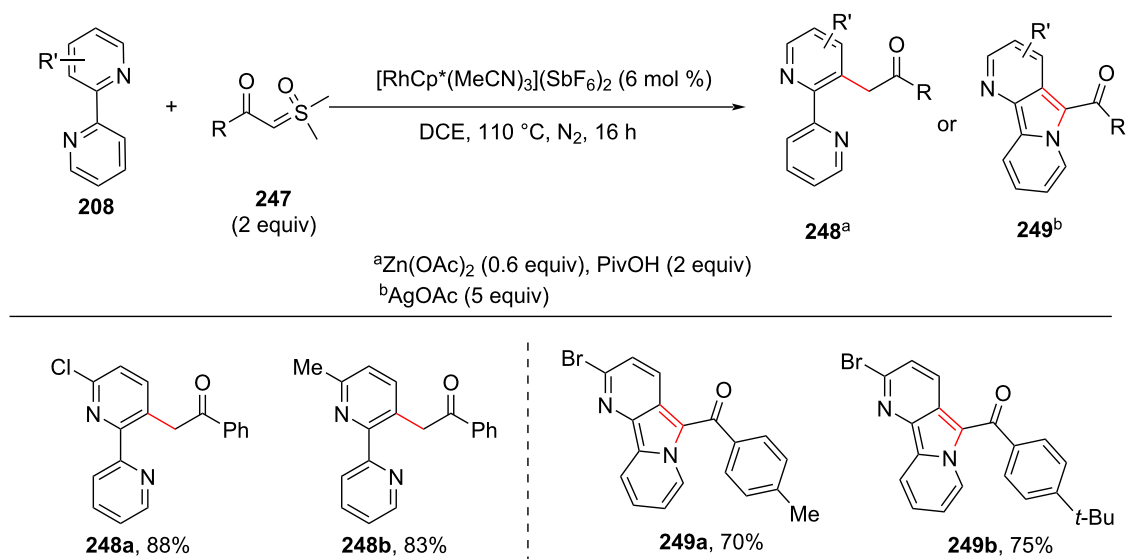
In the subsequent year, the same group reported a method for the rhodium-catalyzed acylmethylation of bipyridines [117]. The group has demonstrated a switchable reaction, wherein changing the additive can deliver the acylmethylated product **248** or the annulation product pyrido[2,3-*a*]indolizine **249** (Scheme 45). Under action of the Rh(III) catalyst, zinc acetate and PivOH as additives, the acylmethylation of bipyridines takes place at the C-2 position to furnish acylmethylated products **248** and the reaction was found suitable for various sub-

strates. On the other hand, the usage of silver acetate as an additive provided the annulated (intramolecular cyclization of bipyridine) product **249**.

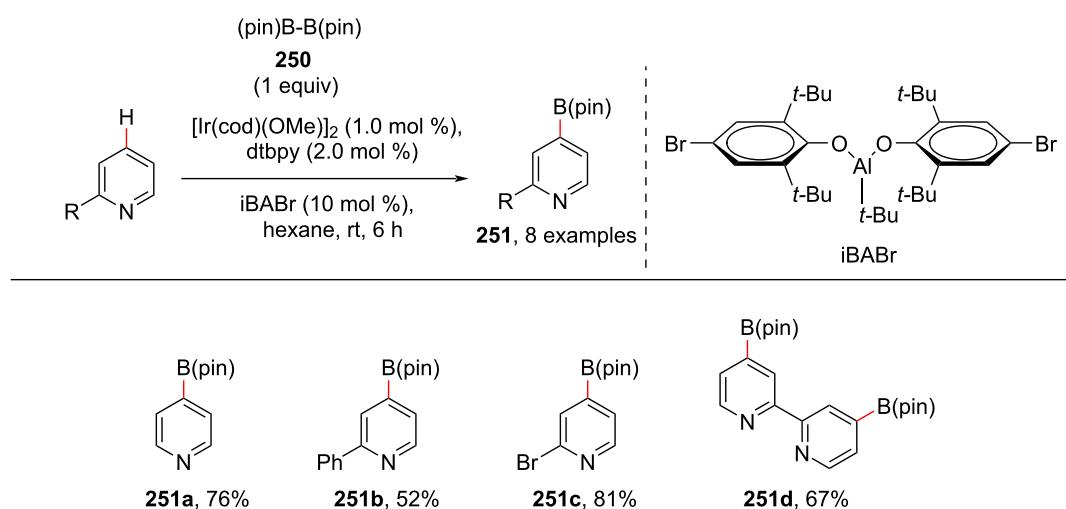
## Miscellaneous reactions

### C–H Borylation

Due to the broad utilities of arylboronic esters in organic synthesis, various protocols have been reported till date for their incorporation into an organic molecule. In 2017, Nakao and group reported a method for the iridium-catalyzed *para*-C–H borylation of pyridines using bis(pinacolato)diboron (**250**) for the synthesis of borylated pyridines **251**, which are important intermediates for various derivatization reactions (Scheme 46) [118]. In common, site-selective borylations have been in less focus, due to the lack of suitable strategies, however, this group achieved



**Scheme 45:** Rh-catalyzed C–H acylmethylation and annulation of bipyridine with sulfoxonium ylides.



**Scheme 46:** Iridium-catalyzed C4-borylation of pyridines.

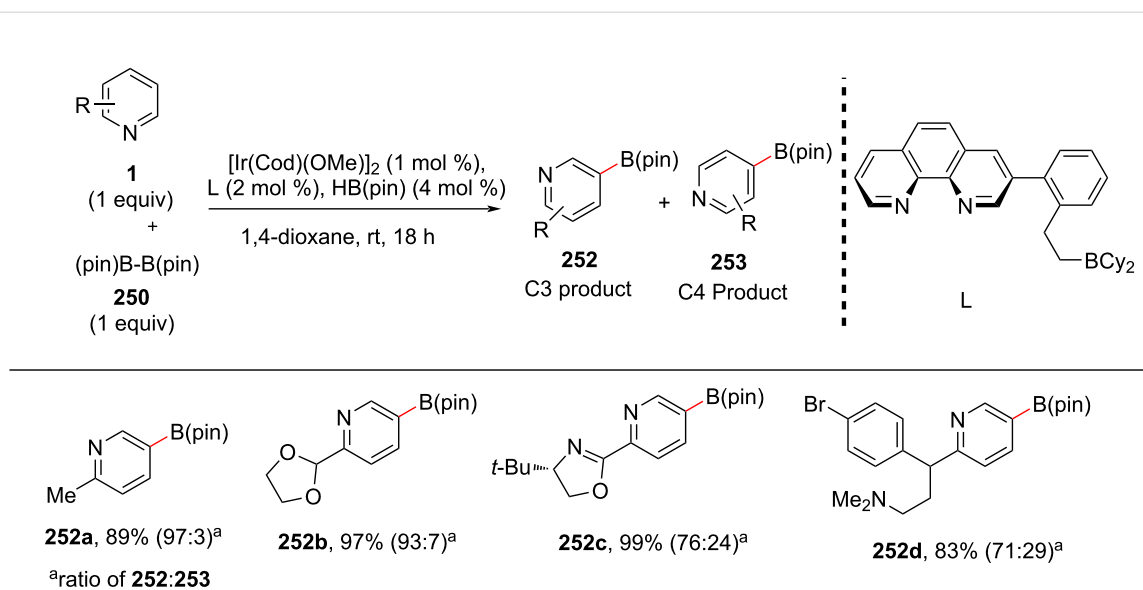
the *para*-selective borylation of pyridines using a cooperative catalyst strategy. The authors used [Ir(cod)(OMe)<sub>2</sub>]<sub>2</sub> as a metal catalyst, along with a sterically bulky Lewis acid such as methylaluminum bis(2,6-di-*tert*-butyl-4-methylphenoxide) as a cooperative catalyst.

Later, in 2019, the same group reported a protocol for the selective C5(C3)-borylation of pyridines under iridium–Lewis acid bifunctional catalysis (Scheme 47) [119]. With the optimized conditions in hands, the authors screened for the substrate scope of substituted pyridines. Also, they employed the reported

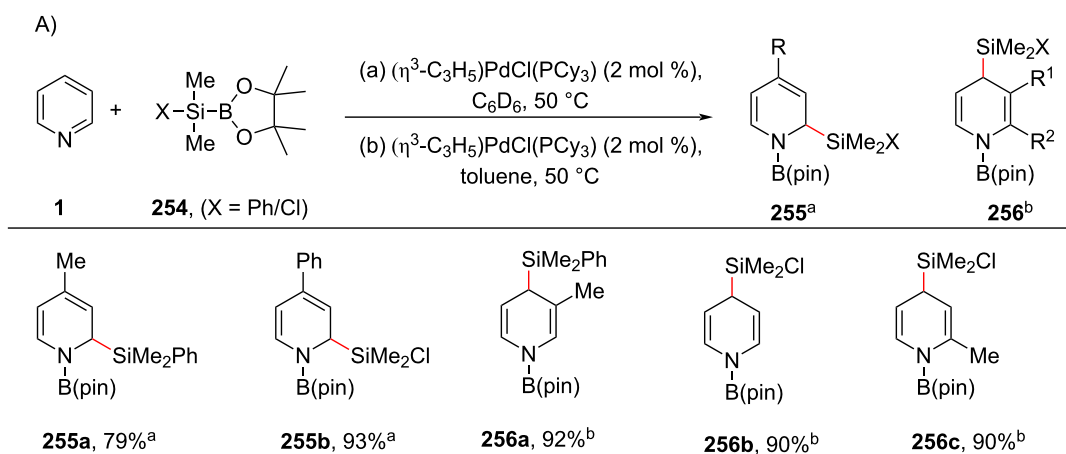
protocol for the late-stage functionalization of brompheniramine (**252d**), an antihistaminic drug.

### C–H Silaboration

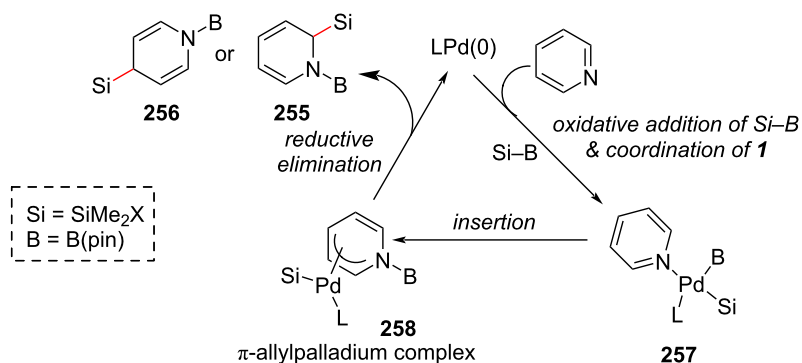
In 2011, a protocol for the synthesis of highly functionalized dihydropyridines via palladium-catalyzed silaboration providing silylated dihydropyridines **255** and **256** (Scheme 48) was developed by Sugimoto and co-workers [120]. This reaction involved a dearomatizing conversion of pyridines to dihydropyridines under mild conditions with the introduction of a silyl group on a carbon atom of pyridine ring. Various pyridines



Scheme 47: C3-Borylation of pyridines.



B) proposed mechanism



Scheme 48: Pd-catalyzed regioselective synthesis of silylated dihydropyridines.

were subjected to this silaboration using the Pd/PCy<sub>3</sub> catalytic system providing the corresponding products in good yields. The proposed mechanism (Scheme 48b) involves the oxidative addition of silylboronic ester **254** to Pd(0) and coordination of pyridine **1** providing the intermediate **257** which on further regioselective insertion of pyridine into the Pd–B bond resulted in the  $\pi$ -allyl palladium complex **258**. Subsequent reductive elimination furnishes the silaboration products **255** and **256** with the regeneration of Pd(0).

## Conclusion

Significant progress has been made in the area of *ortho*- and distal C–H functionalization of pyridines, as evidenced by the reactions outlined in this review. The previous research and their mechanistic insight provided us with more information to approach the new avenue of catalytic C–H functionalization of the pyridine nucleus. The challenges still remain for the distal C–H functionalization, particularly at the C4 position. Even the directing group on pyridine ring system has been less explored for *ortho*- or distal C–H functionalization. Although the C–H functionalization with transition-metal catalysis and rare earth metal catalysis has advanced, the functionalization of the pyridine ring system can further be explored by employing new catalytic systems and merging of different strategies. Taking this into account, we hope that the efforts for the development of novel protocols for the preparation and incorporation of functionalized pyridine scaffolds will continue and could be applicable for applications in industry.

## ORCID® iDs

Haritha Sindhe - <https://orcid.org/0000-0002-4510-2209>

Satyasheel Sharma - <https://orcid.org/0000-0002-4983-1572>

## References

- Attla, A. M.; Mansour, H. A.; Almehdi, A. A.; Abbasi, M. M. *Nucleosides Nucleotides* **1999**, *18*, 2301–2306. doi:10.1080/07328319908044882
- Zav'yalova, V. K.; Zubarev, A. A.; Shestopalov, A. M. *Russ. Chem. Bull.* **2009**, *58*, 1939–1944. doi:10.1007/s11172-009-0265-2
- Vitaku, E.; Smith, D. T.; Njardarson, J. T. *J. Med. Chem.* **2014**, *57*, 10257–10274. doi:10.1021/jm501100b
- El-Naggar, M.; Almahlhi, H.; Ibrahim, H. S.; Eldehna, W. M.; Abdel-Aziz, H. A. *Molecules* **2018**, *23*, 1459. doi:10.3390/molecules23061459
- Chen, Z.; Li, P.; Hu, D.; Dong, L.; Pan, J.; Luo, L.; Zhang, W.; Xue, W.; Jin, L.; Song, B. *Arabian J. Chem.* **2019**, *12*, 2685–2696. doi:10.1016/j.arabjc.2015.05.003
- Khalaf, H. S.; Tolan, H. E. M.; El-Bayaa, M. N.; Radwan, M. A. A.; El-Manawaty, M.; El-Sayed, W. A. *Russ. J. Gen. Chem.* **2020**, *90*, 1706–1715. doi:10.1134/s1070363220090182
- Bhutani, P.; Joshi, G.; Raja, N.; Bachhav, N.; Rajanna, P. K.; Bhutani, H.; Paul, A. T.; Kumar, R. *J. Med. Chem.* **2021**, *64*, 2339–2381. doi:10.1021/acs.jmedchem.0c01786
- Ling, Y.; Hao, Z.-Y.; Liang, D.; Zhang, C.-L.; Liu, Y.-F.; Wang, Y. *Drug Des., Dev. Ther.* **2021**, *15*, 4289–4338. doi:10.2147/dddt.s329547
- Yin, P.; Zhang, Q.; Shreeve, J. N. *M. Acc. Chem. Res.* **2016**, *49*, 4–16. doi:10.1021/acs.accounts.5b00477
- Wang, Q.; Lei, C.-j.; Yang, H.-w.; Cheng, G.-b. *Energ. Mater. Front.* **2022**, *3*, 68–73. doi:10.1016/j.enmf.2022.05.003
- Movassaghi, M.; Hill, M. D.; Ahmad, O. K. *J. Am. Chem. Soc.* **2007**, *129*, 10096–10097. doi:10.1021/ja073912a
- Hill, M. D. *Chem. – Eur. J.* **2010**, *16*, 12052–12062. doi:10.1002/chem.201001100
- Nakao, Y. *Synthesis* **2011**, 3209–3219. doi:10.1055/s-0030-1260212
- Hilton, M. C.; Dolewski, R. D.; McNally, A. J. *Am. Chem. Soc.* **2016**, *138*, 13806–13809. doi:10.1021/jacs.6b08662
- Murakami, K.; Yamada, S.; Kaneda, T.; Itami, K. *Chem. Rev.* **2017**, *117*, 9302–9332. doi:10.1021/acs.chemrev.7b00021
- Proctor, R. S. J.; Phipps, R. J. *Angew. Chem., Int. Ed.* **2019**, *58*, 13666–13699. doi:10.1002/anie.201900977
- Duan, J.; Zhang, L.; Xu, G.; Chen, H.; Ding, X.; Mao, Y.; Rong, B.; Zhu, N.; Guo, K. *J. Org. Chem.* **2020**, *85*, 8157–8165. doi:10.1021/acs.joc.0c01081
- Xie, D.; Wang, Y.; Zhang, X.; Fu, Z.; Niu, D. *Angew. Chem., Int. Ed.* **2022**, *61*, e202204922. doi:10.1002/anie.202204922
- Cen, K.; Usman, M.; Shen, W.; Liu, M.; Yang, R.; Cai, J. *Org. Biomol. Chem.* **2022**, *20*, 7391–7404. doi:10.1039/d2ob01344d
- Hamada, Y. Role of Pyridines in Medicinal Chemistry and Design of BACE1 Inhibitors Possessing a Pyridine Scaffold. In *Pyridine*; Pandey, P. P., Ed.; IntechOpen: Rijeka, 2018; pp 9–26. doi:10.5772/intechopen.74719
- Małkowska, M. *Chem. Soc. Rev.* **2010**, *39*, 2855–2868. doi:10.1039/b822559c
- Haag, B.; Mosrin, M.; Ila, H.; Malakhov, V.; Knochel, P. *Angew. Chem., Int. Ed.* **2011**, *50*, 9794–9824. doi:10.1002/anie.201101960
- Chinchilla, R.; Nájera, C.; Yus, M. *Chem. Rev.* **2004**, *104*, 2667–2722. doi:10.1021/cr020101a
- Wang, H.; Huang, H. *Chem. Rec.* **2016**, *16*, 1807–1818. doi:10.1002/tcr.201500274
- Gandeepan, P.; Müller, T.; Zell, D.; Cera, G.; Warratz, S.; Ackermann, L. *Chem. Rev.* **2019**, *119*, 2192–2452. doi:10.1021/acs.chemrev.8b00507
- Dalton, T.; Faber, T.; Glorius, F. *ACS Cent. Sci.* **2021**, *7*, 245–261. doi:10.1021/acscentsci.0c01413
- Sinha, S. K.; Guin, S.; Maiti, S.; Biswas, J. P.; Porey, S.; Maiti, D. *Chem. Rev.* **2022**, *122*, 5682–5841. doi:10.1021/acs.chemrev.1c00220
- Rogge, T.; Kaplaneris, N.; Chatani, N.; Kim, J.; Chang, S.; Punji, B.; Schafer, L. L.; Musaev, D. G.; Wencel-Delord, J.; Roberts, C. A.; Sarpong, R.; Wilson, Z. E.; Brimble, M. A.; Johansson, M. J.; Ackermann, L. *Nat. Rev. Methods Primers* **2021**, *1*, 43. doi:10.1038/s43586-021-00041-2
- Guillemand, L.; Kaplaneris, N.; Ackermann, L.; Johansson, M. J. *Nat. Rev. Chem.* **2021**, *5*, 522–545. doi:10.1038/s41570-021-00300-6
- Sambiagio, C.; Schönbauer, D.; Blicke, R.; Dao-Huy, T.; Pototschnig, G.; Schaaf, P.; Wiesinger, T.; Zia, M. F.; Wencel-Delord, J.; Besset, T.; Maes, B. U. W.; Schnürch, M. *Chem. Soc. Rev.* **2018**, *47*, 6603–6743. doi:10.1039/c8cs00201k

31. Murali, K.; Machado, L. A.; Carvalho, R. L.; Pedrosa, L. F.; Mukherjee, R.; Da Silva Júnior, E. N.; Maiti, D. *Chem. – Eur. J.* **2021**, *27*, 12453–12508. doi:10.1002/chem.202101004
32. Seth, K. *Org. Chem. Front.* **2022**, *9*, 3102–3141. doi:10.1039/d1qo01859k
33. Sun, Q.; Xu, X.; Xu, X. *ChemCatChem* **2022**, *14*, e202201083. doi:10.1002/cctc.202201083
34. Wu, P.; Cao, F.; Zhou, Y.; Xue, Z.; Zhang, N.; Shi, L.; Luo, G. *Inorg. Chem.* **2022**, *61*, 17330–17341. doi:10.1021/acs.inorgchem.2c02953
35. Jo, W.; Kim, J.; Choi, S.; Cho, S. H. *Angew. Chem., Int. Ed.* **2016**, *55*, 9690–9694. doi:10.1002/anie.201603329
36. Lee, S. H.; Kwon, N. Y.; Lee, J. Y.; An, W.; Jung, Y. H.; Mishra, N. K.; Ghosh, P.; Park, J. S.; Kim, I. S. *Eur. J. Org. Chem.* **2020**, 4886–4892. doi:10.1002/ejoc.202000610
37. Han, S.; Chakrasali, P.; Park, J.; Oh, H.; Kim, S.; Kim, K.; Pandey, A. K.; Han, S. H.; Han, S. B.; Kim, I. S. *Angew. Chem., Int. Ed.* **2018**, *57*, 12737–12740. doi:10.1002/anie.201807159
38. Kim, M.; Koo, Y.; Hong, S. *Acc. Chem. Res.* **2022**, *55*, 3043–3056. doi:10.1021/acs.accounts.2c00530
39. Chakraborty, S.; Biju, A. T. *Angew. Chem., Int. Ed.* **2023**, *62*, e202300049. doi:10.1002/anie.202300049
40. Luo, Y.-R. *Handbook of Bond Dissociation Energies in Organic Compounds*; CRC Press: Boca Raton, FL, U.S.A., 2002. doi:10.1201/9781420039863
41. Dong, Z.; Ren, Z.; Thompson, S. J.; Xu, Y.; Dong, G. *Chem. Rev.* **2017**, *117*, 9333–9403. doi:10.1021/acs.chemrev.6b00574
42. Evano, G.; Theunissen, C. *Angew. Chem., Int. Ed.* **2019**, *58*, 7202–7236. doi:10.1002/anie.201806629
43. Sun, A. C.; McAtee, R. C.; McClain, E. J.; Stephenson, C. R. *Synthesis* **2019**, *51*, 1063–1072. doi:10.1055/s-0037-1611658
44. Mandal, D.; Roychowdhury, S.; Biswas, J. P.; Maiti, S.; Maiti, D. *Chem. Soc. Rev.* **2022**, *51*, 7358–7426. doi:10.1039/d1cs00923k
45. Wang, H.-H.; Wang, X.-D.; Yin, G.-F.; Zeng, Y.-F.; Chen, J.; Wang, Z. *ACS Catal.* **2022**, *12*, 2330–2347. doi:10.1021/acscatal.1c05266
46. Bera, A.; Kabadwal, L. M.; Bera, S.; Banerjee, D. *Chem. Commun.* **2022**, *58*, 10–28. doi:10.1039/d1cc05899a
47. Liu, X.-L.; Jiang, L.-B.; Luo, M.-P.; Ren, Z.; Wang, S.-G. *Org. Chem. Front.* **2022**, *9*, 265–280. doi:10.1039/d1qo01223a
48. Jordan, R. F.; Taylor, D. F. *J. Am. Chem. Soc.* **1989**, *111*, 778–779. doi:10.1021/ja00184a081
49. Yotphan, S.; Bergman, R. G.; Ellman, J. A. *Org. Lett.* **2010**, *12*, 2978–2981. doi:10.1021/ol101002b
50. Guan, B.-T.; Hou, Z. *J. Am. Chem. Soc.* **2011**, *133*, 18086–18089. doi:10.1021/ja208129t
51. Xiao, B.; Liu, Z.-J.; Liu, L.; Fu, Y. *J. Am. Chem. Soc.* **2013**, *135*, 616–619. doi:10.1021/ja3113752
52. Xiao, Q.; Ling, L.; Ye, F.; Tan, R.; Tian, L.; Zhang, Y.; Li, Y.; Wang, J. *J. Org. Chem.* **2013**, *78*, 3879–3885. doi:10.1021/jo4002883
53. Sun, Q.; Chen, P.; Wang, Y.; Luo, Y.; Yuan, D.; Yao, Y. *Inorg. Chem.* **2018**, *57*, 11788–11800. doi:10.1021/acs.inorgchem.8b01959
54. Kundu, A.; Inoue, M.; Nagae, H.; Tsurugi, H.; Mashima, K. *J. Am. Chem. Soc.* **2018**, *140*, 7332–7342. doi:10.1021/jacs.8b03998
55. Hara, N.; Saito, T.; Semba, K.; Kuriakose, N.; Zheng, H.; Sakaki, S.; Nakao, Y. *J. Am. Chem. Soc.* **2018**, *140*, 7070–7073. doi:10.1021/jacs.8b04199
56. Kuriakose, N.; Zheng, J.-J.; Saito, T.; Hara, N.; Nakao, Y.; Sakaki, S. *Inorg. Chem.* **2019**, *58*, 4894–4906. doi:10.1021/acs.inorgchem.8b03493
57. Hara, N.; Aso, K.; Li, Q.-Z.; Sakaki, S.; Nakao, Y. *Tetrahedron* **2021**, *95*, 132339. doi:10.1016/j.tet.2021.132339
58. Lin, H.; Li, Y.; Wang, J.; Zhang, M.; Jiang, T.; Li, J.; Chen, Y. *Appl. Organomet. Chem.* **2021**, *35*, e6345. doi:10.1002/aoc.6345
59. Tran, G.; Hesp, K. D.; Mascitti, V.; Ellman, J. A. *Angew. Chem., Int. Ed.* **2017**, *56*, 5899–5903. doi:10.1002/anie.201702409
60. Li, J.-F.; Pan, D.; Wang, H.-R.; Zhang, T.; Li, Y.; Huang, G.; Ye, M. *J. Am. Chem. Soc.* **2022**, *144*, 18810–18816. doi:10.1021/jacs.2c09306
61. Li, B.-J.; Shi, Z.-J. *Chem. Sci.* **2011**, *2*, 488–493. doi:10.1039/c0sc00419g
62. Nakao, Y.; Yamada, Y.; Kashihara, N.; Hiyama, T. *J. Am. Chem. Soc.* **2010**, *132*, 13666–13668. doi:10.1021/ja106514b
63. Wang, Y.; Li, R.; Guan, W.; Li, Y.; Li, X.; Yin, J.; Zhang, G.; Zhang, Q.; Xiong, T.; Zhang, Q. *Chem. Sci.* **2020**, *11*, 11554–11561. doi:10.1039/d0sc04808a
64. Ma, J.-B.; Zhao, X.; Zhang, D.; Shi, S.-L. *J. Am. Chem. Soc.* **2022**, *144*, 13643–13651. doi:10.1021/jacs.2c04043
65. Cheel, J.; Theoduloz, C.; Rodríguez, J.; Saud, G.; Caligari, P. D. S.; Schmeda-Hirschmann, G. *J. Agric. Food Chem.* **2005**, *53*, 8512–8518. doi:10.1021/jf051294g
66. Grimsdale, A. C.; Leok Chan, K.; Martin, R. E.; Jokisz, P. G.; Holmes, A. B. *Chem. Rev.* **2009**, *109*, 897–1091. doi:10.1021/cr000013v
67. Nguyen, P.-H.; Yang, J.-L.; Uddin, M. N.; Park, S.-L.; Lim, S.-I.; Jung, D.-W.; Williams, D. R.; Oh, W.-K. *J. Nat. Prod.* **2013**, *76*, 2080–2087. doi:10.1021/np400533h
68. Singh, R. S. P.; Michel, D.; Das, U.; Dimmock, J. R.; Alcorn, J. *Bioorg. Med. Chem. Lett.* **2014**, *24*, 5199–5202. doi:10.1016/j.bmcl.2014.09.074
69. Heck, R. F. *Acc. Chem. Res.* **1979**, *12*, 146–151. doi:10.1021/ar50136a006
70. Mc Cartney, D.; Guiry, P. J. *Chem. Soc. Rev.* **2011**, *40*, 5122–5150. doi:10.1039/c1cs15101k
71. Ali, W.; Prakash, G.; Maiti, D. *Chem. Sci.* **2021**, *12*, 2735–2759. doi:10.1039/d0sc05555g
72. Logeswaran, R.; Jegannathan, M. *Adv. Synth. Catal.* **2022**, *364*, 2113–2139. doi:10.1002/adsc.202200193
73. Carral-Menoyo, A.; Sotomayor, N.; Lete, E. *Trends Chem.* **2022**, *4*, 495–511. doi:10.1016/j.trechm.2022.03.007
74. Wen, P.; Li, Y.; Zhou, K.; Ma, C.; Lan, X.; Ma, C.; Huang, G. *Adv. Synth. Catal.* **2012**, *354*, 2135–2140. doi:10.1002/adsc.201200195
75. Goriya, Y.; Ramana, C. V. *Chem. – Eur. J.* **2012**, *18*, 13288–13292. doi:10.1002/chem.201202379
76. Oi, S.; Tanaka, Y.; Inoue, Y. *Organometallics* **2006**, *25*, 4773–4778. doi:10.1021/om060561k
77. Cheng, K.; Yao, B.; Zhao, J.; Zhang, Y. *Org. Lett.* **2008**, *10*, 5309–5312. doi:10.1021/ol802262r
78. Hoffmann-Röder, A.; Krause, N. *Angew. Chem., Int. Ed.* **2004**, *43*, 1196–1216. doi:10.1002/anie.200300628
79. Ma, S. *Chem. Rev.* **2005**, *105*, 2829–2872. doi:10.1021/cr020024j
80. Han, X.-L.; Lin, P.-P.; Li, Q. *Chin. Chem. Lett.* **2019**, *30*, 1495–1502. doi:10.1016/j.ccllet.2019.04.027
81. Song, G.; Wang, B.; Nishiura, M.; Hou, Z. *Chem. – Eur. J.* **2015**, *21*, 8394–8398. doi:10.1002/chem.201501121
82. Li, W.; Tang, J.; Li, S.; Zheng, X.; Yuan, M.; Xu, B.; Jiang, W.; Fu, H.; Li, R.; Chen, H. *Org. Lett.* **2020**, *22*, 7814–7819. doi:10.1021/acs.orglett.0c02679

83. Ye, M.; Gao, G.-L.; Yu, J.-Q. *J. Am. Chem. Soc.* **2011**, *133*, 6964–6967. doi:10.1021/ja2021075
84. Quagliano, J.; Schubert, L. *Chem. Rev.* **1952**, *50*, 201–260. doi:10.1021/cr60156a001
85. Coe, B. J.; Glenwright, S. J. *Coord. Chem. Rev.* **2000**, *203*, 5–80. doi:10.1016/s0010-8545(99)00184-8
86. Cong, X.; Tang, H.; Wu, C.; Zeng, X. *Organometallics* **2013**, *32*, 6565–6575. doi:10.1021/om400890p
87. Shi, B.-F.; Mangel, N.; Zhang, Y.-H.; Yu, J.-Q. *Angew. Chem., Int. Ed.* **2008**, *47*, 4882–4886. doi:10.1002/anie.200801030
88. Zhou, J.; Li, B.; Hu, F.; Shi, B.-F. *Org. Lett.* **2013**, *15*, 3460–3463. doi:10.1021/ol401540k
89. Qian, Z.-C.; Zhou, J.; Li, B.; Hu, F.; Shi, B.-F. *Org. Biomol. Chem.* **2014**, *12*, 3594–3597. doi:10.1039/c4ob00612g
90. Tsai, C.-C.; Shih, W.-C.; Fang, C.-H.; Li, C.-Y.; Ong, T.-G.; Yap, G. P. A. *J. Am. Chem. Soc.* **2010**, *132*, 11887–11889. doi:10.1021/ja1061246
91. Shen, Y.; Chen, J.; Liu, M.; Ding, J.; Gao, W.; Huang, X.; Wu, H. *Chem. Commun.* **2014**, *50*, 4292–4295. doi:10.1039/c3cc48767a
92. Kianmehr, E.; Faghhi, N.; Khan, K. M. *Org. Lett.* **2015**, *17*, 414–417. doi:10.1021/ol503238a
93. Li, M.; Li, X.; Chang, H.; Gao, W.; Wei, W. *Org. Biomol. Chem.* **2016**, *14*, 2421–2426. doi:10.1039/c5ob02409a
94. Zeng, Y.; Zhang, C.; Yin, C.; Sun, M.; Fu, H.; Zheng, X.; Yuan, M.; Li, R.; Chen, H. *Org. Lett.* **2017**, *19*, 1970–1973. doi:10.1021/acs.orglett.7b00498
95. Ye, M.; Gao, G.-L.; Edmunds, A. J. F.; Worthington, P. A.; Morris, J. A.; Yu, J.-Q. *J. Am. Chem. Soc.* **2011**, *133*, 19090–19093. doi:10.1021/ja209510q
96. Dai, F.; Gui, Q.; Liu, J.; Yang, Z.; Chen, X.; Guo, R.; Tan, Z. *Chem. Commun.* **2013**, *49*, 4634–4636. doi:10.1039/c3cc41066h
97. Wasa, M.; Worrell, B. T.; Yu, J.-Q. *Angew. Chem., Int. Ed.* **2010**, *49*, 1275–1277. doi:10.1002/anie.200906104
98. Sirois, J. J.; Davis, R.; DeBoef, B. *Org. Lett.* **2014**, *16*, 868–871. doi:10.1021/ol403634b
99. Salamanca, V.; Toledo, A.; Albéniz, A. C. *J. Am. Chem. Soc.* **2018**, *140*, 17851–17856. doi:10.1021/jacs.8b10680
100. Suresh, R.; Muthusubramanian, S.; Kumaran, R. S.; Manickam, G. *Asian J. Org. Chem.* **2014**, *3*, 604–608. doi:10.1002/ajoc.201400013
101. Liu, W.; Yu, X.; Li, Y.; Kuang, C. *Chem. Commun.* **2014**, *50*, 9291–9294. doi:10.1039/c4cc04129a
102. Odani, R.; Hirano, K.; Satoh, T.; Miura, M. *J. Org. Chem.* **2015**, *80*, 2384–2391. doi:10.1021/acs.joc.5b00037
103. Shang, Y.; Jie, X.; Zhao, H.; Hu, P.; Su, W. *Org. Lett.* **2014**, *16*, 416–419. doi:10.1021/ol403311b
104. Gao, G.-L.; Xia, W.; Jain, P.; Yu, J.-Q. *Org. Lett.* **2016**, *18*, 744–747. doi:10.1021/acs.orglett.5b03712
105. Song, G.; Gong, X.; Li, X. *J. Org. Chem.* **2011**, *76*, 7583–7589. doi:10.1021/jo201266u
106. Thenarukandiyil, R.; Choudhury, J. *Organometallics* **2015**, *34*, 1890–1897. doi:10.1021/acs.organomet.5b00157
107. Zhang, W.-B.; Yang, X.-T.; Ma, J.-B.; Su, Z.-M.; Shi, S.-L. *J. Am. Chem. Soc.* **2019**, *141*, 5628–5634. doi:10.1021/jacs.9b00931
108. Ye, P.; Shao, Y.; Zhang, F.; Zou, J.; Ye, X.; Chen, J. *Adv. Synth. Catal.* **2020**, *362*, 851–857. doi:10.1002/adsc.201901473
109. Hancock, R. D. *Chem. Soc. Rev.* **2013**, *42*, 1500–1524. doi:10.1039/c2cs35224a
110. Hagui, W.; Periasamy, K.; Soulé, J.-F. *Eur. J. Org. Chem.* **2021**, 5388–5402. doi:10.1002/ejoc.202100806
111. Katagiri, T.; Mukai, T.; Satoh, T.; Hirano, K.; Miura, M. *Chem. Lett.* **2009**, *38*, 118–119. doi:10.1246/cl.2009.118
112. Kwak, J.; Ohk, Y.; Jung, Y.; Chang, S. *J. Am. Chem. Soc.* **2012**, *134*, 17778–17788. doi:10.1021/ja308205d
113. Hong, S. Y.; Kwak, J.; Chang, S. *Chem. Commun.* **2016**, *52*, 3159–3162. doi:10.1039/c5cc09960a
114. Yu, J.; Lv, W.; Cheng, G. *Org. Lett.* **2018**, *20*, 4732–4735. doi:10.1021/acs.orglett.8b01632
115. Yu, J.; Wen, S.; Ba, D.; Lv, W.; Chen, Y.; Cheng, G. *Org. Lett.* **2019**, *21*, 6366–6369. doi:10.1021/acs.orglett.9b02253
116. Wu, S.; Wang, Z.; Bao, Y.; Chen, C.; Liu, K.; Zhu, B. *Chem. Commun.* **2020**, *56*, 4408–4411. doi:10.1039/d0cc01077d
117. Chen, M.; Meng, H.; Yang, F.; Wang, Y.; Chen, C.; Zhu, B. *Org. Biomol. Chem.* **2021**, *19*, 4268–4271. doi:10.1039/d1ob00590a
118. Yang, L.; Semba, K.; Nakao, Y. *Angew. Chem., Int. Ed.* **2017**, *56*, 4853–4857. doi:10.1002/anie.201701238
119. Yang, L.; Uemura, N.; Nakao, Y. *J. Am. Chem. Soc.* **2019**, *141*, 7972–7979. doi:10.1021/jacs.9b03138
120. Oshima, K.; Ohmura, T.; Sugimoto, M. *J. Am. Chem. Soc.* **2011**, *133*, 7324–7327. doi:10.1021/ja2020229

## License and Terms

This is an open access article licensed under the terms of the Beilstein-Institut Open Access License Agreement (<https://www.beilstein-journals.org/bjoc/terms>), which is identical to the Creative Commons Attribution 4.0 International License (<https://creativecommons.org/licenses/by/4.0>). The reuse of material under this license requires that the author(s), source and license are credited. Third-party material in this article could be subject to other licenses (typically indicated in the credit line), and in this case, users are required to obtain permission from the license holder to reuse the material.

The definitive version of this article is the electronic one which can be found at:  
<https://doi.org/10.3762/bjoc.19.62>



# Aromatic C–H bond functionalization through organocatalyzed asymmetric intermolecular aza-Friedel–Crafts reaction: a recent update

Anup Biswas

## Review

Open Access

### Address:

Department of Chemistry, Hooghly Women's College, Vivekananda Road, Pipulpati, Hooghly - 712103, WB, India

### Email:

Anup Biswas - a.biitkgp@gmail.com

### Keywords:

asymmetric; aza-Friedel–Crafts reaction; H-bonding; organocatalysis; stereoselectivity

*Beilstein J. Org. Chem.* **2023**, *19*, 956–981.

<https://doi.org/10.3762/bjoc.19.72>

Received: 09 April 2023

Accepted: 15 June 2023

Published: 28 June 2023

This article is part of the thematic issue "C–H bond functionalization: recent discoveries and future directions".

Guest Editor: I. Chatterjee



© 2023 Biswas; licensee Beilstein-Institut.  
License and terms: see end of document.

## Abstract

The aza-Friedel–Crafts reaction allows an efficient coupling of electron-rich aromatic systems with imines for the facile incorporation of aminoalkyl groups into the aromatic ring. This reaction has a great scope of forming aza-stereocenters which can be tuned by different asymmetric catalysts. This review assembles recent advances in asymmetric aza-Friedel–Crafts reactions mediated by organocatalysts. The mechanistic interpretation with the origin of stereoselectivity is also explained.

## Introduction

The ease of a chemical transformation depends on the thermodynamic instability of a chemical bond owing to its fast cleavage under mild reaction conditions. A C–H bond is thermodynamically stable and possesses a high bond dissociation energy opposing the bond to easy chemical transformation. Therefore, harsh reaction conditions and the necessity of an external activator like catalysts are common prerequisites for processes involving C–H bond breaking. Among different types of C–H bonds, an aromatic C–H bond is even more inert rendering this type of bond functionalization more difficult. Herewith the term “bond functionalization” is defined as the cleavage of an existing bond with substitution by another bond.

Aromatic C–H bond functionalizations have gained considerable attention by organic chemists because of the strategic importance of this process as well as the ability to synthesize functionalized aromatic molecules in a straightforward way. Many organic name reactions have been discovered utilizing the C–H bond functionalization concept [1].

Metals were exclusively explored to assist substitutions of aromatic C–H bonds by other bonds and this area of research is more than a century old. However, many disadvantages are associated with metal-mediated organic transformations including harsh reaction conditions (e.g., high temperature) and toxic



solvents. With the tremendous progress in organic chemistry over the last few decades, metal catalysis has been increasingly and successfully replaced by organocatalysis, i.e., accelerating the rate of chemical transformations by using small organic molecules as catalysts. Although being discovered more than 100 years ago, the concept became increasingly accepted and popular only by the last decade of the last century [2,3].

Nowadays, organocatalysis is especially applied to asymmetric synthesis and a huge number of organocatalysts has been introduced in last three decades for the asymmetric synthesis of acyclic, carbocyclic, heterocyclic, and polycyclic molecular architectures with high molecular complexity. In particular, asymmetric organocatalysis plays a pivotal role in the construction of optically active, bioactive, and natural products. The main advantages of organocatalyzed stereoselective reactions include mild reaction conditions and the use of a sole catalyst without the need of other chiral ligands [4,5]. In these reactions, stereoselection in the products is achieved by the chiral environment present in the catalyst itself. Depending upon the reactivities, organocatalysts can be categorized into two major divisions: 1) covalent bonding and 2) noncovalent bonding catalysts. A covalent bonding organocatalyst reacts with a substrate to form an activated chiral intermediate which undergoes a stereoselective reaction with another reagent. A noncovalent bonding catalyst usually assembles the reaction partners in a highly ordered three dimensional transition state through noncovalent interactions (like H-bonding,  $\pi$ - $\pi$  interactions) thus promoting the stereoselective reaction. Examples of covalent bonding organocatalysts are amines [6,7], N-heterocyclic carbenes [8,9], phosphines [10], amidines [11], isothioureas [12,13], whereas thioureas [14,15], ureas [16], phosphoric acids [17,18], and squaramides [19,20] fall into the second category.

The Friedel–Crafts reaction, discovered by Charles Friedel and James Crafts in 1877 allows the aromatic C–H bond functionalization through the formation of a new C–C bond [21]. The reaction requires an electrophilic reagent/intermediate present in the reaction system on which an electrophilic attack by the  $\pi$ -electron cloud of the aromatic ring can occur spontaneously to form a dearomatized species. The latter is rearomatized in a succeeding step with the elimination of a  $H^+$  ion to form the functionalized aromatic moieties. The aza-Friedel–Crafts reaction is a subclass of the originally reported transformation that couples an imine with an aromatic system allowing for a facile incorporation of an alkylamine functionality into the aromatic system. Like the classical Friedel–Crafts reaction, the aza-Friedel–Crafts reaction also requires the presence of a Lewis acid catalyst for rate acceleration. The reaction can be very easily modulated by different Lewis acidic metallic compounds which effectively form a coordinate bond by accepting the lone

pair of electrons of the imine nitrogen to a suitable vacant orbital of the metal center, thus enhancing the electrophilicity of the imine carbon atom by imparting a positive character on the adjacent heteroatom [22,23].

With the advent of different types of organocatalysts, the aza-Friedel–Crafts reaction has also been explored under the influence of organocatalysis. However, here organocatalysts act as Brønsted acids which form noncovalent interactions (H-bonding) with the imine nitrogen to enhance the electrophilicity of the imine component. In addition, by selecting suitable imine components, asymmetric products containing a nitrogen-substituted stereocenter can be obtained. Chiral organocatalysts can easily influence asymmetric aza-Friedel–Crafts reactions. The asymmetric induction is attributed to the formation of a chiral complex through a noncovalent interaction with the imine nitrogen and the catalyst which selectively blocks one face of the imine's plane. This forces the nucleophile to approach from the opposite face thus imparting stereoselectivity into the products.

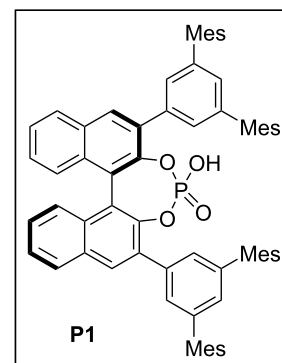
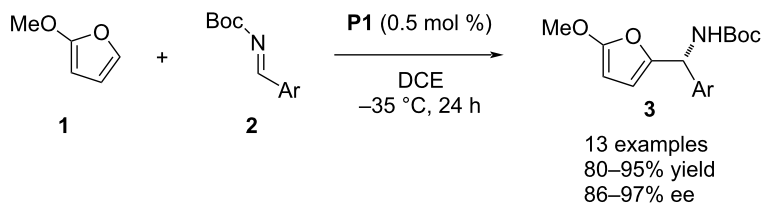
The first organocatalyzed asymmetric aza-Friedel–Crafts protocol was published by Terada and co-workers in 2004. In this methodology, a 1,1'-bi-2-naphthol (BINOL)-derived chiral phosphoric acid **P1** was used as the catalytic reagent to couple 2-methoxyfuran (**1**) and *N*-Boc-protected aldimines **2** to incorporate an aza-tertiary stereocenter into the 2' position of the heteroaromatic products **3** (Scheme 1) [24].

This review summarizes the recent advances (2018 till date) on organocatalyzed asymmetric aza-Friedel–Crafts reactions. The examples have been segmented according to the different types of catalysts.

## Review Phosphoric acids

Chiral phosphoric acids have been envisaged as versatile organocatalysts for various asymmetric chemical transformations. These compounds play a dual role in the catalytic cycle due to their intrinsic Brønsted acidity and the ability to H-bond formation. Organophosphoric acids can perform as both H-bond acceptors and donors. 1,1'-Bi-2-naphthol (BINOL) and 1,1'-spirobiindane-7,7'-diol (SPINOL)-derived phosphoric acids with different substituents in the 2,2'-positions of the aromatic framework have been extensively explored as axially chiral catalysts in the field of asymmetric transformations including aza-Friedel–Crafts reactions.

In 2018, Nakamura and co-workers designed an aza-Friedel–Crafts process between indoles **4** and cyclic *N*-sulfonyl ketimines **5**. The authors employed the BINOL-based chiral

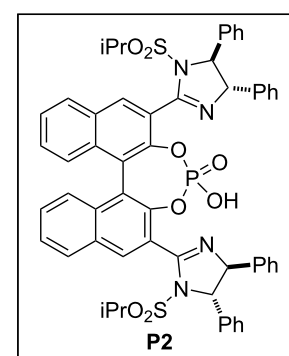
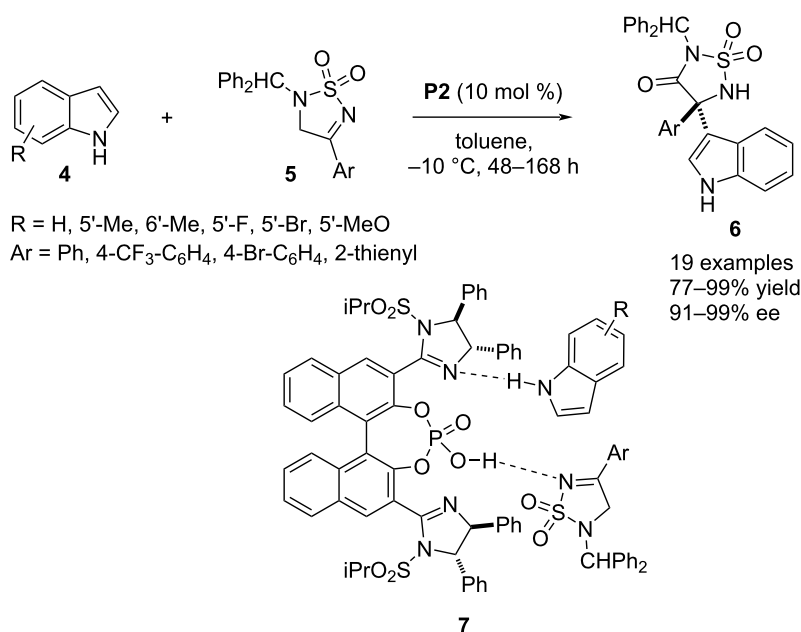


**Scheme 1:** First organocatalyzed asymmetric aza-Friedel–Crafts reaction.

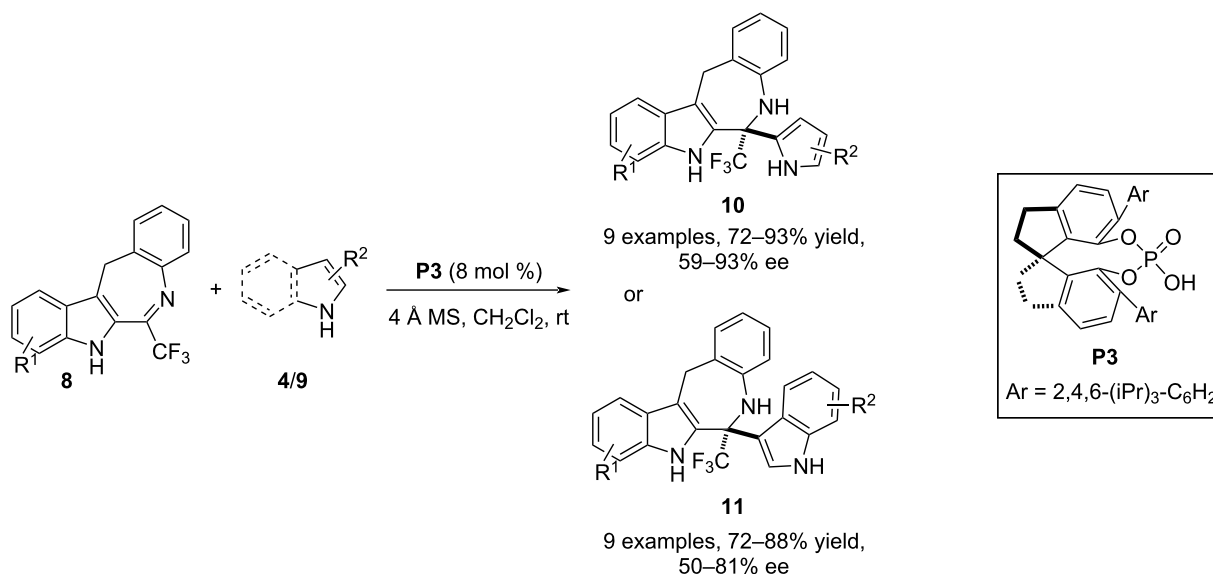
phosphoric acid **P2** bearing two imidazoline moieties at the *ortho*-positions as the catalyst which activates both reactants through H-bonding where the NH group of the nucleophile performs as an H-bond donor towards the imidazoline nitrogen and the electrophile acts as H-bond acceptor from the OH group of the catalyst. These interactions rearrange the three molecules in a chiral pocket as shown by transition state **7**, favoring stereoselection in the products through C3-functionalization of the indole (Scheme 2) [25].

In 2018, Lin and co-workers deployed pyrroles **9** in an aza-Friedel–Crafts reaction with trifluoromethyldihydrobenzoazepinoindoles **8** to achieve the aromatic electrophilic substitu-

tion at the C2 position of the pyrrole ring. A further extension of the scope of this process was achieved through the C3–H functionalization of indole derivatives **4**. The nucleophile favors the attack at the imine carbon included in the seven-membered ring of compound **8** to generate an aza-quaternary stereocenter containing trifluoromethyl, pyrrole/indole, and benzoazepinoindole moieties. Stereoselectivity in the products **10/11** was achieved by using the chiral spirocyclic phosphoric acid catalyst **P3** which, through H-bonding interactions with the nucleophile and the electrophile, forces the nucleophile to approach the C=N plane from the *Re* face. In general, enantiocontrol with pyrroles was better than with indoles (Scheme 3) [26].



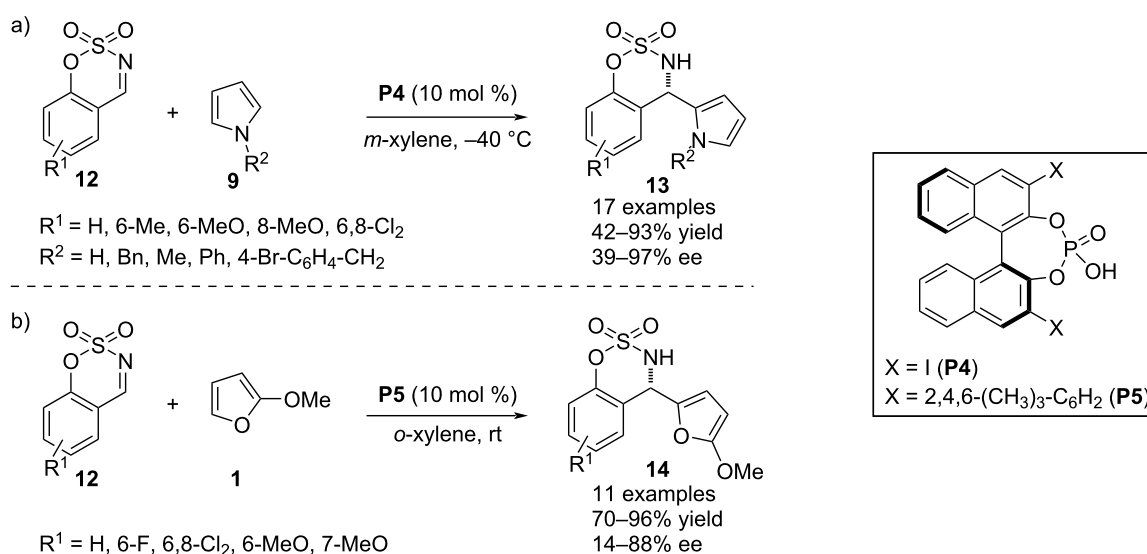
**Scheme 2:** Aza-Friedel–Crafts reaction between indoles and cyclic ketimines.



**Scheme 3:** Aza-Friedel–Crafts reaction utilizing trifluoromethyldihydrobenzoazepinoindoles as electrophiles.

In 2018, Kim and co-workers developed an aza-Friedel–Crafts protocol involving pyrroles **9** as the  $\pi$ -nucleophile in combination with cyclic *N*-sulfinimines **12**. The chiral phosphoric acid **P4** was used to catalyze the introduction of a pyrrole-substituted aza-quaternary stereocenter in cyclic sulfamidate derivatives. *N*-Alkyl and *N*-benzyl-substituted pyrroles responded to the process with appreciable enantioefficiency. However, pyrrole was not proved to be the efficient substrate in terms of stereo-control [27] (Scheme 4a). In the very next year, pyrrole was

successfully replaced by 2-substituted furans **1** as the aromatic reacting partner with imines **12** to execute the asymmetric aza-Friedel–Crafts process modulated by the chiral phosphoric acid **P5** as the catalyst. A major concern of this process was the reduced aromatic character of the furan ring and the C2 methoxy-substituted substrate was exclusively employed to make the aromatic ring sufficiently electron rich. The substrate scope was mainly attributed to alterations of the substituents on the benzene ring of imines **12** (Scheme 4b) [28].



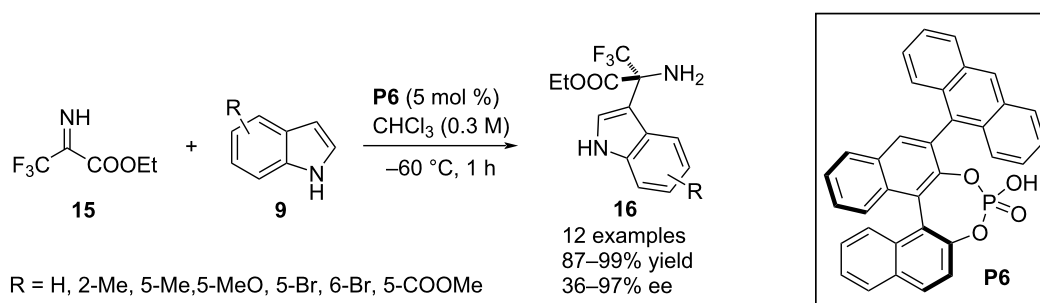
**Scheme 4:** Aza-Friedel–Crafts reaction utilizing cyclic *N*-sulfinimines as electrophiles.

In 2018, Morimoto, Ohshima and co-workers reported an aza-Friedel–Crafts process for the functionalization of the C3–H bond in indoles **9** in the presence of BINOL-derived chiral phosphoric acid **P6** as the catalytic agent. They utilized trifluoromethyl ester-substituted N-unprotected imine **15** as the potential electrophile to install an aza-quaternary stereocenter in the C3 position. The products **16** were achieved with excellent enantioselectivities which were attributed to an attractive interaction between the indole ring and the anthracene substituent of the catalyst's framework (Scheme 5) [29].

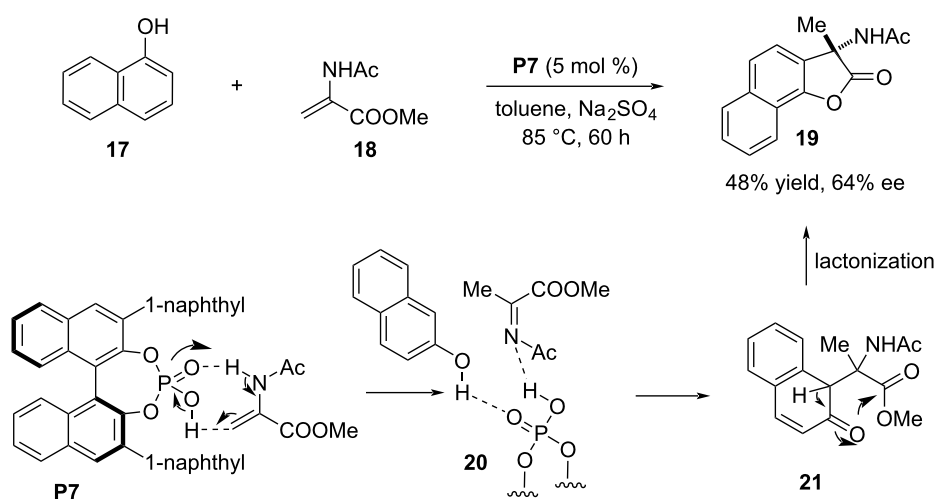
In 2018, Piersanti and co-workers developed a phosphoric acid-catalyzed cascade reaction proceeding through aza-Friedel–Crafts reaction and lactonization steps. Main focus of this article was to demonstrate a racemic process between  $\alpha$ -naphthol or phenol derivatives and in situ-generated *N*-acetyl ketimine from methyl 2-acetamidoacrylate (**18**) in the course of preparing 3-NHAc-naphthofuran or benzofuran analogues. The achiral phosphoric acid (PhO)<sub>2</sub>P(O)OH was the catalytic reagent to execute the process delivering the products with low

to moderate chemical yields. Attempts to make the process stereoselective, a series of chiral phosphoric acid catalysts were screened in the model reaction between  $\alpha$ -naphthol (**17**) and methyl 2-acetamidoacrylate (**18**) but promising selectivity was not achieved. The highest enantiomeric excess of 64% was obtained in the presence of **P7** as the catalyst (Scheme 6) [30].

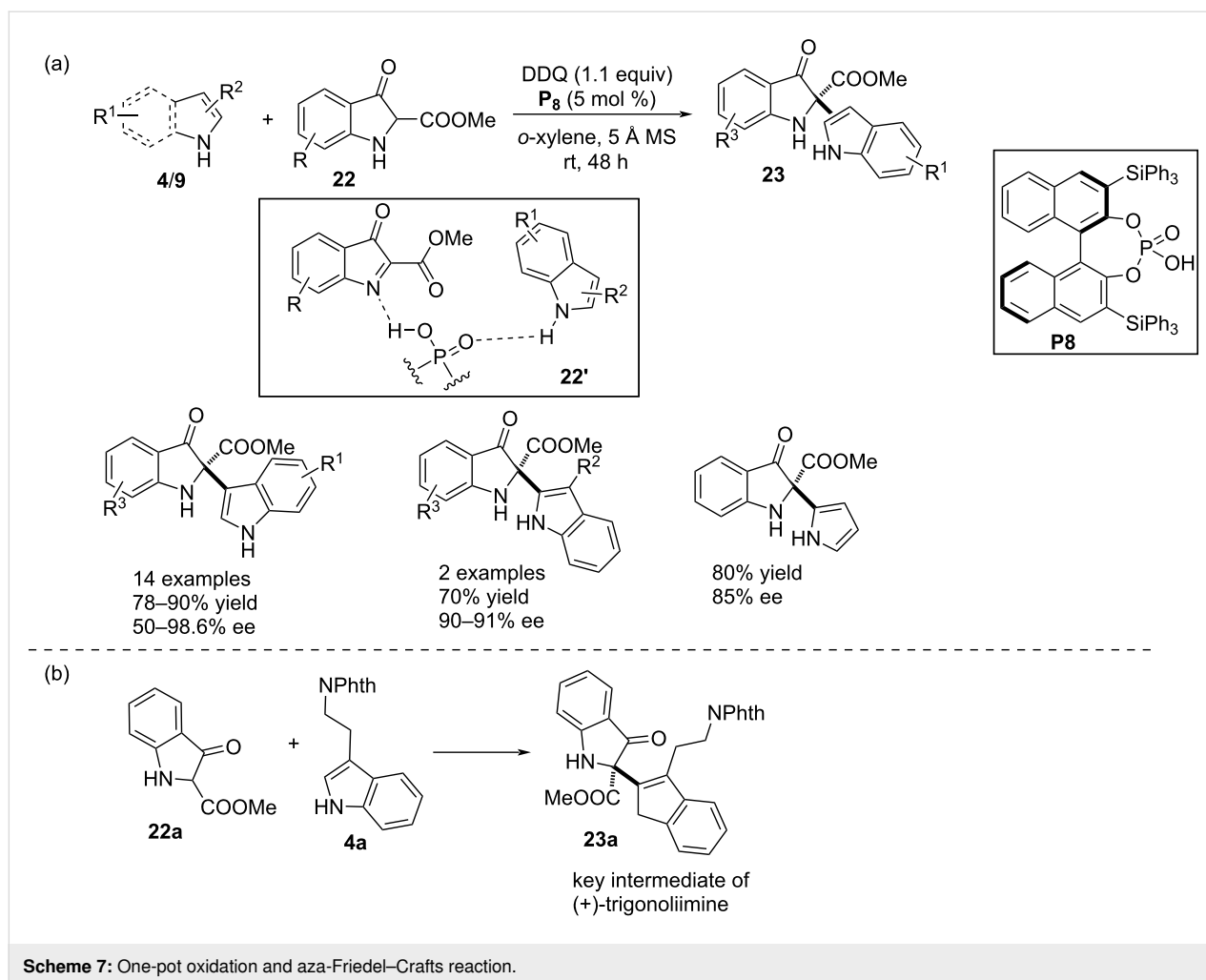
In 2018, Reddy and co-workers developed a one pot protocol comprising oxidation and an enantioselective aza-Friedel–Crafts addition. In the first step, the DDQ-promoted oxidation of 3-indolinonecarboxylate **22** generated indolenines that performed as the potential electrophiles towards indoles **4**. The chiral catalyst effectively assembled the reacting partners in a chiral transition state through H-bonding interactions to facilitate a highly face-selective nucleophilic attack by  $\pi$ -nucleophile to the cyclic imine (see transition state **22'** in Scheme 7a). The BINOL-derived chiral phosphoric acid **P8** was employed as the asymmetric organocatalyst for this transformation to construct the heterodimerized products **23** framed with an aza-quaternary stereocenter. Indole derivatives without any substitution in the



**Scheme 5:** Aza-Friedel–Crafts reaction involving N-unprotected imino ester as electrophile.



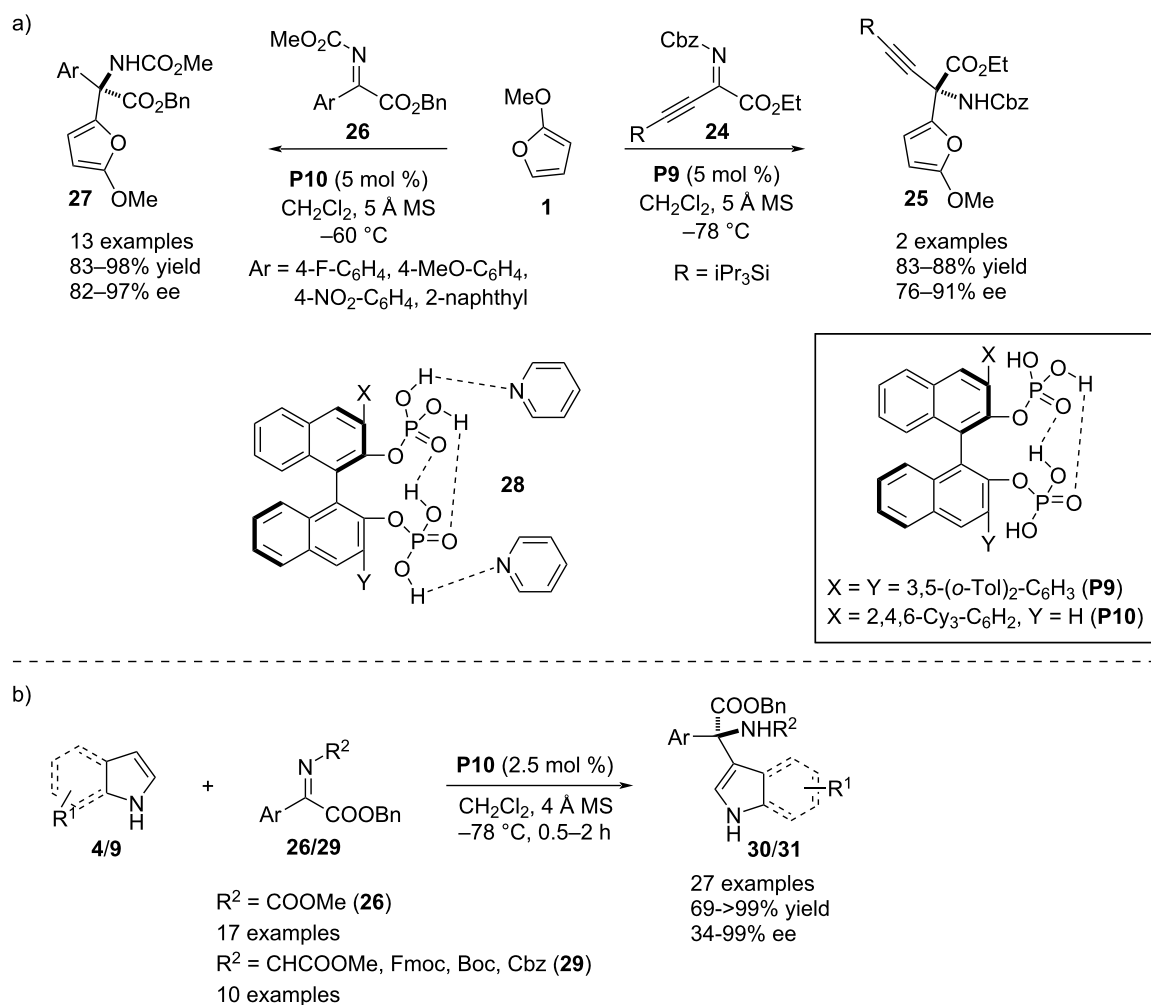
**Scheme 6:** Aza-Friedel–Crafts and lactonization cascade.



heterocyclic ring participated in the reaction through the C3 position smoothly providing the products with appreciable yields and enantiocontrol. Two examples were demonstrated with 3-alkyl-substituted indoles which effectively attacked the electrophile through the C2 position. The reaction was even compatible with pyrroles (Scheme 7a). The utility of this methodology was successfully demonstrated by the synthesis of product **23a**, the key intermediate of natural product (+)-trigonoliimine (Scheme 7b) [31].

In 2018, Ishihara and co-workers developed a novel  $C_2$  and  $C_1$ -symmetric bisphosphoric acid-catalyzed asymmetric aza-Friedel–Crafts reaction. Both catalysts showed intramolecular H-bonding causing a sharp increase in Brønsted acidity of free OH groups and prevention of catalyst dimerization. The  $C_2$ -symmetric **P9** promoted the reaction between 2-methoxyfuran (**1**) and  $\beta,\gamma$ -alkynyl- $\alpha$ -imino esters **24** to effect a C–C bond formation at the C2' position of the heterocyclic ring. Only two examples were shown by varying the alkynyl substituent. The authors further extended the scope by studying the

reaction between 2-methoxyfuran (**1**) and aryl- $\alpha$ -ketimino ester **26** to activate the C2'–H bond in **1**. The  $C_1$ -symmetric catalyst **P10** was the optimal catalyst for the second reaction furnishing the products with excellent chemical yields and enantioselectivities. To understand the activities of the catalysts, the authors were able to obtain X-ray crystallographic data of the pyridine–catalyst complex which showed two intramolecular H-bonding interactions in the molecular framework of the catalyst where two free OH groups were engaged in interactions with the pyridine. This data clearly indicates the activation of the reaction components through H-bonding engagement with free hydroxy groups of the catalysts also favoring stereoselective addition (see structure **28** in Scheme 8a) [32]. Two years later, the same research group utilized the  $C_1$ -symmetric catalyst **P10** for the functionalization of the C3–H bond of indole **9** through aza-Friedel–Crafts reaction with aryl- $\alpha$ -ketimino esters **26/29**. They also utilized unsubstituted and 2,3-disubstituted pyrroles **9** as  $\pi$ -nucleophile towards the same electrophiles to incorporate an amine-substituted quaternary stereocenter at the C2' position (Scheme 8b) [33].



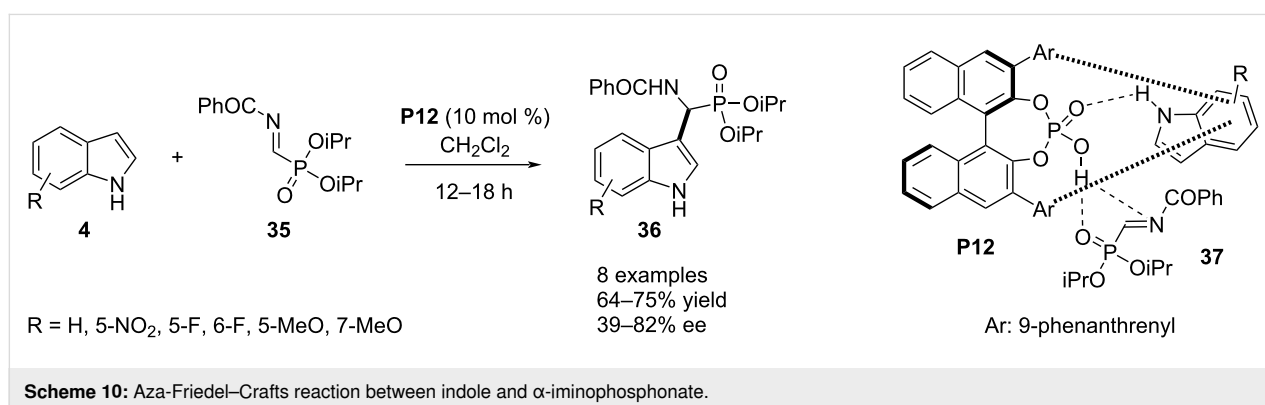
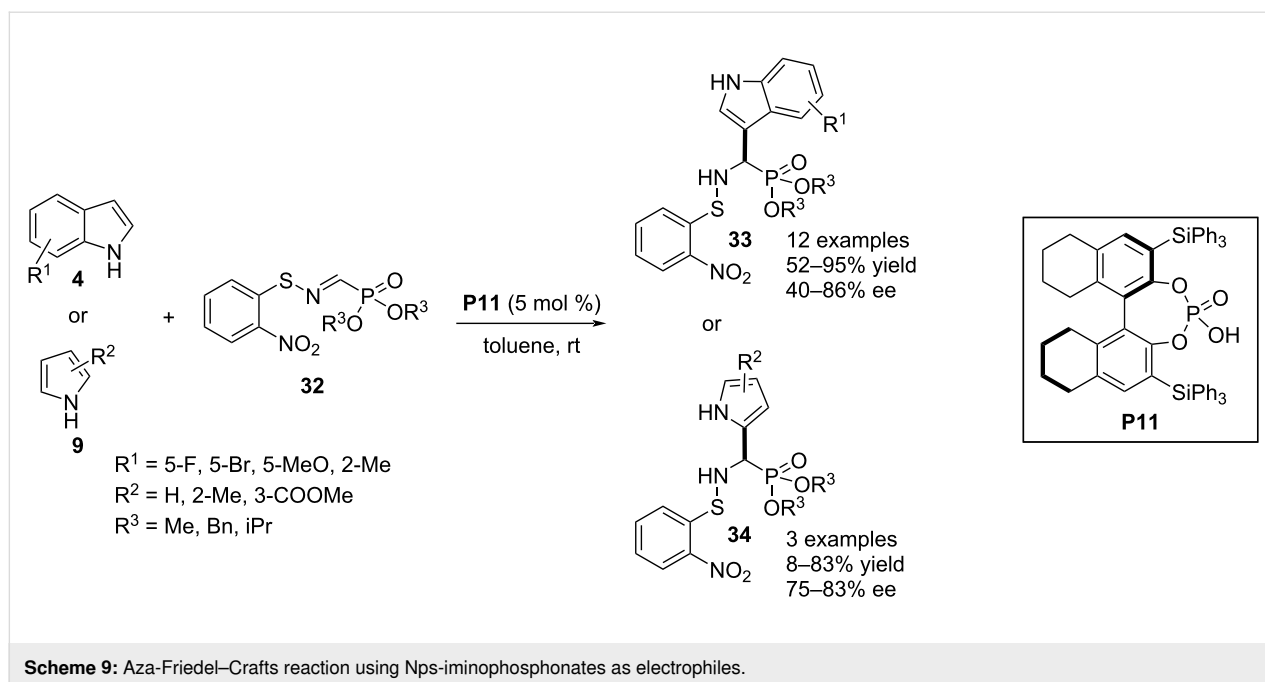
**Scheme 8:** C<sub>1</sub> and C<sub>2</sub>-symmetric phosphoric acids as catalysts.

In 2019, Inokuma, Yamada and co-workers reported the C3–H bond functionalization of indoles **4** through aza-Friedel–Crafts reaction utilizing *N*-*o*-nitrophenylsulfenyl (Nps)-iminophosphonates **32** as electrophiles. The chiral phosphoric acid **P11** was used as H-bonding catalyst to impart stereoselectivities into the products, i.e.,  $\alpha$ -3-indolyl- $\alpha$ -aminophosphonic acids **33**. The reaction was also well compatible with pyrroles **4** proceeding through C2–H substitution. With C2-substituted pyrrole, the electrophile enters into the C5 position (Scheme 9) [34].

In 2019, Palacios, Vicario and co-workers documented an aza-Friedel–Crafts reaction between indole **4** and  $\alpha$ -iminophosphonate **35**. The reaction functionalized the C3 position of the heterocyclic ring with an  $\alpha$ -aminophosphonate group. Chiral phosphoric acid **P12** was the stereoselectivity inducer in the products **36** as explained by  $\pi$ – $\pi$  stacking and H-bonding interactions between the catalyst and the substrates (see transition state **37** in Scheme 10). The presented substrate scope was not

broad and poor to moderate enantioselectivities were obtained. Indoles with a substituent in the carbocyclic ring required shorter reaction times to accomplish in comparison to C2-substituted indoles. The authors also tried the reaction with C3-substituted indoles to functionalize the C2 position. However, a very low enantioselectivity was achieved in the latter case (Scheme 10) [35].

Lin and co-workers designed a planar chiral phosphoric acid containing a [2.2]paracyclophane moiety that efficiently catalyzed the aza-Friedel–Crafts reaction between indole **4** and *N*-tosyl vinylaldehydes **38** to functionalize the C3–H bond of the heterocyclic ring. The authors tried six such catalysts by varying the aromatic substituents, among which **P13** was proved to be the best one in terms of both yields and enantioselectivity. The catalyst **P13** was an even far superior catalyst than conventional BINOL and SPINOL-derived phosphoric acids. The substrate scope was investigated by varying substitu-

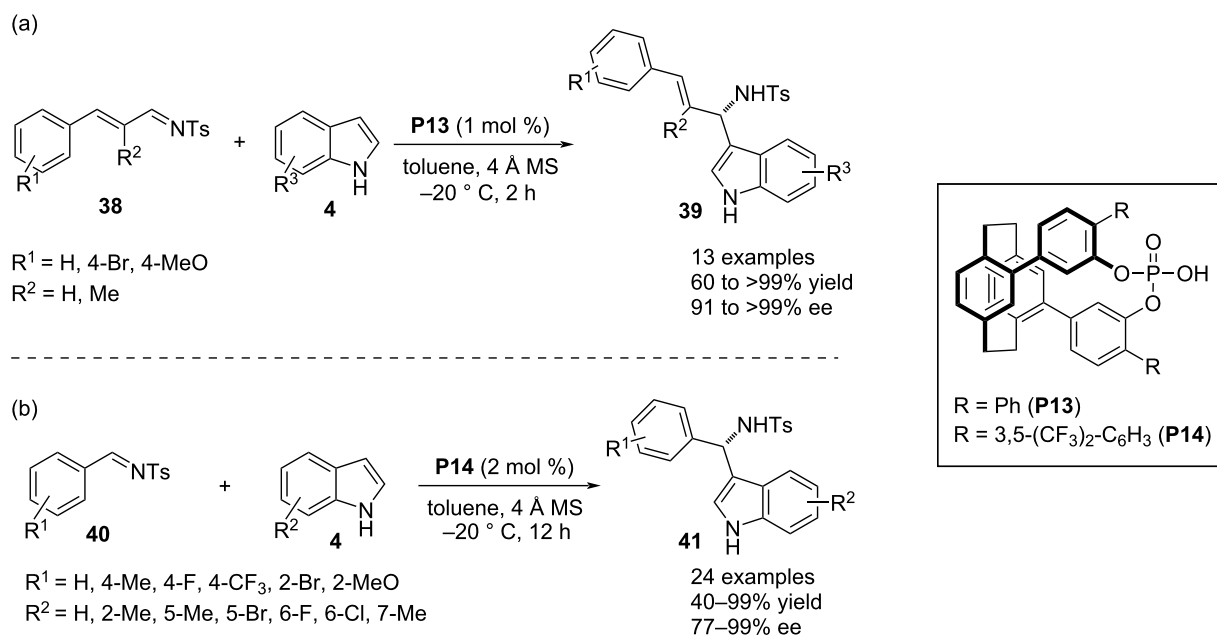


ents in the carbocyclic ring of indole **4**. Changing the  $\beta$ -aryl and  $\alpha$ -substituents in the styryl-derived aldimines further expanded the substrate scope. Only 1 mol % catalyst loading was sufficiently efficient to deliver the enantioenriched products (Scheme 11a). The compatibility of the reaction was further explored by using *N*-tosyl arylaldimines **40** as the electrophilic partner to afford (aryl)(indolyl)methanamines **41** with high enantioselectivities. In this case, **P14** was identified as the optimal catalyst (Scheme 11b) [36].

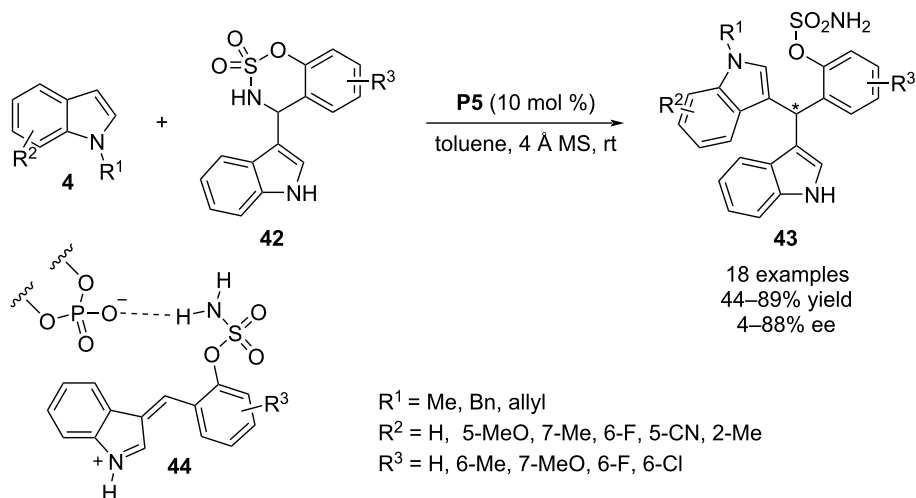
In 2019, Kim and co-workers reported a phosphoric acid-catalyzed enantioselective aza-Friedel–Crafts reaction between *N*-substituted indoles **4** and indol-3-ylsulfamidates **42**. The dual reactivity of catalyst **P5** initiated with the protonation of amidates **42** to generate intermediate **44** through ring cleavage. Then, the intermediate **44** was paired with the anionic conjugate base of catalyst **P5** and acts as electrophile to

facilitate the conjugate Friedel–Crafts reaction involving C3 of indole **4** as the nucleophile. This reaction afforded (bis(indolyl)methyl)benzenesulfonamide derivatives **43** but no promising enantioselectivity was achieved for most of the products (Scheme 12) [37].

In 2019, You, Yuan and co-workers reported another enantioefficient aza-Friedel–Crafts reaction between *N*-unsubstituted pyrroles/indoles **4/9** and isoquinoline-1,3,4(2*H*)-trione-1-imines **45** installing an aza-quaternary stereocenter in isoquinoline-1,3(2*H*,4*H*)-dione frameworks **46/47**. The spinol-derived catalyst **P15** was applied for the asymmetric induction through H-bonding interaction with the NH group of the heteroarene and amide oxygen of **45** forcing the heteroarene to approach from the *Si*-face of the imine moiety predominantly (see transition state **48**) achieving high enantiocontrol for both heterocycles (Scheme 13) [38].



**Scheme 11:** [2,2]-Paracyclophane-derived chiral phosphoric acids as catalyst.

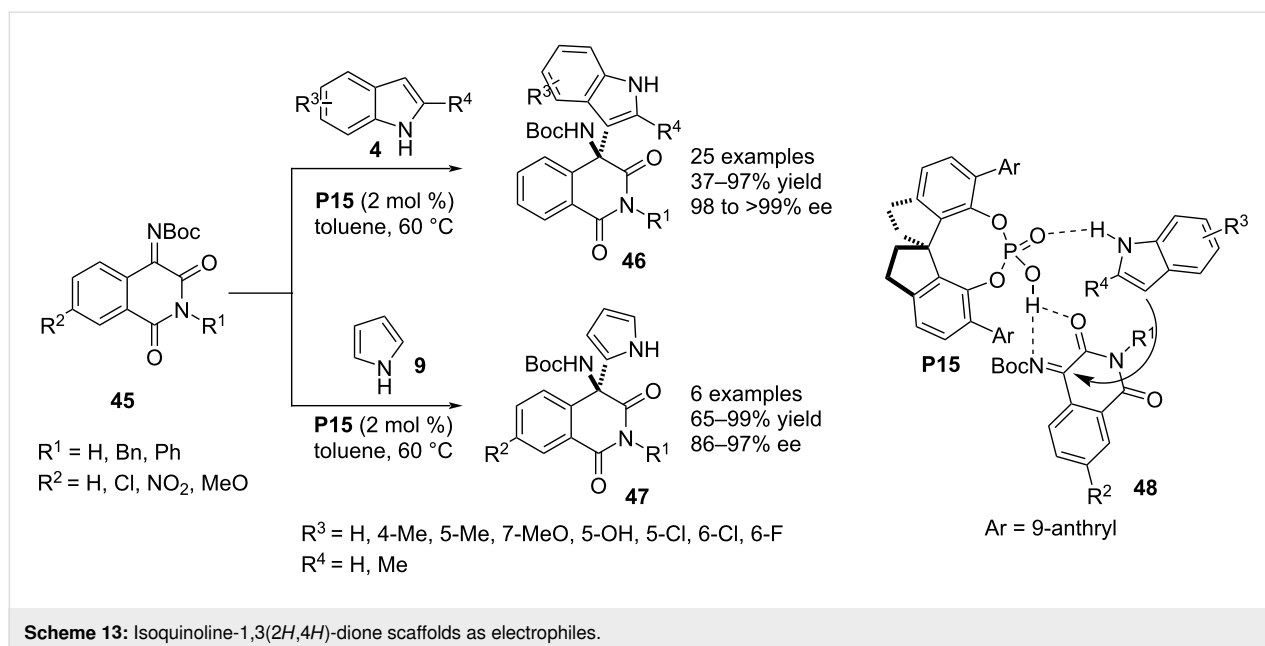


**Scheme 12:** Aza-Friedel–Crafts reaction through ring opening of sulfamidates.

The carbocyclic ring in indoles is less reactive than the heterocyclic ring and hence the presence of an electron-donating functional group is crucial in the ring to activate it for aromatic electrophilic substitution processes. In 2019, Zhang and co-workers succeeded in the C6-selective aminoalkylation of 2,3-disubstituted indoles **4** without the presence of a directing group in the benzene ring. As the electron-demanding reaction partner, isatin-derived *N*-Boc-substituted ketimines **49** were employed which effectively functionalized the C6–H bond of substrate **4** to construct 3-oxindole derivatives **50** bearing an indole-substituted aza-quaternary stereocenter at its C3 position. 2,3-Dialkyl-

substituted indoles having methyl or cycloalkyl substituents of different ring sizes exclusively reacted as nucleophiles. Chiral phosphoric acid **P16** mediated the asymmetric transformation to regulate the stereochemical output of the quaternary stereocenter with good to excellent enantioselectivities. A resonance-assisted accumulation of negative charge on C6 enabled the carbon to add to the electrophile selectively from the *Re* face of the imine plane because of substrate–catalyst H-bonding interactions (see transition state **51**). Beside multiple noncovalent interactions,  $\pi$ – $\pi$  stacking between the anthracenyl group of the catalyst framework and aromatic rings of both substrates was

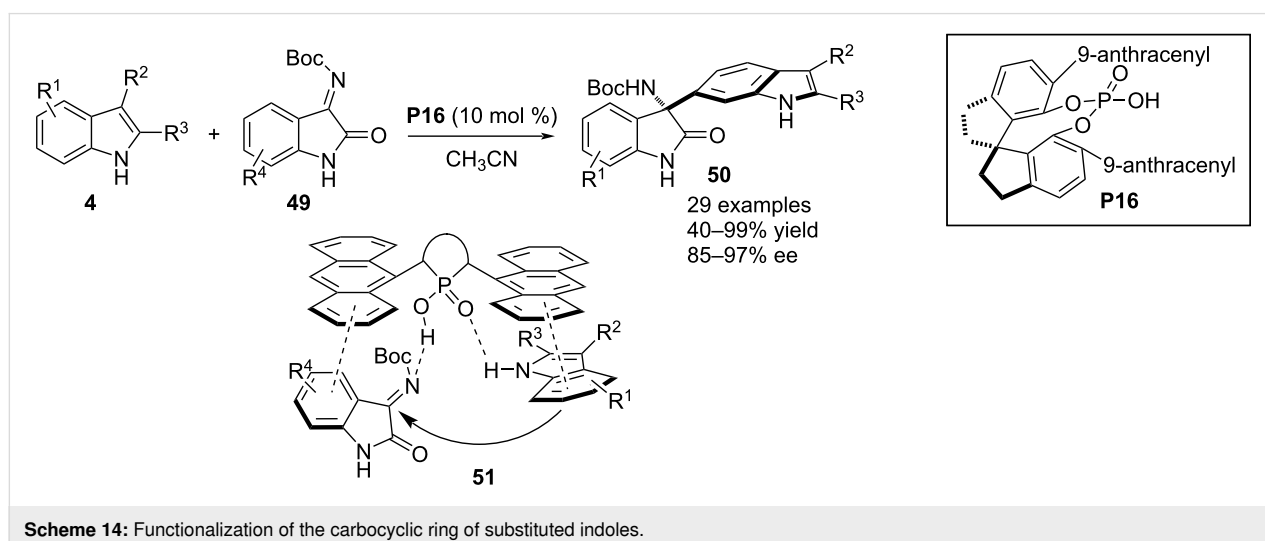


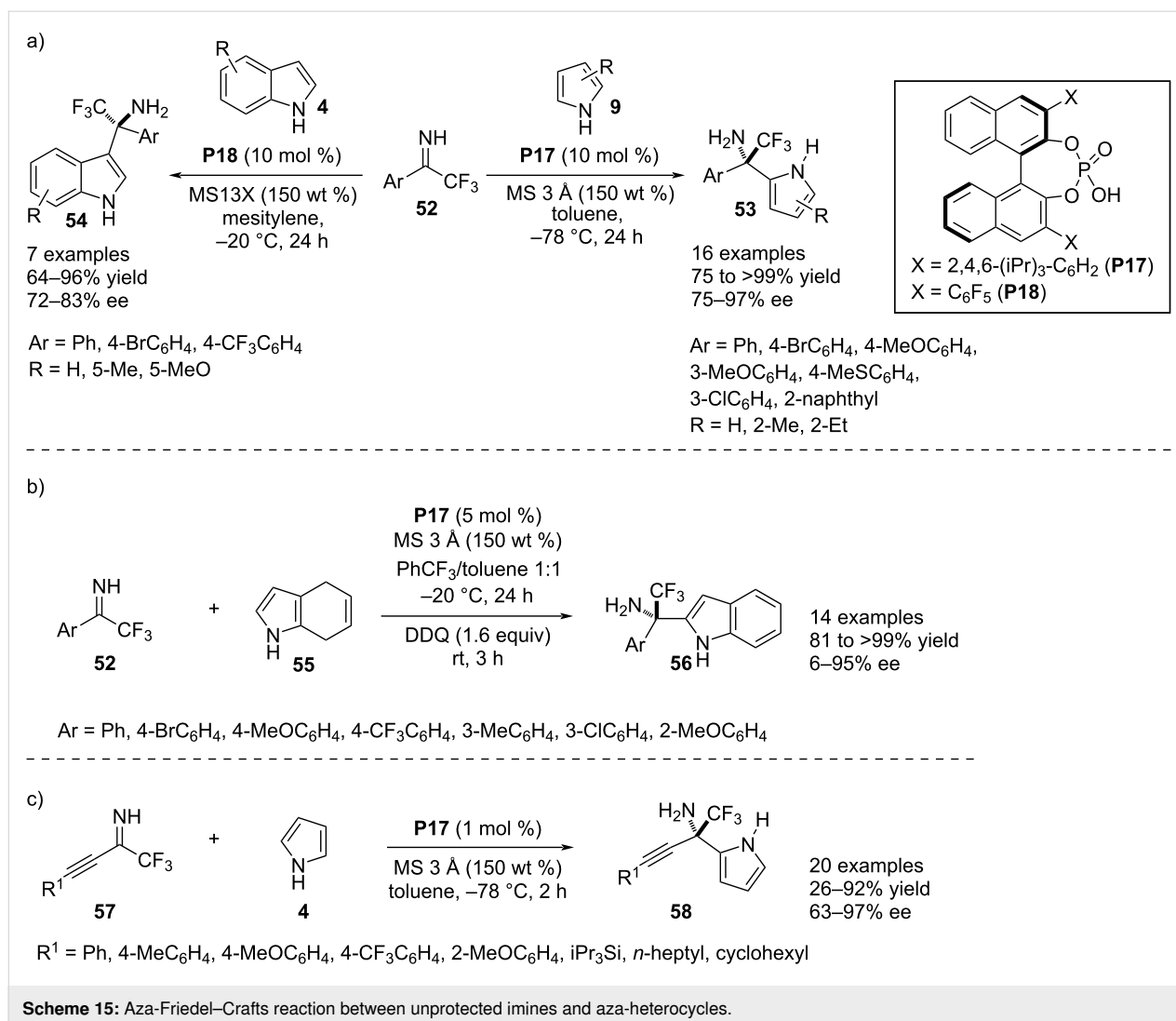


also responsible for the stereoselective addition (Scheme 14) [39].

In 2019, Akiyama and co-workers developed a simple enantioselective aza-Friedel–Crafts process using unprotected pyrroles **9** and indoles **4** mediated by BINOL-derived chiral phosphoric acid catalysts **P17** and **P18**. The electrophile was the  $\alpha$ -trifluoromethyl-containing imine **52** which directed the C2 functionalization in the pyrrole moiety with catalyst **P17** and a C3 substitution in indole derivatives using catalyst **P18** forming the trifluoromethylated aza-quaternary stereocenter. Excellent chemical yields and good to excellent levels of enantioselectivities in the products **53/54** were obtained by the chiral catalysts. The process was robust towards  $\alpha$ -aryl- and  $\alpha$ -trifluoromethylim-

ines and the substrate scope was mainly investigated by the variation of electron-donating groups in the aryl ring of the imines whereas amenability of this methodology was narrow for ring-substituted pyrroles and indoles (Scheme 15a) [40]. In the next year, the same research group reported another aza-Friedel–Crafts reaction between 4,7-dihydroindole (**55**) and N-unsubstituted trifluoromethylated ketimines **52** proceeding through C2 functionlization and follow up oxidation to provide 2-substituted indoles **56** which are typically difficult to obtain directly from unsubstituted indoles through electrophilic substitution. The process was catalyzed by the chiral phosphoric acid **P17** to install a quaternary stereocenter bearing primary amine and trifluoromethyl functionalities associated with appreciable enantiocontrol. The substrate scope was investigated by the

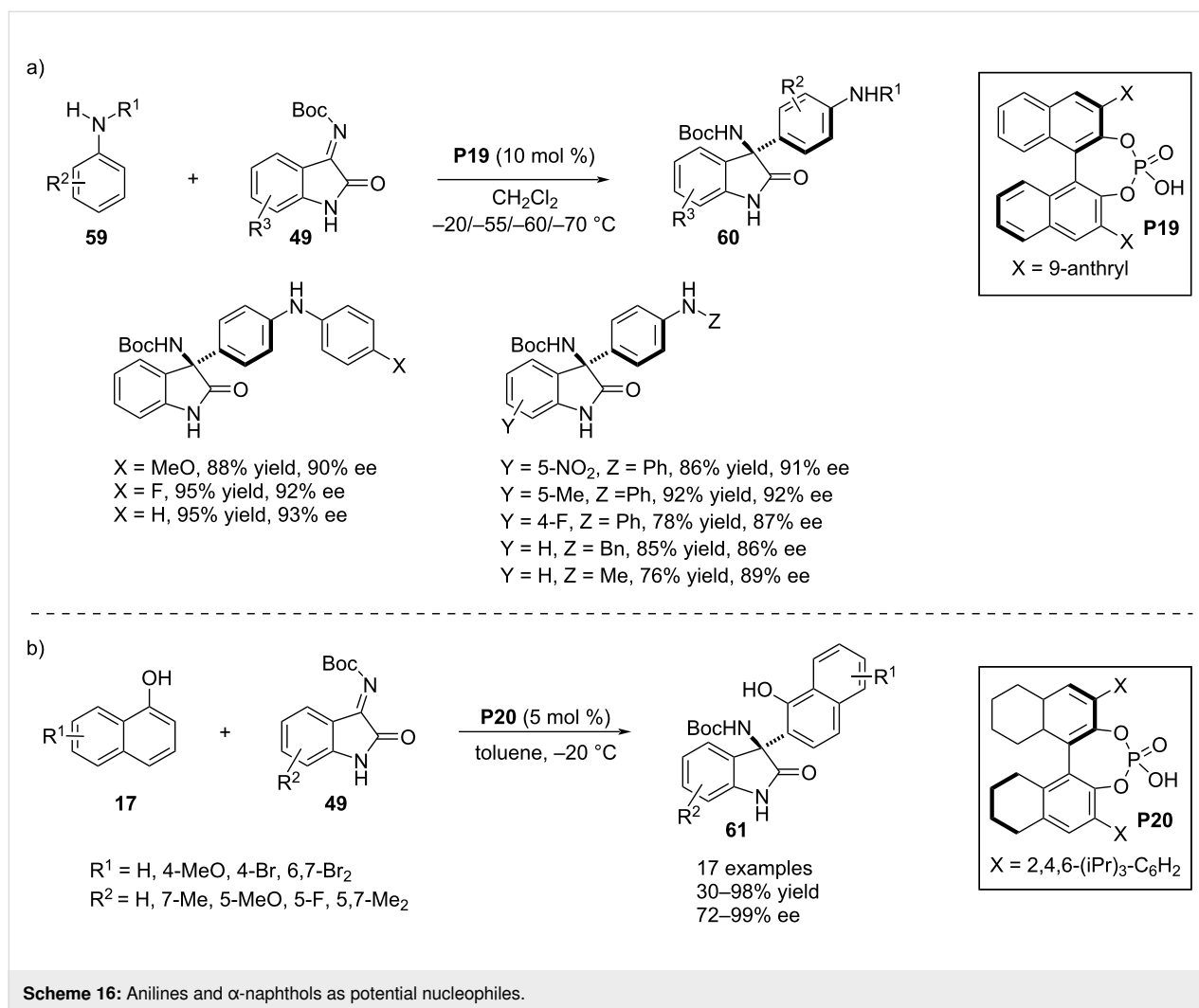




variation of sterically and electronically divergent aryl substituents in the ketimines but the enantioselectivity was markedly lowered with sterically congested reactants (Scheme 15b) [41]. Very recently, Akiyama and co-workers demonstrated a C2-selective aza-Friedel–Crafts reaction of unmodified pyrroles **9** with (alkynyl)(trifluoromethyl)imines **57** catalyzed by the chiral phosphoric acid **P17**. This reaction produced an aza-quaternary stereocenter bearing 2-pyrrolyl, trifluoromethyl and alkynyl as other three substituents (Scheme 15c) [42].

In 2020, a completely *para*-selective aza-Friedel–Crafts protocol with *N*-monosubstituted aniline derivatives **59** catalyzed by the chiral phosphoric acid **P19** was disclosed by Zhu, Zhang and co-workers [43]. The electrophilic aromatic substitution involved isatin-derived ketimines **49** as the electron-demanding partner to achieve this aromatic *p*-C–H bond functionalization framing an all substituted stereocenter at the C3 position of the oxindole scaffold in the products **60**. A very low

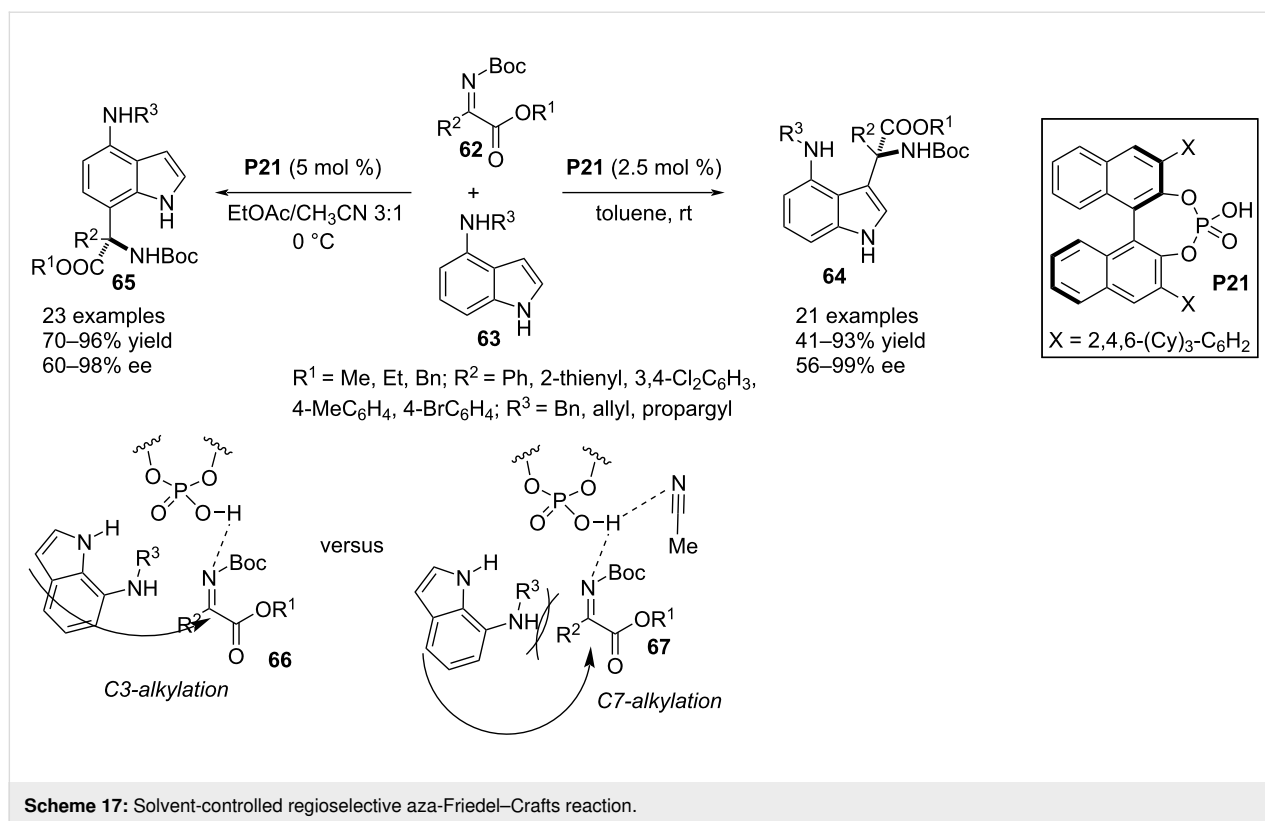
reaction temperature (–55/–60 °C) was ideal to obtain the products with satisfactory enantioselectivities. The reaction was compatible with a broad range of substrates using *para*-substituted phenyl rings as the nitrogen substituents in anilines **59**. Two examples were shown with *N*-benzyl and *N*-methyl-substituted anilines which afforded the desired products as well but an elevated temperature was required for these reactions. Further expansion of the substrate scope was achieved by altering functionalities with contrasting electronic and steric nature in the benzene ring of substrate **49**. Generally high enantioselectivities were obtained with *N*-aryl-substituted anilines **59** which decreased in case of *N*-alkyl-substituted anilines. This observation led to the development of a plausible transition state of the stereoselective electrophilic addition which included dual H-bonding interactions between both the substrates and the catalyst along with  $\pi$ – $\pi$  interactions between the catalyst's aryl group and the aryl substituent at the nitrogen in the aniline **59** (Scheme 16a) [43]. Recently, Fan and co-workers reported a

Scheme 16: Anilines and  $\alpha$ -naphthols as potential nucleophiles.

chiral phosphoric acid **P20**-assisted enantioselective aza-Friedel–Crafts reaction between  $\alpha$ -naphthols **17** and isatin-derived ketimines **49** to construct an aza-quaternary stereocenter at the C3 position of oxindole scaffolds **61** bearing a  $\beta$ -naphtholyl substituent (Scheme 16b) [44].

In 2020, Meng, Chan, Zhao and co-workers reported another C3-selective aza-Friedel–Crafts reaction of 4-aminoindole derivatives **63** utilizing *N*-Boc- $\alpha$ -ketimino esters **62** as potential electrophiles. The chiral phosphoric acid **P21** catalyzed this process facilitating the formation of a quaternary stereocenter containing  $\alpha$ -amino esters. Switching the solvent from non-polar to polar showed a regioselectivity shift to a C7 alkylation of the indole ring. The solvent-controlled regioselectivity switch of this aza-Friedel–Crafts reaction can be explained by the involvement of the polar solvent (acetonitrile) in the H-bonding with the catalyst thus creating a more hindered environment for a C3 alkylation, rather favoring the reaction through the less congested site (see transition states **66** and **67**, Scheme 17) [45].

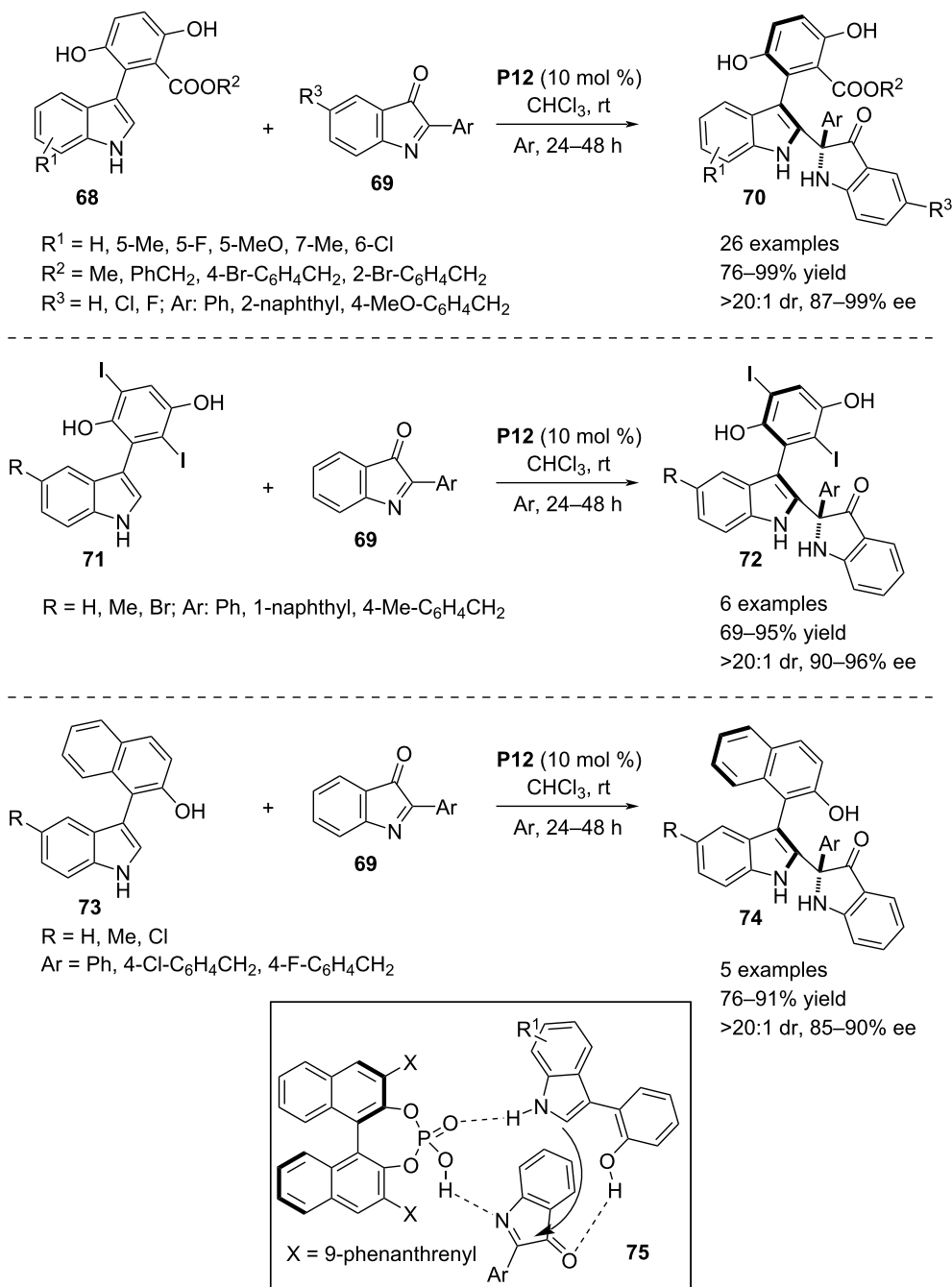
In 2020, Fu and co-workers developed a novel aza-Friedel–Crafts reaction between 3-arylindoles **68** and 2-aryl-3*H*-indol-3-ones **69** activating the C2–H bond of the heteroaromatic ring. Chiral phosphoric acid **P12** catalyzed this transformation generating a complex molecular topology of 2,3-disubstituted indoles bearing both axial and central chirality. The aza-Friedel–Crafts reaction would allow the nucleophile to selectively attack the C=N plane of the electrophile as directed by a triple hydrogen-bonded complex between the catalyst and the substrates (see transition state **75**, Scheme 18). This C–C bond formation affords a 3-indolinone moiety bearing an aza-quaternary stereocenter at the C2 position. In addition, the reaction allows to obtain axially chiral products **70/72/74** through restriction of the C–C bond rotation around the heteroaryl and aryl moieties. For this purpose, sterically bulky substituents need to be present in the aryl ring attached to the C3 position of the starting indoles. The axial chirality was attributed to ester and phenolic OH groups at the *ortho*-positions of the aryl ring and an additional phenolic OH functionality at the *meta*-posi-



tion (substrate **68**). Some more substrates were prepared by introducing a 2,5-diiodo-3,6-dihydroxyphenyl substitution at the C3 position of the indole ring (substrate **71**). The products were formed with high chemical yields and excellent diastereo- and enantioselectivities. A further expansion of the substrate scope was demonstrated by incorporating a  $\beta$ -naphthol ring as the C3 substituent of the indole moiety (substrate **73**). In all classes of bi(heteroaryl) substrates, a phenolic OH group at the *ortho*-position was crucial as it was involved in an intermolecular hydrogen bonding with the carbonyl oxygen of **69** in the ternary complex, thus bringing more rigidity in the three dimensional transition state (Scheme 18) [46].

In 2021, Chen and co-workers documented a chiral phosphoric acid **P17**-catalyzed aza-Friedel–Crafts process between racemic 2,3-dihydroisoxazol-3-ol derivatives **76** and pyrroles/indoles **4/9** allowing access to 2,3-dihydroisoxazoles **77/78** bearing an all-substituted stereocenter at the C3 position. A dual catalytic activity of the Brønsted acid catalyst was illustrated by the authors which was initiated with a smooth protonation of the OH group in **76** with a subsequent dehydration to generate isoxazolium cation **80** paired with a phosphate anion. This chiral phosphate is engaged in H-bonding with the free NH of the heteroarene ring to ease the stereoselective 1,2-addition to in situ generate the cationic heterocyclic scaffold **81**. The reaction proceeded faster with pyrroles than with indole (Scheme 19) [47].

In 2021, Zhang and co-workers used 5-aminoisoxazole scaffolds **82** in an enantioefficient aza-Friedel–Crafts reaction with isatin-derived *N*-Boc ketimines **49**. A 2-oxindole-substituted aza-quaternary stereocenter was installed at the C4 position of the heteroaromatic ring in **83** and the enantiocontrol was achieved by BINOL-derived chiral phosphoric acid **P22**. An amine functionality was crucial in the isoxazole ring to enhance the nucleophilicity of the adjacent carbon atom. In addition, the amine hydrogen forms an H-bond with the catalyst along with another hydrogen bond formed between the imine nitrogen of **49** and the catalyst's OH group (see transition state **84**). These dual H-bonding interactions were assisted by a  $\pi$ – $\pi$  interaction between the arene rings of both the electrophile and nucleophile that helped in the formation of a stereodefined transition state. The substrate scope was achieved by varying the substituents in the C3 position of the isoxazoles **82** and the carbocyclic ring substituents in ketimines **49**. Few more products were added to the library by altering the substituents of the amine in **82** and the ring nitrogen in **49** (Scheme 20a) [48]. The nucleophilicity of C3-substituted 5-aminoisoxazoles **82** was further utilized in another aza-Friedel–Crafts reaction with  $\beta,\gamma$ -alkynyl- $\alpha$ -ketimino esters **86** to provide *N*-Boc  $\alpha$ -amino esters containing a quaternary stereocenter at the  $\alpha$ -carbon. The chiral phosphoric acid **P22** was used as catalyst to introduce the aza-ester quaternary stereocenter in the molecular entities **87** with appreciable chemical yields and excellent enantioselectivities. One

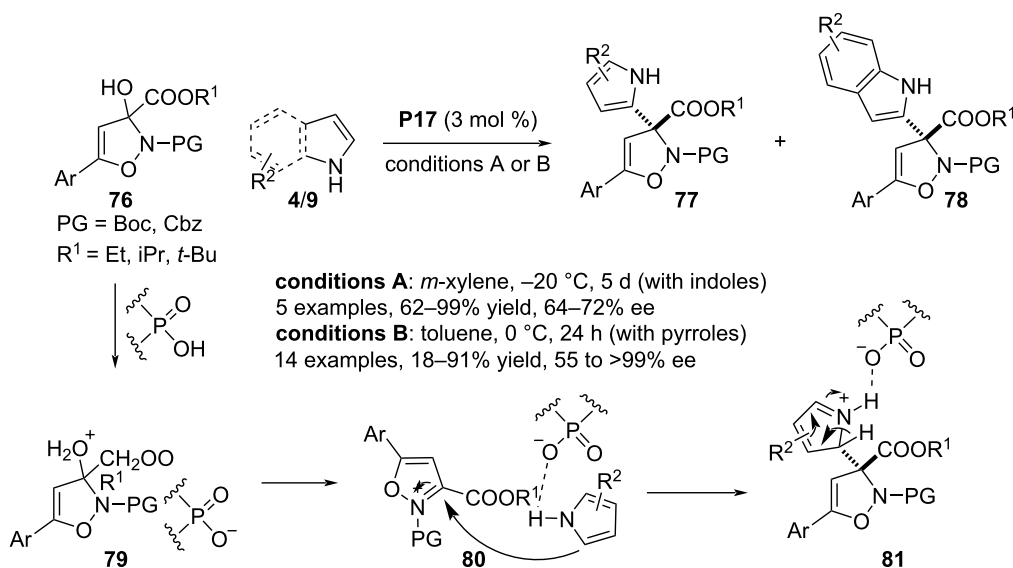


**Scheme 18:** Generating central and axial chirality via aza-Friedel–Crafts reaction.

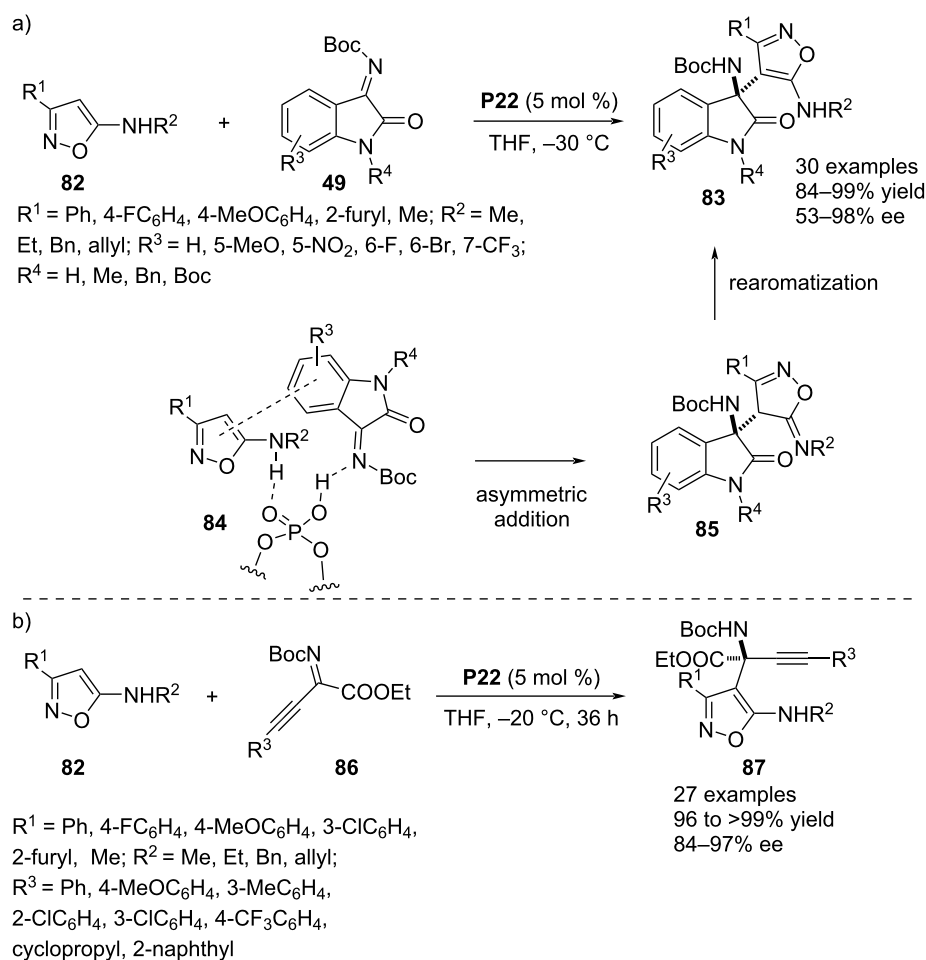
example was presented with a 5-aminoisothiazole motif that gave the product with much decreased yield (70%) and enantioselectivity (36% ee) (Scheme 20b) [49].

In 2022, Sun, Li and co-workers developed an aza-Friedel–Crafts technique involving 3-alkynylated 3-hydroxy-1-oxoisindolines **88** as electrophiles in combination with unsub-

stituted indoles **4** in the presence of chiral phosphoric acid *ent*-**P17** as the catalytic agent. Facile dehydration of **88** was facilitated by the Brønsted acid to generate (*N*-acyl)(propargyl)imine **90** as intermediate which added to the deprotonated phosphoric acid to form phosphate ester **91** as the next intermediate through an equilibrium process. Then, 1,2-addition by the C3 position of the heteroarene ring to the acylimine intermediate afforded the



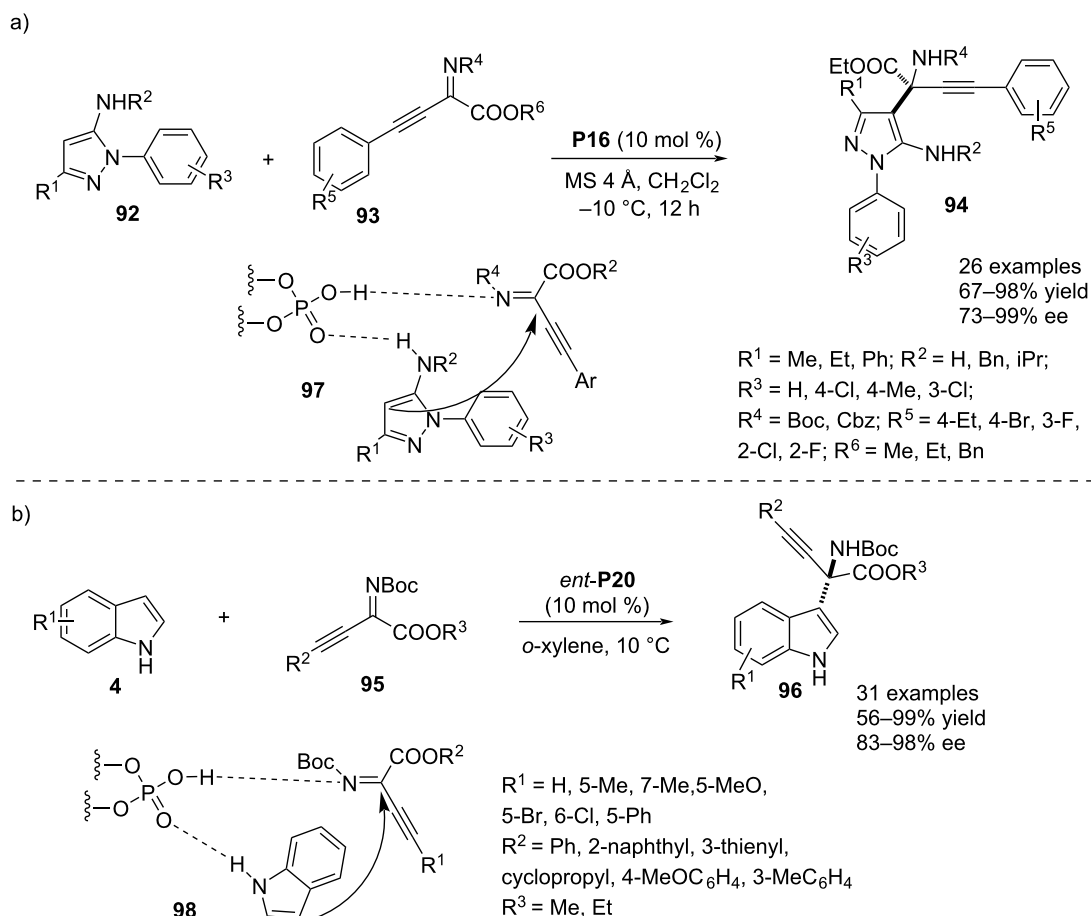
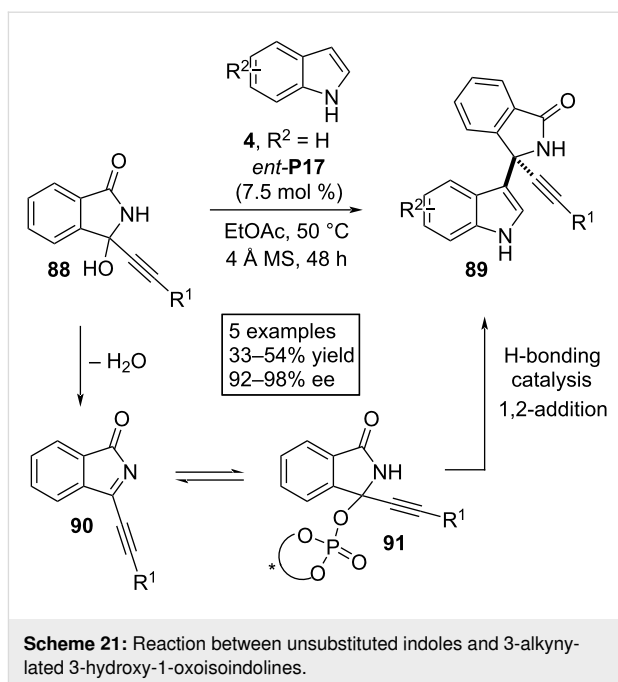
Scheme 19: Reaction between indoles and racemic 2,3-dihydroisoxazol-3-ol derivatives.



Scheme 20: Exploiting 5-aminoisoxazoles as nucleophiles.

3-indolyl-substituted aza-quaternary stereocenter. Here the stereoselectivity was attributed to an H-bonding interaction between the catalyst and the substrates (Scheme 21) [50].

In 2022, Lin and co-workers reported an unusual aza-Friedel–Crafts reaction using *N*-aryl-5-aminopyrazoles **92** as potential  $\pi$ -nucleophiles in combination with  $\beta,\gamma$ -alkynyl- $\alpha$ -imino esters **93** acting as the electrophilic reagent. Chiral phosphoric acid **P16** was the catalytic agent to access a series of enantioenriched  $\alpha$ -amino esters **94** containing 5-aminopyrazolyl and alkynyl substituents at the  $\alpha$ -carbon. A library of products was prepared by varying different parts of both nucleophile and electrophile. The enantioselectivity of the reaction was an obvious result of a dual H-bonding interaction between the catalyst and both substrates where the imine nitrogen of **93** acted as H-bond acceptor and the amine functionality in **92** as H-bond donor to the catalyst (see transition state **97**, Scheme 22a) [51]. Recently, the same research group documented another aza-Friedel–Crafts reaction between indoles **4** and **95** that frames aza-quaternary stereocenter at the  $\alpha$ -carbon



**Scheme 22:** Synthesis of unnatural amino acids bearing an aza-quaternary stereocenter.

of unnatural amino acid derivatives **96**. Enantiocontrol was rationalized by dual H-bonding interactions between both the reagents and the catalyst. The indole's NH performed as the H-bond donor whereas the imine nitrogen of **95** was the H-bond acceptor towards the catalyst enabling a face-selective attack by the  $\pi$ -nucleophile to the electrophile C=N plane (see transition state **98**). The substrate scope comprised mainly varying aryl or heteroaryl-substituents at the alkyne moiety that imparted high degrees of enantioselectivities to the products (Scheme 22b) [52].

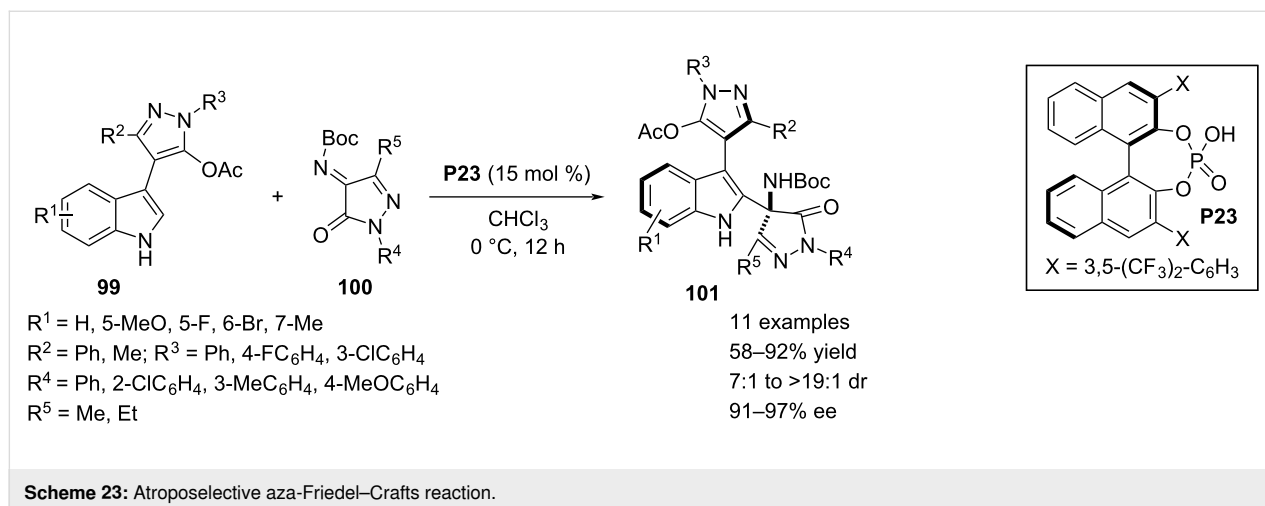
In 2022, Huang and co-workers demonstrated an atroposelective construction of 3,4'-indole-pyrazole frameworks achieved through an asymmetric aza-Friedel–Crafts reaction. As substrate the authors chose the racemate of indole moiety **99** bearing a 5-acetyloxypyrazol substitution at the C3 position which was coupled with the pyrazolone-derived imine **100** to functionalize the C2–H bond of the indole ring. This aromatic electrophilic substitution also gave a quaternary aza-stereocenter in the pyrazolone moiety. Axial chirality associated with central chirality in the product structures was influenced by chiral phosphoric acid catalyst **P23**. To freeze the C–C bond rotation, the pyrazole moiety in **99** required sterically demanding substituents. Excellent dia- and enantioselective synthesis of the products were caused by a chiral environment induced in the transition state through a dual H-bonding interaction between both the substrates and catalyst. In addition,  $\pi$ – $\pi$  stacking between the aromatic moieties in both reagents brought more rigidity in the corresponding transition state (Scheme 23) [53].

In 2023, a chiral phosphoric acid *ent*-**P17**-mediated aza-Friedel–Crafts alkylation was reported between 5-aminopyrazole **92** as the  $\pi$ -nucleophile and 3*H*-indol-3-ones **69** as electrophilic reagents. The presence of an amino group in pyrazole **92** is necessary as it is engaged in the H-bonding interaction with

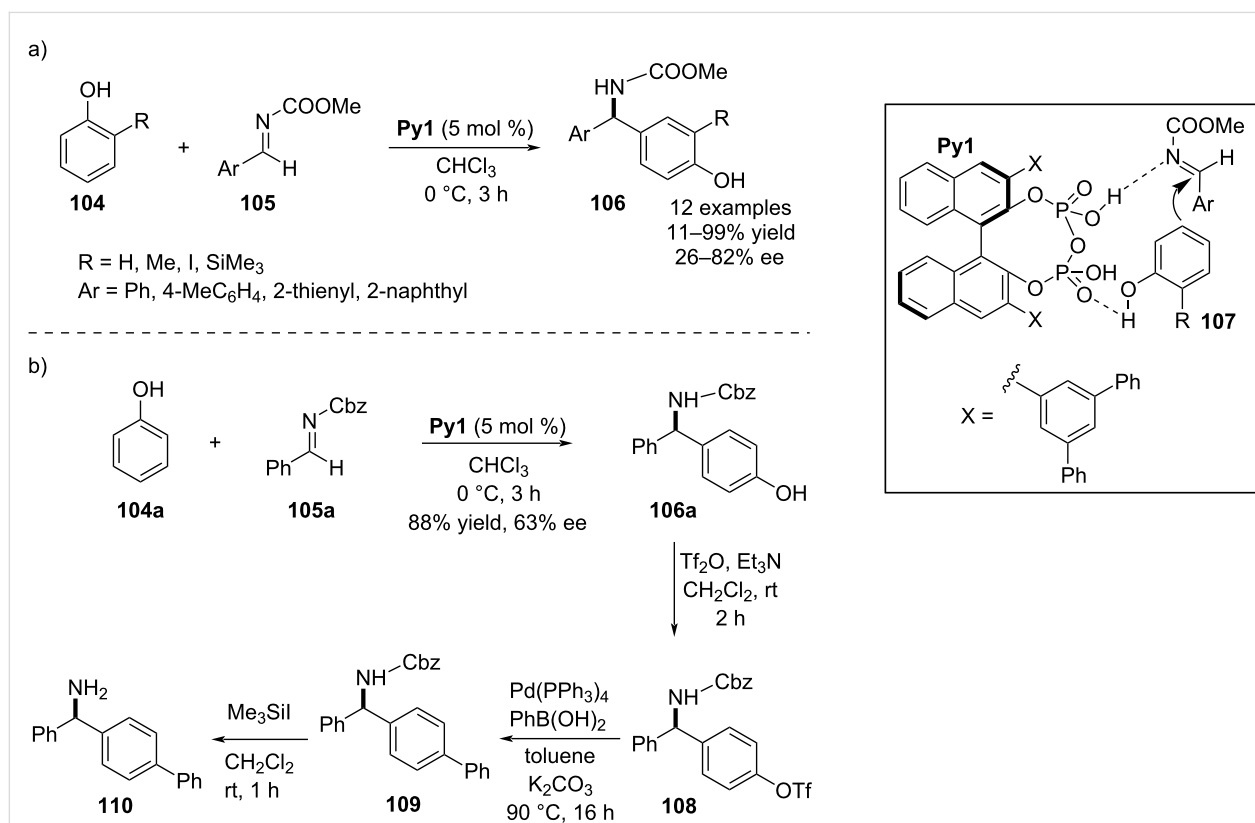
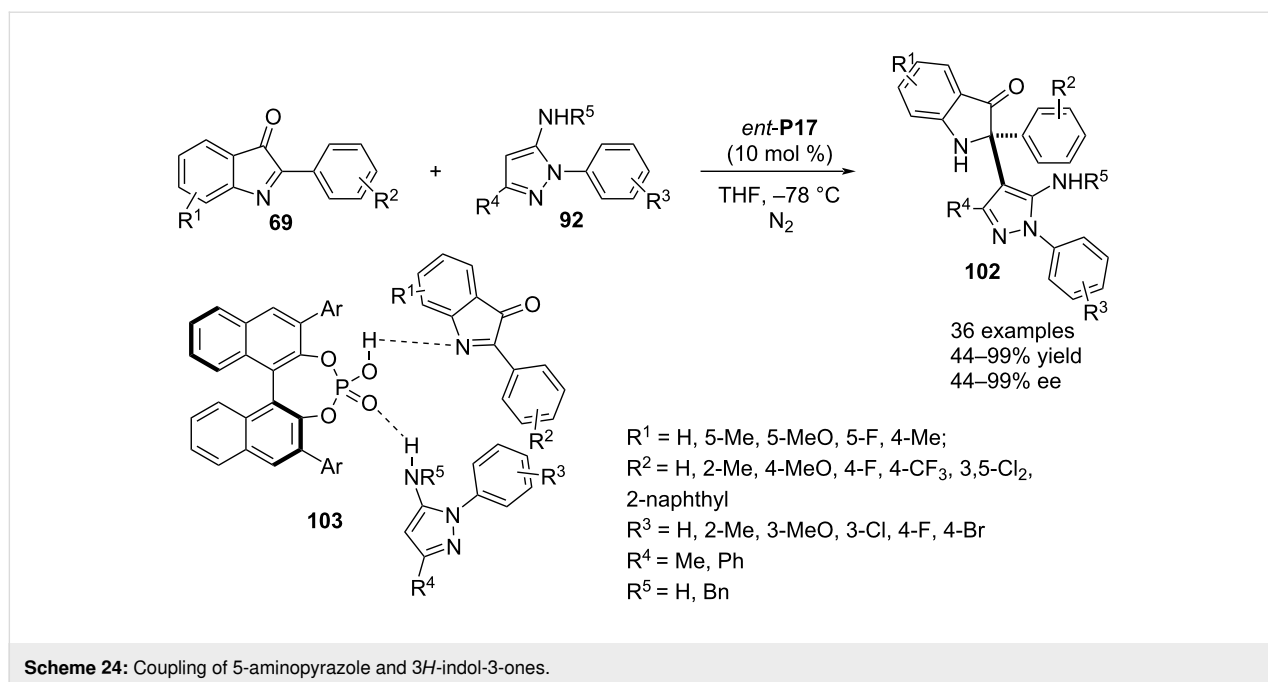
the catalyst P=O moiety whereas the imine nitrogen of **69** accepts an H-bond from the catalyst OH group (see transition state **103**). These dual noncovalent interactions were the reason behind a highly face-selective attack by the *ortho*-carbon of the aromatic amine functionality to the cyclic imine allowing a facile access of indolin-3-ones **102** attached to a 5-aminopyrazolyl-substituted aza-quaternary stereocenter via the C2 position. The reaction was very well compatible with various aryl substituents as well as different groups on the benzene ring of indolones **69**. Further broadening of the substrate scope was achieved by changing the aryl substituent attached to the pyrazole ring nitrogen. For enantioenrichment of the products, the presence of a methyl group at the C3 position of the pyrazole ring was obligatory. One example was included with a phenyl substituent at the aforesaid position for which a much diminished enantioselectivity (44%) was obtained (Scheme 24) [54].

## Pyrophosphoric acids

In 2018, Ishihara and co-workers demonstrated a highly *para*-selective aza-Friedel–Crafts process using phenols and *ortho*-monosubstituted phenol analogues **104**. As potential electrophiles, *N*-methoxycarbonyl-substituted aldimines **105** were explored to activate the *para*-carbon of the phenol derivatives catalyzed by the chiral pyrophosphoric acid **Py1**. The high regioselectivity was mainly caused by catalyst–substrate interactions via intermolecular H-bonding which could force the  $\pi$ -nucleophile to approach from the less sterically congested *para*-position. As *ortho*-substituents in the phenol derivatives, mainly sterically bulky alkyl, silyl, and iodo groups were incorporated to ensure the complete regioselectivity. On the other hand, various aromatic aldehyde-based aldimines were examined as electrophilic partners. Enantioincorporation into the products was explained by a *Si*-face attack of the nucleophile to the C=N plane. However, this process was not very promising in terms of enantioselectivities (Scheme 25a). The synthetic ap-







plicability of this asymmetric process was shown by synthesizing **110**, a key intermediate of (*R*)-bifonazole (Scheme 25b) [55].

## Thioureas and squaramides

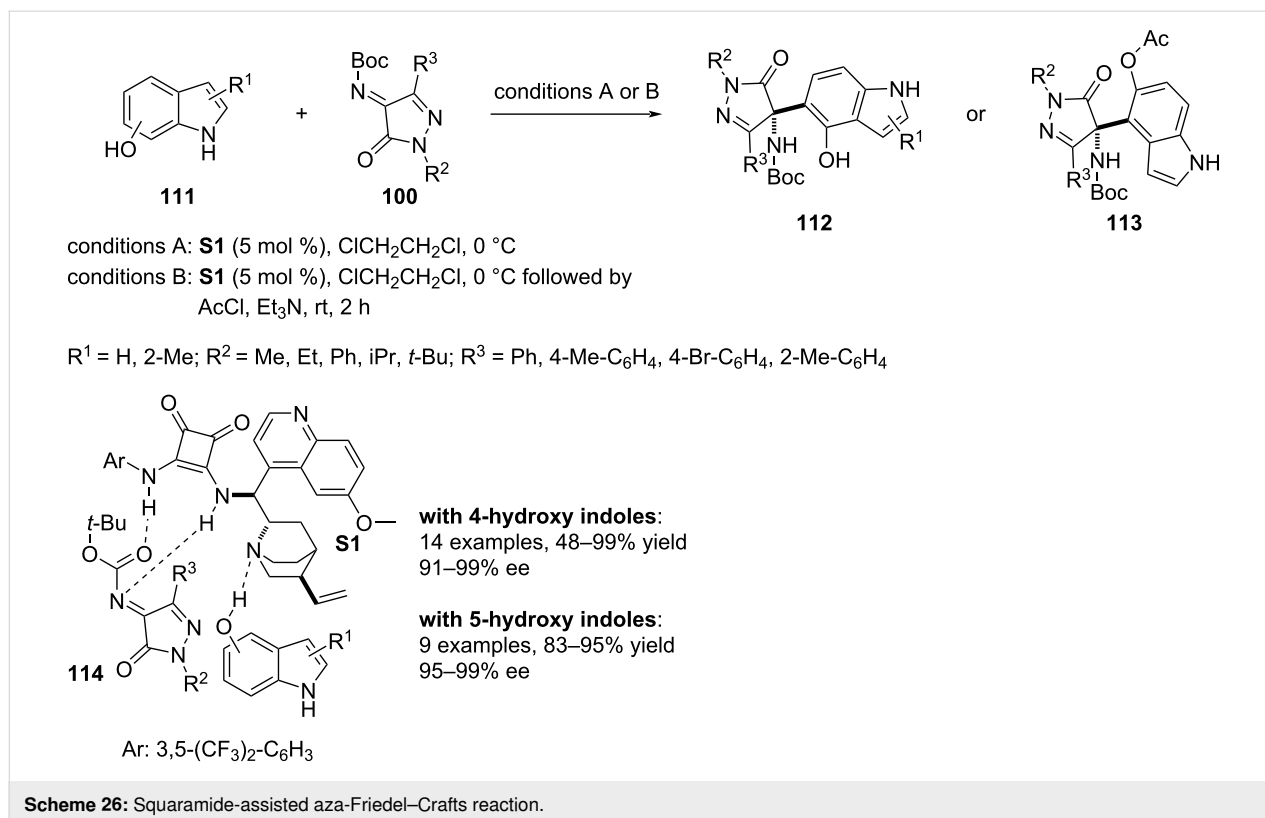
In 2018, Yang, Deng and co-workers developed an aza-Friedel–Crafts aminoalkylation of 4- and 5-hydroxyindoles **111**.

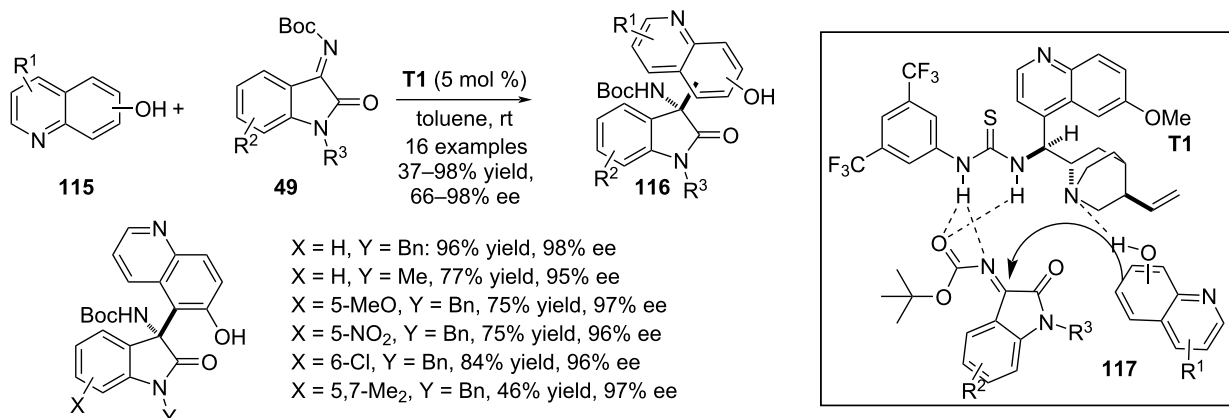
As electron-demanding component, *N*-Boc pyrazolinone ketimines **100** were investigated to install the all-substituted aza-quaternary stereocenter at the C4 position of the pyrazolinone scaffold. Stereoinduction on this chiral center was regulated by the chiral squaramide catalyst **S1** affording the products with excellent enantioselectivities. A stereodefined transition state organized by triple H-bonding interactions between the catalyst and the substrates controls the enantioefficiency of this process (see transition state **114**). The substrate scope was broader with 4-hydroxyindoles to functionalize the C5–H bond whereas a bit narrower substrate scope was achieved with 5-hydroxyindoles allowing the 4-indolyl-substituted stereocenter formation. In both cases, few more products were added by altering N1 and C3 substituents of **100** (Scheme 26) [56].

In the same year, a quinine-derived chiral thiourea-mediated aza-Friedel–Crafts reaction between hydroxyquinolines **115** and isatin-derived ketimines **49** was reported by Vila, Pedro and co-workers. Regioisomeric hydroxyquinolines were tested in this reaction to facilitate the electrophilic aromatic substitution on the *ortho*-carbon atom with respect to the hydroxy group in quinolines **15**. The reaction affords oxindole scaffolds **116** with a hydroxyquinoline-substituted aza-quaternary stereocenter in the 3 position. Most of the examples in this report involved 6-hydroxyquinoline as nucleophile whereas two examples each were presented with 5- and 7-hydroxyquinolines, respectively.

Both the imine nitrogen and the carbonyl oxygen of the *N*-substituted Boc group of **49** were H-bonded with NH groups of the thiourea framework whereas the hydroxy functionality of **116** engaged itself in H-bonding with the quaternary nitrogen of the catalyst (see transition state **117**). These noncovalent interactions were responsible for the stereochemical output of the reaction furnishing the products with moderate to excellent enantioselectivities. Electronically and sterically divergent functionalities in the benzene ring of **49** expanded the substrate scope whereas variation of **115** was very much limited (Scheme 27) [57].

In 2021, Wang and co-workers developed an aza-Friedel–Crafts reaction involving  $\beta$ -naphthols **119** as  $\pi$ -nucleophiles and benzothiazolines **118** as electrophiles. Chiral squaramide **S1**-assisted this process affording enantioenriched 1-((benzothiazol-2-ylamino)methyl)naphthalen-2-ols **120** with high chemical yields. The activation of the electrophile was achieved through acceptance of H-bonds by the nitrogens in **118** from the NH moieties of the catalyst where a free OH group of **119** donated a H-bond to the tertiary amine moiety of **S1**. These noncovalent interactions were responsible for the stereochemical output of the reaction. Different aryl substituents on the imine carbon and functionalities in the carbocyclic ring of **118** were tested. One example was shown with an alkyl-substituted imine which provided the product with much





Scheme 27: Thiourea-catalyzed aza-Friedel–Crafts reaction.

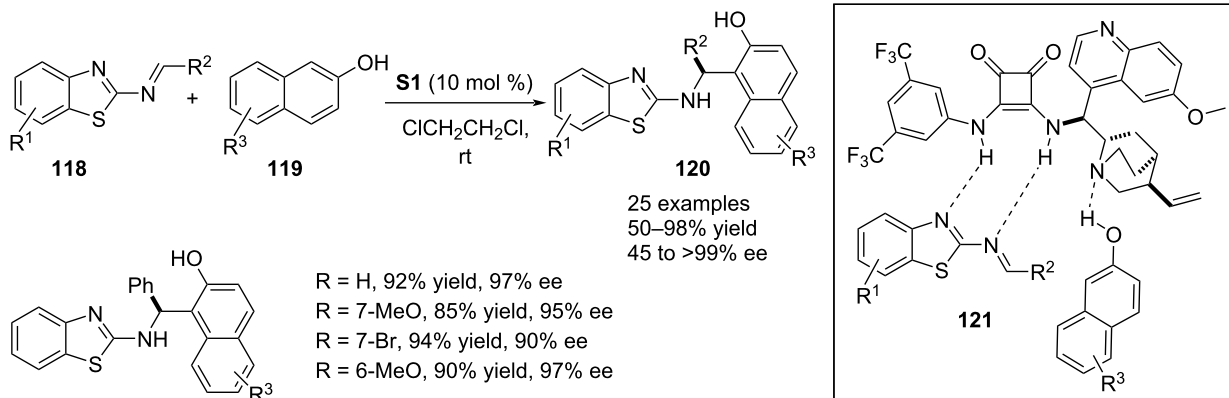
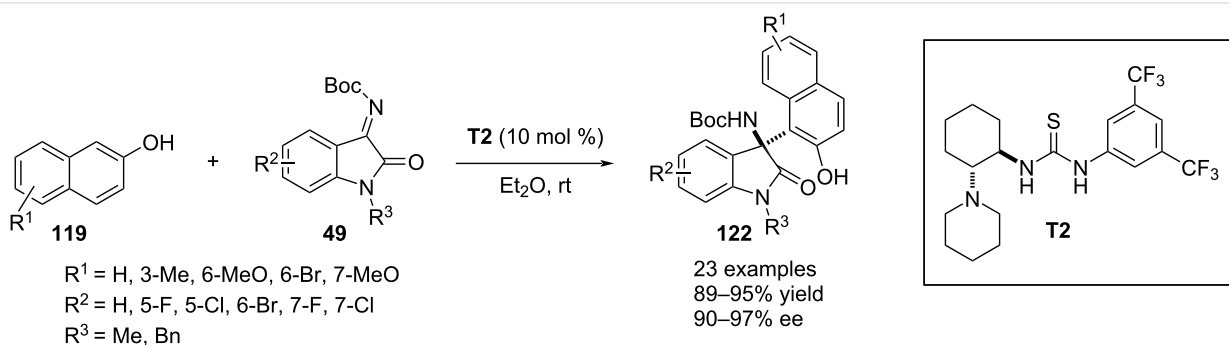
decreased enantioselectivity (45% ee) and four examples were presented by varying the functionalities in the nucleophile (Scheme 28) [58].

In 2021, Wang, Jin and co-workers deployed chiral thiourea **T2** as the catalytic agent for executing a highly enantioselective aza-Friedel–Crafts process between  $\beta$ -naphthols **119** and isatin-

derived ketimines **49** in the course of accessing enantio-enriched 3-amino-2-oxindoles **122** (Scheme 29) [59].

### Other catalysts

In 2019, Vila, Pedro and co-workers reported a functional group-directed activation of the carbocyclic ring of indoles utilizing cyclic imines as electrophiles. The quinine-derived

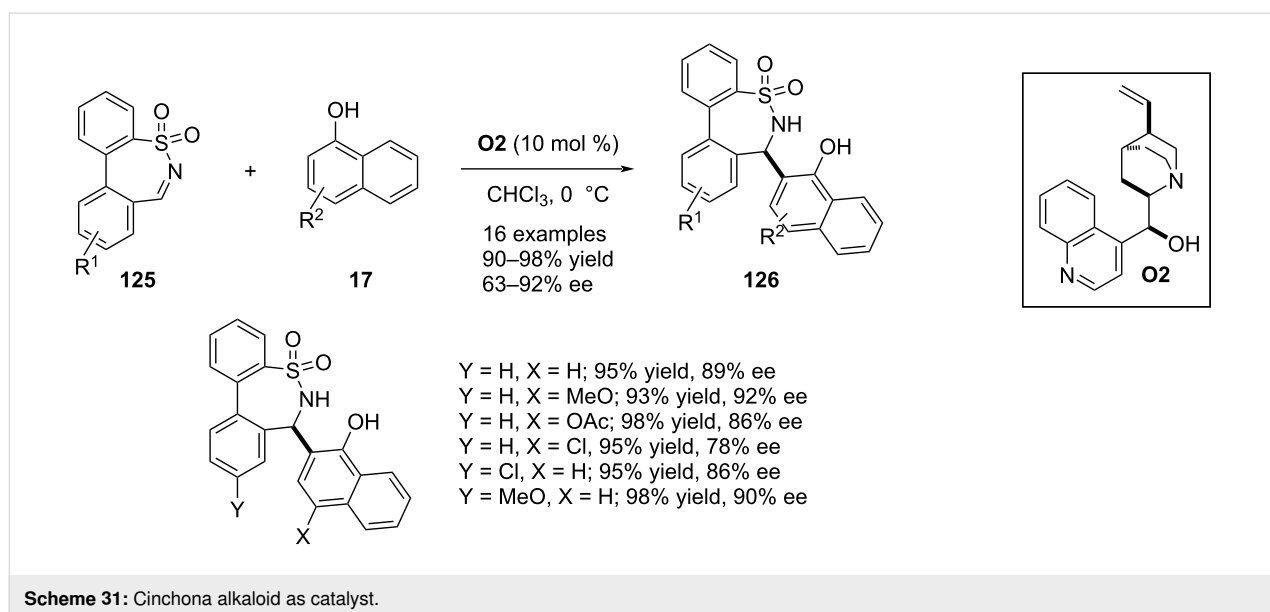
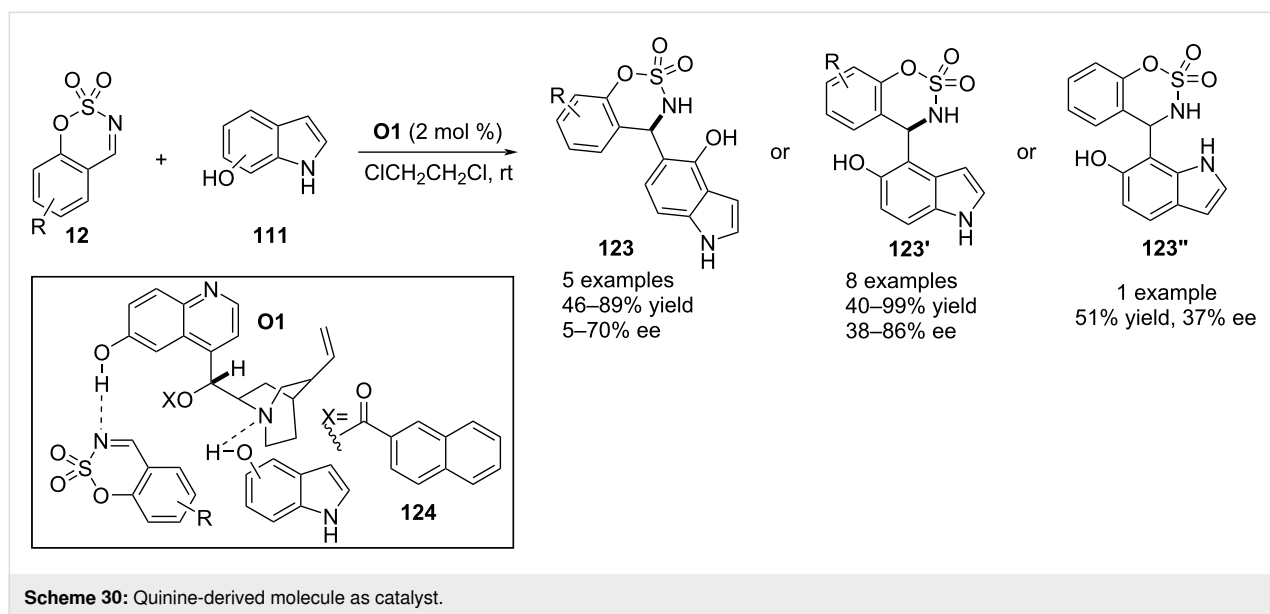
Scheme 28: Squaramide-catalyzed reaction between  $\beta$ -naphthols and benzothiazolines.Scheme 29: Thiourea-catalyzed reaction between  $\beta$ -naphthol and isatin-derived ketamine.

compound **O1** was the catalytic reagent to functionalize the *ortho*-C–H bond of 4-, 5-, and 6-hydroxyindoles **111** via an aza-Friedel–Crafts aminoalkylation involving benzoxathiazine 2,2-dioxides **12** as electron-demanding reagents. H-Bonding engagement of both substrates with the catalyst selectively masked the *Re* face of the imine plane thus forcing the nucleophile to approach from the *Si* face (see transition state **124**, Scheme 30) [60].

In 2019, Zhou and co-workers reported an aza-Friedel–Crafts reaction between  $\alpha$ -naphthol derivatives **17** utilizing 7-membered cyclic *N*-sulfonylimines **125** as electrophiles leading to the facile access of  $\epsilon$ -sultams **126** bearing a sulfonylamine-

substituted stereocenter. Cinchona alkaloid **O2** was the efficient catalyst for this asymmetric C–C bond formation delivering the products with moderate to good enantioselectivities. One example was documented involving  $\beta$ -naphthol as nucleophile and another example included electron-rich phenol (Scheme 31) [61].

Lin, Duan and co-workers demonstrated an enantioselective aza-Friedel–Crafts reaction between indoles **4** and isatin-derived ketimines **49**. A chiral phase transfer catalyst **O3** derived from urea assisted this organic transformation featuring a C3–H bond functionalization of indoles. Different protecting groups for the imine nitrogen and ring nitrogen of **49** were



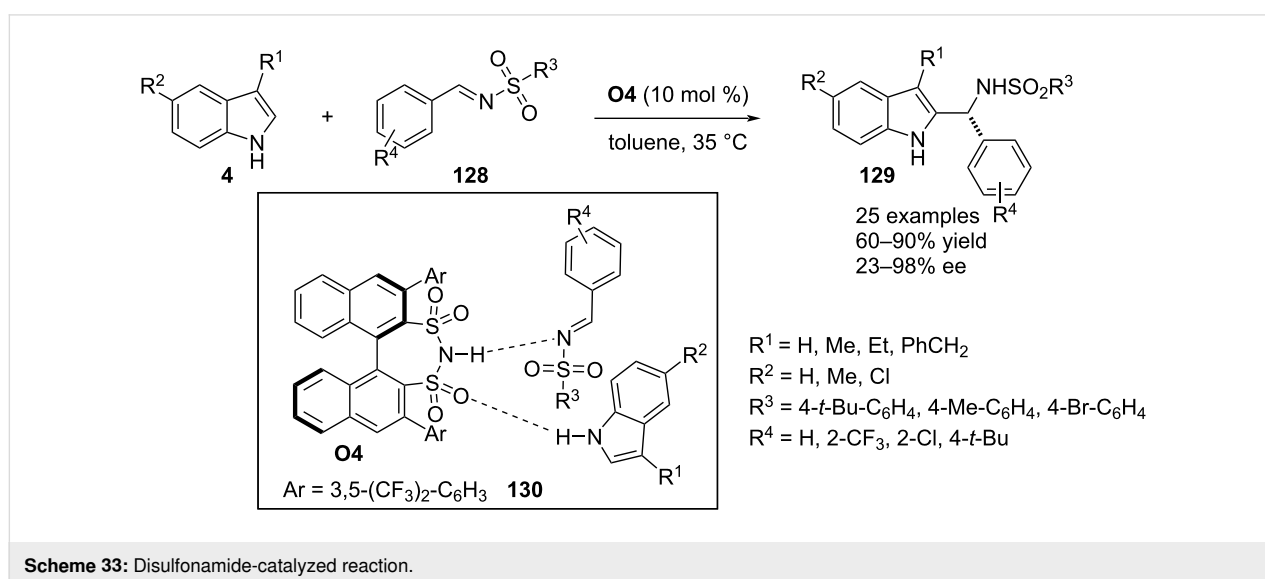
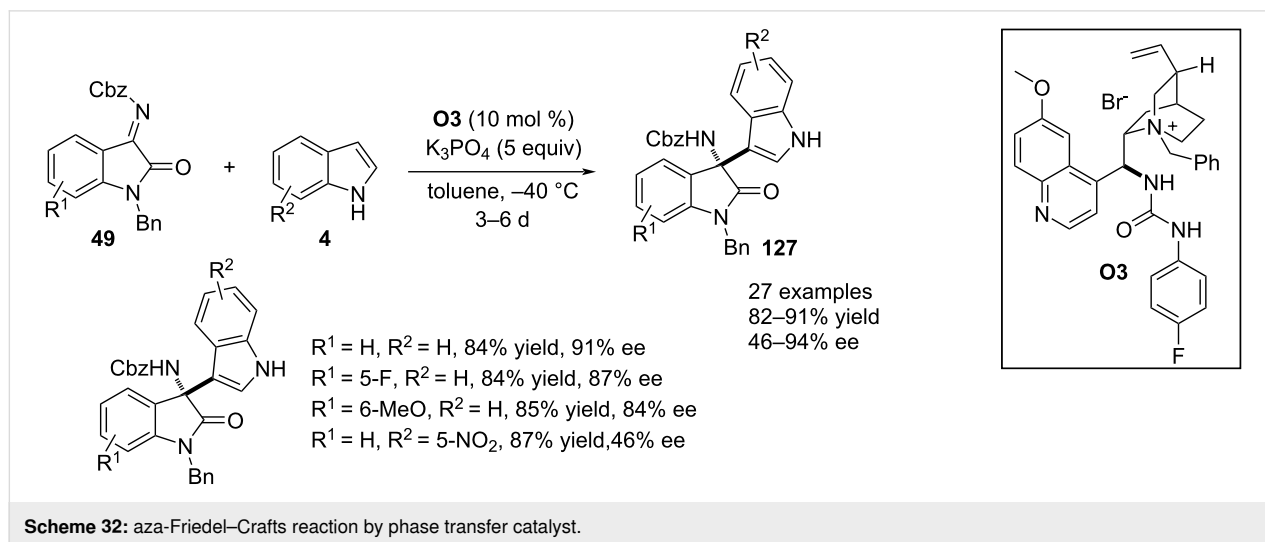
screened under optimal reaction conditions where Cbz and benzyl were the best protecting groups in terms of enantioselectivities. A product library was prepared by varying sterically and electronic divergent functionalities in the carbocyclic rings of both reactants. Enantioincorporation into the products was explained by H-bonding engagement between the catalyst NHs groups and an ionic interaction between the anionic indole and quaternary ammonium moiety of the catalyst (Scheme 32) [62].

In 2022, Li, Chen and co-workers employed the BINOL-derived chiral disulfonimide **O4** as Brønsted acid catalyst to execute a straightforward aza-Friedel–Crafts reaction between 3-substituted indoles **4** and *N*-sulfonyl-substituted aldimines **128**. The reaction successfully installed an aza-tertiary stereocenter at the C2 position of the heterocyclic ring. A broad substrate scope was investigated by varying substituents on both

substrates. A transition state involving dual noncovalent interactions between the catalyst and substrates directed the face-selective addition of the  $\pi$ -nucleophile to the electrophilic carbon of the imine (see transition state **130**, Scheme 33) [63].

## Heterogenous catalysts

In 2020, Pedrosa and co-workers devised a chiral heterogenous thiourea catalyst that was applied in an enantioefficient aza-Friedel–Crafts process. A series of heterogenous catalysts were prepared by condensation between alkaloids and polystyrene-derived isothiocyanates. These polymer-supported materials were utilized as heterogenous catalyst to execute the aza-Friedel–Crafts reaction between 1-naphthols **17** and isatin-derived ketimines **49** to produce oxindole motif **61** bearing a 1-hydroxynaphth-2-yl-substituted aza-quaternary stereocenter at the C3 position. The best result was obtained with the hydroqui-



nine-based supported catalyst **H1** which efficiently promoted five catalytic cycles without loss of its activity. *N*-Alkyl-substituted ketimines **49** with different functionalities in the benzene ring were well responsive towards the heterogenous reaction to afford the products **61** with moderate to excellent enantiomeric excesses. However, *N*-unsubstituted **49** ( $R^1 = H$ ) resulted in a much diminished stereoselectivity. As the electrophilic partner, isatin-derived ketimine was also utilized which furnished the product with 68% enantiomeric excess. Replacement of the nucleophile in this methodology for substrate scope expansion was carried out by employing 2-naphthol and 4-hydroxyindole (Scheme 34) [64].

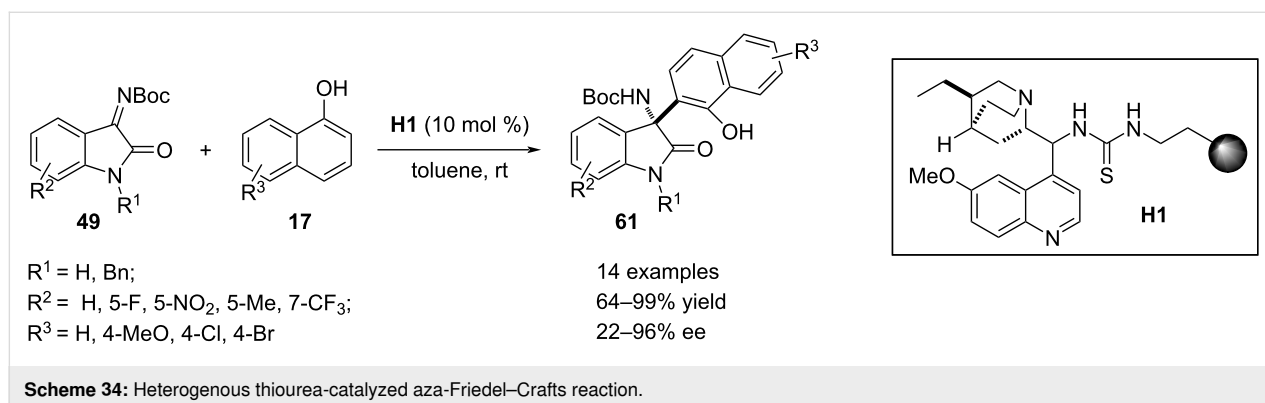
## Application in total synthesis

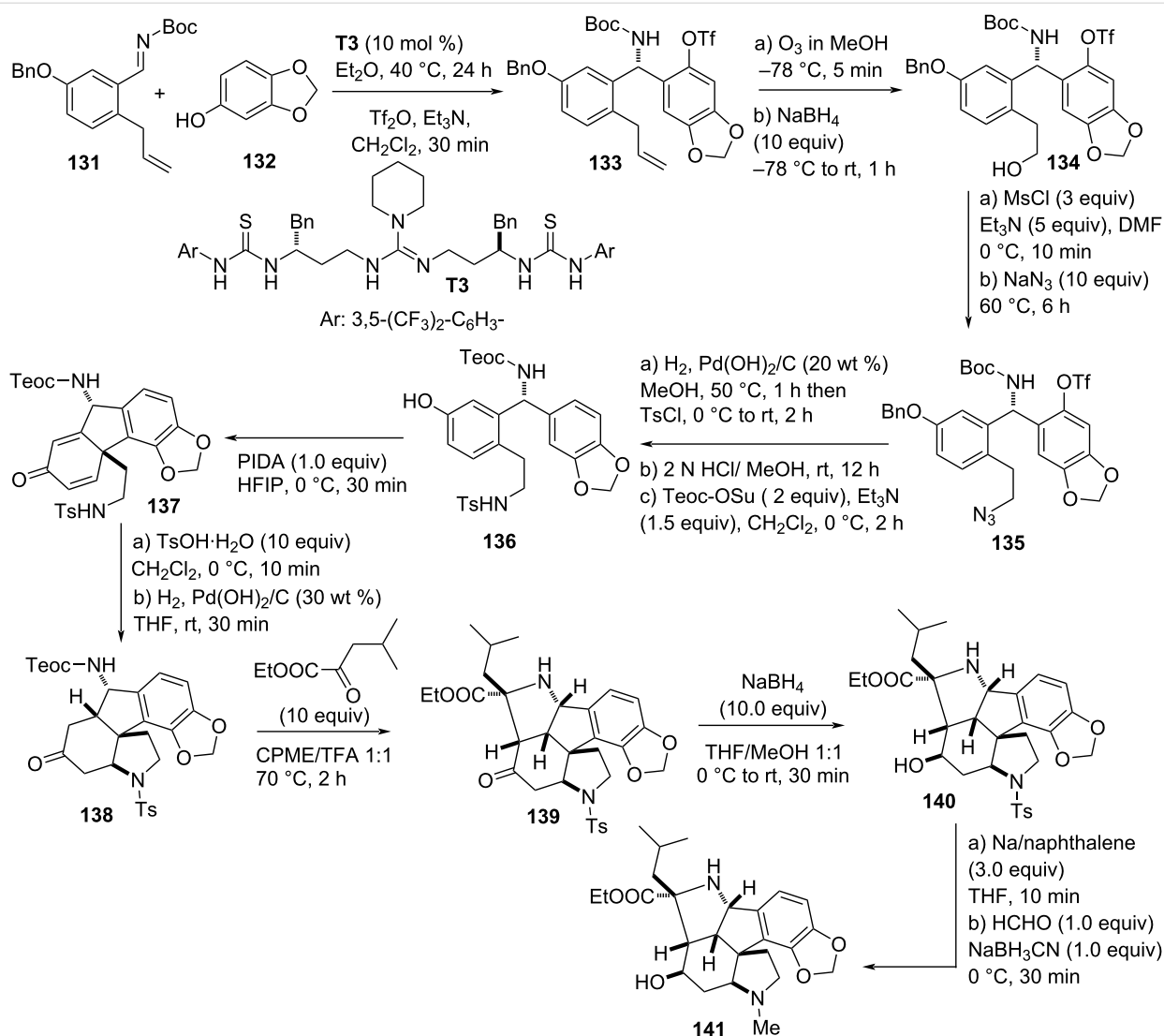
In 2018, a guanidine bistiourea-catalyzed highly enantioselective aza-Friedel–Crafts reaction was applied as a central step in the total synthesis of (+)-gracilamine. The reaction was designed between sesamol (**132**) and *N*-Boc-protected ketimine **131** in the presence of **T3** as catalyst to introduce the electrophile at the *ortho*-position with respect to the phenolic OH group. The aza-Friedel–Crafts product was obtained with 94% yield and converted into triflate **133** with 74% yield and 99% ee after recrystallization. Subsequent ozonolysis of the terminal alkene functionality with a follow-up reduction furnished primary alcohol **134** which was transformed into the azide **135**. Reduction of the azide **135** was accompanied by debenzylation, was followed by tosylation of the primary amine and exchange of the Boc-protecting group with the Teoc group then gave phenol **136**. Compound **136** was then subjected to a highly diastereoselective oxidative phenolic coupling giving fused tetracyclic architecture **137**. Follow-up acid-mediated intramolecular aza-Michael addition and subsequent alkene reduction provided ketone **138** which was reacted with an  $\alpha$ -keto ester in an intramolecular 5-*endo-trig*-cyclization process to afford **139**. Treatment of compound **139** with sodium borohydride afforded secondary alcohol **140** which after conversion of the tosyl group into a methyl group gave the final product **141** (Scheme 35) [65].

In 2019, Piersanti and co-workers reported an organocatalyzed enantioselective aza-Friedel–Crafts/lactonization domino reaction sequence as the key step in the course of synthesizing (+)- and (–)-fumimycin. (–)-Fumimycin was first isolated from *Aspergillus fumisynnematus* and exhibits antibacterial activity against resistant *S. aureus* strains. It is also an inhibitor of the enzyme peptide deformylases (PDFs). The synthesis comprised the reaction between the highly substituted hydroquinone **142** and dehydroalanine **143** in the presence of chiral phosphoric acid **P7** as catalyst to prepare benzofuran-2(3*H*)-one derivative **144** having an aza-quaternary stereocenter. The achiral Lewis acid tris(pentafluorophenyl)borane was required as additive in the reaction system to enhance the chemical yield and enantioselectivity. After two additional steps, i.e., demethylation of the phenolic ether and ester hydrolysis, (–)-fumimycin (**146**) was obtained (Scheme 36) [66].

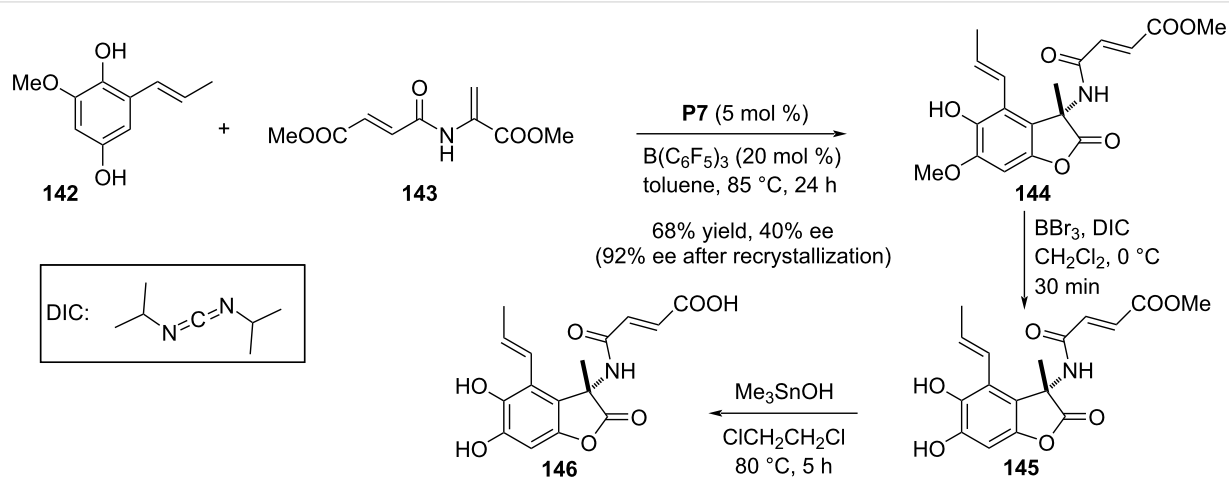
## Conclusion

The aza-Friedel–Crafts reaction is a powerful reaction that allows the incorporation of an aminoalkyl functionality in aromatic systems through C–C bond formation. This C–H bond functionalization methodology of aromatic systems also has the possibility of incorporating aza stereocenters into a product depending upon the choice of a suitable electrophile, i.e., imines. The present review assembled recent (from 2018 till date) examples of asymmetric versions of this important method mediated by different organocatalysts. The mechanistic approaches with explanation about the origin of stereoselectivities has also been elaborated. This reaction has been successfully utilized as the key step in the syntheses of different important natural products which have been included in this article as well. On searching the literature, it has been found that mainly H-bonding chiral organic molecules have been envisaged as the catalytic systems for stereoreinduction into products. The asymmetric induction is caused by effective noncovalent interactions between the catalysts and substrates to force a face-selective attack by the nucleophile, i.e., the aromatic  $\pi$ -system to the electrophile.





Scheme 35: Total synthesis of (+)-gracilamine.



Scheme 36: Total synthesis of (-)-fumimycin.

## ORCID® iDs

Anup Biswas - <https://orcid.org/0000-0002-6985-1247>

## References

- Davies, H. M. L.; Morton, D. J. *Org. Chem.* **2016**, *81*, 343–350. doi:10.1021/acs.joc.5b02818
- List, B. *Chem. Rev.* **2007**, *107*, 5413–5415. doi:10.1021/cr078412e
- MacMillan, D. W. C. *Nature* **2008**, *455*, 304–308. doi:10.1038/nature07367
- Mancheño, O. G.; Waser, M. *Eur. J. Org. Chem.* **2023**, *26*, e202200950. doi:10.1002/ejoc.202200950
- Han, B.; He, X.-H.; Liu, Y.-Q.; He, G.; Peng, C.; Li, J.-L. *Chem. Soc. Rev.* **2021**, *50*, 1522–1586. doi:10.1039/d0cs00196a
- Mukherjee, S.; Yang, J. W.; Hoffmann, S.; List, B. *Chem. Rev.* **2007**, *107*, 5471–5569. doi:10.1021/cr0684016
- Erkkilä, A.; Majander, I.; Pihko, P. M. *Chem. Rev.* **2007**, *107*, 5416–5470. doi:10.1021/cr068388p
- Enders, D.; Niemeier, O.; Henseler, A. *Chem. Rev.* **2007**, *107*, 5606–5655. doi:10.1021/cr068372z
- Hopkinson, M. N.; Richter, C.; Schedler, M.; Glorius, F. *Nature* **2014**, *510*, 485–496. doi:10.1038/nature13384
- Methot, J. L.; Roush, W. R. *Adv. Synth. Catal.* **2004**, *346*, 1035–1050. doi:10.1002/adsc.200404087
- Taylor, J. E.; Bull, S. D.; Williams, J. M. J. *Chem. Soc. Rev.* **2012**, *41*, 2109–2121. doi:10.1039/c2cs15288f
- Biswas, A.; Mondal, H.; Maji, M. S. *J. Heterocycl. Chem.* **2020**, *57*, 3818–3844. doi:10.1002/jhet.4119
- McLaughlin, C.; Smith, A. D. *Chem. – Eur. J.* **2021**, *27*, 1533–1555. doi:10.1002/chem.202002059
- Taylor, M. S.; Jacobsen, E. N. *Angew. Chem., Int. Ed.* **2006**, *45*, 1520–1543. doi:10.1002/anie.200503132
- Connon, S. J. *Chem. – Eur. J.* **2006**, *12*, 5418–5427. doi:10.1002/chem.200501076
- Atashkar, B.; Zolfigol, M. A.; Mallakpour, S. *Mol. Catal.* **2018**, *452*, 192–246. doi:10.1016/j.mcat.2018.03.009
- Parmar, D.; Sugiono, E.; Raja, S.; Rueping, M. *Chem. Rev.* **2014**, *114*, 9047–9153. doi:10.1021/cr5001496
- Woldegiorgis, A. G.; Lin, X. *Beilstein J. Org. Chem.* **2021**, *17*, 2729–2764. doi:10.3762/bjoc.17.185
- Chauhan, P.; Mahajan, S.; Kaya, U.; Hack, D.; Enders, D. *Adv. Synth. Catal.* **2015**, *357*, 253–281. doi:10.1002/adsc.201401003
- Biswas, A.; Ghosh, A.; Shankhdhar, R.; Chatterjee, I. *Asian J. Org. Chem.* **2021**, *10*, 1345–1376. doi:10.1002/ajoc.202100181
- Friedel, C.; Crafts, J. M. C. *R. Hebd. Seances Acad. Sci.* **1877**, *84*, 1450–1454.
- Calloway, N. O. *Chem. Rev.* **1935**, *17*, 327–392. doi:10.1021/cr60058a002
- Rueping, M.; Nachtsheim, B. J. *Beilstein J. Org. Chem.* **2010**, *6*, No. 6. doi:10.3762/bjoc.6.6
- Uraguchi, D.; Sorimachi, K.; Terada, M. *J. Am. Chem. Soc.* **2004**, *126*, 11804–11805. doi:10.1021/ja046185h
- Nakamura, S.; Furukawa, T.; Hatanaka, T.; Funahashi, Y. *Chem. Commun.* **2018**, *54*, 3811–3814. doi:10.1039/c8cc00594j
- Rahman, A.; Xie, E.; Lin, X. *Org. Biomol. Chem.* **2018**, *16*, 1367–1374. doi:10.1039/c8ob00055g
- Choi, S.; Kim, S.-G. *Bull. Korean Chem. Soc.* **2018**, *39*, 1340–1343. doi:10.1002/bkcs.11593
- Lee, J.; Kim, S.-G. *Bull. Korean Chem. Soc.* **2019**, *40*, 606–609. doi:10.1002/bkcs.11731
- Yonesaki, R.; Kondo, Y.; Akkad, W.; Sawa, M.; Morisaki, K.; Morimoto, H.; Ohshima, T. *Chem. – Eur. J.* **2018**, *24*, 15211–15214. doi:10.1002/chem.201804078
- Bartoccini, F.; Mari, M.; Retini, M.; Bartolucci, S.; Piersanti, G. *J. Org. Chem.* **2018**, *83*, 12275–12283. doi:10.1021/acs.joc.8b01774
- Yarlagadda, S.; Sridhar, B.; Subba Reddy, B. V. *Chem. – Asian J.* **2018**, *13*, 1327–1334. doi:10.1002/asia.201800300
- Hatano, M.; Okamoto, H.; Kawakami, T.; Toh, K.; Nakatsuji, H.; Sakakura, A.; Ishihara, K. *Chem. Sci.* **2018**, *9*, 6361–6367. doi:10.1039/c8sc02290a
- Hatano, M.; Toh, K.; Ishihara, K. *Org. Lett.* **2020**, *22*, 9614–9620. doi:10.1021/acs.orglett.0c03662
- Inokuma, T.; Sakakibara, T.; Someno, T.; Masui, K.; Shigenaga, A.; Otaka, A.; Yamada, K.-i. *Chem. – Eur. J.* **2019**, *25*, 13829–13832. doi:10.1002/chem.201903572
- Maestro, A.; Martinez de Marigorta, E.; Palacios, F.; Vicario, J. *J. Org. Chem.* **2019**, *84*, 1094–1102. doi:10.1021/acs.joc.8b02843
- Xie, E.; Huang, S.; Lin, X. *Org. Lett.* **2019**, *21*, 3682–3686. doi:10.1021/acs.orglett.9b01127
- Kim, Y.; Lee, J.; Jung, J.; Kim, S.-G. *Tetrahedron Lett.* **2019**, *60*, 1625–1630. doi:10.1016/j.tetlet.2019.05.003
- You, Y.; Lu, W.-Y.; Xie, K.-X.; Zhao, J.-Q.; Wang, Z.-H.; Yuan, W.-C. *Chem. Commun.* **2019**, *55*, 8478–8481. doi:10.1039/c9cc04057a
- Zhou, J.; Zhu, G.-D.; Wang, L.; Tan, F.-X.; Jiang, W.; Ma, Z.-G.; Kang, J.-C.; Hou, S.-H.; Zhang, S.-Y. *Org. Lett.* **2019**, *21*, 8662–8666. doi:10.1021/acs.orglett.9b03276
- Miyagawa, M.; Yoshida, M.; Kiyota, Y.; Akiyama, T. *Chem. – Eur. J.* **2019**, *25*, 5677–5681. doi:10.1002/chem.201901020
- Uchikura, T.; Suzuki, R.; Suda, Y.; Akiyama, T. *ChemCatChem* **2020**, *12*, 4784–4787. doi:10.1002/cctc.202000920
- Uchikura, T.; Aruga, K.; Suzuki, R.; Akiyama, T. *Org. Lett.* **2022**, *24*, 4699–4703. doi:10.1021/acs.orglett.2c01972
- Liu, C.; Tan, F.-X.; Zhou, J.; Bai, H.-Y.; Ding, T.-M.; Zhu, G.-D.; Zhang, S.-Y. *Org. Lett.* **2020**, *22*, 2173–2177. doi:10.1021/acs.orglett.0c00262
- Duan, M.; Chen, J.; Wang, T.; Luo, S.; Wang, M.; Fan, B. *J. Org. Chem.* **2022**, *87*, 15152–15158. doi:10.1021/acs.joc.2c01659
- Zhao, Y.; Cai, L.; Huang, T.; Meng, S.; Chan, A. S. C.; Zhao, J. *Adv. Synth. Catal.* **2020**, *362*, 1309–1316. doi:10.1002/adsc.201901380
- Yuan, X.; Wu, X.; Peng, F.; Yang, H.; Zhu, C.; Fu, H. *Chem. Commun.* **2020**, *56*, 12648–12651. doi:10.1039/d0cc05432a
- Cheng, Y.-S.; Chan, S.-H.; Rao, G. A.; Gurubrahmam, R.; Chen, K. *Adv. Synth. Catal.* **2021**, *363*, 3502–3506. doi:10.1002/adsc.202100408
- Liu, H.; Yan, Y.; Li, M.; Zhang, X. *Org. Biomol. Chem.* **2021**, *19*, 3820–3824. doi:10.1039/d1ob00374g
- Li, M.; Chen, Y.; Yan, Y.; Liu, M.; Huang, M.; Li, W.; Cao, L.; Zhang, X. *Org. Biomol. Chem.* **2022**, *20*, 8849–8854. doi:10.1039/d2ob01746f
- Qian, C.; Liu, M.; Sun, J.; Li, P. *Org. Chem. Front.* **2022**, *9*, 1234–1240. doi:10.1039/d1qo01864g
- Woldegiorgis, A. G.; Han, Z.; Lin, X. *Adv. Synth. Catal.* **2022**, *364*, 274–280. doi:10.1002/adsc.202101011
- Woldegiorgis, A. G.; Gu, H.; Lin, X. *Chirality* **2022**, *34*, 678–693. doi:10.1002/chir.23422
- Li, C.; Zuo, W.-F.; Zhou, J.; Zhou, W.-J.; Wang, M.; Li, X.; Zhan, G.; Huang, W. *Org. Chem. Front.* **2022**, *9*, 1808–1813. doi:10.1039/d2qo00021k



54. Qiao, X.-X.; He, Y.; Ma, T.; Zou, C.-P.; Wu, X.-X.; Li, G.; Zhao, X.-J. *Chem. – Eur. J.* **2023**, *29*, e202203914. doi:10.1002/chem.202203914
55. Okamoto, H.; Toh, K.; Mochizuki, T.; Nakatsuji, H.; Sakakura, A.; Hatano, M.; Ishihara, K. *Synthesis* **2018**, *50*, 4577–4590. doi:10.1055/s-0037-1610250
56. Yang, Z.-T.; Yang, W.-L.; Chen, L.; Sun, H.; Deng, W.-P. *Adv. Synth. Catal.* **2018**, *360*, 2049–2054. doi:10.1002/adsc.201800181
57. Vila, C.; Rendón-Patiño, A.; Montesinos-Magraner, M.; Blay, G.; Muñoz, M. C.; Pedro, J. R. *Adv. Synth. Catal.* **2018**, *360*, 859–864. doi:10.1002/adsc.201701217
58. Li, C.-Y.; Xiang, M.; Zhang, J.; Li, W.-S.; Zou, Y.; Tian, F.; Wang, L.-X. *Org. Biomol. Chem.* **2021**, *19*, 7690–7694. doi:10.1039/d1ob01443a
59. Chen, Z.; Zhang, T.; Sun, Y.; Wang, L.; Jin, Y. *New J. Chem.* **2021**, *45*, 10481–10487. doi:10.1039/d1nj01421h
60. Vila, C.; Tortosa, A.; Blay, G.; Muñoz, M. C.; Pedro, J. R. *New J. Chem.* **2019**, *43*, 130–134. doi:10.1039/c8nj05577g
61. Zhao, Z.-B.; Shi, L.; Li, Y.; Meng, F.-J.; Zhou, Y.-G. *Org. Biomol. Chem.* **2019**, *17*, 6364–6368. doi:10.1039/c9ob01158g
62. Li, J.; Wei, Z.; Cao, J.; Liang, D.; Lin, Y.; Duan, H. *J. Org. Chem.* **2022**, *87*, 2532–2542. doi:10.1021/acs.joc.1c02477
63. Sun, P.; Jia, Z.-H.; Tang, L.; Zheng, H.; Li, Z.-R.; Chen, L.-Y.; Li, Y. *Org. Biomol. Chem.* **2022**, *20*, 1916–1925. doi:10.1039/d1ob02281d
64. Rodríguez-Rodríguez, M.; Maestro, A.; Andrés, J. M.; Pedrosa, R. *Adv. Synth. Catal.* **2020**, *362*, 2744–2754. doi:10.1002/adsc.202000238
65. Odagi, M.; Yamamoto, Y.; Nagasawa, K. *Angew. Chem., Int. Ed.* **2018**, *57*, 2229–2232. doi:10.1002/anie.201708575
66. Retini, M.; Bartolucci, S.; Bartocchini, F.; Mari, M.; Piersanti, G. *J. Org. Chem.* **2019**, *84*, 12221–12227. doi:10.1021/acs.joc.9b02020

## License and Terms

This is an open access article licensed under the terms of the Beilstein-Institut Open Access License Agreement (<https://www.beilstein-journals.org/bjoc/terms>), which is identical to the Creative Commons Attribution 4.0 International License (<https://creativecommons.org/licenses/by/4.0>). The reuse of material under this license requires that the author(s), source and license are credited. Third-party material in this article could be subject to other licenses (typically indicated in the credit line), and in this case, users are required to obtain permission from the license holder to reuse the material.

The definitive version of this article is the electronic one which can be found at:  
<https://doi.org/10.3762/bjoc.19.72>